

FIELD ORIENTED CONTROL OF A PERMANENT MAGNET
SYNCHRONOUS MOTOR USING SPACE VECTOR MODULATED DIRECT
AC-AC MATRIX CONVERTER

A THESIS SUBMITTED TO
THE GRADUATE SCHOOL OF NATURAL AND APPLIED SCIENCES
OF
MIDDLE EAST TECHNICAL UNIVERSITY

BY

DOĞAN YILDIRIM

IN PARTIAL FULLFILLMENT OF THE REQUIREMENTS
FOR
THE DEGREE OF MASTER OF SCIENCE
IN
ELECTRICAL AND ELECTRONICS ENGINEERING

MAY 2012

Approval of the thesis:

**FIELD ORIENTED CONTROL OF A PERMANENT MAGNET
SYNCHRONOUS MOTOR USING SPACE VECTOR MODULATED
DIRECT AC-AC MATRIX CONVERTER**

submitted by **DOĞAN YILDIRIM** in partial fulfillment of the requirements for the degree of **Master of Science in Electrical and Electronics Engineering Department, Middle East Technical University** by,

Prof. Dr. Canan ÖZGEN
Dean, Graduate School of **Natural and Applied Sciences** _____

Prof. Dr. İsmet ERKMEN
Head of Department, **Electrical and Electronics Engineering** _____

Prof. Dr. Aydın ERSKAK
Supervisor, **Electrical and Electronics Engineering Dept., METU** _____

Examining Committee Members:

Prof. Dr. Muammer ERMIŞ
Electrical and Electronics Engineering Dept., METU _____

Prof. Dr. Aydın ERSKAK
Electrical and Electronics Engineering Dept., METU _____

Prof. Dr. Işık ÇADIRCI
Electrical and Electronics Engineering Dept., HU _____

Dr. Faruk BİLGİN
Space Technologies Research Institute, TÜBİTAK _____

Dr. Bilge MUTLUER
Space Technologies Research Institute, TÜBİTAK _____

Date: _____ 10.05.2012 _____

I hereby declare that all information in this document has been obtained and presented in accordance with academic rules and ethical conduct. I also declare that, as required by these rules and conduct, I have fully cited and referenced all material and results that are not original to this work.

Name, Last name : Dođan YILDIRIM

Signature :

ABSTRACT

FIELD ORIENTED CONTROL OF A PERMANENT MAGNET SYNCHRONOUS MOTOR USING SPACE VECTOR MODULATED DIRECT AC-AC MATRIX CONVERTER

Yıldırım, Doğan

M. Sc., Department of Electrical and Electronics Engineering

Supervisor: Prof. Dr. Aydın Ersak

May 2012, 167 pages

The study designs and constructs a three-phase to three-phase direct AC-AC matrix converter based surface mounted permanent magnet synchronous motor (PMSM) drive system. First, the matrix converter topologies are analyzed and the state-space equations describing the system have been derived in terms of the input and output variables. After that, matrix converter commutation and modulation methods are investigated. A four-step commutation technique based on output current direction provides safe commutation between the matrix converter switches. Then, the matrix converter is simulated for both the open-loop and the closed-loop control. For the closed-loop control, a current regulator (PI controller) controls the output currents and their phase angles. Advanced pulse width modulation and control techniques, such as space vector pulse width modulation and field oriented control, have been used for the closed-loop control of the system. Next, a model of diode-rectified two-level voltage source inverter is developed for simulations. A comparative study of indirect space vector modulated direct matrix converter and space vector modulated diode-rectified two-level voltage source inverter is given in terms of input/output waveforms to verify that the matrix converter fulfills the two-level voltage source inverter operation. Following the verification of matrix converter operation

comparing with the diode-rectified two-level voltage source inverter, the simulation model of permanent magnet motor drive system is implemented. Also, a direct matrix converter prototype is constructed for experimental verifications of the results. As a first step in experimental works, filter types are investigated and a three-phase input filter is constructed to reduce the harmonic pollution. Then, direct matrix converter power circuitry and gate-driver circuitry are designed and constructed. To control the matrix switches, the control algorithm is implemented using a DSP and a FPGA. This digital control system measures the output currents and the input voltages with the aid of sensors and controls the matrix converter switches to produce the required PWM pattern to synthesize the reference input current and output voltage vectors, as well. Finally, the simulation results are tested and supported by laboratory experiments involving both an R-L load and a permanent magnet synchronous motor load. During the tests, the line-to-line supply voltage is set to 26 V peak value and a 400 V/3.5 kW surface mounted permanent magnet motor is used.

Keywords: Direct matrix converter, bi-directional switch, space vector PWM, field oriented control, SMPMS motor, three-phase diode rectifier, two-level inverter

ÖZ

UZAY VEKTÖR MODULASYONLU DİREK AC-AC MATRİS ÇEVİRİCİ KULLANARAK KALICI MIKNATISLI SENKRON MOTORUN ALAN YÖNLENDİRMELİ DENETİMİ

Yıldırım, Doğan

Yüksek Lisans, Elektrik Elektronik Mühendisliği Bölümü

Tez Yöneticisi: Prof. Dr. Aydın Ersak

Mayıs 2012, 167 sayfa

Bu çalışmada üç faz giriş ve üç faz çıkışlı matris çevirici topolojisine dayalı yüzey monte kalıcı mıknatıslı eşzamanlı motor sürücü sistemi tasarlanmakta ve inşa edilmektedir. İlk olarak, matris çevirici topolojileri analiz edilmektedir ve giriş - çıkış değişkenleri cinsinden sistemi tanımlayacak durum uzayı denklemleri çıkarılmaktadır. Daha sonra matris çevirici komutasyon ve modülasyon metotları incelenmektedir. Çıkış akımının yönüne dayalı dört basamaklı komutasyon tekniği ile matris çeviricinin güvenilir komutasyonu yapılmaktadır. Sonra, matris çevirici kontrolü için açık ve kapalı döngü benzetim modelleri oluşturulmaktadır. Çıkış akımları ve faz açıları kapalı döngü kontrolü, PI kontrolcüsü kullanılarak gerçekleştirilmektedir. Uzay vektör darbe genişlik modülasyonu ve alan yönlendirmeli kontrol teknikleri gibi gelişmiş modülasyon ve kontrol teknikleri kullanılmaktadır. Daha sonra, diyot doğrultmalı iki seviyeli voltaj kaynaklı evirici modeli geliştirilmektedir. Matris çeviricinin bu evirici yapısının fonksiyonlarını yerine getirebildiğini doğrulamak amacıyla bu iki topolojinin giriş ve çıkış dalga formları birbirleri ile karşılaştırılmaktadır. Matris çeviricinin bu iki seviyeli yapının fonksiyonlarını yerine getirebildiği doğrulandıktan sonra kalıcı mıknatıslı motor sürücü sistemi benzetim modeli gerçekleştirilmektedir. Bununla birlikte, deneysel doğrulamalar için matris çevirici devresi inşa

edilmektedir. Deneysel çalışmalarda ilk olarak, filtre türleri incelenmekte ve harmonik kirliliği önlemek amaçlı üç faz giriş filtresi inşa edilmektedir. Sonra, direk matris çevirici güç devresi ve “gate” sürücü devresi tasarlanmakta ve üretilmektedir. Matris çevirici üzerinde bulunan anahtarları kontrol etmek için FPGA ve DSP kullanılmaktadır. Dijital kontrol sistemi ile çıkış akımları ve giriş gerilim bilgileri okunmakta, hesaplanan akım ve voltaj vektörlerinin sentezlenmesi için gerekli anahtarlama işaretleri oluşturulmaktadır. Son olarak, simülasyon sonuçları pasif R-L yük ve motor yükü kullanılarak deneysel çalışma sonuçlarıyla test edilmekte ve desteklenmektedir. Testler boyunca, fazdan faza olan besleme voltaj değeri 26 V tepe gerilim değerine ayarlanmakta ve 400 V/3.5 kW'lık yüzey monte kalıcı mıknatıslı motor deneysel çalışmalarda kullanılmaktadır.

Anahtar Kelimeler: Direk matris çevirici, çift yönlü anahtar, uzay vektörü darbe genişliği modülasyonu, alan yönlendirmeli kontrol, yüzey monte kalıcı mıknatıslı senkron motor, üç faz diyot doğrultucu, iki seviyeli evirici

To My Family

ACKNOWLEDGEMENTS

I express my gratitude to my supervisor Prof. Dr. Aydın ERSAK for his guidance, support, criticism, encouragement and contributions throughout my graduate education.

I would also like to thank my colleagues and managers at ASELSAN Inc. for their understanding, help and support. I am also grateful to ASELSAN Inc. for the financial support.

Finally, I would like to thank my parents and wife, who have always been enriching my life with their continuous support and love.

TABLE OF CONTENTS

ABSTRACT	IV
ÖZ.....	VI
ACKNOWLEDGEMENTS.....	IX
TABLE OF CONTENTS.....	X
LIST OF FIGURES	XIII
LIST OF TABLES	XVIII
LIST OF ABBREVIATIONS.....	XIX
NOMENCLATURE.....	XX
CHAPTERS	
1. INTRODUCTION	1
1.1 AC/AC POWER CONVERSION	1
1.1.1 Overview of Indirect (DC-link) Two-Level Voltage Source Converters.....	3
1.1.2 History of Direct AC/AC Converters	5
1.1.3 Concept of Matrix Converter	7
1.2 SCOPE OF THESIS AND STRUCTURE OF CHAPTERS	8
2. THE PERMANENT MAGNET SYNCHRONOUS MACHINE (PMSM) DRIVE SYSTEM USING DIRECT MATRIX CONVERTER.....	10
2.1 STRUCTURE OF PERMANENT MAGNET MACHINE DRIVE SYSTEM.....	10
2.2 FUNDAMENTALS OF MATRIX CONVERTER	12
2.3 INPUT-OUTPUT CHARACTERISTICS OF MATRIX CONVERTER.....	12
2.3.1 Output Voltages and Currents.....	12
2.3.2 Input Voltages and Currents	14
2.4 STRUCTURAL ISSUES OF MATRIX CONVERTER	16
2.4.1 Direct Matrix Converter.....	17
2.4.2 Indirect Matrix Converter	18
2.4.3 Bi-directional Switches.....	20

2.4.4 Commutation Problem.....	23
2.4.5 Safe Operation	23
2.4.6 Switch Commutation	26
3. PERMANENT MAGNET SYNCHRONOUS MACHINES.....	42
3.1 STEADY-STATE MODELING OF SMPM SYNCHRONOUS MACHINE.....	43
3.2 DYNAMIC MODELING OF THE SMPM SYNCHRONOUS MACHINE.....	46
4. OPERATIONAL ISSUES OF MATRIX CONVERTER.....	50
4.1 STATE-SPACE MODEL OF MATRIX CONVERTER	50
4.2 VOLTAGE AND CURRENT WAVEFORMS GENERATION IN MATRIX CONVERTERS	53
4.2.1 Matrix Converter Modulation Methods of Alesina and Venturini.....	55
4.2.2 Space Vector.....	58
4.2.3 Application of Space Vector PWM Methods in the Matrix Converter	60
4.2.4 Application of the Indirect Space Vector PWM for Direct Matrix Converter	76
5. SYSTEM MODELING AND SIMULATIONS	83
5.1 MODELING OF DIRECT MATRIX CONVERTER.....	83
5.1.1 Input Filter Design.....	84
5.1.2 Construction of Bi-directional Power Switch Structures	89
5.1.3 Steps for the Simulation of Indirect Space Vector PWM for the Direct Matrix Converter	89
5.2 SIMULATIONS ON DIRECT MATRIX CONVERTER REGARDING TO OUTPUT CHARACTERISTICS.....	90
5.2.1 Simulations of Open-Loop System with Balanced R-L Load.....	91
5.2.2 Closed-Loop Simulations with Balanced Three-Phase R-L Load	105
5.3 SIMULATIONS ON DIRECT MATRIX CONVERTER REGARDING TO INPUT CHARACTERISTICS.....	111
5.4 SIMULATIONS ON DIODE-RECTIFIED TWO-LEVEL VOLTAGE SOURCE INVERTER STRUCTURE.....	113
5.5 COMPARISON OF THE DIODE-RECTIFIED TWO-LEVEL VOLTAGE SOURCE INVERTER AND DIRECT MATRIX CONVERTER.....	116
5.6 MODELING OF THE DIRECT MATRIX CONVERTER INTEGRATED DRIVE SYSTEM AND SIMULATIONS.....	118
5.6.1 Field Oriented Control of a Permanent Magnet Synchronous Motor	118
5.6.2 Model of the PMSM and Simulation Results	122

6. EXPERIMENTAL WORK	129
6.1 HARDWARE IMPLEMENTATION	129
6.2 MEASUREMENT EQUIPMENTS	134
6.3 EXPERIMENTAL RESULTS	135
6.3.1 Open-Loop Output Characteristics with Balanced R-L Load	135
6.3.2 Closed-Loop Output Characteristics with Balanced R-L Load	141
6.3.3 Unity Power Factor Control.....	148
6.3.4 Experiments with Surface Mounted Permanent Magnet Machine Load	151
7. CONCLUSIONS AND FUTURE WORKS	155
REFERENCES.....	159
APPENDIX.....	164
A. PARK AND CLARKE TRANSFORMATIONS	164
A.1. CLARKE TRANSFORMATION	164
A.2. PARK TRANSFORMATION	166

LIST OF FIGURES

FIGURES

Fig.1. 1 Classifications of converters low-to-high power drives	2
Fig.1. 2 Three-phase two-level voltage source inverter circuit topology	2
Fig.1. 3 Diode rectifier stage	3
Fig.1. 4 Diode rectifier based VSI.....	4
Fig.1. 5 Back to back voltage source converter.....	4
Fig.1. 6 Phase-controlled thyristor-based three-phase to three-phase cycloconverter.....	5
Fig.1. 7 Basic direct matrix converter circuit	6
Fig.2. 1 PMSM drive basic architecture.....	11
Fig.2. 2 Block diagram of PMSM drive system.....	11
Fig.2. 3 Structure of matrix converter system	13
Fig.2. 4 Line-to-line output voltage waveform generated by direct matrix converter	13
Fig.2. 5 Three-phase output currents of a direct matrix converter	14
Fig.2. 6 Three-phase input voltages of direct matrix converter.....	14
Fig.2. 7 Unfiltered input phase “A” current	15
Fig.2. 8 Harmonic spectrum of unfiltered input phase A current ($f_s = 10$ kHz)	15
Fig.2. 9 Filtered input phase A current.....	16
Fig.2. 10 Harmonic spectrum of filtered input phase A current ($f_s = 10$ kHz)	16
Fig.2. 11 Structure of direct matrix converter	17
Fig.2. 12 Structure of three-phase to four-phase direct matrix converter	18
Fig.2. 13 Indirect three-phase to three-phase matrix converter	19
Fig.2. 14 An equivalent switching combination of direct and indirect matrix converter	19
Fig.2. 15 Diode bridge structure.....	20
Fig.2. 16 Common source AC switch configuration.....	21
Fig.2. 17 Common drain AC switch configuration	22
Fig.2. 18 Anti-parallel series diode-MOSFET configuration	23
Fig.2. 19 The use of clamp circuit in direct matrix converter	25
Fig.2. 20 Input/output varistor/suppressor diode protection scheme.....	25
Fig.2. 21 Line to line short circuit condition.....	27
Fig.2. 22 Output current interrupt	27
Fig.2. 23 One output phase structure of direct matrix converter	29

Fig.2. 24 One output phase structure.....	30
Fig.2. 25 Freewheeling current path in Leg2	31
Fig.2. 26 Control signals of unidirectional switches	34
Fig.2. 27 Inductive current path in two step commutation	35
Fig.2. 28 Inter-Switches Commutation	35
Fig.2. 29 Allowed current directions ($V_B > V_A$)	37
Fig.2. 30 Critical and uncritical intervals for detecting of input voltage polarities	39
Fig.2. 31 Critical and uncritical intervals for output current direction and input voltage polarity based commutations.....	40
Fig.3. 1 Permanent magnet rotor construction using surface mounted magnets	42
Fig.3. 2 Permanent magnet rotor construction using embedded magnets	43
Fig.3. 3 Per-phase equivalent circuit of non-salient surface mounted permanent magnet synchronous machine.....	44
Fig.3. 4 Phasor diagram of the non-salient SMPM machine	45
Fig.3. 5 Phase equivalent circuit of a SMPM.....	47
Fig.3. 6 Two-phase (d, q) equivalent model of SMPM synchronous machine	48
Fig.4. 1 Simplified three-phase to three-phase matrix converter.....	51
Fig.4. 2 A possible switching pattern	56
Fig.4. 3 Three variables of balanced three-phase system (x_a, x_b, x_c)	59
Fig.4. 4 Space vector X_s and its components	59
Fig.4. 5 Switching constraints (a) possible short circuit states at input terminal (b) open circuit state at output terminals	62
Fig.4. 6 (a) Output phase voltage vector (b) input line current vector hexagons.....	64
Fig.4. 7 Indirect matrix converter circuit.....	66
Fig.4. 8 Active current vectors, related sectors, and the reference phase current vector I_i in complex plane	69
Fig.4. 9 Relationships between the input line current waveforms and the sectors in time domain	69
Fig.4. 10 Reference phase current vector construction.....	70
Fig.4. 11 Active output voltage space vectors, related sectors, and the reference output phase voltage vector, V_o in complex plane	73
Fig.4. 12 Time domain relationship between the output phase voltage waveforms and sectors	74
Fig.4. 13 Reference phase voltage vector construction	74
Fig.4. 14 (a) Voltage space vectors (b) current space vectors	78
Fig.4. 15 Nine switching pulses for a carrier frequency of 10 kHz with single-sided switching pattern	81

Fig.4. 16 Nine switching pulses for a carrier frequency of 10 kHz with double-sided switching pattern	82
Fig.5. 1 Input filter configurations used for matrix converter input filters.....	85
Fig.5. 2 Laplace transform of per-phase equivalent circuit	86
Fig.5. 3 Magnitude and phase plot of the LC filter with $R_f = 94$ Ohm.....	87
Fig.5. 4 Magnitude and phase plot of the LC filter without damping resistor.....	87
Fig.5. 5 The block diagram of the direct matrix converter model for simulation.....	88
Fig.5. 6 Per-phase equivalent circuit model of three-phase balanced passive load	91
Fig.5. 7 Block diagram of direct matrix converter in open-loop and a R-L load	92
Fig.5. 8 Block diagram for the direct matrix converter with unity gain assumption and the R-L load	92
Fig.5. 9 Theoretical magnitude and phase plots of load transfer function.....	93
Fig.5. 10 Output phase “a” to neutral voltage, V_{an} ($f_o = 50$ Hz).....	94
Fig.5. 11 Output phase “b” to neutral voltage, V_{bn} ($f_o = 50$ Hz).....	94
Fig.5. 12 Output phase “c” to neutral voltage, V_{cn} ($f_o = 50$ Hz).....	95
Fig.5. 13 Output line-to-line voltage V_{ab} ($f_o = 50$ Hz)	95
Fig.5. 14 Output line-to-line voltage V_{bc} ($f_o = 50$ Hz)	96
Fig.5. 15 Output line-to-line voltage V_{ca} ($f_o = 50$ Hz)	96
Fig.5. 16 Harmonic spectrum of output line-to-line voltage V_{ab} ($f_o = 50$ Hz)	97
Fig.5. 17 Waveforms of the load currents ($f_o = 50$ Hz).....	97
Fig.5. 18 Harmonic spectrum of the output phase “a” current ($f_o = 50$ Hz)	98
Fig.5. 19 Output phase “a” to neutral voltage, V_{an} ($f_o = 100$ Hz).....	99
Fig.5. 20 Output line-to-line voltage V_{ab} ($f_o = 100$ Hz).....	99
Fig.5. 21 Harmonic spectrum of output line-to-line voltage V_{ab} ($f_o = 100$ Hz)	99
Fig.5. 22 Waveforms of the load currents ($f_o = 100$ Hz)	100
Fig.5. 23 Harmonic spectrum of the output phase “a” current ($f_o = 100$ Hz)	100
Fig.5. 24 Reference and observed output line-to-line voltage waveform, V_{ab}	102
Fig.5. 25 Output current and voltage waveforms and the control signals of the semiconductor switches at a commutation instant	103
Fig.5. 26 Single phase output circuit structure	104
Fig.5. 27 Block diagram of the closed-loop system involving the direct matrix converter with RL load	105
Fig.5. 28 Simple block diagram form of closed-loop direct matrix converter control system	105
Fig.5. 29 Output phase “a” to neutral voltage, V_{an} ($f_o = 50$ Hz)	106
Fig.5. 30 Output line-to-line voltage V_{ab} ($f_o = 50$ Hz).....	107
Fig.5. 31 Close-loop output currents ($f_o = 50$ Hz).....	107

Fig.5. 32 Harmonic spectrum of output line-to-line voltage V_{ab} ($f_o = 50$ Hz).....	108
Fig.5. 33 Harmonic spectrum of output phase “a” current ($f_o = 50$ Hz).....	108
Fig.5. 34 Output phase “a” to neutral voltage, V_{an} ($f_o = 100$ Hz).....	109
Fig.5. 35 Output line-to-line voltage V_{ab} ($f_o = 100$ Hz).....	109
Fig.5. 36 Harmonic spectrum of output line-to-line voltage V_{ab} ($f_o = 100$ Hz).....	110
Fig.5. 37 Closed-loop output currents ($f_o = 100$ Hz).....	110
Fig.5. 38 Harmonic spectrum of output phase “a” current ($f_o = 100$ Hz).....	110
Fig.5. 39 Unfiltered and filtered input phase “A” current vs. input phase “A” voltage, V_{AN}	111
Fig.5. 40 Harmonic spectrum of unfiltered input phase current, I_A	112
Fig.5. 41 Harmonic spectrum of filtered input phase current, I_A	112
Fig.5. 42 Output phase “a” to neutral voltage, V_{an} ($f_o = 50$ Hz).....	113
Fig.5. 43 Output line-to-line voltage V_{ab} ($f_o = 50$ Hz).....	114
Fig.5. 44 Harmonic spectrum of output line-to-line voltage V_{ab} ($f_o = 50$ Hz).....	114
Fig.5. 45 Three-phase output currents ($f_o = 50$ Hz).....	114
Fig.5. 46 Harmonic spectrum of output phase “a” current ($f_o = 50$ Hz).....	115
Fig.5. 47 Three-phase input currents ($f_i = 50$ Hz).....	115
Fig.5. 48 Harmonic spectrum of input phase “A” current, I_A	116
Fig.5. 49 Voltage linearity characteristics.....	117
Fig.5. 50 Basic scheme of FOC for permanent magnet synchronous motor.....	120
Fig.5. 51 Simulation model of the stator windings.....	122
Fig.5. 52 One-phase equivalent circuit model of SMPMSM.....	123
Fig.5. 53 Block diagram of closed-loop drive control system.....	124
Fig.5. 54 Dynamic responses of d-axis (i_d) and q-axis (i_q) currents.....	125
Fig.5. 55 Zoomed-in view of i_q reference and i_q	125
Fig.5. 56 Output phase “a” to neutral voltage, V_{an} ($f_o = 5.5$ Hz).....	126
Fig.5. 57 Output line-to-line voltage, V_{ab} ($f_o = 5.5$ Hz).....	126
Fig.5. 58 Closed-loop three-phase output currents ($f_o = 5.5$ Hz).....	127
Fig.5. 59 Developed electromechanical motor torque and three-phase motor currents.....	127
Fig.6. 1 Overall structure of the matrix converter circuit.....	130
Fig.6. 2 One phase filter elements.....	130
Fig.6. 3 Photograph of power circuit board.....	131
Fig.6. 4 Top view of gate-driver board.....	133
Fig.6. 5 Bottom view of gate-driver board.....	133
Fig.6. 6 The photograph of direct matrix converter circuit.....	134
Fig.6. 7 Output phase “a” to neutral voltage, V_{an} ($f_o = 50$ Hz).....	136
Fig.6. 8 Output line-to-line voltage V_{ab} ($f_o = 50$ Hz).....	137

Fig.6. 9 Harmonic spectrum of output line-to-line voltage V_{ab} ($f_o = 50$ Hz).....	137
Fig.6. 10 Three-phase output currents ($f_o = 50$ Hz).....	138
Fig.6. 11 Harmonic spectrum of the output phase “a” current ($f_o = 50$ Hz)	138
Fig.6. 12 Output phase “a” to neutral voltage, V_{an} ($f_o = 100$ Hz).....	139
Fig.6. 13 Output line-to-line voltage V_{ab} ($f_o = 100$ Hz).....	139
Fig.6. 14 Harmonic spectrum of output line-to-line voltage V_{ab} ($f_o = 100$ Hz).....	140
Fig.6. 15 Three-phase output currents ($f_o = 100$ Hz).....	140
Fig.6. 16 Harmonic spectrum of the output phase “a” current ($f_o = 100$ Hz)	141
Fig.6. 17 Dynamic responses of the matrix converter circuit.....	142
Fig.6. 18 Output phase “a” to neutral voltage, V_{an} ($f_o = 50$ Hz).....	143
Fig.6. 19 Output line-to-line voltage V_{ab} ($f_o = 50$ Hz).....	144
Fig.6. 20 Harmonic spectrum of output line-to-line voltage V_{ab} ($f_o = 50$ Hz).....	144
Fig.6. 21 Three-phase output currents at 50 Hz	144
Fig.6. 22 Harmonic spectrum of the output phase “a” current ($f_o = 50$ Hz)	145
Fig.6. 23 Output phase “a” to neutral voltage, V_{an} ($f_o = 100$ Hz).....	146
Fig.6. 24 Output line-to-line voltage V_{ab} ($f_o = 100$ Hz).....	146
Fig.6. 25 Harmonic spectrum of output line-to-line voltage V_{ab} ($f_o = 100$ Hz).....	146
Fig.6. 26 Three-phase output currents ($f_o = 100$ Hz).....	147
Fig.6. 27 Harmonic spectrum of the output phase “a” current ($f_o = 100$ Hz)	147
Fig.6. 28 Input phase “A” to neutral voltage, V_{AN} and unfiltered input current, I_A	148
Fig.6. 29 Harmonic spectrum of the unfiltered input phase “A” current ($f_i = 50$ Hz)	149
Fig.6. 30 Input phase “A” to neutral voltage, V_{AN} and filtered input current, I_A ($f_i = 50$ Hz)	150
Fig.6. 31 Harmonic spectrum of the filtered input phase “A” current ($f_i = 50$ Hz)	150
Fig.6. 32 Three-phase input currents.....	150
Fig.6. 33 Output phase “a” to neutral voltage, V_{an} ($f_o = 5.5$ Hz)	152
Fig.6. 34 Output line-to-line voltage V_{ab} ($f_o = 5.5$ Hz).....	152
Fig.6. 35 Three-phase output currents ($f_o = 5.5$ Hz).....	153
Fig.6. 36 Developed motor torque and converter output currents	153

LIST OF TABLES

TABLES

Table 2. 1 The allowable current directions according to the switch state combinations.....	30
Table 2. 2 All switching combinations for current based commutation	33
Table 4. 1 All possible safe switching configurations.....	63
Table 4. 2 All allowed switching configurations and the corresponding DC-link voltage and input line currents	68
Table 4. 3 All allowable switching configurations for the inversion stage	72
Table 4. 4 Sector pairs and useable vectors.....	79
Table 5. 1 Simulation parameters.....	90
Table 5. 2 Calculated theoretical gain and phase angles for R-L load	101
Table 5. 3 Parameters of the test motor	122

LIST OF ABBREVIATIONS

AC	: Alternating Current
DC	: Direct Current
DMC	: Direct Matrix Converter
FOC	: Field Oriented Control
IGBT	: Insulated Gate Bipolar Transistor
IGCT	: Integrated Gate Commutated Thyristor
IMC	: Indirect Matrix Converter
IPM	: Interior Permanent Magnet
MC	: Matrix Converter
MMF	: Magneto Motive Force
MOSFET	: Metal Oxide Semiconductor Field Effect Transistor
PCB	: Printed Circuit Board
PI	: Proportional Integral
PWM	: Pulse Width Modulation
SPWM	: Sinusoidal Pulse Width Modulation
SMPM	: Surface Mounted Permanent Magnet
SVPWM	: Space Vector Pulse Width Modulation
THD	: Total Harmonic Distortion
VSI	: Voltage Source Inverter

NOMENCLATURE

V_A, V_B, V_C	: Three-Phase Input Voltages
$\mathcal{V}_A(t), \mathcal{V}_B(t), \mathcal{V}_C(t)$: Instantaneous Input Phase Voltages
V_{AB}, V_{BC}, V_{CA}	: Line-to-Line Input Voltages
$\mathcal{V}_{AB}(t), \mathcal{V}_{BC}(t), \mathcal{V}_{CA}(t)$: Instantaneous Line-to-Line Input Voltages
V_i	: Peak Value of Input Line-to-Line Voltages
I_i	: Peak Value of Three-Phase Input Currents
ω_i	: Input Angular Frequency
φ_i	: Angle between Input Phase Voltages and Currents
i_A, i_B, i_C	: Three-Phase Input Currents
$i_A(t), i_B(t), i_C(t)$: Instantaneous Input Line Currents
V_a, V_b, V_c	: Three-Phase Output Voltages
$\mathcal{V}_a(t), \mathcal{V}_b(t), \mathcal{V}_c(t)$: Instantaneous Output Phase Voltages
V_{ab}, V_{bc}, V_{ca}	: Line-to-Line Output Voltages
i_a, i_b, i_c	: Three-Phase Output Currents
$i_a(t), i_b(t), i_c(t)$: Instantaneous Output Phase Currents
V_o	: Peak Value of Output Phase Voltages
I_o	: Peak Value of Output Phase Currents
ω_o	: Output Angular Frequency
φ_o	: Angle between Output Phase Voltages and Currents
V_{DC}	: Mean Value of DC-link Voltage
I_{DC}	: Mean Value of DC-link Current
C_p	: Clamp Capacitor
R_p	: Clamp Resistor
C_{AB}, C_{BC}, C_{AC}	: Input Filter Capacitors
L_A, L_B, L_C	: Input Filter Inductors
R_A, R_B, R_C	: Input Filter Resistors
R_f	: Input Filter Resistance
L_f	: Input Filter Inductance
C_f	: Input Filter Capacitance
S	: Switch State

P_{out}	: Output Power
P_{in}	: Input Power
P_{cu}	: Total Copper Loss
p_{out}	: Instantaneous Value of Output Power
p_{in}	: Instantaneous Value of Input Power
E_a	: Rms Value of Back-emf Voltage
ω_e	: Electrical Rotor Speed
ω_r	: Angular Velocity of Motor
p	: Pole Number
λ_f	: Permanent Magnet Flux Linkage
λ_q	: Quadrature Axis Stator Flux Linkage
λ_d	: Direct Axis Stator Flux Linkage
λ_m	: Magnet Flux Linkage
L_a, L_b, L_c	: Self Inductances of Stator Windings
R_a, R_b, R_c	: Stator Winding Resistances
$L_{ab}, L_{ba}, L_{ca}, L_{ac}, L_{bc}, L_{cb}, M$: Mutual Inductances
R_s	: Per-Phase Equivalent Stator Winding Resistance
L_s	: Per-Phase Equivalent Stator Winding Inductance
e_a, e_b, e_c	: Phase Back-emf Voltages
L_d	: Direct Axis Inductance
L_q	: Quadrature Axis Inductance
v_q	: Quadrature Axis Voltage
v_d	: Direct Axis Voltage
i_q	: Rotating Quadrature Axis Stator Current
i_d	: Rotating Direct Axis Stator Current
ϕ	: Angle between Induced Back-emf and Stator Current
θ	: Angle between Stator Phase Voltage and Current
$M(t)$: Modulation Matrix
q	: Input to Output Voltage Transfer Ratio
x_a, x_b, x_c	: Three Variables of Balanced Three-Phase System
\vec{V}_i	: Input Phase Voltage Vector
\vec{V}_o	: Output Phase Voltage Vector

\bar{I}_i	: Input Line Current Vector
\bar{I}_o	: Output Phase Current Vector
α_i	: Angle of Input Voltage Vector
α_o	: Angle of Output Voltage Vector
β_i	: Angle of Input Current Vector
β_o	: Angle of Output Current Vector
d_x, d_y	: Duty Ratios of Input Current Vectors
d_α, d_β	: Duty Ratios of Output Voltage Vectors
d_{c0}	: Duty Ratio of Zero Current Vectors
d_{v0}	: Duty Ratio of Zero Voltage Vectors
T_x, T_y	: Applied Time Durations of Active Current Vectors
T_{c0}	: Applied Time Duration of Zero Current Vectors
T_α, T_β	: Applied Time Durations of Active Voltage Vectors
T_{v0}	: Applied Time Duration of Zero Voltage Vectors
d_0	: Duty Ratio of Zero Vectors
R_L	: Per-Phase Load Resistor
L_L	: Per-Phase Load Inductor
f_s	: Switching Frequency
f_o	: Output Frequency
f_i	: Input Supply Frequency
T_s	: Switching Period
K_p	: Proportional Gain
K_i	: Integrator Gain
pu	: Per-Unit
N	: Neutral Point of Input Supply
n	: Neutral Point of Output
$G_{I_o V_o}$: Output Voltage to Output Current Transfer Function
$G_{I_o I_o^*}$: Output Current Reference to Output Current Transfer Function
m_c	: Current Modulation Index
m_v	: Voltage Modulation Index
T_{DMC}	: Transfer Function of Direct Matrix Converter

T_{VSI}	: Transfer Function of Two-level Voltage Source Inverter
T_{VSR}	: Transfer Function of Voltage Source Rectifier
ω_0	: Filter Cut-off Frequency
$v_o(t)$: Instantaneous Output Voltage
$i_o(t)$: Instantaneous Output Current

CHAPTER 1

INTRODUCTION

Electrical energy is widely utilized from low to high power areas in numerous modern industrial and domestic applications in the world. However, in many applications, the AC mains power cannot be directly utilized. For example, in variable speed drives, in order to run AC motors at different speeds; it is necessary to have a variable frequency and amplitude AC power supply. Also in order to run DC motor at different speeds; AC/DC power conversion is necessary. Hence, many parts of industrial application require power conversions. In the past, DC motors had been widely preferred since the torque of a DC motor can be easily controlled. Today, DC motors are replaced by AC motors because of the maintenance problems of DC motors due to the presence of commutators and brushes. As a result, AC motor drives have gained substantial attention. In order to effectively control the AC motors, many special devices that maintain the AC/AC power conversion process, have been designed and produced.

1.1 AC/AC POWER CONVERSION

The variable AC electrical power should be achieved through AC/AC power conversion from utility AC power with fixed amplitude and frequency. AC/AC converters take power from an AC system and deliver it to another with waveforms of adjustable amplitudes and frequencies.

Nowadays, various power converter circuits are used which improve the performance, efficiency and reliability of the systems they take place. Fig.1. 1 displays a classification of converter families used in electrical drive applications. The AC/AC converters are classified into two groups such as; indirect (DC-link) converters which include DC-link

components between the two AC systems and direct converters that provide direct AC/AC power conversion.

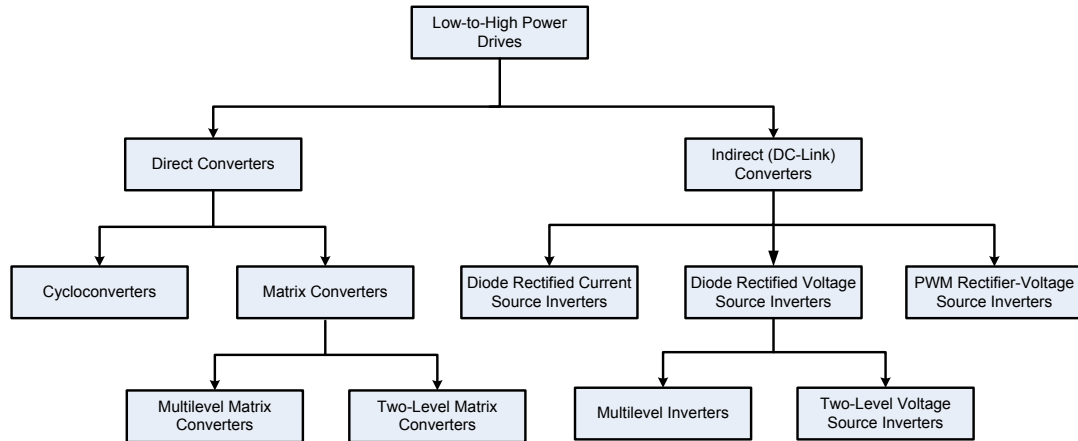


Fig.1. 1 Classifications of converters low-to-high power drives

In all indirect power converter circuits, diode-rectified two-level voltage source inverters (VSI) are totally widespread nowadays. VSI is a DC/AC converter that generates AC output voltages from a DC input voltage. Three-phase two-level VSI shown in Fig.1. 2, is one of the most widely used inverter topology for three-phase applications.

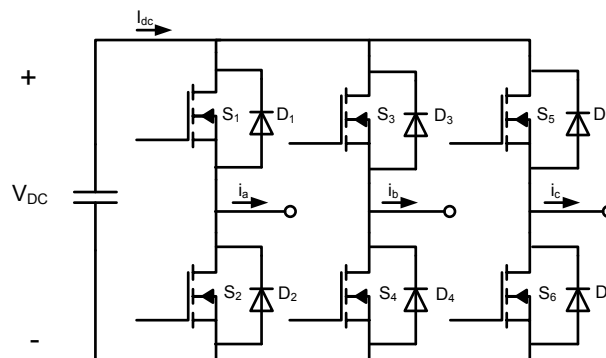


Fig.1. 2 Three-phase two-level voltage source inverter circuit topology

In direct AC/AC converters, the cycloconverter is the most commonly employed topology in three-phase to three-phase applications, which uses semiconductor switches to connect directly the power supply to the load, converting a three-phase AC voltage to a three-phase AC voltage with adjustable magnitude and variable frequency. It allows power flow in either direction. The operating output frequency of this direct converter should be less than

the input frequency. In addition to the cycloconverters, matrix converters have enjoyed increasing interest as direct converters in recent years. This interest is reflected in the number of articles and papers written about matrix converters in the last ten years.

1.1.1 Overview of Indirect (DC-link) Two-Level Voltage Source Converters

As mentioned earlier, two-level voltage source inverter is a DC/AC converter. However, DC voltage is not common voltage. To generate DC voltage, rectifier structures are commonly used. A rectifier is a device that converts alternating voltage to direct voltage. This process is also called as rectification. The most commonly used rectifier structure is three-phase diode rectifier shown in Fig.1. 3. The circuit also contains a DC-link capacitor to ensure ripple free DC-link voltage.

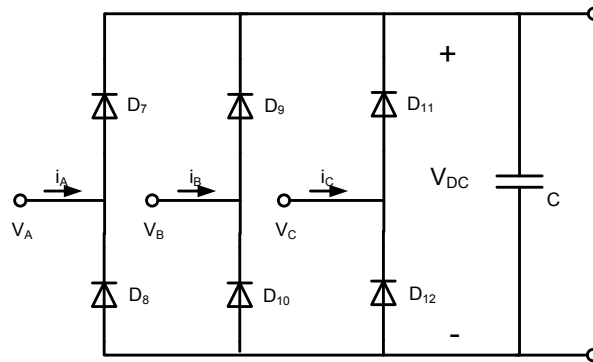


Fig.1. 3 Diode rectifier stage

Most of the converters use diode-rectifiers (followed by a DC-link capacitor), which draw non-sinusoidal currents (i_A , i_B , i_C) even when fed with a balanced sinusoidal voltages (V_A, V_B, V_C). Only considering the load side currents (i_a , i_b , i_c), the diode rectifier based VSI may be is a good solution, but its supply side currents (i_A , i_B , i_C) are highly distorted, containing high amounts of low order harmonics which may further interfere with the other electric systems in the network. In addition, the current flow on diodes cannot be reversed. Thus, bi-directional power flow cannot be provided without using an auxiliary circuit. This is another drawback of this topology. Fig.1. 4 represents the diode rectifier based VSI structure.

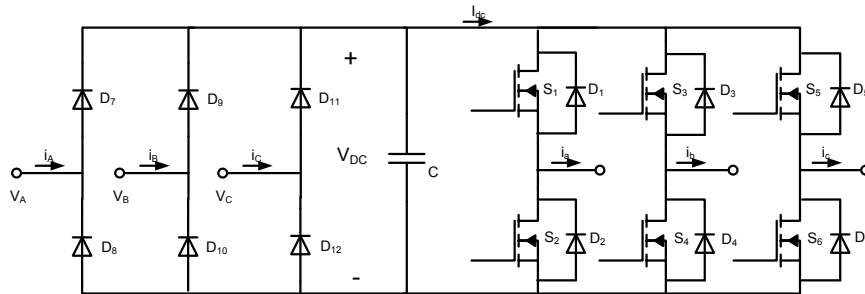


Fig.1. 4 Diode rectifier based VSI

A conventional solution for the harmonics in input current waveforms and bi-directional power flow problems is to use a controlled bridge rectifier instead of diode rectifier as shown in Fig.1. 5. This structure is called back-to-back voltage source converter (BBVSC). The BBVSC was introduced in the late 1970s. The BBVSC draws sinusoidal current waveforms (i_A , i_B , i_C) from the AC supply. It contains a DC-link capacitor between controlled bridge rectifier and the inverter bridge and supply filter inductors.

The DC-link capacitor is a bulky component with a limited lifetime. Moreover, supply filter inductors (L_s) placed at the input terminals of the controlled bridge rectifier are also bulkier and heavier than the DC-link capacitor in low and medium power conversion. Therefore, this conventional indirect converter has also big volume.

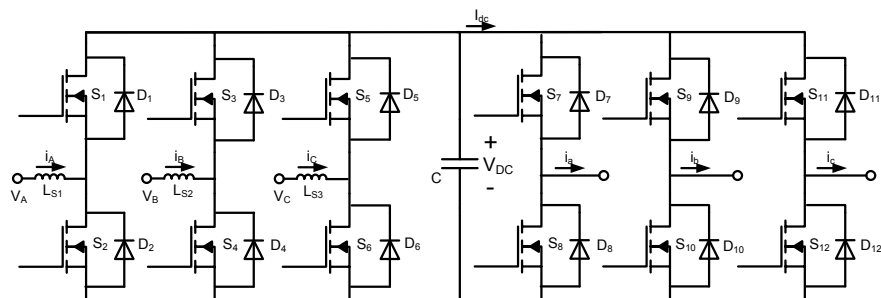


Fig.1. 5 Back to back voltage source converter

1.1.2 History of Direct AC/AC Converters

The idea of direct frequency conversion was originally presented in the 1920s ^[1]. In general, direct AC/AC converters can be classified in two distinct groups. Converters in the first group are those which can be used if the operating output frequencies are lower than the input supply frequency. This converter was called cycloconverter. It converts AC voltage waveforms, such as that of the main supply, to other AC voltage waveforms with lower frequency. After the invention of thyristor, the first semiconductor based cycloconverter were developed in the 1960s ^[2]. A possible typical phase-controlled thyristor-based three-phase to three-phase cycloconverter is displayed in Fig.1. 6.

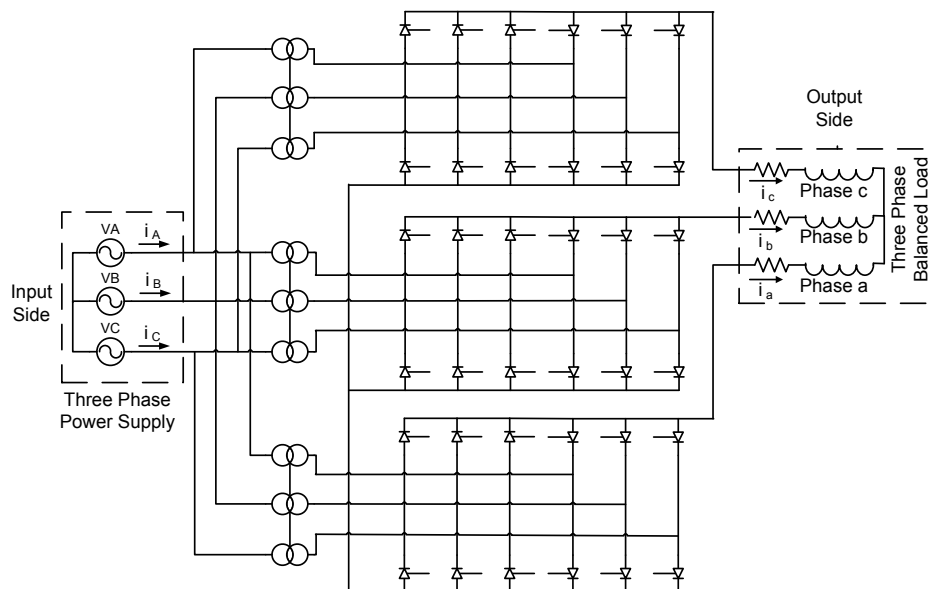


Fig.1. 6 Phase-controlled thyristor-based three-phase to three-phase cycloconverter

They are commonly employed in three-phase applications. In most power systems, the amplitude and the frequency of input voltage applied to a cycloconverter have fixed magnitudes, whereas both the amplitude and the frequency of output waveforms of a cycloconverter tend to be variable. The load voltage and input current waveforms in the cycloconverter are heavily distorted and power factor of the input is quite poor. However, the quality of the output waveforms can be enhanced if more switching devices are employed ^[2]. Moreover, its output frequency is also usually limited to half frequency of the

input supply. Because, normal loads cannot tolerate the voltage distortion produced with higher input to output frequency ratios. Thus, the only advantages remaining are robustness of the thyristor and low losses.

Considering all mentioned above, the cycloconverter cannot be seen as an optimal solution for low and medium power level converters because of restricted output frequencies and poor harmonic performance. However, for the high power levels, cycloconverter can be seen as an optimal solution due to the low losses and robustness.

The second class of direct converters is the matrix converter (MC). It is much versatile without imposing any limits on the operating output frequencies. A matrix converter performs direct AC/AC power conversion process from AC utility to AC load, with neither intermediate DC conversion nor DC energy storage elements. Thus, it replaces the multiple conversion stages by a single power conversion stage. By the way, the converter size and volume can be greatly reduced compared to the indirect AC/AC power converters which have DC-link components. Thus, direct converter topologies may provide a solution for application where large passive components are not allowed. A basic circuit of the MC is shown in Fig.1. 7.

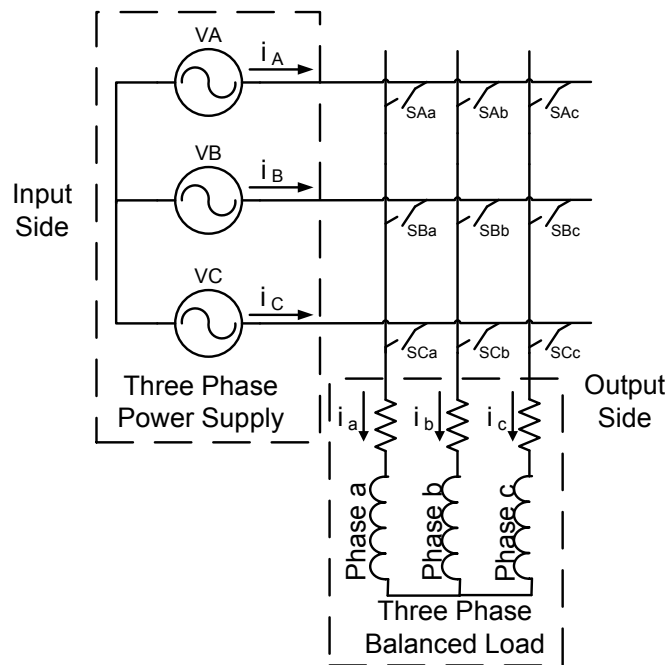


Fig.1. 7 Basic direct matrix converter circuit

1.1.3 Concept of Matrix Converter

MC is basically a switch-mode direct AC/AC power conversion device without requiring the use of a bulky storage electrolytic capacitor. They are gaining considerable attention as an alternative to the classical structures such as back-to-back voltage source converters and diode-rectified two-level voltage source inverters, due to the system level advantages such as; the possibility to increase the power density of the power conversion system; inherent four-quadrant operation capability; allowing bi-directional power flow; producing sinusoidal input and output current waveforms (low harmonic contents in the input currents); controllability of the input power factor; and increasing the reliability and compact design ^[3].

The matrix converter topology consists of controlled bi-directional switches which directly connect the load to the source. Hence, in this converter input and output sides are directly linked. The output voltage and current waveforms with adjustable magnitude and frequency are constructed by single-stage power conversion process. The single stage power conversion principle has given distinct structure to the matrix converter. This aspect makes the modulation control of the matrix converter quite different and complicated. However, the matrix converter topology can be implemented with much compact in size and volume compared with the diode-rectifier based two-level VSI and back-to-back voltage source converter. In addition to its compact design, it draws sinusoidal input currents with unity power factor as well as sinusoidal output currents and the matrix converter can operate at high temperature surroundings due to the lacking of DC-link capacitors, which is very vulnerable in high temperature. Therefore, the converter also has longer lifetime. Considering these advantages, the matrix converters have become increasingly attractive for AC/AC power conversion.

In practice, an input filter is also necessary to attenuate the input currents harmonics. This can be interpreted as a realistic advantage if the filter size is also optimized, by employing the semiconductor devices with sufficiently high switching frequency. This means that a consensus between the size of input filter and the semiconductor losses must be found. Considering all factors mentioned above which are fundamental for good power supply and electric drive applications. The main feature of this converter is to allow these fundamentals for power supply and electric drive applications.

The matrix converters were first mentioned in the early 1980's by Alesina and Venturini ^[4]. They developed a rigorous mathematical description of matrix converter and presented the concept of the duty-cycle modulation matrix. This pulse width modulation method is known as the Venturini Modulation method. Unfortunately, this method had a serious drawback. The initial Venturini Modulation was limited to a maximum 50% input to output voltage transfer ratio. They later proposed an improved method to increase this limit, thus third harmonics were successfully included in the output voltage waveforms. The maximum input voltage to output voltage transfer ratio became 86.6%.

A different waveform synthesis approach was proposed by P. Ziogas et al. in ^[2]. They split the matrix converter into a fictitious rectifier and a fictitious inverter and instead of using the matrix converter to assemble its output voltage directly from three-phase AC input voltage; the input voltage was first rectified to create an imaginary DC-link voltage and later inverted at the required output frequency. This technique was referred as the indirect function approach and it allowed the use of well-known techniques for controlling the fictitious rectifier and inverter.

Space vector pulse width modulation technique was first employed by Huber et al. in 1989 ^[5] which has been well established to obtain satisfactory input/output performance to control a matrix converter. The modulation technique which employed space vectors in both the rectifier and inverter process allows obtaining the maximum output to input voltage ratio (0.86), sinusoidal input current and control of the input displacement factor.

1.2 SCOPE OF THESIS AND STRUCTURE OF CHAPTERS

This study focuses on closed-loop field oriented control of a surface mounted permanent magnet synchronous motor using space vector modulated direct AC-AC matrix converter. In this thesis, the first objective is to analyze the matrix converter topologies. The second objective is to investigate the modulation methods and implement the most suitable one. The other objective is to develop a matrix converter simulation model to demonstrate the feasibility of developed algorithm. And the last objective is to design and produce a matrix converter circuit and verify the converter operation.

This thesis is categorized in seven chapters in the following style.

Chapter 1 gives the basic information about AC/AC power converters, their advantages and disadvantages.

Chapter 2 presents the structure of matrix converter integrated permanent magnet drive system, fundamentals of matrix converter topologies, input-output characteristics and structures of matrix converters.

Chapter 3 focuses on the steady-state and dynamic modeling of permanent magnet synchronous machines.

Chapter 4 gives the state-space equations of matrix converter terminal voltages and currents. Then, matrix converter modulation methods are presented and space vector definition is introduced. Finally, space vector modulation methods for matrix converter are investigated in detail.

Chapter 5 demonstrates the modeling of the matrix converter system. Then, the open-loop and closed-loop performances of direct matrix converter are investigated by the simulations. The comparison of the direct matrix converter and the diode-rectified two-level voltage source inverter is studied in simulations. Finally, the operational analysis of matrix converter integrated surface mounted permanent magnet synchronous machine drive system is presented.

Chapter 6 presents the conducted tests on matrix converter circuit using a passive R-L load and a surface mounted permanent magnet synchronous machine. The operation of the direct matrix converter system is examined based on the experimental results. During the tests, the line-to-line supply voltage is set to 26 V peak value and a 400 V/3.5 kW surface mounted permanent magnet motor is used.

Chapter 7 summarizes the overall study conducted in the thesis and concludes the performance of the indirect space vector modulated direct AC/AC matrix converter.

CHAPTER 2

THE PERMANENT MAGNET SYNCHRONOUS MACHINE (PMSM) DRIVE SYSTEM USING DIRECT MATRIX CONVERTER

In this chapter, the structure of permanent magnet synchronous machine (PMSM) drive system with matrix converter is presented first. After that, fundamentals of matrix converter topology are introduced. That is followed by a presentation of input-output characteristics of matrix converter. At the end of this chapter, structural issues of matrix converter are investigated.

2.1 STRUCTURE OF PERMANENT MAGNET MACHINE DRIVE SYSTEM

A permanent magnet synchronous machine, a power converter (i.e. only power stage) and a controller (PWM is considered in controller) are the three major components of an electrical drive system. The structure of a permanent magnet synchronous machine drive is given in Fig.2. 1 in block diagrams. Parts of the block diagrams are also discussed in this chapter.

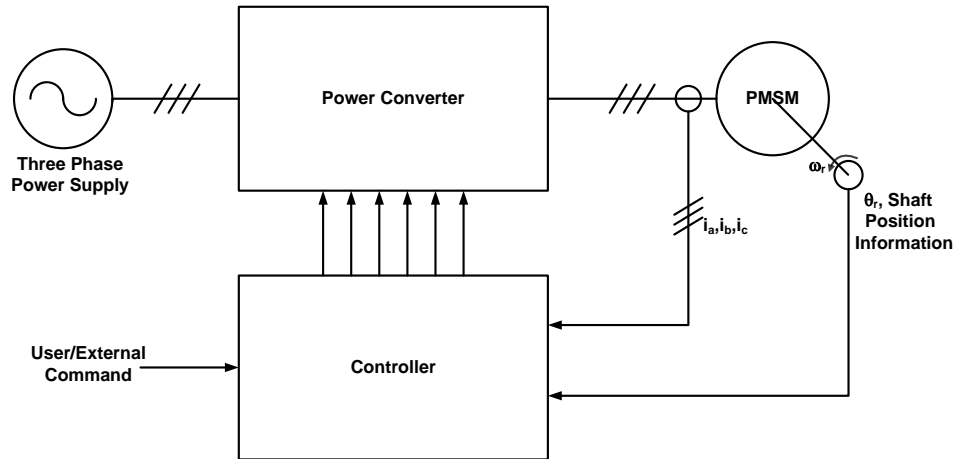


Fig.2. 1 PMSM drive basic architecture

The power converter typically involves a rectifier, DC-link capacitors, an inverter, gate drivers for the power transistors placed in the inverter and current transducers.

The controller involves a microcontroller or a digital signal processor (DSP) and peripheral interface circuits to gather the sensor data (e.g. data from current transducers and position sensor).

In general, diode-rectified three-phase two-level PWM voltage source inverters drive the permanent magnet synchronous machines. Besides that, matrix converters can also be used, especially in high power density applications where the large electrolytic capacitors are inappropriate. The block diagram of the permanent magnet synchronous machine drive system with vector controlled matrix converter is presented in Fig.2. 2.

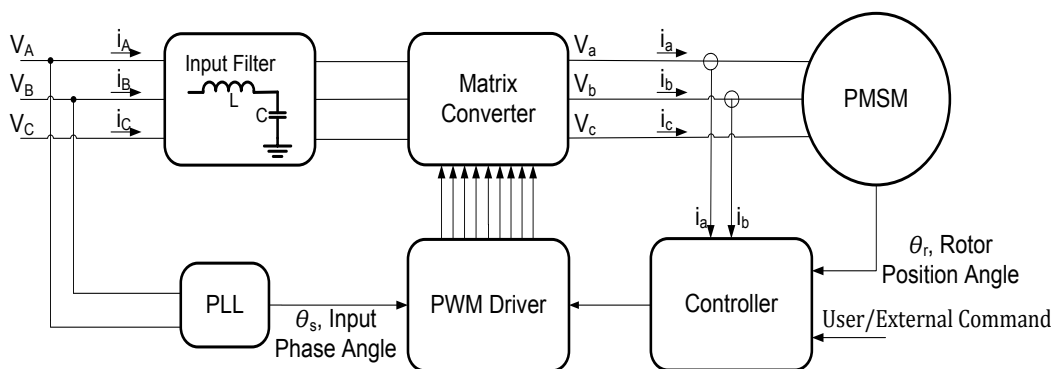


Fig.2. 2 Block diagram of PMSM drive system

2.2 FUNDAMENTALS OF MATRIX CONVERTER

The matrix converter is an alternative to the conventional AC-DC-to-DC-AC converter. It has several advantages over them such as ^[61];

- Matrix converter provides sinusoidal input current and output waveforms,
- Matrix converter allows inherently bidirectional power flow,
- Matrix converter allows inherently four-quadrant operation,
- Matrix converter has compact design (e.g. small size) due to the absence of large energy storing elements,
- Matrix converter has the possibility to increase the power density of the power conversion system,
- Matrix converter has the capability of fully controlled input power factor.

The matrix converter has also disadvantages such as;

- The input voltage to output voltage transfer ratio is 0.86,
- Matrix converter is sensitive to the disturbances on the AC mains.

2.3 INPUT-OUTPUT CHARACTERISTICS OF MATRIX CONVERTER

This section presents a brief description of main characteristics of matrix converter.

2.3.1 Output Voltages and Currents

The matrix converter connects input lines to all three output lines for any desired time duration. It does not need presence of any large energy storage elements between the input and output sides as shown in Fig.2. 3.

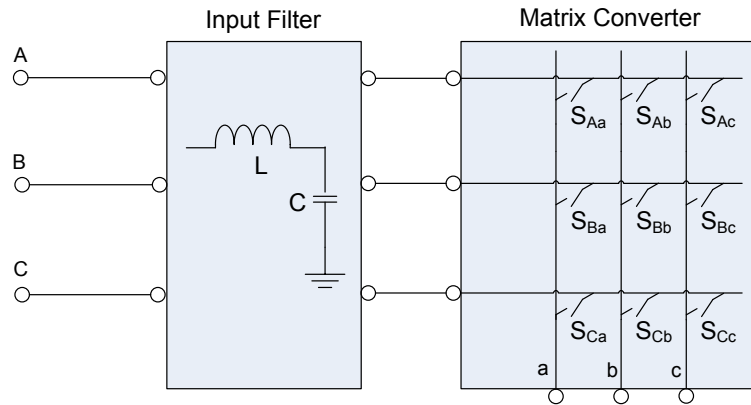


Fig.2. 3 Structure of matrix converter system

AC output voltage waveforms are synthesized directly from the AC input voltage waveforms. Thus, the sampling and switching rate has to be set much higher than both of the input and output frequencies. In Fig.2. 4, the line-to-line output voltage waveform for a 10 kHz switching frequency is shown [6]. The red colored waveform is the fundamental component of the output line-to-line voltage.

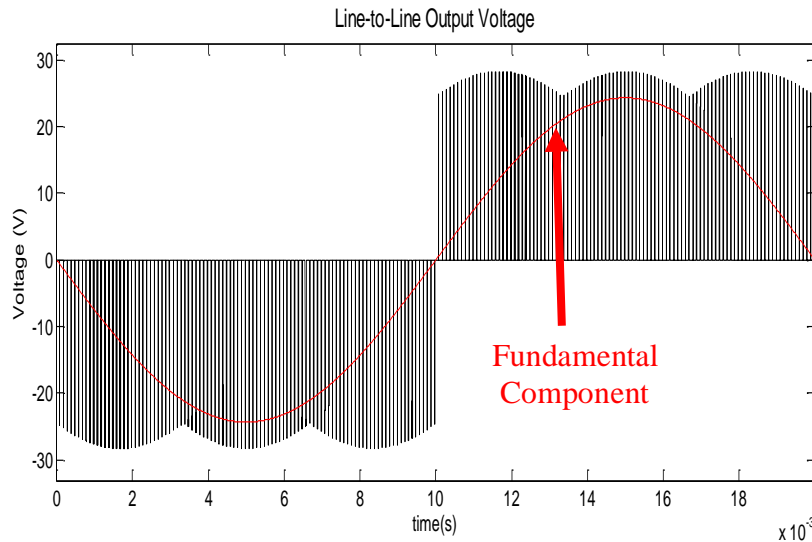


Fig.2. 4 Line-to-line output voltage waveform generated by direct matrix converter

Due to the inductive nature of the permanent magnet synchronous motor, smooth output currents are observed, as shown in Fig.2. 5.

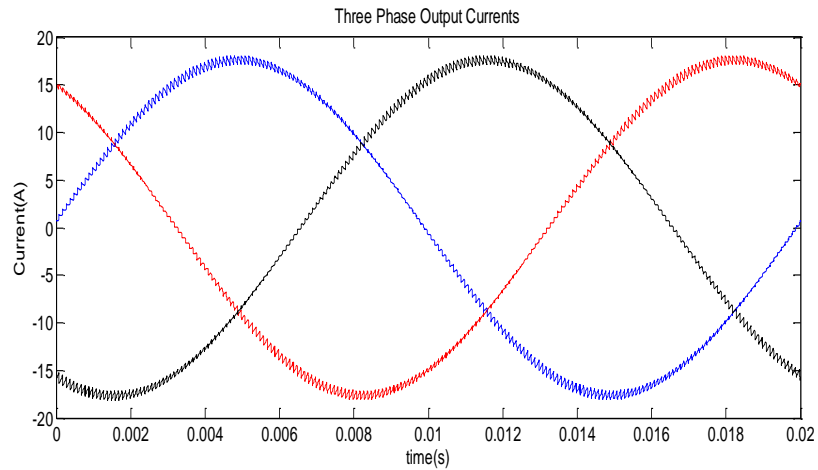


Fig.2. 5 Three-phase output currents of a direct matrix converter

2.3.2 Input Voltages and Currents

The input of a matrix converter needs to be a balanced three-phase voltage waveforms as shown in Fig.2. 6.

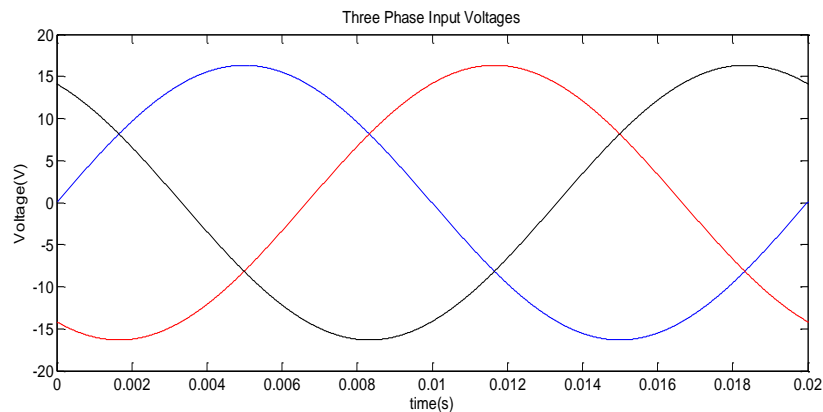


Fig.2. 6 Three-phase input voltages of direct matrix converter

Likewise to the output voltage waveforms of matrix converter, the input currents are directly synthesized from the balanced and sinusoidal output current waveforms. In Fig.2. 7, one phase discontinuous input current of a matrix converter for a 10 kHz switching frequency (f_s) and in Fig.2. 8, its harmonic spectrum is presented. As seen in Fig.2. 7, the discontinuous input currents drawn by the matrix converter may cause the considerable harmonic currents injected to back into the AC mains. Referring Fig.2. 8, the magnitudes of switching harmonic components are comparable with the fundamental component. So,

these considerable harmonic currents flowing through line impedances distort the line voltage and create power quality problems for the other consumers. Thus, these harmonics have to be reduced at least.

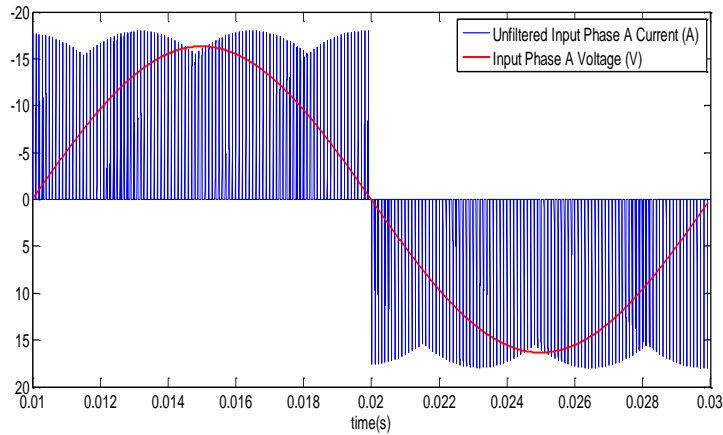


Fig.2. 7 Unfiltered input phase “A” current

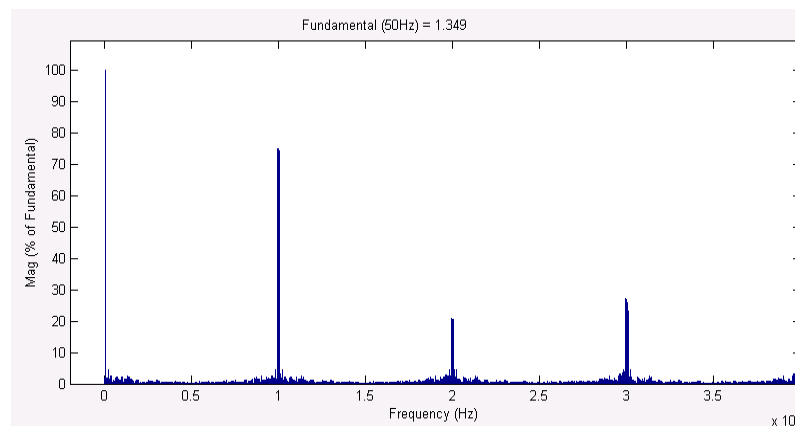


Fig.2. 8 Harmonic spectrum of unfiltered input phase A current ($f_s = 10 \text{ kHz}$)

Reduction of harmonics generated by static converters simply requires filtering which uses storage elements [7]. The drive system also involves a small three-phase input filter. It prevents unwanted harmonic currents flowing in to the AC mains. As a result, the input currents drawn from three-phase AC supply are smoothed out by the input filter. The smoothed current waveform and harmonic spectrum are presented in Fig.2. 9 and Fig.2. 10. Fig.2. 10 shows that the considerable high order frequency harmonics were suppressed.

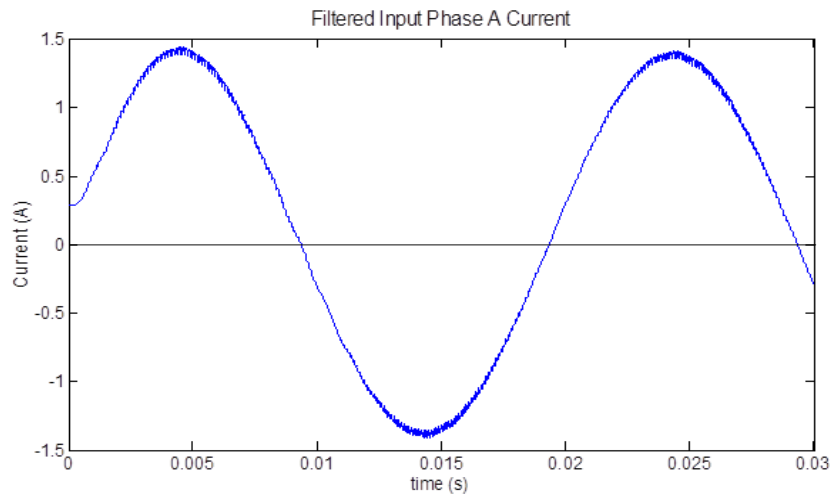


Fig.2. 9 Filtered input phase A current

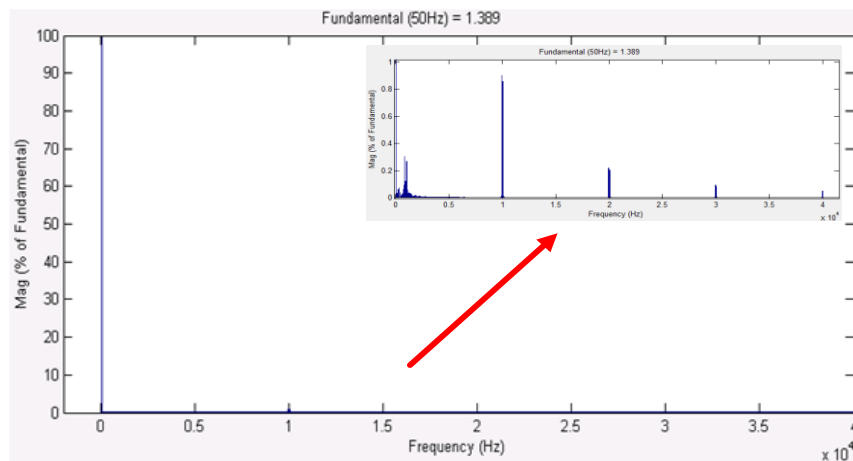


Fig.2. 10 Harmonic spectrum of filtered input phase A current ($f_s = 10$ kHz)

2.4 STRUCTURAL ISSUES OF MATRIX CONVERTER

This section is concerned with structural issues of the matrix converter. Firstly, direct (single-stage) and indirect (two-stage) matrix converter topologies are presented. The matrix converter involves bi-directional switches, which are frequently named as bilateral switch, AC switch or four-quadrant switch. The switches must be able to block voltages of either polarity and be able to conduct current in either direction. Such switches are not available in practice and should be constructed with a combination of the available

semiconductor switches and diodes [8, 9]. Possible bi-directional switch structures and practical problems related to the implementation of them are presented here.

The section discusses also commutation problems happen in the converter. In order to ensure the commutation even under abnormal conditions (e.g. load failure, input voltage failure, emergency stop), some protective techniques are also introduced. Finally, commutation strategies which are applicable for the matrix converter will be introduced as well.

2.4.1 Direct Matrix Converter

Direct (single-stage) matrix converters have single power conversion stage so that they accomplish AC to AC power conversion directly. There are not any intermediate power conversion stages such as rectification (AC to DC conversion) and inversion (DC to AC conversion). Fig.2. 11 shows a three-phase to three-phase direct matrix converter (DMC).

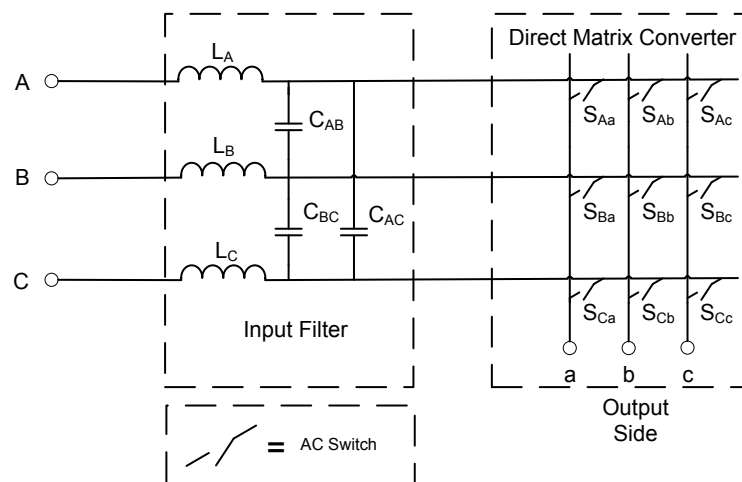


Fig.2. 11 Structure of direct matrix converter

This structure consists of nine bi-directional switches and involves a small three-phase input filter. The input filter is used to prevent unwanted harmonic currents which flow into AC mains. In a three-phase to three-phase direct matrix converter each of the input phases A, B, C are directly connected to corresponding output phase a, b, c. Besides this, the converter shown in Fig.2. 11 is not the only possible direct (single-stage) matrix converter topology. In general, the direct matrix converter is an array of $m \times n$ bi-directional power

switches to connect directly m-phases of the voltage source to n-phases of a load ^[10]. Several studies have been conducted on single-to-single phase and single-to-two phase matrix converters ^[11-13]. In the case of direct matrix converters with more than three output phases, a three-phase to four-phase matrix converter proposed ^[14] and applied as well ^[15]. The neutral line here is understood as the fourth output phase. Fig.2. 12 shows such a three-phase to four-phase matrix converter.

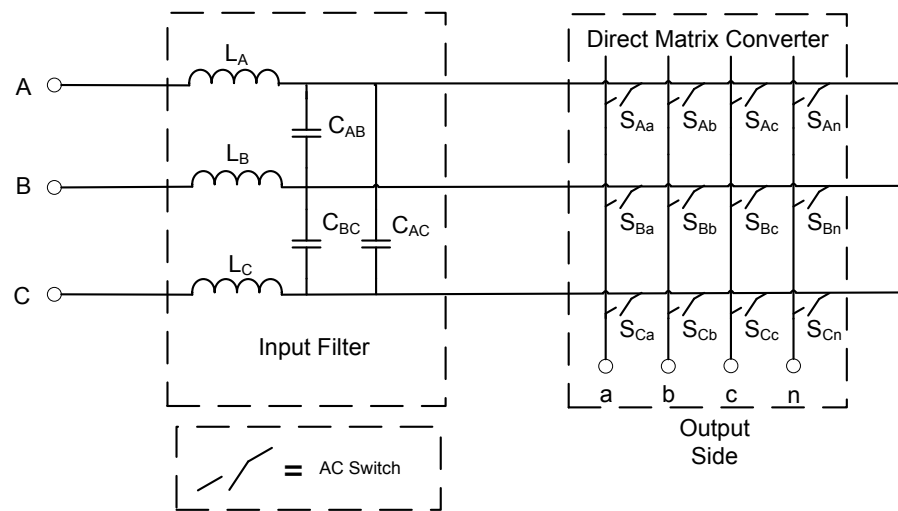


Fig.2. 12 Structure of three-phase to four-phase direct matrix converter

A three-phase to three-phase direct matrix converter has higher practical value because it connects a three-phase voltage supply to a three-phase load, typically a motor.

2.4.2 Indirect Matrix Converter

An indirect (two-stage) matrix converter is made of two back-to-back converters without a DC-link capacitor in between as shown in Fig.2. 13. One of them is a rectifier and other is the inverter stage.

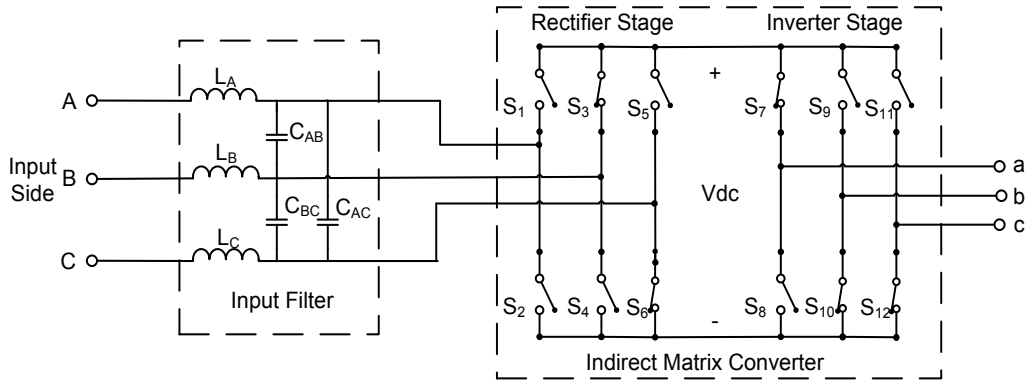


Fig.2. 13 Indirect three-phase to three-phase matrix converter

In indirect (two-stage) matrix converters instantaneous direct connection of three input lines to the three output phases is not possible. Indirect matrix converter has limitations on possible connection states. Due to the rectification stage, only two different input phase lines can be connected to the output phases at most. Hence the flexibility of direct matrix converter is not possible for the indirect (two-stage) matrix converters yet the performance is nearly same in practice. It can be seen in Fig.2. 14 that the input phase “B” is connected to the output phase “a”, the input phase “C” is connected to both output phase “b” and “c” in both matrix converter topologies.

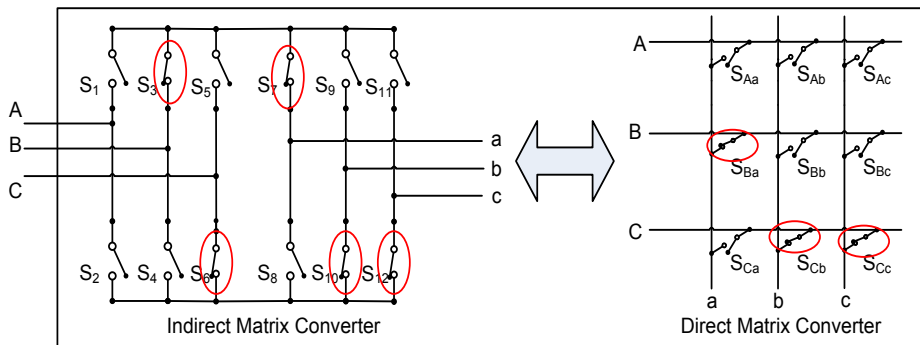


Fig.2. 14 An equivalent switching combination of direct and indirect matrix converter

The indirect matrix converter has gained remarkable attention as it provides a good alternative to back-to-back converters (e.g. voltage source rectifier – voltage source inverter) having advantage of inherent bi-directional power flow, sinusoidal input current

waveforms with minimum harmonics and sinusoidal output waveforms, the possibility of compact design due to the lack of DC-link reactive components and controllable input power factor independent from the output current phase angle ^[16].

2.4.3 Bi-directional Switches

A bi-directional switch is used to conduct currents and block voltages in both polarities, the energy can flow from source to the load and from load to the source depending on control signal. However, commercially a proper switch is still not available on the market. For this reason, an alternative AC switch is realized by a combination of conventional unidirectional devices. That is other fully controllable semiconductor switches and diodes can be used to construct AC switches. In general, AC switch topologies can be classified into two groups; diode bridge topology and switching devices with anti-parallel diode topologies ^[8, 9]. We can see the advantages and disadvantages of these structures at below.

2.4.3.1 Diode Bridge Switch

Fig.2. 15 shows the bi-directional diode bridge switch configuration proposed in the literature with a semiconductor switching device. The switching device could be a MOSFET, an IGBT or an IGCT. But also, other switching devices may be used.

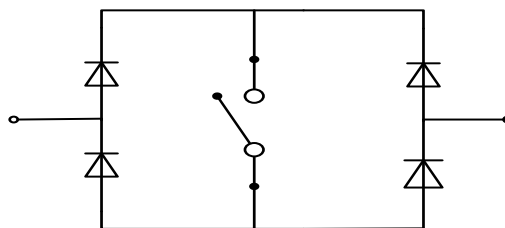


Fig.2. 15 Diode bridge structure

The main advantages of this structure are that it consists of only one active device. As a result of that, the cost of the power circuit, the complexity of control and the complexity of gate drive circuit are reduced. Besides that, there are three semiconductor devices in each conduction path causing increased conduction losses. Moreover, the current direction cannot be controlled by this structure ^[17].

2.4.3.2 Switches with Anti-Parallel Diode

There are different configurations for AC switches with anti-parallel diode proposed in the literature. In this group, each combinational switch (bi-directional) consists of two semiconductor switches and two anti-parallel diodes. The switching devices could be MOSFETs, IGBTs or IGCTs. But also, other switching devices may be used. In this study, MOSFETs and their free-wheeling diodes were used for implementing the hardware. Hence, in the next expressions, MOSFETs are preferred to create relevant knowledge with the hardware realization.

2.4.3.2.1 Common Source Configurations

This switch structure consists of two diodes and two MOSFETs connected in anti-parallel as shown in Fig.2. 16. Since the reverse blocking capability is relatively weak of MOSFET technology, diodes are placed in a series with the MOSFET switches to provide better reverse blocking capability. Hence, one MOSFET and one diode anti-parallel structure can be connected as series to provide the required diode and MOSFET serial connection form. According to the diode bridge topologies, common source AC switch structure has a few advantages. The first advantage of this structure is that only two semiconductor devices carry the current, so conduction losses are reduced. And also, the current can be controlled in both directions independently from current direction ^[17, 18].

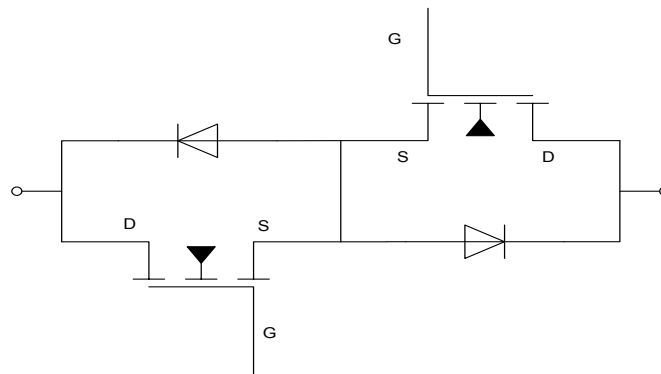


Fig.2. 16 Common source AC switch configuration

2.4.3.2.2 Common Drain Configurations

This structure is nearly similar to the structure which is presented in the previous configuration. The difference exists into the common connection point of anti-parallel diode-MOSFET structures. In this configuration, common connection point is selected as MOSFETs' drain terminals. As in the common source structure, to increase the reverse blocking capability, diodes should be placed in series with the switches. A MOSFET - diode anti-parallel structure connected in series with another such pair may be a suitable solution for increasing the voltage blocking capability as shown in Fig.2. 17. The conduction losses are same as the previous configuration. One possible advantage of the common drain configuration proposed in the literature could be that the need for the use of isolated power supplies could be reduced although it is not possible in general. The stray inductances between the switches must be same and low if this advantage is to be achieved in practice. However, at high power levels stray inductances between the switches become more effective, and the complexity of the control process increases. For that reason, common mode source structure is preferred for higher power levels ^[17, 18].

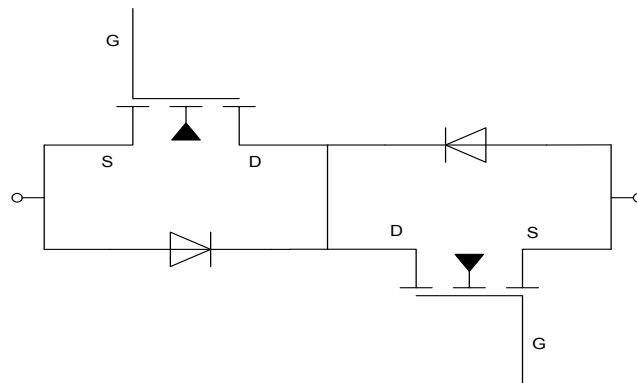


Fig.2. 17 Common drain AC switch configuration

2.4.3.2.3 Series Diode-MOSFET Structure with Anti-Parallel Form

These structures can be realized from both of the Common Drain and Common Source structures when the common connection is left unconnected. The structure is presented in Fig.2. 18. As in the common source and drain structures, two semiconductor devices, an active switch and a diode, carry the current. Hence, the conduction losses are also same as the common drain and common source structures. However, in the case of common source

connection left unconnected eighteen isolated supplies are required for the gate drive control, whereas the common drain structure requires six isolated supplies and common source structure requires nine isolated supplies for the gate drives of switches. For that reason, series diode-MOSFET connected anti-parallel form is not commonly used as the common drain and source structures ^[17, 18].

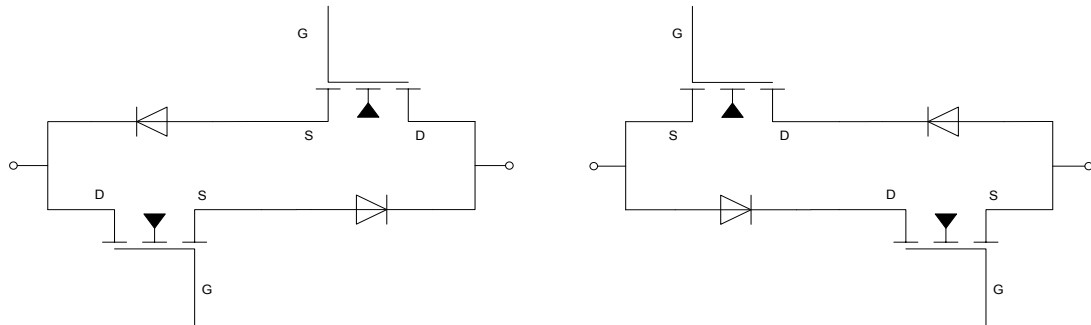


Fig.2. 18 Anti-parallel series diode-MOSFET configuration

2.4.4 Commutation Problem

In matrix converter topologies, the commutation problem basically caused from the lack of static freewheeling paths. In practice, purely resistive loads do not exist and therefore the load current path must always be provided with the active control of semiconductor switches. Also, the matrix converter commonly works at the switching frequencies from 2 to 10 kHz. Hence, reliable and fast current commutation between AC switches in matrix converter becomes critical, and safe commutation of the current from one bi-directional switch to another becomes difficult. Therefore, additional care is to be paid in to the synchronization of the switching signals ^[19].

2.4.5 Safe Operation

Likewise the other static converter, the protection issue is also needed for matrix converter to protect against the overvoltage and the overcurrent due to the restricted capability of semiconductor switches and diodes. Therefore, an effective protection circuit has an important role for the reliable operation.

2.4.5.1 Overvoltage Protection

A voltage surge from the AC mains may cause commutation failure in the converter operation. To avoid from a possible damage requires the use of some protective schemes in practice. There are two different protection schemes commonly proposed in the literature. The first protection scheme uses a clamp circuit to clamp the voltage spikes, the second uses varistor/suppressor diode protections at the input and output terminals ^[20].

2.4.5.1.1 Clamp Circuit

The clamp circuit includes a capacitor, two three-phase full-bridge diode rectifier structures and a discharge resistor as shown in Fig.2. 19. The clamp circuit protects the all nine bi-directional (18 unidirectional) switches against the surge coming from the utility and the voltage spikes caused during the emergency shutdown of the converter or a load failure. If the current flow through the inductive load is interrupted due to an emergency or a load failure, the stored energy in the load inductance is going to be transferred to the clamp capacitor. Thus, no overvoltage is going to be produced provided that the clamp capacitor sufficiently large. Also, output voltage spikes are generated by the parasitic inductances of power switches and by the timing inaccuracies during the switching task as well. Since the voltage of clamp capacitor increases at each inaccurate switching operation or voltage surge coming from the AC mains, a path is needed to discharge the clamp capacitor. Therefore, although not an efficient solution a resistor is used to discharge the clamp capacitor. This circuit has the advantage of being very simple. This scheme provides protection for all operating conditions and has simple hardware requirements. However, it also increases the number of semiconductor devices and required reactive component. These are the drawbacks of the clamp circuit protection scheme ^[21].

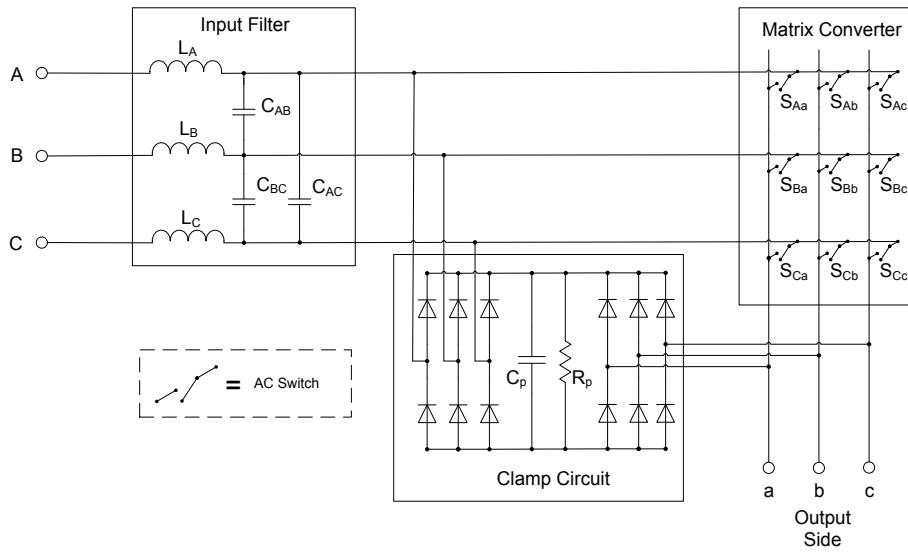


Fig.2. 19 The use of clamp circuit in direct matrix converter

2.4.5.1.2 Input/Output Varistor/Suppressor Diode Protection

In this strategy, the overvoltage protection is achieved by using varistors or suppressors ^[22]. This protection scheme is shown in Fig.2. 20. These varistors/suppressors limit the maximum voltage under overvoltage conditions. This strategy is suitable for low power ratings. For high power applications, the clamp circuit should be used.

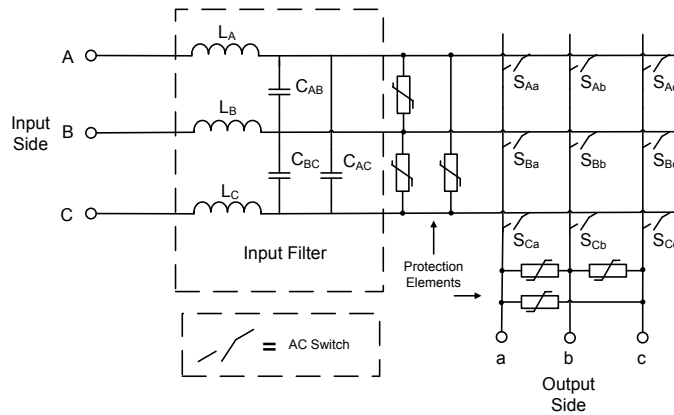


Fig.2. 20 Input/output varistor/suppressor diode protection scheme

2.4.5.2 Overcurrent Protection

Overcurrent can be a result of a short circuit existing on two (or more) input lines or two (or more) output phases. In both cases to prevent the damage will be caused from overcurrent, similar protection strategy can be followed up. Basically, phase currents both of input phases and output phases are monitored and if any of the phase currents is at above a predetermined safe value, all semiconductor switches are forced to turn-off. Since the freewheeling paths are provided with active control of semiconductor switches, at that time the freewheeling path is destroyed. We know that the freewheeling path is important to prevent switches from overvoltage spike that will be caused from the inductive load current interrupt. Therefore, the overcurrent and overvoltage protection strategies must be used together in matrix converter ^[19].

2.4.6 Switch Commutation

Based on the discussions given in previous sections, safe current commutation between the bi-directional switches is more difficult task comparing with the conventional voltage source inverters and it requires additional attention in timing and synchronization of the switching signals due to absence of natural freewheeling path. Therefore, active control of semiconductor switches is always required. Since the matrix converter is supplied by an AC utility and usually feeds an inductive load, the input lines must not be short circuited and the output lines must not be open circuited. Considering one output phase of three-phase to three-phase matrix converter, it is important that two bi-directional switches must not be switched on at the same time as shown in Fig.2. 21. In this condition, the two bi-directional switches on output phase “a” are turned - on at the same time. This would result in line-to-line short circuit and the destruction of the semiconductor switches due to overcurrent.

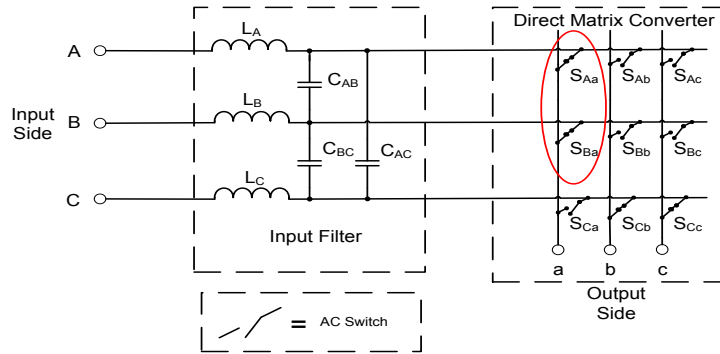


Fig.2. 21 Line to line short circuit condition

Moreover, all of the bi-directional switches for any output phase must never be switched - off at the same time. Otherwise, large overvoltages will result on the switch due to the lack of a path for inductive load current. Fig.2. 22 represents this situation. In this condition, any current path does not exist on output phase “c”. This would result high voltage spikes and the semiconductor switches may be destroyed due to overvoltage.

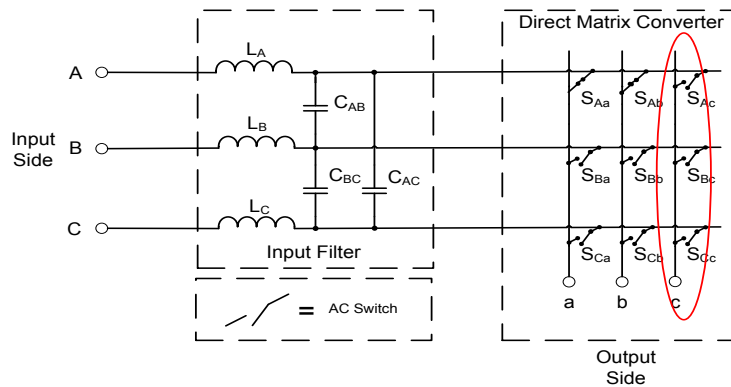


Fig.2. 22 Output current interrupt

Therefore, to provide safe commutation for matrix converter structures, logical switching states must be selected. In the literature, many studies were conducted on safe commutation strategies of matrix converter. Considering the reliability and efficiency, these commutation strategies can be divided in two different groups. In early implementation of matrix converters, dead-time and overlap techniques were used. The first group includes these two techniques. However, these techniques produce overcurrent and voltage spikes. Hence, they

are not so safe and require additional elements like as snubbers, clamping circuit and additional line inductors. Later, multi step commutation methods were implemented in the literature. The multi step commutation methods have been named as “Output Current Direction Based Commutation”, “Input Voltage Polarity Based Commutation” and “Mixed Commutation Method” which is a combination of both “Output Current Direction Based Commutation” and “Input Voltage Polarity Based Commutation” methods. The basic idea in these methods is to perform the required switch commutations by complying with the basic matrix converter rules. The first commutation method is based on the output current direction information, the second method is required to sense the input voltage polarities and the last one needs the both information.

In the literature, two and four step commutation strategies are generally evaluated to perform current direction based and input voltage polarity based commutation methods. The four-step current commutation technique was proposed in the literature ^[9], and it did not require any snubbing or limiting elements. Besides this, other current based commutation methods which require two steps are proposed in ^[23-24] in the literature. Moreover, another idea which uses input voltage magnitude was introduced in ^[25]. The purpose of this proposed input voltage magnitude based modulation techniques is to eliminate the complexity of control and reduce the number of steps used at the commutation instant. This technique exactly requires two steps for the bi-directional switch commutation. And it is also named as two-step voltage polarity based commutation method. Also, four-step commutation based on input voltage polarity has also been implemented ^[26]. However, both of the current direction based and voltage polarity based commutation techniques rely on the accurate measurement of current polarity or voltage polarity, otherwise these may lead to commutation failure. Therefore, new modulation technique has been introduced ^[27] to increase the reliability of these commutation techniques. In this technique, both the input voltage and the output current polarities feed the control structure to perform the commutation process.

In this section, current direction based commutation method is explained first. Then, the voltage polarity based commutation methods are mentioned. After the explanation of current direction based and voltage polarity based modulation techniques, the mixed commutation technique is introduced.

2.4.6.1 Output Current Direction Based Commutation Methods

In this section output current direction based commutation strategies are introduced.

2.4.6.1.1 Four-Step Commutation Strategy Based on Current Direction

The main idea of the safe commutation is to eliminate the switch state combinations which lead to the short circuit between input lines and open circuit at output phases. Before explaining the principle of the current direction based four-step commutation strategy, one output phase of three-phase to three-phase direct matrix converter is presented in the Fig.2. 23 to provide better understanding on switch commutations.

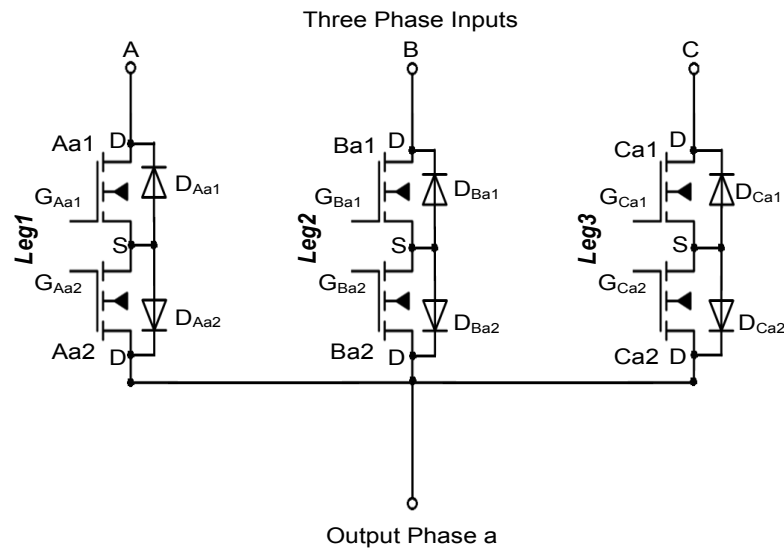
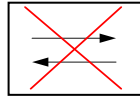
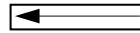


Fig.2. 23 One output phase structure of direct matrix converter

Each leg involves two common source connected N-channel MOSFETs and two anti-parallel diodes. The bi-directional switches formed in common source configuration. The switch state of these MOSFETs have very important role for safe commutation. Firstly, consider only the Leg1 of the output phase "a" of the direct matrix converter structure to simplify the role of switches on the commutation strategy. The allowable current flow directions are shown in Table 2. 1 according to the switch state combinations. The remaining legs may also be considered in the same manner.

Table 2. 1 The allowable current directions according to the switch state combinations

Description	Switch States		Input Phase	Current Direction	Output Phase
	Aa1	Aa2			
Current cannot flow in both direction	Open	Open	A		a
Current can flow in one direction	Open	Close	A		a
Current can flow in one direction only	Close	Open	A		a
Current can flow in both directions	Close	Close	A		a

The “Current Direction” arrows in the Table 2. 1, show directions of the current flow between the “Input Phase, A and Output Phase, a” columns. When a commutation from a bi-directional switch to another bi-directional switch is to take place, the current direction plays an important role to select steps of switch commutation. The following explanation assumes that the load current is in the direction of arrows (e.g from input phase to output phase) shown in Fig.2. 24 and initially the switches, in the Leg1, are turned-on.

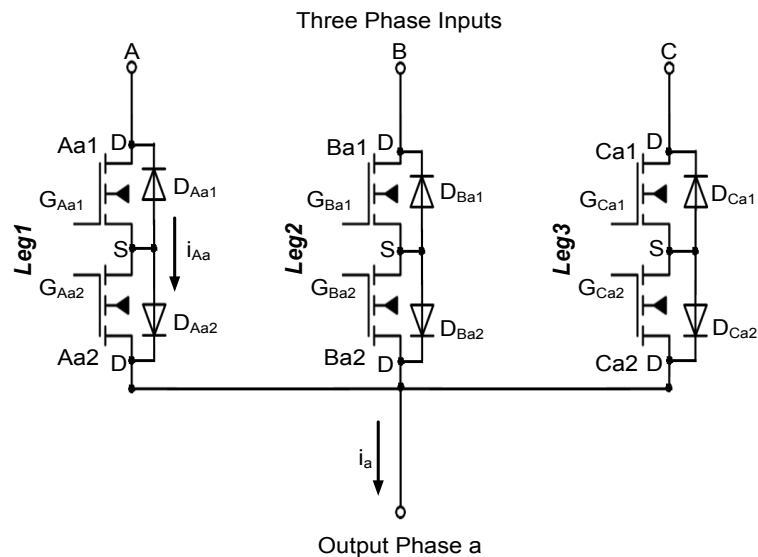


Fig.2. 24 One output phase structure

At a time instant, the commutation of the i_a current from input phase “A” to input phase “B” is required. Since the semiconductor switches have different turn - on / turn - off times and propagation delays, simultaneous turn - off of the switches in Leg1 and turn - on of the switches in Leg2 are not possible. Therefore, after switching-off the switches in Leg1, a dead-time should be introduced to ensure that they are turned - off before the turning - on of the switches in Leg2. However, this time, the inductive output current is interrupted and a voltage spike is induced on opened switches. From the above discussions it is clear that this basic strategy is also harmful. Since this transition cannot be made by using this strategy, a logical switching sequence should be selected during the commutation of the output phases between two input lines. The solution of this problem requires particular care to be paid in the timing and synchronization of the switching signals using only appropriate switch state combinations according to the current direction ^[28].

In order to prevent the voltage spike, the inductive load current which is drawn from the output phase “a” should be able to continue without any interruption when both unidirectional switches in Leg1 are turned-off. Therefore, the inductive current should have a current path to flow in Leg2, as shown in Fig.2. 25.

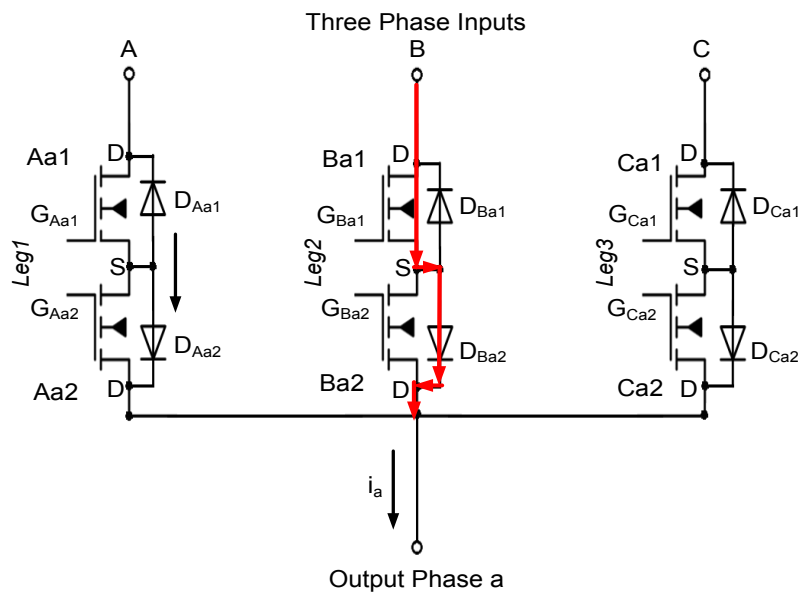


Fig.2. 25 Freewheeling current path in Leg2

Basically, the current paths in Leg1 and Leg2 which allow current to flow in the direction of i_a current can be provided in four different combinations. However, one of these combinations is nonhazardous. Now, consider the switch state combinations one by one.

- First Combination

All switches in Leg1 and Leg2 are turned-on. Referring to Table 2. 1, the switch state allows bi-directional power flow and a path for the current flow is established. However, this leads to the short circuit of input phase lines.

- Second Combination

All switches in Leg1 and only upper switch (Ba1) of Leg2 are turned-on. Referring to Table 2. 1, the switch state allows bi-directional power flow in Leg1 and a unidirectional power flow in Leg2. A current flow path is again established. However, this leads to the short circuiting of input lines if input voltage of phase “B” is greater than the input voltage of phase “A”. The short circuit current flows from input phase “B” to the input phase “A”.

- Third Combination

All switches in Leg2 and only upper switch of Leg1 (Aa1) are turned-on. Referring to Table 2. 1, the switch state allows bidirectional power flow in Leg2 and a unidirectional power flow in Leg1 thus establishing a path for the current flow. However, this connection scheme also leads to be short circuiting of input phase lines if the input voltage of phase “A” is greater than the input voltage of phase “B”.

- Fourth Combination

Only upper switches in Leg1 (Aa1) and Leg2 (Aa2) are turned-on. As displayed in Table 2. 1, the switch state allows only a unidirectional power flow in both, Leg1 and Leg2. There is no risk of short circuiting of input lines in this connection scheme.

There are two restrictions for the safe commutation of matrix converter as mentioned previous parts.

- While providing a path for the current of an inductive load, input lines must not be short circuited.
- While changing the switch states, the current of the inductive load should not be interrupted.

By considering these two limitations, only the fourth combination is appropriate condition to eliminate these dangerous situations. Similarly, all appropriate switch state (S : switch state) combinations can be given by considering the output current directions.

Table 2. 2, displays all switching combinations for four-step current direction based commutation strategy as a summary.

Table 2. 2 All switching combinations for current based commutation

S	MOSFET Switches						Ia Direction
	Aa1	Aa2	Ba1	Ba2	Ca1	Ca2	
1	close	close	open	open	open	open	+,-
2	open	open	close	close	open	open	+,-
3	open	open	open	open	close	close	+,-
4	close	open	open	open	open	open	+
5	open	close	open	open	open	open	-
6	open	open	close	open	open	open	+
7	open	open	open	close	open	open	-
8	open	open	open	open	close	open	+
9	open	open	open	open	open	close	-
10	close	open	close	open	open	open	+
11	open	close	open	close	open	open	-
12	open	open	close	open	close	open	+
13	open	open	open	close	open	close	-
14	close	open	open	open	close	open	+
15	open	close	open	open	open	close	-

In accordance with the above explanations, a commutation is required from S = 1 to S = 2 (Leg1 to Leg2) with the direction of inductive load current being positive. Positive current direction means that current flows from input to output. Then, interim steps should only cover the switch states which affect the current commutation in the Leg1 and Leg2. As a result, fourth, sixth and tenth switch states can be used as interim steps considering the current direction so that the switching sequence should be the following:

- I. Turning-off Aa2 (S = 4)
- II. Turning-on Ba1 (S = 10)
- III. Turning-off Aa1 (S = 6)

IV. Turning-on Ba1 (S = 2).

Also, a dead-time should be introduced between interim steps. Hence, the gate control signals should be applied according to sequence which is shown above. Fig.2. 26 presents the timing diagram of gate control signals.

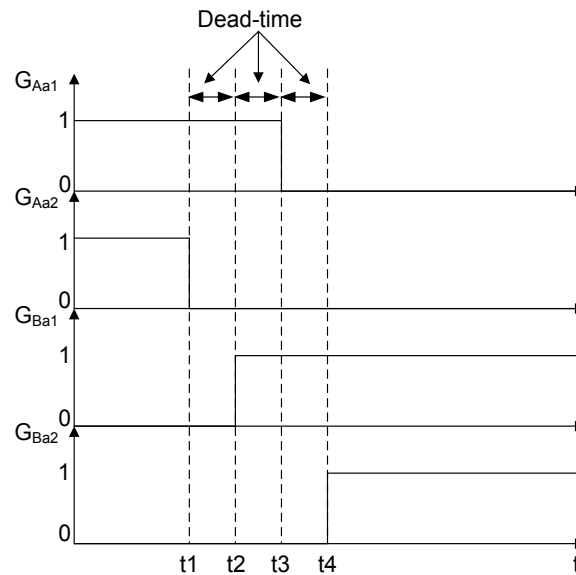


Fig.2. 26 Control signals of unidirectional switches

2.4.6.1.2 Two Step Commutation Strategy Based on the Current Direction

The main idea of this strategy is to keep the non-conducting switches turned - off during the commutation process including the non-conducting switch on active bi-directional switch. The two-step commutation strategy was proposed in ^[28]. When a commutation is required to a different leg, only the switch which is required to generate the path for inductive load current in the sensed direction will be turned - on. After the creation of the new current path, first activated switch is turned - off by the second step. This method is effectively used when the output current is absolutely higher than a small predefined positive threshold value. If the absolute output current level drops down to a smaller level than the threshold value, the sense of the output current direction becomes unreliable and this situation makes that two-step method is much complicated ^[28].

Fig.2. 27 reflects this strategy. If the current, i_a is higher than the threshold, only the upper switch (Aa1) is turned-on.

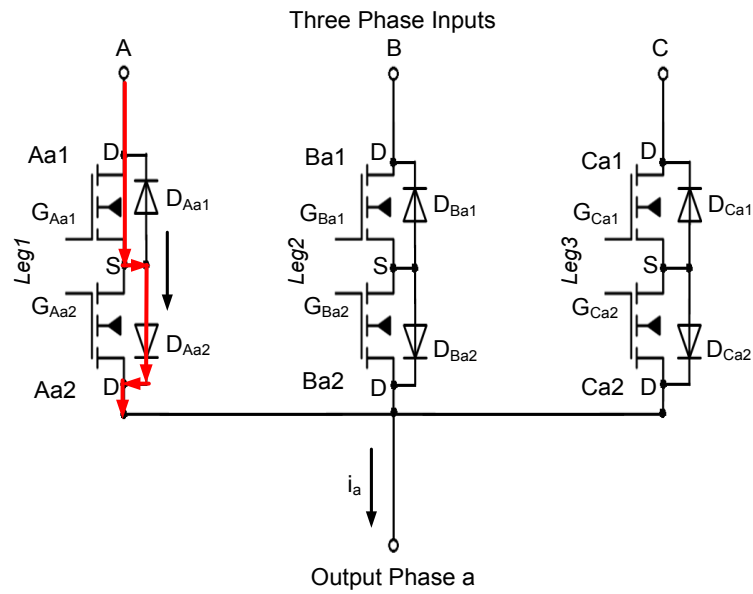


Fig.2. 27 Inductive current path in two step commutation

However, if the current is smaller than the threshold, the use of the on switch only will cause the current interrupt due to change of the current direction or wrong current direction detection. Therefore, both switches on a leg should be turned-on for low current levels to allow a change in the current direction. The commutation type occurring at the instant of the current direction change in the same current path (in a leg) is called as “Inter Switches Commutation”. To provide the reverse current path, both switches (Aa1 and Aa2) must be turned-on as shown in Fig.2. 28.

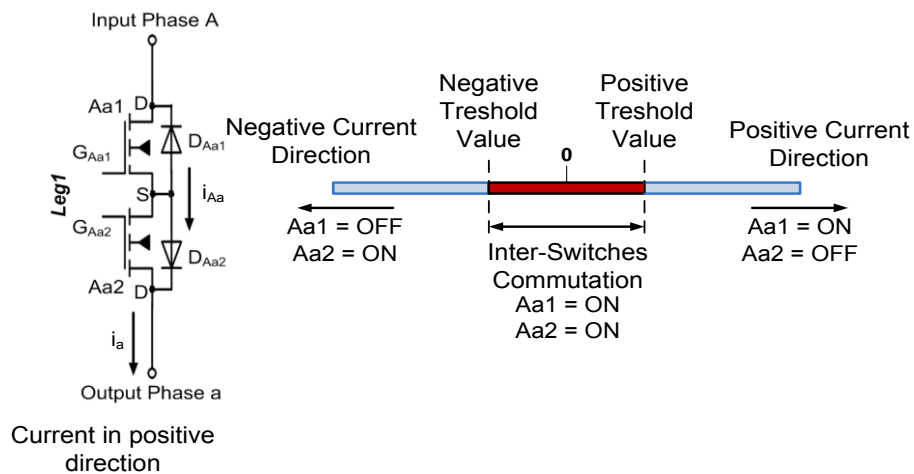


Fig.2. 28 Inter-Switches Commutation

When a commutation between different phases (e.g. between two input lines) is required, the “Inter Switches Commutation” should be disabled to avoid line-to-line short-circuit. This can be realized in two different ways. The first one is based on disabling the current commutation between different input lines until the current level abandons the threshold value. In other words, the last switch state will not be changed until the current reach threshold value. After that value, the output current direction will be sensed correctly. Then switch states can be reliably selected. This method is known as “two-steps commutation with threshold”. However, this compulsory time interval can affect the quality of the output current waveforms seriously because of in this time interval, the output current cannot reverse direction. That means, if the turned-on unidirectional switch is not an appropriate switch state, the current level rises in the opposite direction. In the second way, if the commutation is to happen between different input lines and the current is close to the threshold or within threshold value, a dead-time can be used between the switch commutations. Firstly turned-on switch is opened and after the dead-time duration, the new unidirectional switch in other leg is turned-on. During this time interval, the current commutation is interrupted. This commutation process is known as two-step commutation with dead-time in threshold. The switch commutation interval is half of that resulting in four-step commutation strategies. Hence, faster commutation process can be possible. However, the two-step method is much complicated ^[28] and causes the disruptive effects on output current as mentioned above.

2.4.6.2 Input Voltage Polarity Based Commutation Methods

In the previous section output current direction based commutation methods have been investigated. In this section, commutation techniques depending on the input voltage polarity information have been introduced.

2.4.6.2.1 Four-Step Commutation Strategy Based On the Input Voltage Polarity

The basic idea in this strategy is to provide the same operating conditions of a commutation process as in a traditional DC-link inverter. In order to establish the same operating conditions, the input phase voltages have to be known in real time. While the output phase

is remaining connected to an input line, both switches which are used for constructing the bi-directional switch are turned - on. Besides when a commutation of output phase between different input lines is to happen, real time input line voltages must be known so that we can decide whether upper or lower switch should be turned - on (assume commutation is to happen between Input Phase “A” and Input Phase “B” and also $V_B > V_A$) in the newly current commutation required leg. After this process a freewheeling path should be established in between the new input line and output line by turning-on MOSFET B_{a2} . The remaining semiconductor switch (B_{a1}) prevents the short circuit between the input lines. Then the other freewheeling path can be formed by turning - off one of the switches in firstly current commutated leg (Leg1). Fig.2. 29 illustrates this strategy.

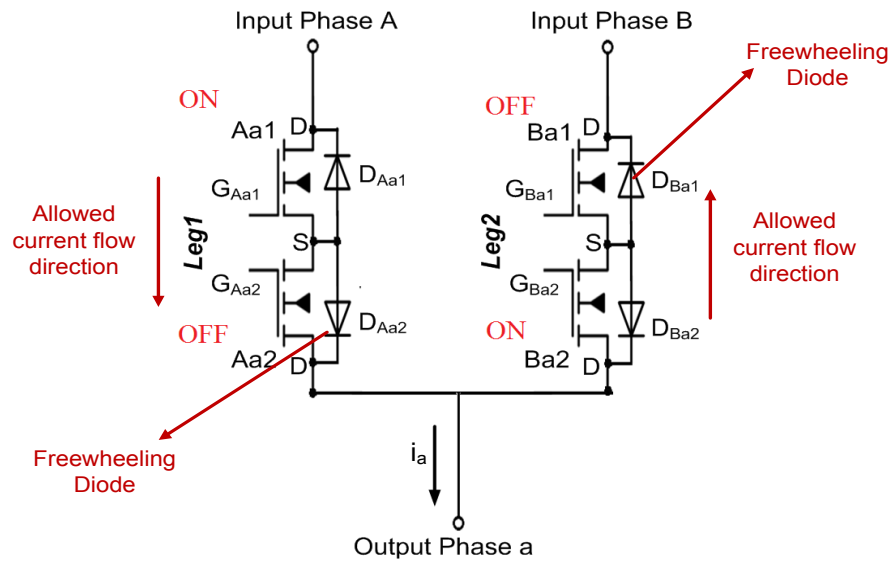


Fig.2. 29 Allowed current directions ($V_B > V_A$)

The freewheeling paths allow the current flows in both directions. The active switch in Leg1 provides a path for the current flow from input phase to output phase and the active switch in Leg2 provides the current flow in the opposite direction. The switching sequences with possible input voltage polarities are introduced as follow:

- If the input phase A voltage level is lower than the input phase B voltage level:
 - I. Turning-on Ba2
 - II. Turning-off Aa2

III. Turning-on Ba1

IV. Turning-off Aa1

- If the input phase A voltage level is higher than the input phase B voltage level:

I. Turning-on Ba1

II. Turning-off Aa1

III. Turning-on Ba2

IV. Turning-off Aa2

Since the turn - on and turn - off delays of semiconductor switches are different, in order to avoid from a probable short circuit between the input lines a blanking time should be inserted between the steps. In this commutation strategy, any hazard of open-circuiting the current flow path is completely removed due to freewheeling paths provided in both directions. However, it is not true for the hazard of the short circuiting. In other words, near the crossing points of input voltages (e.g. critical regions for voltage based strategies), the input voltage polarity may have not been sensed correctly. As a result of this situation a short circuit path may be established. Therefore, a reliable measurement of input line voltages is required ^[26].

2.4.6.2.2 Two-Step Commutation Strategy Based On the Input Voltage Polarity

In this section, a two-step commutation strategy is investigated. The commutation strategy is also called Metzi commutation and proposed in ^[29]. The basic principle of this strategy is based on the operating condition which establishes freewheeling paths for both output current polarities at any time. Since the switching sequences are determined using the information of input line voltages, the Metzi strategy also requires reliable measurement of input line voltages near the crossing points presented as in Fig.2. 30.

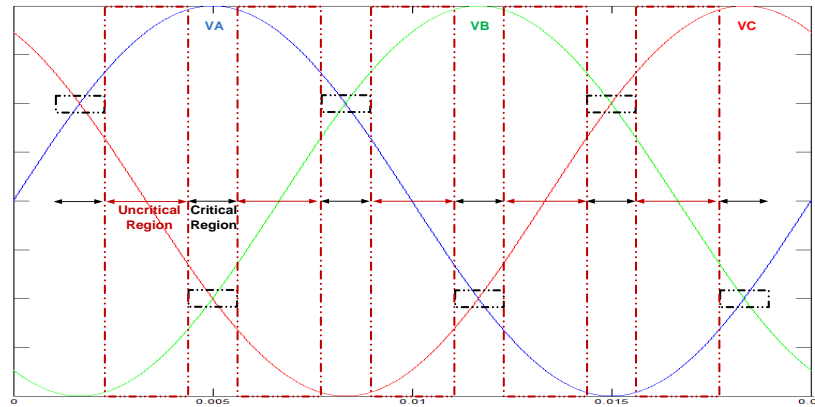


Fig.2. 30 Critical and uncritical intervals for detecting of input voltage polarities

The area in the red dashed rectangle is demonstrated the uncritical region. The potential difference between the input line voltages is high in this interval. Hence, the possibility of wrong detection of input voltage polarities is really low. However, it is not true for the area in the black dashed rectangle which demonstrates the critical region of commutation process. There are a few ways to manage a commutation required within this interval. The first is based on disabling (postponing the request) the commutation until the potential difference abandons the critical region and this is called as “Prohibition”. However, the connection time of the output phase to input phases should be recalculated considering this fact in this time interval. Actually, in this time interval the input line voltage levels are nearly equal. Therefore, this situation does not affect the output voltage and current waveforms. But, it will distort the input currents. A second way called as “Replacement” is to change the switching sequence by adding uncritical commutations. However, this strategy increases the converter switching losses and commutation time due to the additional commutations in this interval. These are the disadvantages of this strategy ^[30].

2.4.6.3 Multi-Step Commutation Strategy Based On Output Current and Input Voltage Polarity

In the previous sections, commutation methods based on the output current direction and the input voltage polarity have been introduced. This section introduces another commutation strategy based on both output current direction and input voltage polarity. Fig.2. 31 shows the principle of this hybrid commutation method.

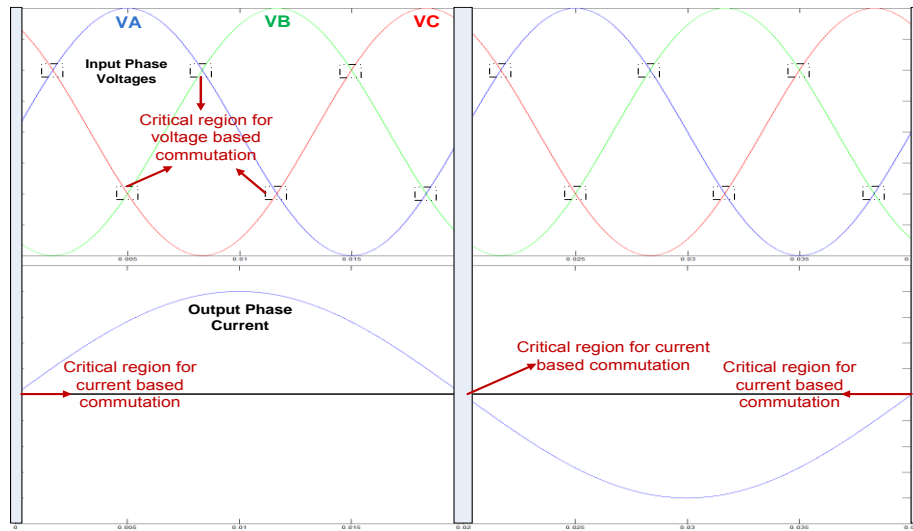


Fig.2. 31 Critical and uncritical intervals for output current direction and input voltage polarity based commutations

One of the former commutation methods based on the output current direction may cause an open-circuit in the current path if the load current is around zero, and the other commutation method based on the input voltage polarity may lead a line-to-line short circuit for a voltage difference of around zero. The proposed method combines both commutation methods based on current and voltage as follows ^[29]:

- At the zero crossing point of the load current, voltage based commutation method is used.
- At the zero crossing point of the voltage difference, current based commutation method is used.

Thus, this mixed method can decrease possibility of the commutation failure without the need for a high accuracy detection circuit. There are two types of these hybrid commutation methods used in practice; one that mostly uses the current based commutation method, and the other that mostly uses the voltage based commutation method. When the output phase current frequency is lower than the input voltage frequency, current based commutation technique will be preferred. Because, the selection process, whether the current based commutation method or voltage based commutation method should be used, decreases.

Hence, for the lower output current frequencies current based commutation technique is suitable. Besides that, if the output current frequency is higher than the input voltage frequency, opposite case is suitable ^[27].

CHAPTER 3

PERMANENT MAGNET SYNCHRONOUS MACHINES

The permanent magnet synchronous machine has permanent magnets instead of field windings. The permanent magnet synchronous machines can be classified into two main groups according to the installation of the permanent magnet materials on the rotor, Surface Mounted Permanent Magnet (SMPM) machines and Interior Permanent Magnet (IPM) machines. The magnets can be mounted on the rotor surface or they can be internal to the rotor. The permanent magnets are located on the outer surface of the rotor core in surface mounted permanent magnet machines, as shown in Fig.3. 1 ^[31].

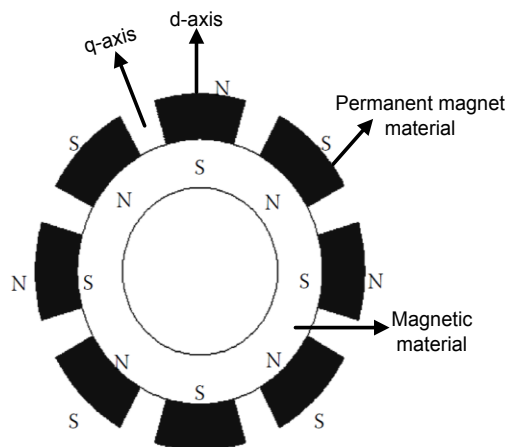


Fig.3. 1 Permanent magnet rotor construction using surface mounted magnets

In interior permanent magnet machines, the permanent magnets are embedded inside the rotor core. The structure of the interior permanent magnet machine is given in Fig.3. 2.

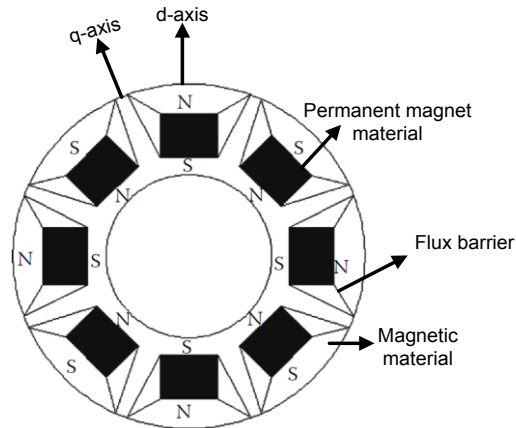


Fig.3. 2 Permanent magnet rotor construction using embedded magnets

The rotor magnetic axis is called direct axis (d-axis) or field flux axis and the principal path of the flux is through the magnets. The torque axis (quadrature axis or q-axis) of rotor is electrically orthogonal to the direct axis. Regardless of the manner of mounting the permanent magnets on the rotor, the basic principle of operation of machines are same. An important difference exists between the direct and quadrature axes inductances for different types of permanent magnet synchronous machines. The SMPM machines have many small permanent magnet materials that are placed whole surface of the rotor. Therefore, they have symmetrical reluctance in both axes and they are non-salient pole synchronous machines. In other words, the d and q axes reactances of SMPM machines are equal ($L_q = L_d$). The arrangement of the permanent magnets to the rotor surface provides the highest air gap flux density as is directly faces the air gap without the interruption of any other medium such as part of rotor laminations. Drawbacks of such an arrangement are; lower structural integrity and lower mechanical robustness. Besides that, the interior construction relieves the problem of retaining the magnets against centrifugal force. Therefore the interior construction is suitable for high-speed applications ^[31].

3.1 STEADY-STATE MODELING OF SMPM SYNCHRONOUS MACHINE

This section presents steady-state analysis of the surface mounted synchronous machines considering the per-phase steady-state equivalent circuit shown as in Fig.3. 3 ^[32].

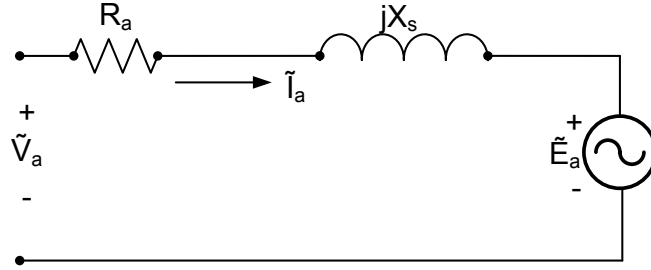


Fig.3. 3 Per-phase equivalent circuit of non-salient surface mounted permanent magnet synchronous machine

In Fig.3. 3, \tilde{V}_a is the motor terminal voltage, \tilde{E}_a is the back-emf voltage induced due to the permanent magnet flux and \tilde{I}_a is the motor phase current. And R_a and X_s are the per-phase winding resistance and synchronous reactance. From the equivalent circuit, we can write

$$\tilde{V}_a = \tilde{E}_a + \tilde{I}_a R_a + j\tilde{I}_a X_s \quad (3-1)$$

The average power input to the machine;

$$P_{in} = 3V_a I_a \cos \theta \quad (3-2)$$

where θ is the power-factor angle between the applied voltage and the phase current. V_a and I_a are the rms values of phase voltage and current.

The total copper (electrical) loss in a surface mounted permanent magnet synchronous machine is;

$$P_{cu} = 3I_a^2 R_a \quad (3-3)$$

By subtracting the total copper loss from the power input, we obtain the power developed by a surface mounted permanent magnet synchronous machine as;

$$P_{out} = 3V_a I_a \cos \theta - P_{cu} \quad (3-4)$$

Eddy current and hysteresis losses are also assumed as negligible.

Steady-state phasor diagram for the SMPM machine by neglecting the winding resistor is given in Fig.3. 4.

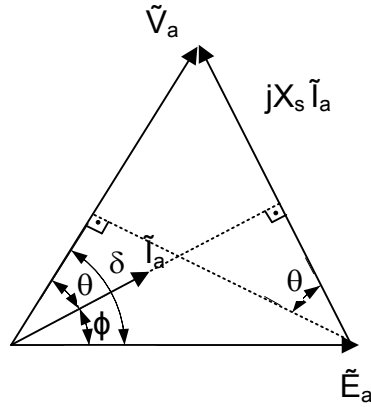


Fig.3. 4 Phasor diagram of the non-salient SMPM machine

From the per-phase equivalent circuit in Fig.3. 3, the total output power can be written as [32],

$$P_{out} = 3I_a E_a \cos \phi \quad (3-5)$$

For the flux linkage λ_f due the permanent magnets and the electrical speed w_e , the back-emf is given by;

$$E_a = w_e \lambda_f \quad (3-6)$$

If w_r is the angular velocity (rad/s) of the motor, the electromagnetic torque developed by the motor is then given as;

$$T = \frac{P_{out}}{w_r} = \frac{3I_a E_a \cos \phi}{w_r} \quad (3-7)$$

w_r and w_e are related by;

$$w_e = w_r \frac{P}{2} \quad (3-8)$$

where P is the pole number.

Then, from (3-6) – (3-8) the electromagnetic torque equation can be obtained as;

$$T = 3 \frac{P}{2} \lambda_f I_a \cos \phi \quad (3-9)$$

It is obvious that the maximum torque can be achieved by controlling the magnitude and phase of the phase current \tilde{I}_a .

3.2 DYNAMIC MODELING OF THE SMPM SYNCHRONOUS MACHINE

In the previous section, steady-state analysis of the surface mounted permanent magnet synchronous machines was introduced. This section presents the dynamic model of permanent magnet synchronous machine. The mathematical model of permanent magnet synchronous machine is developed with the help of Park and Clarke transformations which are derived in Appendix A. Actually; the model of permanent magnet synchronous machine is nonlinear. For simplicity, the following assumptions are made in the derivation:

- Saturation in machine is neglected,
- The back-emf is purely sinusoidal,
- Eddy currents and hysteresis losses are negligible,
- Balanced three-phase voltage source is considered.

There is no external voltage supply connected to the rotor side and the permanent magnet flux variation is negligible. Therefore, rotor voltage equations need not to be taken into account in the SMPM synchronous machine modeling ^[33].

The circuit equations of the three stator windings in terms of phase variables can be written as:

$$\begin{bmatrix} v_a \\ v_b \\ v_c \end{bmatrix} = \begin{bmatrix} R_a & 0 & 0 \\ 0 & R_b & 0 \\ 0 & 0 & R_c \end{bmatrix} \begin{bmatrix} i_a \\ i_b \\ i_c \end{bmatrix} + \frac{d}{dt} \begin{bmatrix} L_a & L_{ab} & L_{ac} \\ L_{ba} & L_b & L_{bc} \\ L_{ca} & L_{cb} & L_c \end{bmatrix} \begin{bmatrix} i_a \\ i_b \\ i_c \end{bmatrix} + \begin{bmatrix} e_a \\ e_b \\ e_c \end{bmatrix} \quad (3-10)$$

where R_a , R_b , and R_c are the stator resistances, L_a , L_b , L_c the self inductances, and L_{ab} , L_{ba} , L_{ca} , L_{ac} , L_{bc} , L_{cb} the mutual inductances. Assume that the stator windings are balanced and there is no change in the rotor reluctance with rotor position change for surface mounted permanent magnet synchronous machines, then

$$R_a = R_b = R_c = R_s \quad (3-11)$$

$$L_a = L_b = L_c = L$$

$$L_{ab} = L_{ba} = L_{ac} = L_{ca} = L_{bc} = L_{cb} = M$$

$$\begin{bmatrix} v_a \\ v_b \\ v_c \end{bmatrix} = \begin{bmatrix} R_s & 0 & 0 \\ 0 & R_s & 0 \\ 0 & 0 & R_s \end{bmatrix} \begin{bmatrix} i_a \\ i_b \\ i_c \end{bmatrix} + \frac{d}{dt} \begin{bmatrix} L & M & M \\ M & L & M \\ M & M & L \end{bmatrix} \begin{bmatrix} i_a \\ i_b \\ i_c \end{bmatrix} + \begin{bmatrix} e_a \\ e_b \\ e_c \end{bmatrix} \quad (3-12)$$

where $i_a = -i_b - i_c$ and we have that;

$$\begin{bmatrix} v_a \\ v_b \\ v_c \end{bmatrix} = \begin{bmatrix} R_s & 0 & 0 \\ 0 & R_s & 0 \\ 0 & 0 & R_s \end{bmatrix} \begin{bmatrix} i_a \\ i_b \\ i_c \end{bmatrix} + \frac{d}{dt} \begin{bmatrix} L-M & 0 & 0 \\ 0 & L-M & 0 \\ 0 & 0 & L-M \end{bmatrix} \begin{bmatrix} i_a \\ i_b \\ i_c \end{bmatrix} + \begin{bmatrix} e_a \\ e_b \\ e_c \end{bmatrix} \quad (3-13)$$

In Fig.3. 5, a dynamic phase equivalent circuit of SMPM is presented.

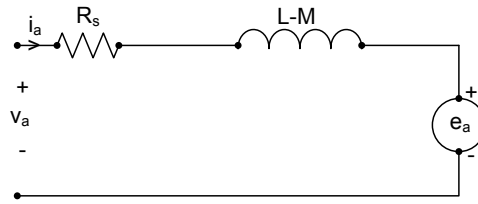


Fig.3. 5 Phase equivalent circuit of a SMPM

A two-phase equivalent equations and d-q model of a permanent magnet synchronous machine rotating at the synchronous speed is obtained by using Park and Clarke transformations which are given in Appendix A.

$$\begin{bmatrix} v_d \\ v_q \end{bmatrix} = \frac{2}{3} \begin{bmatrix} \cos(\Phi) & \cos(\Phi - \frac{2\pi}{3}) & \cos(\Phi + \frac{2\pi}{3}) \\ -\sin(\Phi) & -\sin(\Phi - \frac{2\pi}{3}) & -\sin(\Phi + \frac{2\pi}{3}) \end{bmatrix} \begin{bmatrix} v_a \\ v_b \\ v_c \end{bmatrix} \quad (3-14)$$

$$v_q = R_s i_q + L_q \frac{d}{dt} i_q + w_e L_d i_d + w_e \lambda_m \quad (3-15)$$

$$v_d = R_s i_d + L_d \frac{d}{dt} i_d - w_e L_q i_q \quad (3-16)$$

Fig.3. 6(a) and Fig.3. 6(b) show the dynamic two-phase equivalent circuit.

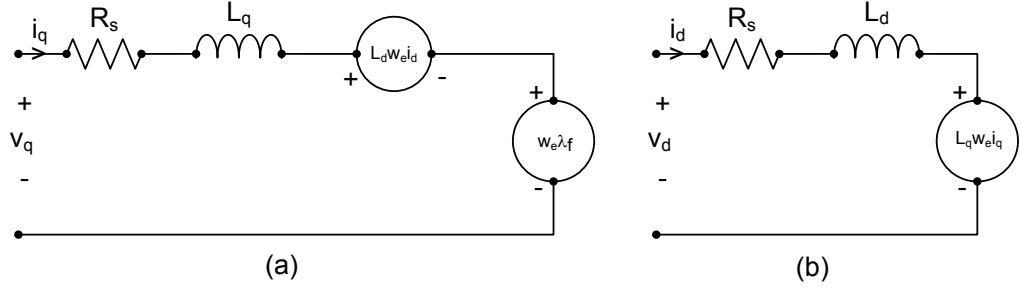


Fig.3. 6 Two-phase (d, q) equivalent model of SMPM synchronous machine

For three-phase permanent magnet synchronous machines, the input power (p_{in}) can be represented as:

$$p_{in} = v_a i_a + v_b i_b + v_c i_c \quad (3-17)$$

which in terms of d, q variables is;

$$p_{in} = \frac{3}{2} (v_d i_d + v_q i_q). \quad (3-18)$$

The output power, p_{out} can be obtained from the (3-18) by ignoring the copper losses.

$$p_{out} = \frac{3}{2} (-w_e \lambda_q i_d + w_e \lambda_d i_q) \quad (3-19)$$

where,

$$\lambda_q = L_q i_q \quad (3-20)$$

$$\lambda_d = L_d i_d + \lambda_m. \quad (3-21)$$

The instantaneous torque T is obtained by dividing the output power, p_{out} by mechanical speed w_r .

$$T = \frac{3}{2} \left(\frac{P}{2} \right) (\lambda_m i_q + (L_d - L_q) i_q i_d) \quad (3-22)$$

The torque equation includes two terms. First term is called as “the mutual reaction torque” that is produced from the interaction between the permanent magnet flux, λ_m and i_q current component. The second term corresponds to the “reluctance torque” due to the differences between d-axis and q-axis reluctances. In order to produce additive reluctance torque, i_d

must be negative and L_q must be greater than L_d . Besides that, the reluctance variation between the direct (d-axis) and quadrature (q-axis) axes is fairly small in non-salient surface mounted permanent magnet synchronous machine. Therefore, the second term, “reluctance torque”, can be neglected for this machine type ^[33]. The output torque (T) is linearly dependent with the magnet flux and q-axis current;

$$T = \frac{3}{2} \left(\frac{P}{2} \right) \lambda_m i_q. \quad (3-23)$$

CHAPTER 4

OPERATIONAL ISSUES OF MATRIX CONVERTER

In this chapter, the modulation strategies for matrix converter are introduced. First, a state-space model of matrix converter is presented to provide basic background on input/output characteristics. That is followed by a review of matrix converter modulation methods presented in the literature. Then, space vector definition is described. Finally, the derivations of the space vector pulse width modulation (SVPWM) methods for matrix converter topologies are presented.

4.1 STATE-SPACE MODEL OF MATRIX CONVERTER

A simplified three-phase to three-phase direct matrix converter model is shown in Fig.4. 1. This model consists of nine ideal AC (bi-directional) semiconductor switches which allow each of the three output lines to be connected to any of the three input lines. In this topology, a three-phase output voltage with adjustable magnitude and frequency is directly synthesized from three-phase AC mains.

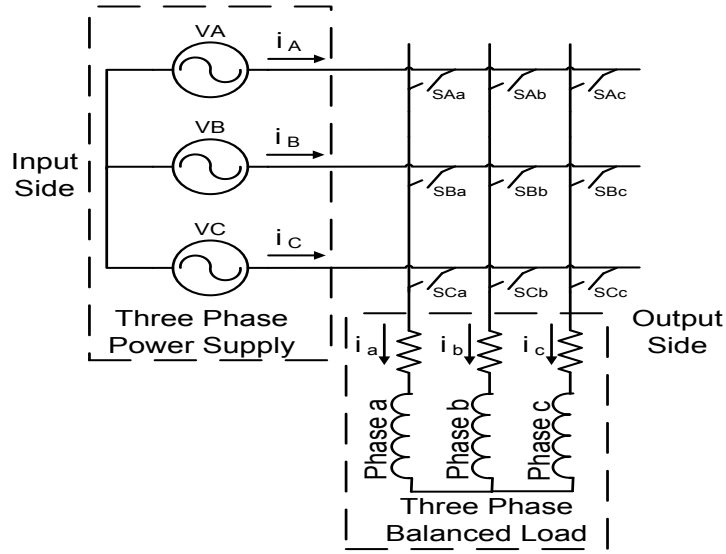


Fig.4. 1 Simplified three-phase to three-phase matrix converter

There is another matrix converter topology with no DC-link capacitor, known as indirect matrix converter as mentioned in Section 2.4.2. In indirect matrix converter topology, the three-phase AC mains voltage is first converted into a fictitious DC-link voltage. Then, the fictitious DC-link voltage is inverted in to the required AC output voltages. Besides these differences, the input–output voltages and currents show similar characteristics. The instantaneous input phase voltages and currents are given by the following equations;

$$\mathcal{V}_{inputs} = \begin{bmatrix} \mathcal{V}_A(t) \\ \mathcal{V}_B(t) \\ \mathcal{V}_C(t) \end{bmatrix} = \frac{V_i}{\sqrt{3}} \begin{bmatrix} \cos\left(w_i t - \frac{\pi}{6}\right) \\ \cos\left(w_i t - \frac{\pi}{6} - \frac{2}{3}\pi\right) \\ \cos\left(w_i t - \frac{\pi}{6} - \frac{4}{3}\pi\right) \end{bmatrix}. \quad (4-1)$$

Then, the instantaneous input line-to-line voltages can be written as,

$$\begin{bmatrix} \mathcal{V}_{AB}(t) \\ \mathcal{V}_{BC}(t) \\ \mathcal{V}_{CA}(t) \end{bmatrix} = V_i \begin{bmatrix} \cos(w_i t) \\ \cos\left(w_i t - \frac{2}{3}\pi\right) \\ \cos\left(w_i t - \frac{4}{3}\pi\right) \end{bmatrix} \quad (4-2)$$

where V_i is the peak value of the input line-to-line voltages and w_i is the input angular frequency.

The input line currents are given as;

$$i_{inputs} = \begin{bmatrix} i_A(t) \\ i_B(t) \\ i_C(t) \end{bmatrix} = I_i \begin{bmatrix} \cos(w_i t - \frac{\pi}{6} - \varphi_i) \\ \cos(w_i t - \frac{\pi}{6} - \varphi_i - \frac{2}{3}\pi) \\ \cos(w_i t - \frac{\pi}{6} - \varphi_i - \frac{4}{3}\pi) \end{bmatrix} \quad (4-3)$$

where I_i is the peak value of three-phase input currents. The input currents have a phase angle φ_i with respect to the input phase voltages. This angle φ_i can be set to zero to obtain unity power factor control. The output phase voltages and currents are given by;

$$\mathcal{V}_{outputs} = \begin{bmatrix} \mathcal{V}_a(t) \\ \mathcal{V}_b(t) \\ \mathcal{V}_c(t) \end{bmatrix} = V_o \begin{bmatrix} \cos(w_o t) \\ \cos(w_o t - \frac{2}{3}\pi) \\ \cos(w_o t - \frac{4}{3}\pi) \end{bmatrix}, \quad (4-4)$$

$$i_{outputs} = \begin{bmatrix} i_a(t) \\ i_b(t) \\ i_c(t) \end{bmatrix} = I_o \begin{bmatrix} \cos(w_o t - \varphi_o) \\ \cos(w_o t - \varphi_o - \frac{2}{3}\pi) \\ \cos(w_o t - \varphi_o - \frac{4}{3}\pi) \end{bmatrix}. \quad (4-5)$$

where V_o is the peak value of output voltages, I_o is the peak value of the output currents, w_o is the output angular frequency and φ_o is the phase difference between the output voltages and currents.

Then, the instantaneous input and output voltages are related by;

$$\mathcal{V}_{outputs} = \begin{bmatrix} \mathcal{V}_a(t) \\ \mathcal{V}_b(t) \\ \mathcal{V}_c(t) \end{bmatrix} = \begin{bmatrix} s_{Aa}(t) & s_{Ba}(t) & s_{Ca}(t) \\ s_{Ab}(t) & s_{Bb}(t) & s_{Cb}(t) \\ s_{Ac}(t) & s_{Bc}(t) & s_{Cc}(t) \end{bmatrix} \begin{bmatrix} \mathcal{V}_A(t) \\ \mathcal{V}_B(t) \\ \mathcal{V}_C(t) \end{bmatrix} \quad (4-6)$$

and the instantaneous input and output currents are related as;

$$i_{inputs} = \begin{bmatrix} i_A(t) \\ i_B(t) \\ i_C(t) \end{bmatrix} = \begin{bmatrix} s_{Aa}(t) & s_{Ba}(t) & s_{Ca}(t) \\ s_{Ab}(t) & s_{Bb}(t) & s_{Cb}(t) \\ s_{Ac}(t) & s_{Bc}(t) & s_{Cc}(t) \end{bmatrix}^T \begin{bmatrix} i_a(t) \\ i_b(t) \\ i_c(t) \end{bmatrix}. \quad (4-7)$$

The switching function s_{Yx} in (4-6) – (4-7) denotes the instantaneous states of AC switches and it is either “0” when the switch is “off” or “1” when the switch is “on”. Note that $Y \in \{A, B, C\}$ and $x \in \{a, b, c\}$.

Since in the matrix converter only one AC switch must be closed on each output phase at any time this prevents the line-to-line short circuit of the input supply. Moreover, all AC switches in an output phase must not be opened at the same time to avoid the open circuit at the load sides because any natural freewheeling path exists for the inductive load current. These constraints can be stated formally by;

$$S_{Ax} + S_{Bx} + S_{Cx} = 1 \text{ and } x \in \{a, b, c\} \quad (4-8)$$

4.2 VOLTAGE AND CURRENT WAVEFORMS GENERATION IN MATRIX CONVERTERS

In principle, the aims of the modulation methods to synthesize the voltage and current waveforms are identical. All modulation methods are used to create target waveforms at the converter input and output terminals. Actually, these modulation methods show difference in quality of the generated input and output waveforms. Considering this fact, the ideal modulation methods to generate the input-output current and voltage waveforms of matrix converter should provide the following specifications ^[34]:

- Independent control of frequency and magnitude of the generated output voltages,
- Sinusoidal input currents with full control of power factor,
- Maximum input voltage to output voltage transfer ratio,
- Minimum low order harmonics, low total harmonic distortion and minimum switching losses,
- Efficient implementation.

The matrix converter control strategies were first mentioned by Alesina and Venturini. The first modulation method for current and voltage waveforms generated by matrix converters were proposed in 1980, by Venturini ^[35]. This is the first modulation method proposed for the generation of input-output waveforms of matrix converter. However, the first method has the drawback of low input voltage to output voltage transfer ratio as 0.5.

In 1985 a control technique based on a different approach was proposed ^[2,36]. Input voltages are first rectified to generate an imaginary DC-link voltage, later the DC-link voltage is

inverted to generate desired output voltages. This approach provides higher voltage transfer ratio of 0.86. However, it still had limitation in the input power factor control.

In 1988, Alesina and Venturini proposed a new PWM modulation method to generate input-output waveforms of matrix converter ^[37]. This method also eliminates the drawback of first modulation method of Venturini and known as Venturini's Optimal Method. By this method, the voltage transfer ratio is increased at a maximum value of 0.86.

In 1989 Roy and April proposed a scalar PWM method as an alternative method for matrix converter input-output waveforms generation ^[38].

The space vector pulse width modulation method for matrix converter was first mentioned in ^[39] in 1989. The first SVPWM method had also two distinct control stages. Those are a rectification stage which provides a constant fictitious DC voltage and an inverter stage which generates the three-phase target voltage waveforms. This modulation method is named as indirect or two-stage SVPWM in the literature. By this method, control of input power factor is not possible. An advanced space vector PWM method was proposed in 1991 which allowed to the control of the input power factor ^[5].

In 1993 Casadei, Grandi, Serra and Tani proposed a space vector PWM method in ^[40]. It does not involve any rectification and inversion process. The power was converted directly from an AC form to another AC form by this method.

The matrix converter PWM methods described in the literature can be classified into two categories, the direct PWM approach and the indirect PWM approach.

The Alesina and Venturini method, single-stage or direct space vector PWM and scalar PWM methods are examples of direct PWM approaches.

The two-stage or indirect space vector PWM methods are classified in indirect PWM approach in the literature.

The indirect matrix converter topology can be fully matched the physical implementation of the indirect space vector PWM method ^[41]. As mentioned in Section 2.4.2, the indirect matrix converter topology consists of a rectifier stage at the input side and a conventional voltage source inverter (VSI) at the output side. These two stages are fictitious rectification and fictitious inversion stage. Modulation methods of rectifier and inverter stages can be analyzed separately for simplification.

4.2.1 Matrix Converter Modulation Methods of Alesina and Venturini

By the first modulation methods of Venturini, reachable maximum input to output voltage transfer ratio is 0.5 because fundamental voltage waveform is always between the negative and positive envelope of the input voltage waveforms ^[4]. The method uses a switching frequency much higher than both frequencies at the input and at the output. The aim in using the Alesina and Venturini PWM method is to find a modulation matrix $M(t)$ which satisfies ^[42],

$$\mathcal{V}_{outputs} = \begin{bmatrix} \mathcal{V}_a(t) \\ \mathcal{V}_b(t) \\ \mathcal{V}_c(t) \end{bmatrix} = [M(t)] \begin{bmatrix} \mathcal{V}_A(t) \\ \mathcal{V}_B(t) \\ \mathcal{V}_C(t) \end{bmatrix}, \quad (4-9)$$

$$i_{inputs} = \begin{bmatrix} i_A(t) \\ i_B(t) \\ i_C(t) \end{bmatrix} = [M(t)]^T \begin{bmatrix} i_a(t) \\ i_b(t) \\ i_c(t) \end{bmatrix}, \quad (4-10)$$

where the modulation matrix $M(t)$ defined above has the following matrix form;

$$M(t) = \begin{bmatrix} m_{Aa}(t) & m_{Ba}(t) & m_{Ca}(t) \\ m_{Ba}(t) & m_{Bb}(t) & m_{Cb}(t) \\ m_{Ca}(t) & m_{Cb}(t) & m_{Cc}(t) \end{bmatrix}. \quad (4-11)$$

Due to the use of high switching frequency the desired output voltage waveforms can be constructed from the input voltage waveforms. This also allows constructing the desired input currents from the output currents.

By considering (4-8), a typical switching pattern for the matrix converter can be illustrated as in the Fig.4. 2. For the following illustration, it is assumed that the switches can change their states instantaneously at the switching instant.

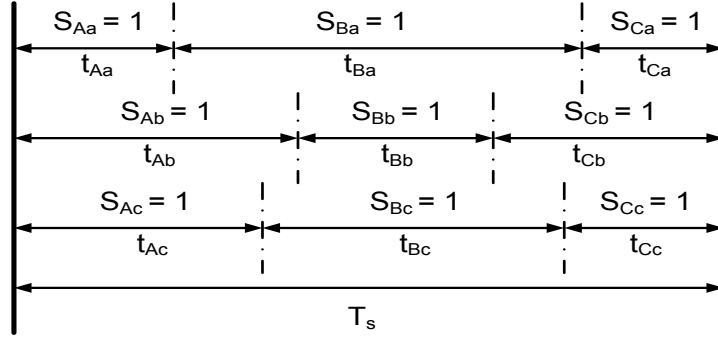


Fig.4. 2 A possible switching pattern

“ T_s ” represents the switching period or complete PWM cycle and t_{Yx} represents the on period of the corresponding switches, where

$$t_{Ax} + t_{Bx} + t_{Cx} = T_s$$

and $x \in \{a, b, c\}$. Then, the modulation duty-ratio (i.e. duty ratio of switch S_{Yx}) can be defined as

$$m_{Yx}(t) = \frac{t_{Yx}}{T_s} \quad (4-12)$$

with $0 \leq m_{Yx}(t) \leq 1$, and $\sum_x m_{Yx}(t) = 1$, where $Y \in \{A, B, C\}$ and $x \in \{a, b, c\}$.

The construction of PWM waveforms based on proposed method by Venturini and Alesina is based on the direct calculation of the modulation matrix $M(t)$ ^[35];

$$M(t) = \frac{1}{3}\alpha_1 M_1(t) + \frac{1}{3}\alpha_2 M_2(t) \quad (4-13)$$

where

$$M_1(t) = \begin{bmatrix} 1 + 2q\cos(w_m t) & 1 + 2q\cos(w_m t - \frac{2\pi}{3}) & 1 + 2q\cos(w_m t + \frac{2\pi}{3}) \\ 1 + 2q\cos(w_m t + \frac{2\pi}{3}) & 1 + 2q\cos(w_m t) & 1 + 2q\cos(w_m t - \frac{2\pi}{3}) \\ 1 + 2q\cos(w_m t - \frac{2\pi}{3}) & 1 + 2q\cos(w_m t + \frac{2\pi}{3}) & 1 + 2q\cos(w_m t) \end{bmatrix} \quad (4-14)$$

$$M_2(t) = \begin{bmatrix} 1 + 2q\cos(w_n t) & 1 + 2q\cos(w_n t - \frac{2\pi}{3}) & 1 + 2q\cos(w_n t + \frac{2\pi}{3}) \\ 1 + 2q\cos(w_n t - \frac{2\pi}{3}) & 1 + 2q\cos(w_n t + \frac{2\pi}{3}) & 1 + 2q\cos(w_n t) \\ 1 + 2q\cos(w_n t + \frac{2\pi}{3}) & 1 + 2q\cos(w_n t) & 1 + 2q\cos(w_n t - \frac{2\pi}{3}) \end{bmatrix} \quad (4-15)$$

where w_o and w_i are the output and input angular frequencies,

$$w_m = (w_o - w_i),$$

$$w_n = (w_o + w_i),$$

$$\alpha_1 = \frac{1}{2} \left[1 + \frac{\tan(\varphi_i)}{\tan(\varphi_o)} \right],$$

$$\alpha_2 = 1 - \alpha_1, \quad (4-16)$$

$$q = \frac{V_o}{V_i},$$

with the following restrictions;

$$\alpha_1 \geq 0, \alpha_2 \geq 0, 0 \leq q \leq \frac{1}{2}.$$

The maximum value of input to output voltage transfer ratio, q is 0.5. This is the drawback of this modulation technique.

In 1988 Venturini and Alesina proposed an improved PWM technique applicable to the matrix converters which increased the maximum input voltage to output voltage transfer ratio to 0.86. The idea was based on the injection of third order harmonic component of input and output voltages to the output reference voltage. When the magnitudes of those third-order components were chosen correctly, the voltage transfer ratio could be raised to 0.86. As a result of that, matrix converter output voltages can be defined as follows ^[6]:

$$V_{outputs} = \begin{bmatrix} \mathcal{V}_a(t) \\ \mathcal{V}_b(t) \\ \mathcal{V}_c(t) \end{bmatrix} = v_o \begin{bmatrix} \cos(w_o t) + \frac{1}{4} \cos(3w_i t) - \frac{1}{6} \cos(3w_o t) \\ \cos(w_o t - \frac{2}{3}\pi) + \frac{1}{4} \cos(3w_i t) - \frac{1}{6} \cos(3w_o t) \\ \cos(w_o t - \frac{4}{3}\pi) + \frac{1}{4} \cos(3w_i t) - \frac{1}{6} \cos(3w_o t) \end{bmatrix} \quad (4-17)$$

The entries in the PWM matrix, $M(t)$ of improved solution can be described as follows ^[6]:
 Note that the subscript 6 in (4-18) indicating that the argument in brackets is to be computed modulo 6.

$$\begin{aligned}
 m_{kh}(t) = & \frac{1}{3} \left\{ 1 + \sqrt{\frac{3}{2}} p \left[Z_1^1(2(k+h) - 4)_{(6)}(t) + Z_1^{-1}(2(k-h) \right. \right. \\
 & \left. \left. h)_{(6)}(t) - \frac{1}{6} Z_3^1(2(h-1))_{(6)}(t) - \frac{1}{6} Z_3^{-1}(2(1-h))_{(6)}(t) + \right. \right. \\
 & \left. \left. \text{sgn}(p) \left(-\frac{1}{6\sqrt{3}} Z_0^4(2(h-1))_{(6)}(t) + \frac{7}{6\sqrt{3}} Z_0^2(2(h-1))_{(6)}(t) \right) \right] + \right. \\
 & \left. \alpha_1 Z_1^1(2(k+h) - 4)_{(6)}(t) + \alpha_2 Z_1^{-1}(2(k-h))_{(6)}(t) \right\}
 \end{aligned} \tag{4-18}$$

where $k, h \in \{1, 2, 3\}$ and

$$Z_n^m(\gamma)(t) = \cos\left((nw_o + mw_i)t + \frac{\gamma\pi}{3}\right)$$

$$\theta = \frac{\tan(\varphi_i)}{\tan(\varphi_o)}, \quad \alpha = \frac{2|\theta|\varphi_o}{\varphi_i}$$

$$p = \frac{\frac{2\varphi_o}{\varphi_i} - \alpha}{\sqrt{3}},$$

$\alpha_1 = \alpha$ and $\alpha_2 = 0$ if $\theta < 0$,

$\alpha_1 = 0$ and $\alpha_2 = \alpha$ if $\theta > 0$,

$\alpha_1 = \alpha_2 = 0$ if $\theta = 0$.

Also the entries (e.g. $m_{kh}(t)$) of PWM matrix, $M(t)$ have the following relation:

$$M(t) = \begin{bmatrix} m_{11}(t) & m_{12}(t) & m_{13}(t) \\ m_{21}(t) & m_{22}(t) & m_{23}(t) \\ m_{31}(t) & m_{32}(t) & m_{33}(t) \end{bmatrix} = \begin{bmatrix} m_{Aa}(t) & m_{Ba}(t) & m_{Ca}(t) \\ m_{Ba}(t) & m_{Bb}(t) & m_{Cb}(t) \\ m_{Ca}(t) & m_{Cb}(t) & m_{Cc}(t) \end{bmatrix}$$

4.2.2 Space Vector

Assume x_a , x_b and x_c are magnitudes of three variables in a balanced three-phase system. Vector forms of the variables are represented with $\overline{x_k}$, $k \in \{a, b, c\}$. These variables can represent currents or voltages of balanced three-phase systems.

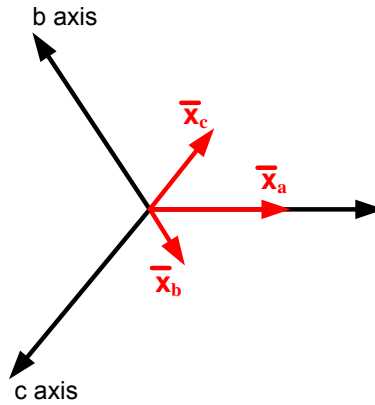


Fig.4. 3 Three variables of balanced three-phase system ($\bar{x}_a, \bar{x}_b, \bar{x}_c$)

Now, define the space vector \bar{X}_s as follows:

$$\bar{X}_s = k(x_a + ax_b + a^2x_c) \tag{4-19}$$

where a and a^2 are the spatial operators and k is the transformation constant, $k = 2/3$.

$$a = e^{j2\pi/3}$$

$$a^2 = e^{j4\pi/3}$$

Fig.4. 4 shows the space vector \bar{X}_s based on the variables of Fig.4. 3.

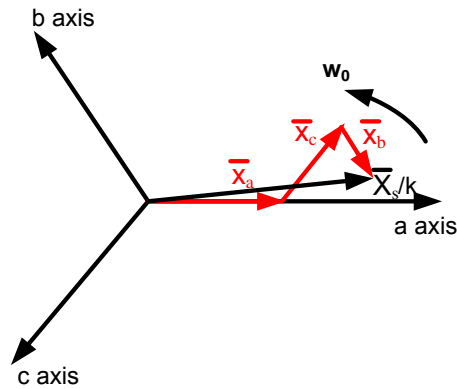


Fig.4. 4 Space vector \bar{X}_s and its components

Assuming the three-phase variables being purely sinusoidal and symmetric with an angular frequency of w_o , then the space vector \bar{X}_s can be expressed in the form;

$$\overline{X_s} = |\overline{X_s}|e^{j\omega_o t} \quad (4-20)$$

where $|\overline{X_s}|$ is the magnitude of the space vector ($\overline{X_s}$) and t is time. In case the three-phase variables are not symmetric, then a zero sequence component is to be added.

Also recalling the relationships between sine, cosine and their exponential forms are useful in the analysis with space vectors:

$$\sin \theta = \frac{e^{j\theta} - e^{-j\theta}}{2j}, \theta \in R \quad (4-21)$$

$$\cos \theta = \frac{e^{j\theta} + e^{-j\theta}}{2}, \theta \in R \quad (4-22)$$

4.2.3 Application of Space Vector PWM Methods in the Matrix Converter

The applications of the space vector PWM methods in the matrix converter control can be classified in two groups; applications of the direct space vector PWM (DSVPWM) method and applications of the indirect space vector PWM (ISVPWM) method.

4.2.3.1 Direct Space Vector PWM Method

The direct space vector PWM technique for the direct matrix converter is based on the instantaneous representation of the three-phase input currents from three-phase output currents and the three-phase output voltages from the three-phase input voltages ^[44]. The space vector algorithm for matrix converter has inherent capability to achieve the control of both the output phase voltage vector and the instantaneous input line current displacement angle.

Under symmetrical and balanced three-phase conditions, the input and output equations of a matrix converter can be described by four vectors in a complex plane.

$$\overline{V}_i = \frac{2}{3}(v_A(t) + a v_B(t) + a^2 v_C(t)) = v_i(t)e^{j\alpha_i(t)} \quad (4-23)$$

$$\overline{V}_o = \frac{2}{3}(v_a(t) + a v_b(t) + a^2 v_c(t)) = v_o(t)e^{j\alpha_o(t)} \quad (4-24)$$

$$\overline{I}_i = \frac{2}{3}(i_A(t) + a i_B(t) + a^2 i_C(t)) = i_i(t)e^{j\beta_i(t)} \quad (4-25)$$

$$\bar{I}_o = \frac{2}{3}(i_a(t) + a i_b(t) + a^2 i_c(t)) = i_o(t)e^{j\beta_o(t)} \quad (4-26)$$

Where \bar{V}_i is the input phase voltage vector, \bar{I}_i is the input line current vector, \bar{V}_o is the output phase voltage vector and \bar{I}_o represents the output phase current vector. In the matrix converter model, \bar{V}_o and \bar{I}_i are the respective reference voltage and current vectors to be synthesized. By using these reference vectors \bar{V}_o and \bar{I}_i , the output voltage regulation, the input power factor control and the regenerative energy handling (e.g. regenerative braking for motor applications) can be achieved ^[45].

The space vector PWM algorithm has four major steps:

- Synchronization with input phase voltages;
- Selection of a set of vectors for synthesizing the reference voltage and current vectors;
- Calculation of duty ratios of selected vectors by using the reference vectors in space;
- Determination of switching patterns in each switching period.

As aforementioned the three-phase to three-phase direct matrix converter consists of nine bi-directional switches and each output phase can be connected to the each input phase at any time. In fact, there are 512 possible switch state combinations by nine AC switches. However, some limitations exist on switch states combinations for the safe switching process of matrix converter structure. The switching operation must not cause the short circuit at the input terminals and open circuit at the output terminals as shown in Fig.4. 5(a) and Fig.4. 5(b).

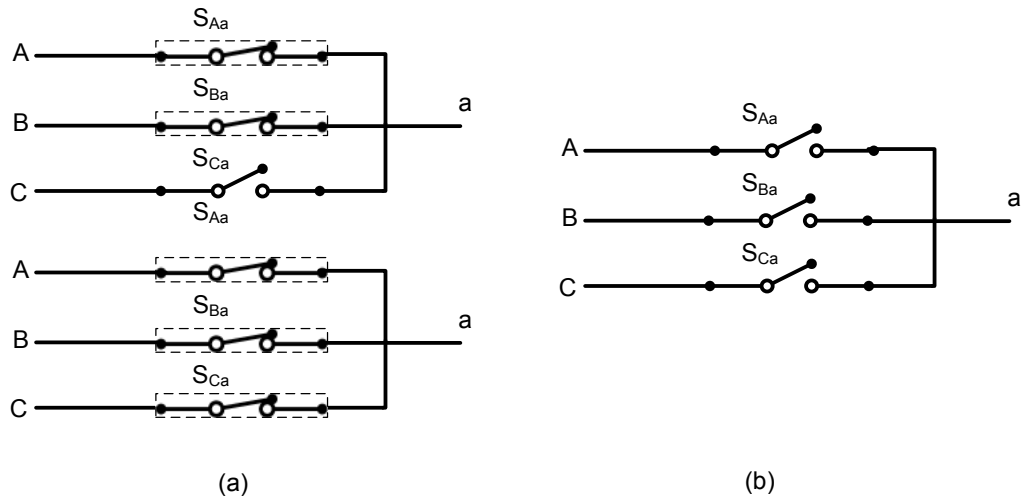


Fig.4. 5 Switching constraints (a) possible short circuit states at input terminal (b) open circuit state at output terminals

Excluding these two constraints on the switching of bi-directional switches in a matrix converter, there are only twenty seven different allowable states are left. The allowed states are listed in Table 4. 1. The table also shows which input lines and output lines are connected, as well as the resulting output line-to-line voltages and input line currents for each allowed switching combination.

Table 4. 1 All possible safe switching configurations

Group	Switching Configurations (S.C.)			Line-to-Line Output Voltages			Output Phase Voltage Vector		Input Line Currents			Input Line Current Vector		
	S.C. No.	Switches On			V_{ab}	V_{bc}	V_{ca}	V_o	α_0	i_A	i_B	i_C	I_i	β_i
1	NA	SaA	SbB	ScC	V_{AB}	V_{BC}	V_{CA}	X	X	i_a	i_b	i_c	X	X
	NA	SaA	ScB	SbC	$-V_{CA}$	$-V_{BC}$	$-V_{AB}$	X	X	i_a	i_c	i_b	X	X
	NA	SbA	SaB	ScC	$-V_{AB}$	$-V_{CA}$	$-V_{BC}$	X	X	i_b	i_a	i_c	X	X
	NA	SbA	ScB	SaC	V_{BC}	V_{CA}	V_{AB}	X	X	i_c	i_a	i_b	X	X
	NA	ScA	SaB	SbC	V_{CA}	V_{AB}	V_{BC}	X	X	i_b	i_c	i_a	X	X
	NA	ScA	SbB	SaC	$-V_{BC}$	$-V_{AB}$	$-V_{CA}$	X	X	i_c	i_b	i_a	X	X
2	0a	SaA	SaB	SaC	0	0	0	0	X	0	0	0	0	X
	0b	SbA	SbB	SbC	0	0	0	0	X	0	0	0	0	X
	0c	ScA	ScB	ScC	0	0	0	0	X	0	0	0	0	X
3	+1	SaA	SbB	SbC	V_{AB}	0	$-V_{AB}$	$2/3 V_{AB}$	0	i_a	$-i_a$	0	$2/\sqrt{3}i_a$	$-\pi/6$
	-1	SbA	SaB	SaC	$-V_{AB}$	0	V_{AB}	$-2/3 V_{AB}$	0	$-i_a$	i_a	0	$-2/\sqrt{3}i_a$	$-\pi/6$
	+2	SbA	ScB	ScC	V_{BC}	0	$-V_{BC}$	$2/3 V_{BC}$	0	0	i_a	$-i_a$	$2/\sqrt{3}i_a$	$\pi/2$
	-2	ScA	SbB	SbC	$-V_{BC}$	0	V_{BC}	$-2/3 V_{BC}$	0	0	$-i_a$	i_a	$2/\sqrt{3}i_a$	$\pi/2$
	+3	ScA	SaB	SaC	V_{CA}	0	$-V_{CA}$	$2/3 V_{CA}$	0	$-i_a$	0	i_a	$2/\sqrt{3}i_a$	$7\pi/6$
	-3	SaA	ScB	ScC	$-V_{CA}$	0	V_{CA}	$-2/3 V_{CA}$	0	i_a	0	$-i_a$	$-2/\sqrt{3}i_a$	$7\pi/6$
	+4	SbA	SaB	SbC	$-V_{AB}$	V_{AB}	0	$2/3 V_{AB}$	$2\pi/3$	i_b	$-i_b$	0	$2/\sqrt{3}i_b$	$-\pi/6$
	-4	SaA	SbB	SaC	V_{AB}	$-V_{AB}$	0	$-2/3 V_{AB}$	$2\pi/3$	$-i_b$	i_b	0	$-2/\sqrt{3}i_b$	$-\pi/6$
	+5	ScA	SbB	ScC	$-V_{BC}$	V_{BC}	0	$2/3 V_{BC}$	$2\pi/3$	0	i_b	$-i_b$	$2/\sqrt{3}i_b$	$\pi/2$
	-5	SbA	ScB	SbC	V_{BC}	$-V_{BC}$	0	$-2/3 V_{BC}$	$2\pi/3$	0	$-i_b$	i_b	$2/\sqrt{3}i_b$	$\pi/2$
	+6	SaA	ScB	SaC	$-V_{CA}$	V_{CA}	0	$2/3 V_{CA}$	$2\pi/3$	$-i_b$	0	i_b	$2/\sqrt{3}i_b$	$7\pi/6$
	-6	ScA	SaB	ScC	V_{CA}	$-V_{CA}$	0	$-2/3 V_{CA}$	$2\pi/3$	i_b	0	$-i_b$	$-2/\sqrt{3}i_b$	$7\pi/6$
	+7	SbA	SbB	SaC	0	$-V_{AB}$	V_{AB}	$2/3 V_{AB}$	$4\pi/3$	i_c	$-i_c$	0	$2/\sqrt{3}i_c$	$-\pi/6$
	-7	SaA	SaB	SbC	0	V_{AB}	$-V_{AB}$	$-2/3 V_{AB}$	$4\pi/3$	$-i_c$	i_c	0	$-2/\sqrt{3}i_c$	$-\pi/6$
	+8	ScA	ScB	SbC	0	$-V_{BC}$	V_{BC}	$2/3 V_{BC}$	$4\pi/3$	0	i_c	$-i_c$	$2/\sqrt{3}i_c$	$\pi/2$
-8	SbA	SbB	ScC	0	V_{BC}	$-V_{BC}$	$-2/3 V_{BC}$	$4\pi/3$	0	$-i_c$	i_c	$2/\sqrt{3}i_c$	$\pi/2$	
+9	SaA	SaB	ScC	0	$-V_{CA}$	V_{CA}	$2/3 V_{CA}$	$4\pi/3$	$-i_c$	0	i_c	$2/\sqrt{3}i_c$	$7\pi/6$	
-9	ScA	ScB	SaC	0	V_{CA}	$-V_{CA}$	$-2/3 V_{CA}$	$4\pi/3$	i_c	0	$-i_c$	$-2/\sqrt{3}i_c$	$7\pi/6$	

Referring the Fig.4. 6, α_0 and β_i are the phase angles of the reference current and voltage vectors, respectively. Also, the symbol “X” is used for some undefined values.

The switching states can be classified in three distinct groups. The first group consists of six switching configurations where each output line is directly connected to the different input lines. In this case, the phase angle of the output phase voltage vector is dependent to the phase angle of the supply. Both the magnitude and the phase of the vectors, which constructed from the first group switching combinations, are variable. There are three switching configurations in the second group which consists of zero vectors. In this case, all output lines are connected to the same input line. And there are eighteen switching combinations in the last group which consists of the active vectors. In this case, the phase angle of the output space vector is independent from the phase angle of supply. The output space vectors can be formed at variable amplitude and frequency and the input current space vector can be formed at variable amplitude at input voltage frequency as shown in Fig.4. 6(a) and Fig.4. 6(b) ^[46]. The tips of these vectors form a regular hexagon, and the adjacent space vectors have an angle 60° with respect to each other. Hence the space vector diagram is divided into six sectors.

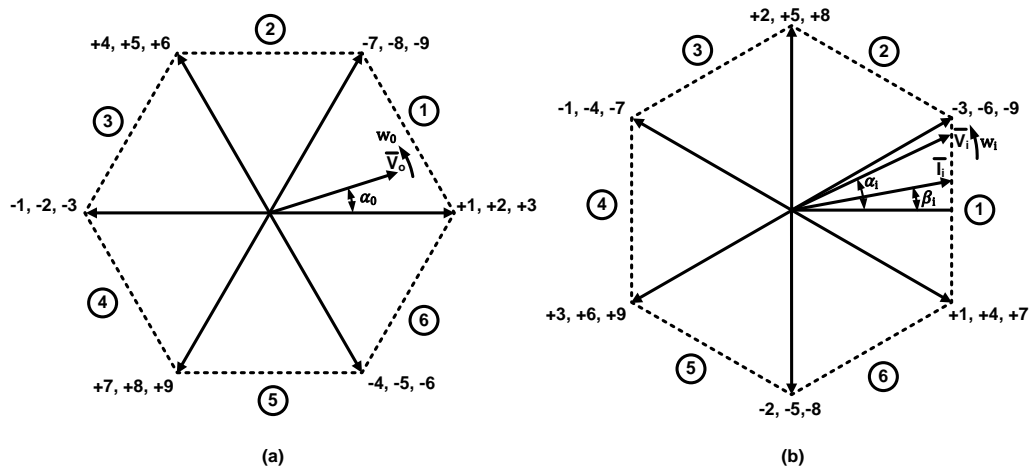


Fig.4. 6 (a) Output phase voltage vector (b) input line current vector hexagons

In principle, the direct space vector PWM algorithm depends on the selection of four switch configurations that are applied for suitable time intervals within each period T_s to synthesize the reference input line current and output phase voltage vectors.

In order to determine the switch states, it should be decided that in which sectors the input line current vector and output phase voltage vector stay. There are 36 possible combinations for sector pair of output voltage and input current vectors. The sectors are determined by using the phase angles for the current and the voltage vectors. The zero and active switching patterns are changed periodically according to sector information and output current requirements ^[45]. More discussion on the application of the space vector PWM method for a three-phase to three-phase matrix converter is presented in next section.

4.2.3.2 Indirect Space Vector PWM Method

The indirect space vector PWM technique is used to generate the desired output line-to-line voltage and the input line current vectors and the phase angle with respect to the input phase voltages. Determining the phase angle is necessary for the input power factor control ^[34, 36].

In the indirect space vector PWM, the required output voltages and input current waveforms are obtained through two fictitious steps: rectification and inversion. The input AC voltages are rectified to build up a constant virtual DC-link voltage. Then, the inversion stage generates desired output voltages. In order to maximize the input voltage to output voltage transfer ratio, the rectification stage continuously selects the maximum input line-to-line voltages.

Unlike the direct space vector PWM method, twenty-one possible switch state combinations can be suitably applied in indirect space vector PWM. Eighteen of them form the active vectors and the remaining form the zero vectors. Actually, switch state combinations are restricted due to the fictitious DC-link structure. This PWM technique assumes that there is a DC-link between the rectifier and inverter. Therefore, it is impossible to connect each output phase to three different input phases at the same time. These six states which include rotating vectors as listed in Table 4.1 cannot be effectively utilized in indirect space vector PWM technique. The method uses only two input phases during the modulation period. Despite that, the full input to output voltage transfer ratio of $\frac{\sqrt{3}}{2}$ and sinusoidal input currents with unity power factor control are still always achieved ^[42].

The difference between the direct space vector PWM technique and indirect space vector PWM technique is that the switching combinations in group 1 stated in Table 4. 1 are not used in indirect space vector PWM technique. Moreover, the indirect space PWM techniques can be implemented by using both direct and indirect matrix converter structure. However, direct PWM technique can only be implemented with direct matrix converter structure.

4.2.3.2.1 Principle of Indirect Space Vector PWM Method

The indirect space vector PWM can be introduced better with the indirect matrix converter circuit shown in Fig.4. 7. The indirect space vector PWM can also be implemented with direct matrix converter topology as it is done in this study. The implementation of indirect space vector PWM with direct matrix converter is introduced in Section 4.2.4.

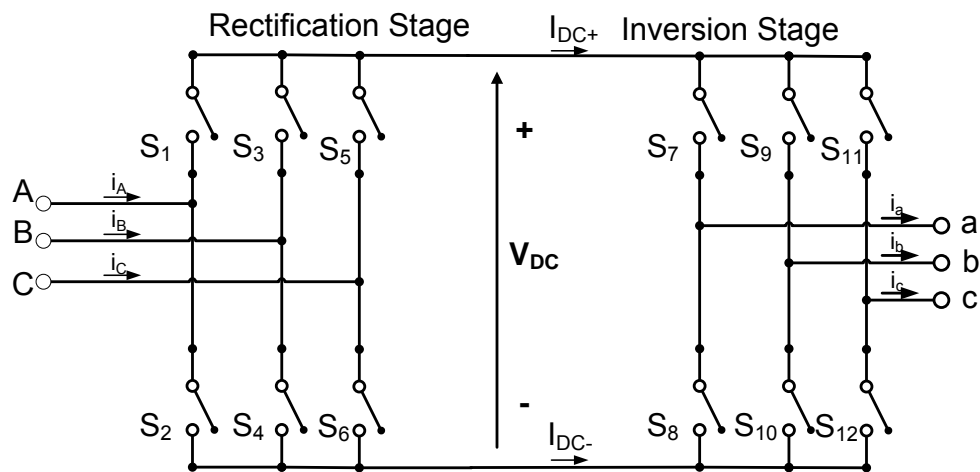


Fig.4. 7 Indirect matrix converter circuit

In order to generate balanced sets of sinusoidal input-output waveforms, PWM is incorporated into the indirect matrix converter in such a way that the rectification and inversion stages can be individually forced to generate input-output waveforms in space vector PWM (SVM) form. The rectification stage provides a constant fictitious DC voltage and the inverter stage produces the three-phase PWM output voltage waveforms. Hence, the space vector PWM is used to determine possible switching combinations and also

calculate the on periods of switches by considering power flow through virtual DC-link. By considering the matrix converter rules and the limitation arising from DC-link, there are twenty-one permissible combinations. Eighteen of them are active vector combinations and the remaining three are zero vector combinations. At any switching instant, the output phase voltage vector \overline{V}_o and the instantaneous input current displacement angle φ_i with respect to the input phase voltages are used as references. In each stage, vector combinations are selected separately to generate input and output reference vectors.

I. Rectification stage

Referring the Fig.4. 7, the rectification stage consists of six bi-directional switches and it is directly connected to the input supply. Thus, the bi-directional switches must never short the input lines. Also, this fact are mathematically expressed for the rectifier stage in a switching period with the equation (4-27). Note that “S_i” (i = 1, 2, 3, 4, 5, 6) is the name of a switch and “s_i” (i = 1,2,3,4,5,6) is the state of the corresponding switch.

$$\begin{aligned} s_1 + s_3 + s_5 &= 1 \\ s_2 + s_4 + s_6 &= 1 \end{aligned} \tag{4-27}$$

Table 4. 2 displays all allowable switching combinations of the rectifier and corresponding generated DC-link voltages and input currents. Referring the Table 4. 2, the first six witching configurations (e.g. 1, 2, 3, 4, 5, 6) show the active vectors which produce a non-zero DC-link voltage and the remaining three switching combinations (e.g. 7, 8, 9) represent the zero vectors which produce zero DC-link voltage. The six active vectors \overline{I}_j , (j=1- 6) shown in Fig.4. 8 have fixed directions in complex plane, and each of them refers to specific connections of the input line voltages to the fictitious DC-link.

Table 4. 2 All allowed switching configurations and the corresponding DC-link voltage and input line currents

Switching Configuration	Switch States $\begin{bmatrix} S_1 & S_3 & S_5 \\ S_2 & S_4 & S_6 \end{bmatrix}$	Input Line Currents			Input Line Current Vector		DC-link Voltage
		i_A	i_B	i_C	$ \bar{I}_i $	$\angle \bar{I}_i$	V_{DC}
1	$\begin{bmatrix} 1 & 0 & 0 \\ 0 & 1 & 0 \end{bmatrix}$	I_{DC+}	I_{DC-}	0	$\frac{2}{\sqrt{3}}I_{DC}$	$-\frac{\pi}{6}$	V_{AB}
2	$\begin{bmatrix} 1 & 0 & 0 \\ 0 & 0 & 1 \end{bmatrix}$	I_{DC+}	0	I_{DC-}	$\frac{2}{\sqrt{3}}I_{DC}$	$\frac{\pi}{6}$	V_{AC}
3	$\begin{bmatrix} 0 & 1 & 0 \\ 0 & 0 & 1 \end{bmatrix}$	0	I_{DC+}	I_{DC-}	$\frac{2}{\sqrt{3}}I_{DC}$	$\frac{\pi}{2}$	V_{BC}
4	$\begin{bmatrix} 0 & 1 & 0 \\ 1 & 0 & 0 \end{bmatrix}$	I_{DC-}	I_{DC+}	0	$\frac{2}{\sqrt{3}}I_{DC}$	$\frac{5\pi}{6}$	V_{BA}
5	$\begin{bmatrix} 0 & 0 & 1 \\ 1 & 0 & 0 \end{bmatrix}$	I_{DC-}	0	I_{DC+}	$\frac{2}{\sqrt{3}}I_{DC}$	$-\frac{5\pi}{6}$	V_{CA}
6	$\begin{bmatrix} 0 & 0 & 1 \\ 0 & 1 & 0 \end{bmatrix}$	0	I_{DC-}	I_{DC+}	$\frac{2}{\sqrt{3}}I_{DC}$	$-\frac{\pi}{2}$	V_{CB}
7	$\begin{bmatrix} 1 & 0 & 0 \\ 1 & 0 & 0 \end{bmatrix}$	0	0	0	0	-	0
8	$\begin{bmatrix} 0 & 1 & 0 \\ 0 & 1 & 0 \end{bmatrix}$	0	0	0	0	-	0
9	$\begin{bmatrix} 0 & 0 & 1 \\ 0 & 0 & 1 \end{bmatrix}$	0	0	0	0	-	0

The rectifier has to generate both the DC-link voltage and the sinusoidal input line currents with controllable displacement angle φ_i with respect to the input phase voltages. In order to generate sinusoidal input line currents with controllable displacement angle (φ_i), the input current reference vector has to be synchronized with the input phase voltages. By using space vector transformation, balanced and sinusoidal three-phase input line currents can be transformed into a reference vector.

$$\bar{I}_i = \frac{2}{3}(i_A(t) + a i_B(t) + a^2 i_C(t)) = i_i(t)e^{j\beta_i(t)} \quad (4-28)$$

where $i_i(t)$ is the instantaneous magnitude for the current reference vector \bar{I}_i and $\beta_i(t)$ is the instantaneous angle of the reference vector \bar{I}_i in the complex plane shown in Fig.4. 8 at time t.

The active current vectors in complex plane are presented in Fig.4. 8. The time domain relationships between the sectors (1, 2, 3, 4, 5, 6) and input line current (i_A , i_B , i_C) waveforms are shown in Fig.4. 9.

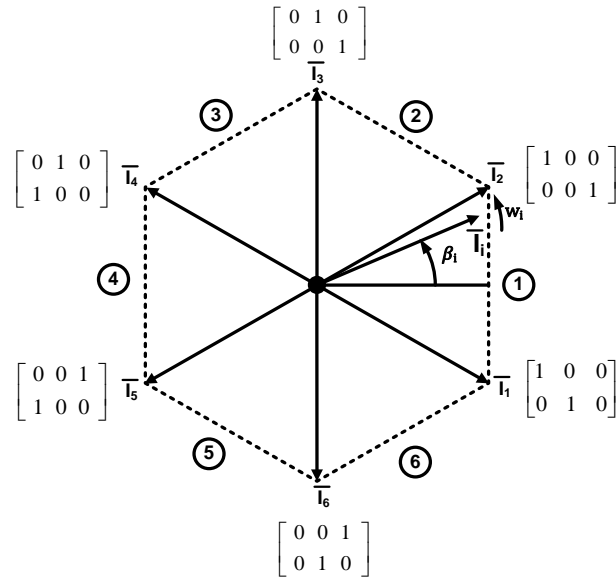


Fig.4. 8 Active current vectors, related sectors, and the reference phase current vector \bar{I}_i in complex plane

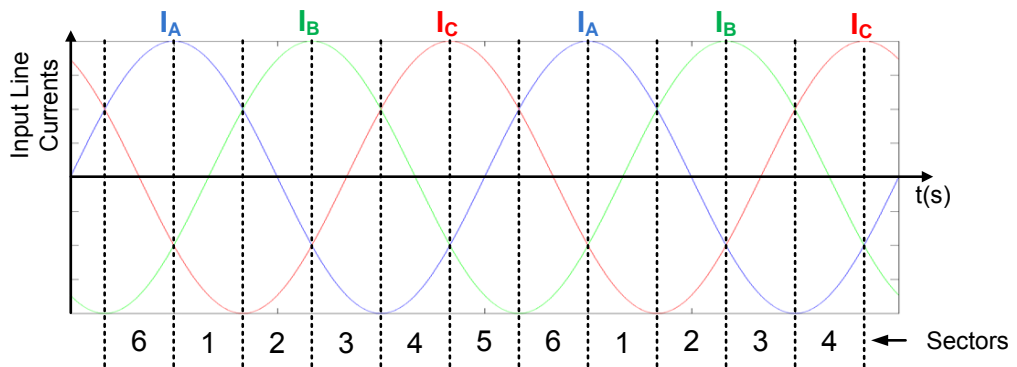


Fig.4. 9 Relationships between the input line current waveforms and the sectors in time domain

The reference phase current vector \bar{I}_i in a sector can be synthesized by two adjacent (active) space vectors (\bar{I}_1 and \bar{I}_2 in Fig. 4.8) and a zero current vector (stated in Table 4. 2). The angular position of the reference phase current vector, \bar{I}_i is determined by the active vectors. The magnitude of the reference vector, $i_i(t)$ is determined by both the use of zero and the active vectors. For a switching period T_s , the reference phase current vector, \bar{I}_i can be synthesized as described below.

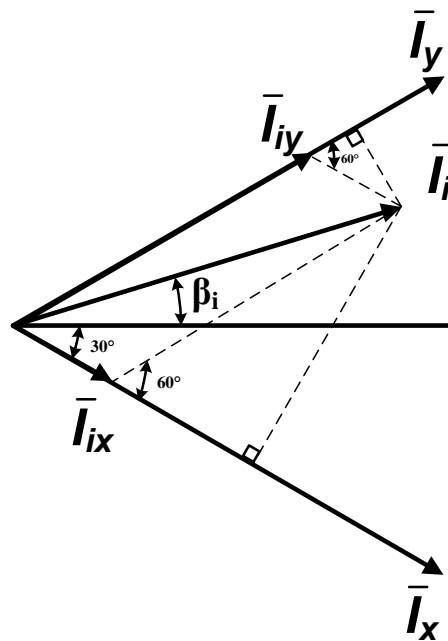


Fig.4. 10 Reference phase current vector construction

The reference phase current vector, \bar{I}_i , is synthesized by using two adjacent active vectors, \bar{I}_x and \bar{I}_y which are contributing to \bar{I}_i with the duty ratios d_x and d_y and a zero vector \bar{I}_0 with the duty ratio d_{c0} will be selected. To synthesize a rotating reference vector at different magnitude and phase, it is necessary to compute duty ratio for each switching period. The reference phase current vector can be written in basic form as follow;

$$\bar{I}_i = \bar{I}_{ix} + \bar{I}_{iy} \quad (4-29)$$

with

$$\overline{I_{ix}} = \overline{I_x} d_x, \quad \overline{I_{iy}} = \overline{I_y} d_y. \quad (4-30)$$

Then, the duty ratios are;

$$d_x = \frac{|\overline{I_{ix}}|}{|\overline{I_x}|}, \quad d_y = \frac{|\overline{I_{iy}}|}{|\overline{I_y}|}$$

Also,

$$|\overline{I_{ix}}| = \frac{|\overline{I_i}| \sin(\frac{\pi}{6} - \beta_i)}{\sin(\frac{\pi}{3})}, \quad |\overline{I_{iy}}| = \frac{|\overline{I_i}| \sin(\frac{\pi}{6} + \beta_i)}{\sin(\frac{\pi}{3})}$$

$$d_x = \frac{|\overline{I_i}|}{\sqrt{\frac{3}{2}}|\overline{I_x}|} \sin(\frac{\pi}{6} - \beta_i), \quad d_y = \frac{|\overline{I_i}|}{\sqrt{\frac{3}{2}}|\overline{I_y}|} \sin(\frac{\pi}{6} + \beta_i) \quad (4-31)$$

$$|\overline{I_x}| = |\overline{I_y}| = \frac{2}{\sqrt{3}} |I_{DC}|, \quad \frac{|\overline{I_i}|}{|I_{DC}|} = m_c, \quad 0 \leq m_c \leq 1$$

where m_c is the current modulation index which represents the current transfer ratio and I_{DC} is the average value of the DC-link current. Thus, the duty ratio of the active vectors can be written as;

$$d_x = m_c \sin\left(\frac{\pi}{6} - \beta_i\right) = \frac{T_x}{T_s}$$

$$d_y = m_c \sin\left(\frac{\pi}{6} + \beta_i\right) = \frac{T_y}{T_s} \quad (4-32)$$

$$d_{c0} = 1 - d_x - d_y = \frac{T_{c0}}{T_s}$$

T_x , T_y and T_{c0} are the applied time durations of corresponding vectors in a switching period.

For unity input current transfer ratio (e.g. $m_c = 1$) the zero current vector is not used in the construction of $\overline{I_i}$. Thus,

$$T_s = T_x + T_y,$$

for unity current modulation index ^[47].

II. Inversion stage

A similar analysis can be carried out to explain the operating principle of inversion stage. The inversion stage is two-level voltage source inverter as shown in Fig.4. 7. Note that “S_i”, (i = 7, 8, 9, 10, 11, 12) is the name of a switch and “s_i”, (i = 7, 8, 9, 10, 11, 12) is the state of the corresponding switch.

The matrix converter rules can be stated as;

$$\begin{aligned}
 s_7 + s_8 &= 1 \\
 s_9 + s_{10} &= 1 \\
 s_{11} + s_{12} &= 1
 \end{aligned}
 \tag{4-33}$$

for a switching period of T_s.

The switches of the voltage source inverter in each leg must never be turned-off so that possibility of an open circuit can be avoided, and likewise both switches must not be turned-on to avoid from a possible short circuit at the output side. Table 4. 3 displays all allowed switching combinations for the inversion stage.

Table 4. 3 All allowable switching configurations for the inversion stage

Switching Configuration	Switch States	Output line-to-line Voltages			Output Phase Voltage Vector		DC-link Current
	$\begin{bmatrix} S_7 & S_9 & S_{11} \\ S_8 & S_{10} & S_{12} \end{bmatrix}$	V _{ab}	V _{bc}	V _{ca}	$ \bar{V}_o $	$\angle \bar{V}_o$	I _{DC+}
1	$\begin{bmatrix} 1 & 0 & 0 \\ 0 & 1 & 1 \end{bmatrix}$	V _{DC}	0	-V _{DC}	$\frac{2}{3}V_{DC}$	0	i _a
2	$\begin{bmatrix} 1 & 1 & 0 \\ 0 & 0 & 1 \end{bmatrix}$	0	V _{DC}	-V _{DC}	$\frac{2}{3}V_{DC}$	$\frac{\pi}{3}$	-i _c
3	$\begin{bmatrix} 0 & 1 & 0 \\ 1 & 0 & 1 \end{bmatrix}$	-V _{DC}	V _{DC}	0	$\frac{2}{3}V_{DC}$	$\frac{2\pi}{3}$	i _b
4	$\begin{bmatrix} 0 & 1 & 1 \\ 1 & 0 & 0 \end{bmatrix}$	-V _{DC}	0	V _{DC}	$\frac{2}{3}V_{DC}$	π	-i _a
5	$\begin{bmatrix} 0 & 0 & 1 \\ 1 & 1 & 0 \end{bmatrix}$	0	-V _{DC}	V _{DC}	$\frac{2}{3}V_{DC}$	$-\frac{2\pi}{3}$	i _c
6	$\begin{bmatrix} 1 & 0 & 1 \\ 0 & 1 & 0 \end{bmatrix}$	V _{DC}	-V _{DC}	0	$\frac{2}{3}V_{DC}$	$-\frac{\pi}{3}$	-i _b
7	$\begin{bmatrix} 1 & 1 & 1 \\ 0 & 0 & 0 \end{bmatrix}$	0	0	0	0	-	0
8	$\begin{bmatrix} 0 & 0 & 0 \\ 1 & 1 & 1 \end{bmatrix}$	0	0	0	0	-	0

Referring the Table 4. 3, the first six switching configurations (1, 2, 3, 4, 5, 6) explain the active vectors which produce a non-zero output voltage and the remaining two configurations (7, 8) represent the zero vectors which produce zero output voltage. The six active vectors have fixed angular positions in complex plane. Each vector refers to the connections of DC-link voltage to the output. In order to generate balanced and sinusoidal output line currents, the output phase voltage reference vector \overline{V}_o has to be synthesized by using voltage space vectors. The magnitude of the phase voltage vector, $v_o(t)$ is also proportional to the DC-link voltage. By using space vector transformation, balanced and sinusoidal three-phase output phase voltages can be transformed into a reference output phase voltage vector, \overline{V}_o as;

$$\overline{V}_o = \frac{2}{3}(v_a(t) + a v_b(t) + a^2 v_c(t)) = v_o(t)e^{j\alpha_o(t)} \quad (4-34)$$

where $v_o(t)$ is the instantaneous magnitude and $\alpha_o(t)$ is the instantaneous angular position of the reference vector with respect to the \overline{V}_1 at time t in complex plane as can be seen in Fig.4. 11.

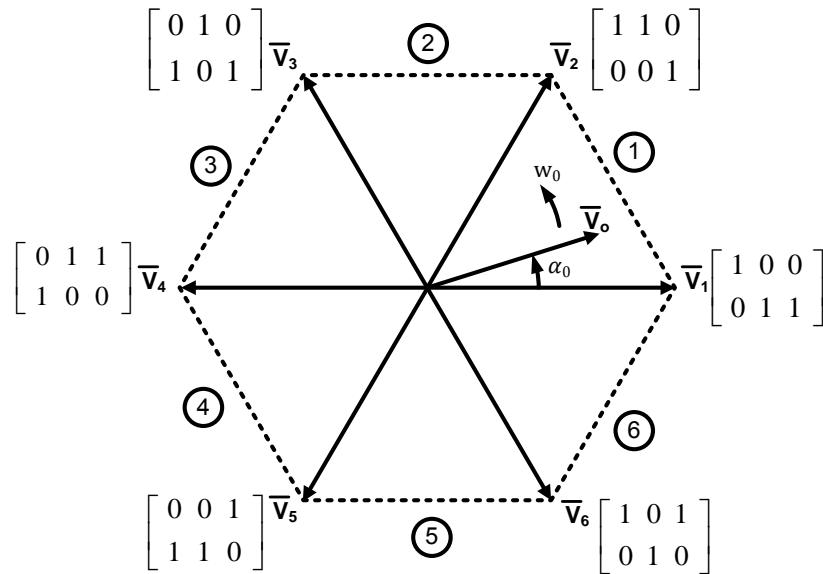


Fig.4. 11 Active output voltage space vectors, related sectors, and the reference output phase voltage vector, \overline{V}_o in complex plane

The space vector diagram for the voltage source inverter is divided into six sectors. In the same way as in the rectification stage, the reference output phase voltage vector can be

synthesized by two adjacent (active) space vectors and a zero voltage vector. The angular position of the reference phase voltage vector is determined by the active vectors. The magnitude of the reference vector, \bar{V}_o is determined by both the zero and the active vectors. The time domain relationships between the output phase voltage waveforms and the sectors are shown in Fig.4. 12.

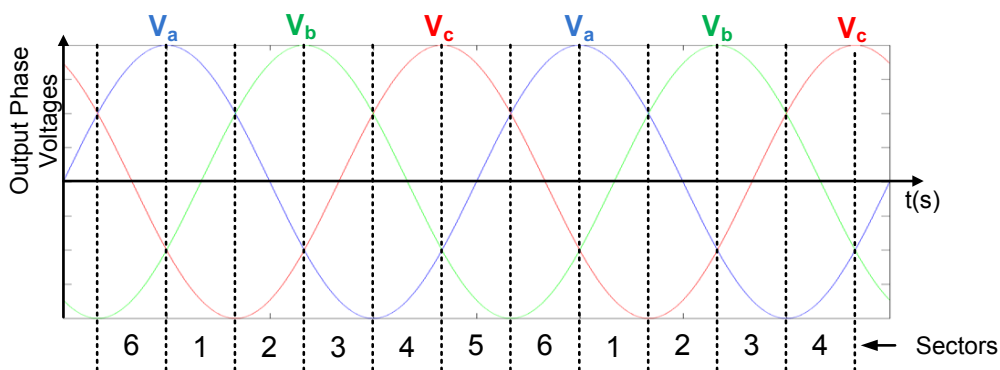


Fig.4. 12 Time domain relationship between the output phase voltage waveforms and sectors

For a switching period T_s , the reference phase voltage vector \bar{V}_o can be synthesized as below.

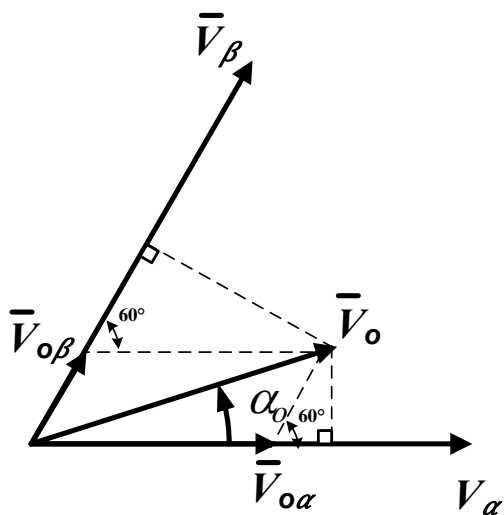


Fig.4. 13 Reference phase voltage vector construction

Two adjacent active vectors, \overline{V}_α and \overline{V}_β which are contributing to \overline{V}_o with the duty ratios d_α and d_β and a zero vector with duty ratio d_{v0} are used in the synthesis. To synthesize rotating reference voltage vectors at different magnitudes and phases, it is necessary to compute duty ratios for each switching period. The reference phase voltage vector can be written in basic form as follows;

$$\overline{V}_o = \overline{V}_{o\alpha} + \overline{V}_{o\beta} \quad (4-35)$$

with

$$\overline{V}_{o\alpha} = \overline{V}_\alpha d_\alpha, \quad \overline{V}_{o\beta} = \overline{V}_\beta d_\beta \quad (4-36)$$

Then, the duty ratios are;

$$d_\alpha = \frac{|\overline{V}_{o\alpha}|}{|\overline{V}_\alpha|}, \quad d_\beta = \frac{|\overline{V}_{o\beta}|}{|\overline{V}_\beta|}.$$

Also,

$$|\overline{V}_{o\alpha}| = \frac{|\overline{V}_o| \sin(\frac{\pi}{3} - \alpha_0)}{\sin(\frac{\pi}{3})}, \quad |\overline{V}_{o\beta}| = \frac{|\overline{V}_o| \sin(\alpha_0)}{\sin(\frac{\pi}{3})}.$$

Hence, the duty ratios can be written as;

$$d_\alpha = \frac{|\overline{V}_o|}{\sqrt{\frac{3}{2}}|\overline{V}_\alpha|} \sin(\frac{\pi}{3} - \alpha_0), \quad d_\beta = \frac{|\overline{V}_o|}{\sqrt{\frac{3}{2}}|\overline{V}_\beta|} \sin(\alpha_0) \quad (4-37)$$

$$|\overline{V}_\alpha| = |\overline{V}_\beta| = \frac{2}{3} |V_{DC}|, \quad \frac{\sqrt{3}|\overline{V}_o|}{|V_{DC}|} = m_v \quad \text{and} \quad 0 \leq m_v \leq 1$$

where m_v is the voltage modulation index which represents the input to output voltage transfer ratio and V_{DC} is the average value of the DC-link voltage. Thus, the duty ratios of the active vectors can be written as;

$$d_\alpha = m_v \sin(\frac{\pi}{3} - \alpha_0) = \frac{T_\alpha}{T_s} \quad (4-38)$$

$$d_\beta = m_v \sin(\alpha_0) = \frac{T_\beta}{T_s}$$

After calculating the duty ratios d_α and d_β , the duty ratio of zero phase voltage vector can be written as follow;

$$d_{v0} = 1 - d_\alpha - d_\beta = \frac{T_{v0}}{T_s} \quad (4-39)$$

III. Synchronization Between the Rectification and Inversion Stages

In the previous two sections, applications of space vector PWM for the rectification and the inversion stages are investigated separately. In fact, both stages are dependent with each other due to the power flow on imaginary DC-link. Since there is no energy storage element in the converter, the power flow from input to output can be assumed as equal by neglecting the switching losses. The space vector PWM is applied in the rectification stage so that it supplies maximum average DC voltage to maximize the overall input voltage to output voltage transfer ratio. That means the modulation index of rectification stage, m_c , is set to unity. On the other hand, the rectifier stage always provides a conduction path between the input terminals and DC-link. The magnitude of the input currents depends on DC-link current. Besides that, the DC-link current I_{DC} depends on the amplitude of output load currents, voltage modulation index m_v and the output load displacement angle, φ_o . Hence, the synchronization of both stages can be achieved inherently by setting the modulation index of rectification stage to unity for same switching period, T_s ^[47].

4.2.4 Application of the Indirect Space Vector PWM for Direct Matrix Converter

As referred to Chapter 2, the functionality of the direct matrix converter and the indirect matrix converter are very similar in most cases. Referring the Table 4. 1, the states of group 1 cannot be used in indirect space vector PWM method, because the instantaneous connection of three input phases to three output phases is not possible. If the switching configurations placed in group 1 are not used in direct matrix converter structure, it is also described as an equivalent circuit combining current source rectifier and voltage source inverter connected through imaginary DC-link as shown in Fig.4. 7. In other words, direct matrix converter can be modeled as an indirect matrix converter.

Also, an electrically equivalent state of direct and indirect matrix converter structure is expressed as visually in Fig.2. 14. Similarly, the other switching configurations stated in

Table 4. 1, except the switching configurations in Group1, can be verified. This situation is also providing the opportunity for implementing the indirect space vector PWM strategy to the direct matrix converter topology. However, indirect space vector PWM strategy described separately for rectification and inversion stages (e.g. two separate transfer functions) in previous two sections should be merged into one transfer function for the direct matrix converter structure. The single transfer function can be constructed by multiplying the transfer functions of rectifier and inverter stages. Then, the transfer function of direct matrix converter system can be modeled as a product of separate transfer functions,

$$T_{DMC} = T_{VSI}T_{VSR} \quad (4-40)$$

where T_{DMC} is the transfer function of direct matrix converter, T_{VSI} is the transfer function of two-level voltage source inverter and T_{VSR} is the transfer function of voltage source rectifier. Then the input current/voltage, fictitious DC-link current/voltage and output current/voltage variables can be derived as follow;

$$T_{VSR} = \begin{bmatrix} s_1 & s_2 & s_3 \\ s_4 & s_5 & s_6 \end{bmatrix} \quad (4-41)$$

$$T_{VSI} = \begin{bmatrix} s_7 & s_9 & s_{11} \\ s_8 & s_{10} & s_{12} \end{bmatrix}^T \quad (4-42)$$

From the required simultaneous output currents, the DC-link current can be as follows;

$$\begin{bmatrix} I_{DC+} \\ I_{DC-} \end{bmatrix} = T_{VSI}^T \begin{bmatrix} I_a \\ I_b \\ I_c \end{bmatrix}. \quad (4-43)$$

The maximum DC-link voltage can be constructed from the input voltages;

$$\begin{bmatrix} V_{DC+} \\ V_{DC-} \end{bmatrix} = T_{VSR} \begin{bmatrix} V_A \\ V_B \\ V_C \end{bmatrix}. \quad (4-44)$$

Also, the input current and output voltage variables can be synthesized from the DC-link variables.

$$\begin{bmatrix} I_A \\ I_B \\ I_C \end{bmatrix} = T_{VSR}^T \begin{bmatrix} I_{DC+} \\ I_{DC-} \end{bmatrix} \quad (4-45)$$

$$\begin{bmatrix} V_a \\ V_b \\ V_c \end{bmatrix} = T_{VSI} \begin{bmatrix} V_{DC+} \\ V_{DC-} \end{bmatrix} \quad (4-46)$$

Then, the input current and output voltage variables for the direct matrix converter can be written in the following form;

$$\begin{bmatrix} V_a \\ V_b \\ V_c \end{bmatrix} = T_{VSI} T_{VSR} \begin{bmatrix} V_A \\ V_B \\ V_C \end{bmatrix}, \quad (4-47)$$

$$\begin{bmatrix} I_A \\ I_B \\ I_C \end{bmatrix} = T_{VSR}^T T_{VSI}^T \begin{bmatrix} I_a \\ I_b \\ I_c \end{bmatrix}. \quad (4-48)$$

Both the input current reference vector and output voltage reference vector have to be synthesized within each switching cycle. This objective will be achieved by selecting the equivalent switch states for control of virtual inverter stage and virtual rectifier stage with direct matrix converter structure. In order to explain the space vector PWM method, reference vectors for the output voltage and the input current are assumed as in Fig.4. 14(a) and Fig.4. 14(b). This assumption does not affect the general validity of the analysis. Similarly, the other possible vector combinations can be used. Also note that the space vectors are stated in Table 4. 1.

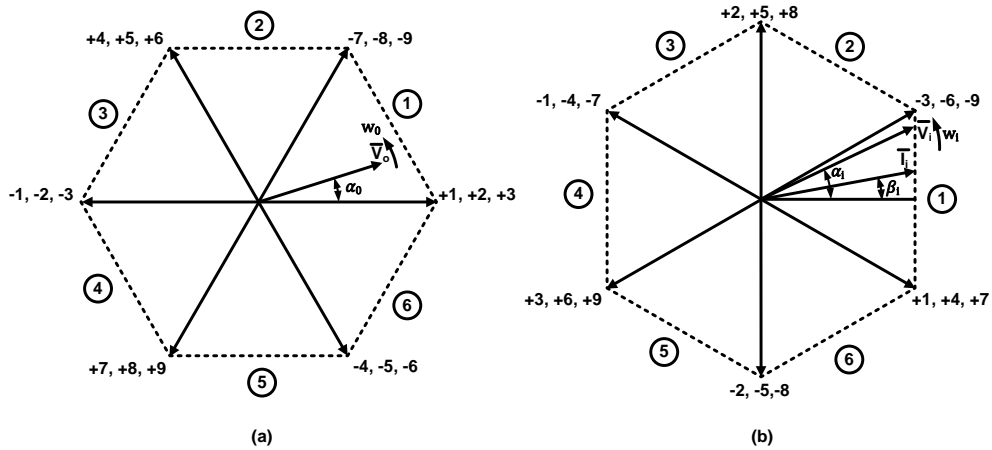


Fig.4. 14 (a) Voltage space vectors (b) current space vectors

Both the voltage and current vector hexagons contain six sectors. Therefore, there are 36 combinations of sector pairs (1-1, 1-2, 1-3, ..., 2-1, 2-2, ...) as listed in Table 4. 4.

The reference vectors, \bar{V}_o and \bar{I}_l shown in Fig.4. 14 can be constructed with the following four vectors within one switching period, to create average output voltages as close as possible to expected output fundamental phase voltages in form of space vector and simultaneously to keep the input line current displacement angle as close as to unity ^[48]. It is noted that the definitions of the vectors are stated in Table 4. 1.

Table 4. 4 Sector pairs and useable vectors

		Sector of Output Phase Voltage Vector					
		1	2	3	4	5	6
Sector of Input Phase Line Vector	1	-3 1 9 -7	9 -7 -6 4	-6 4 3 -1	3 -1 -9 7	-9 7 6 -4	6 -4 -3 1
	2	2 -3 -8 9	-8 9 5 -6	5 -6 -2 3	-2 3 8 -9	8 -9 -5 6	-5 6 2 -3
	3	-1 2 7 -8	7 -8 -4 5	-4 5 1 -2	1 -2 -7 8	-7 8 4 -5	4 -5 -1 2
	4	3 -1 -9 7	-9 7 6 -4	6 -4 -3 1	-3 1 9 -7	9 -7 -6 4	-6 4 3 -1
	5	-2 3 8 -9	8 -9 -5 6	-5 6 2 -3	2 -3 -8 9	-8 9 5 -6	5 -6 -2 3
	6	1 -2 -7 8	-7 8 4 -5	4 -5 -1 2	-1 2 7 -8	7 -8 -4 5	-4 5 1 -2

These vectors are applied for a fraction of a period T_s . Two of the four vectors are used to form the current reference vector. And the other two vectors are responsible for forming the output voltage reference vector. Similarly, it is possible to determine the four switches configurations corresponding to any possible combination of input and output reference vectors, which are listed in Table 4. 1 according to the input and output sector areas.

I. Duty cycle calculation for each vector

In previous section, the duty ratio calculations of rectifier and inverter stage are derived separately. In this section, the five new duty ratios of four active vector pair and a zero vector can be derived from the product of rectifier duty ratios in equations (4-32) and inverter duty ratios in (4-38). $d_{x\alpha}, d_{x\beta}, d_{y\alpha}$ and $d_{y\beta}$ are the four new duty ratios of four

vectors listed in Table 4. 4, respectively. The new duty ratios for these vectors can be written as follows;

$$d_{x\alpha} = d_x d_\alpha = m_c \sin\left(\frac{\pi}{6} - \beta_i\right) m_v \sin\left(\frac{\pi}{3} - \alpha_0\right) = \frac{T_{x\alpha}}{T_s} \quad (4-49)$$

$$d_{x\beta} = d_x d_\beta = m_c \sin\left(\frac{\pi}{6} - \beta_i\right) m_v \sin(\alpha_0) = \frac{T_{x\beta}}{T_s} \quad (4-50)$$

$$d_{y\alpha} = d_y d_\alpha = m_c \sin\left(\frac{\pi}{6} + \beta_i\right) m_v \sin\left(\frac{\pi}{3} - \alpha_0\right) = \frac{T_{y\alpha}}{T_s} \quad (4-51)$$

$$d_{y\beta} = d_y d_\beta = m_c \sin\left(\frac{\pi}{6} + \beta_i\right) m_v \sin(\alpha_0) = \frac{T_{y\beta}}{T_s} \quad (4-52)$$

Then the duty ratio of zero vector, d_0 can be written as;

$$d_0 = 1 - d_{x\alpha} - d_{x\beta} - d_{y\alpha} - d_{y\beta} = \frac{T_0}{T_s} \quad (4-53)$$

Consequently, if the six switching configurations in Group 1 are not used, the direct matrix converter can be modeled as a virtual indirect matrix converter and the indirect space vector PWM method can be applicable for direct matrix converter structure. The implementation of this modulation method is digitally simple and this modulation scheme is able to provide input power factor control and maximum input to output voltage transfer ratio as 0.86. In this study by taking these items into account, indirect space vector modulation technique is preferred with direct matrix converter structure ^[48].

II. Construction of switching patterns

During the construction of vector sequences single-sided or double sided switching patterns can be used. The ordered patterns have a high influence on the performance and the efficiency of converter. To prefer one of these, two criteria are considered;

- Harmonic performance of the converter,
- Minimum switching losses.

Single-sided switching pattern is usually used to minimize total switching losses while the double-sided switching pattern is preferred for better harmonic performance at the input and output sides ^[3]. Fig.4. 15 shows a single-sided and Fig.4. 16 shows a double-sided switching pattern. In double-sided switching, the switching period is divided into two equal intervals and in both these intervals the four selected active vectors and a zero vector are applied. In the last of these two intervals, the sequence order of the active vectors is

reversed. The zero vectors can be applied anywhere in the switching period. In this study, for the better harmonic performance double-sided switching pattern is preferred and the zero vectors are applied in the center of the switching period.

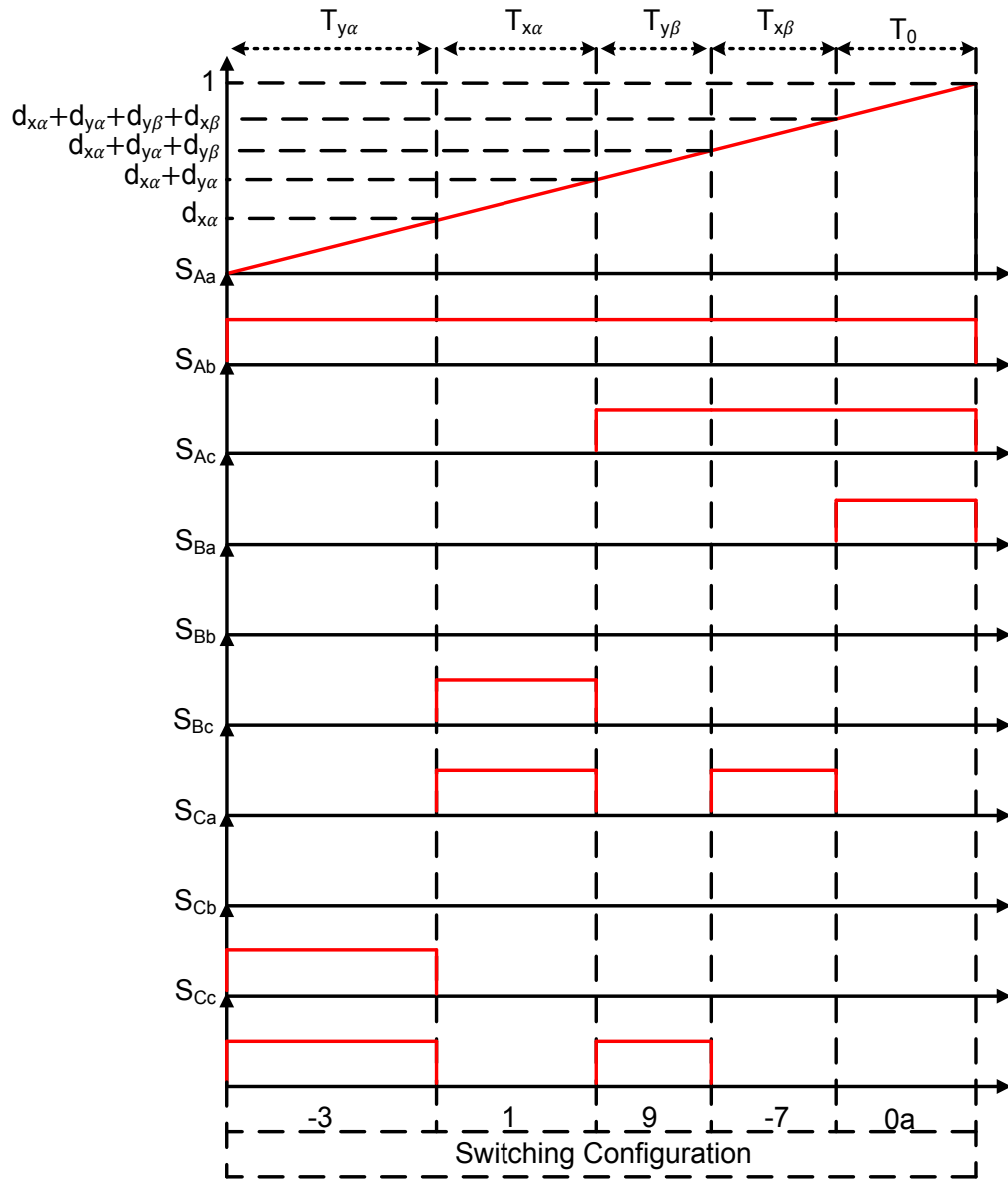


Fig.4. 15 Nine switching pulses for a carrier frequency of 10 kHz with single-sided switching pattern

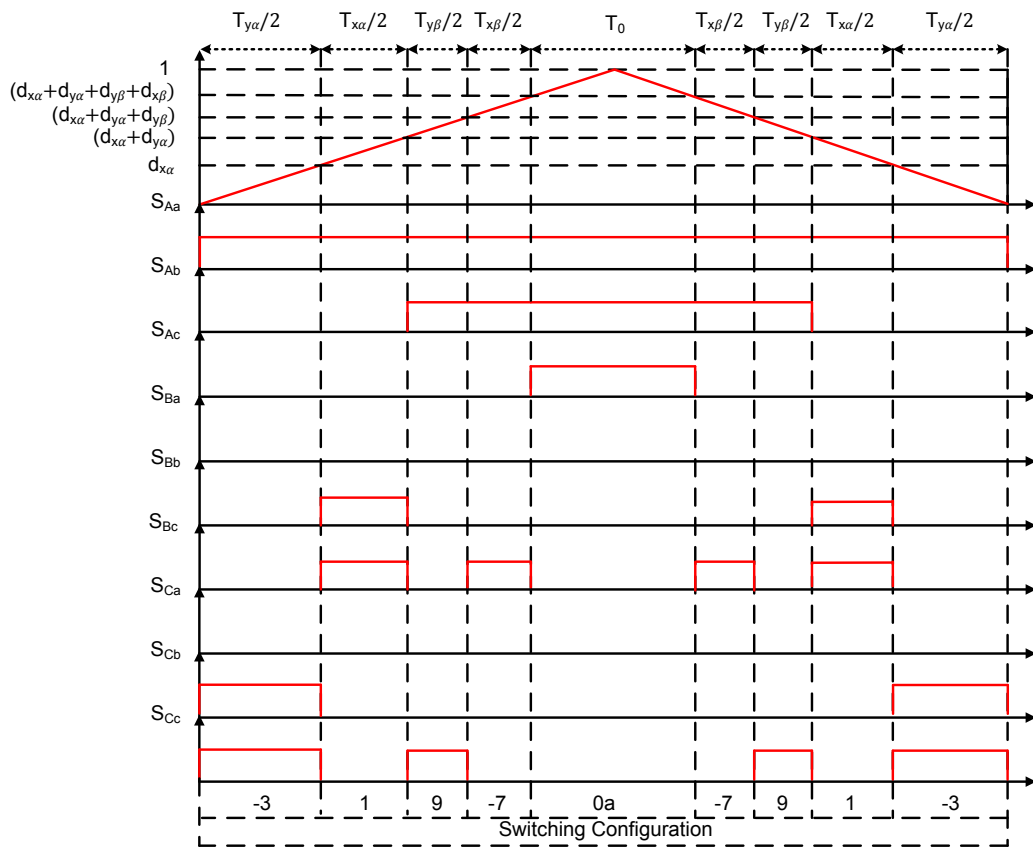


Fig.4. 16 Nine switching pulses for a carrier frequency of 10 kHz with double-sided switching pattern

CHAPTER 5

SYSTEM MODELING AND SIMULATIONS

In this chapter, detailed MATLAB/Simulink models for simulation of direct matrix converter and permanent magnet synchronous motor drive system are developed and simulation results are presented. The drive system model consists of a three-phase power supply, a three-phase input filter, the direct matrix converter, control logic and a surface mounted permanent magnet synchronous motor. The overall simulation model is implemented by using Simpower System Tool Box.

The modeling and simulation play important role in the design, analysis and evaluation of power systems which require complex control. In this study, simulation model of direct matrix converter feeding a balanced three-phase passive load is constructed first. The open-loop and closed-loop operations of direct matrix converter are investigated by using indirect space vector modulation technique. Then, the simulation model of diode-rectified two-level voltage source inverter is introduced and performance analysis of direct matrix converter is carried out by comparing with diode-rectified two-level voltage source inverter. Finally, the overall performance evaluation of direct matrix converter integrated permanent magnet synchronous motor drive system is provided. During the closed-loop simulations, field oriented control theory is utilized. The purpose of the simulations is to verify the characteristics of direct matrix converter. Also, the simulation results of direct matrix converter model and integrated drive system model are verified experimentally in next chapter.

5.1 MODELING OF DIRECT MATRIX CONVERTER

The input filter is needed to be designed first to develop the main circuit simulation model.

5.1.1 Input Filter Design

Although a matrix converter draws sinusoidal current from the input and deliver sinusoidal current to the load with a sinusoidal voltage actually, it is a switched-mode device and draws discontinuous currents from the AC-grid. Unfiltered (discontinuous) input phase “A” current and its harmonic spectrum are shown in Fig.2. 7 and Fig.2. 8. The harmonic currents flowing through the line impedances distort the line voltage and create power quality problems for other consumers. The harmonics may also create spurious resonance problems in the line due to distributed line inductances and capacitances, or extra passive filters installed in the line. In order to attenuate the harmonics injected to the three-phase AC mains, an input filter is needed. The input filter must attenuate the current harmonics at switching frequency and its multiples. Hence, the cut-off frequency of input filter must be much lower than the switching frequency. Also, the cut-off frequency of input filter must be much higher than the frequency of AC-grid system ^[17]. Thus, the design criteria for the input filter are:

- The input filter must have a cut-off frequency lower than the switching frequency. Let L_f and C_f be the filter inductor and the filter capacitor and w_0 be the resonance frequency of the input filter;

$$w_0 = \frac{1}{\sqrt{L_f C_f}}$$

- The cut-off frequency of filter should be much higher than the AC mains,
- The volume and the weight of the input filter should be minimum,
- The input filter should cause a low phase shift between the input phase voltages and the line currents,
- The input filter should not reduce the overall system stability. That is, the input filter should not amplify any harmonic component at any frequency,
- The voltage drops on the filter inductances at the rated current should be kept in minimum in order to let the input to output transfer ratio to the maximum. In other words, the filter impedance at the operating frequency should be minimized.

Considering all the criteria, a simple LC filter can be used to filter out these undesirable switching frequency harmonics. The harmonic contents of the input current can be analyzed first performing some operational tests on converter circuit without using input filter and then filter resonance frequency may be selected by considering the harmonic contents of the input currents. This analysis is important since each component used in the hardware implementation has different manufacturing tolerances and these differences may cause inevitable inaccuracies during the commutation period. As a result of this situation, the harmonic content of the input currents may show differences from theoretically expected harmonic contents (e.g. harmonics at switching frequency and its multiple, no subharmonic content is expected). Therefore, this situation should also be taken into account. Moreover, basic LC filter has high gain at its cut-off frequency. Thus, additional damping is required for stable converter operation. If there is no damping, these unexpected current harmonics can be amplified excessively jeopardizing the stability of the system. The reliability of the system can be enhanced by increasing the damping present in the filter through resistors paralleled with the filtering inductors. Different configurations of input filters have been proposed in the literature ^[34, 49, 50] as shown in Fig.5. 1.

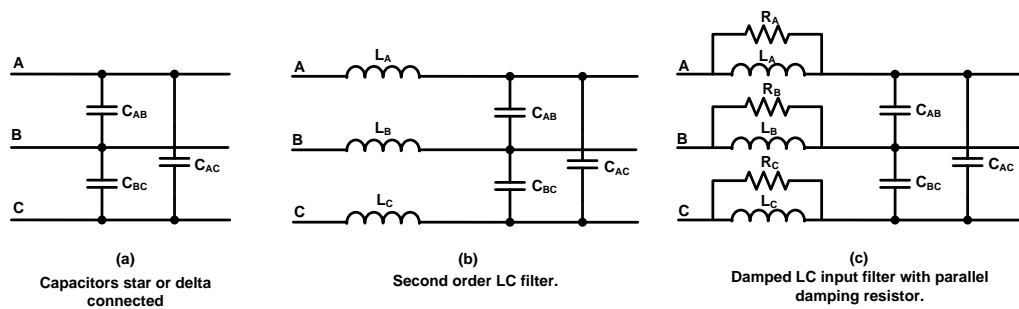


Fig.5. 1 Input filter configurations used for matrix converter input filters

The input filter configuration in Fig.5. 1(a) is not commonly used for practical applications, because, it does not offer a good solution for converter topologies. In order to reduce harmonic components at switching frequency (10 kHz for this study) and multiples with this configuration, size of the capacitance becomes large. Hence, this configuration is not feasible. The input filter configurations in Fig.5. 1(b) and Fig.5. 1(c) are used in various applications with components of moderate sizes. Hence, a second order LC filter

configuration is chosen usually. The per-phase equivalent form of Fig.5. 1(c) in frequency domain is as shown in Fig.5. 2.

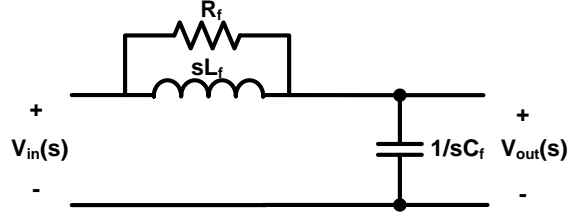


Fig.5. 2 Laplace transform of per-phase equivalent circuit

The transfer function ($G_{RLC}(s)$) of this filter with elements L_f and C_f with a damping resistor, R_f is expressed by equation (5-1).

$$G_{RLC}(s) = \frac{V_{out}(s)}{V_{in}(s)} = \frac{\frac{1}{sC_f}}{\frac{1}{sC_f} + \left(\frac{1}{R_f} + \frac{1}{sL_f}\right)^{-1}} \quad (5-1)$$

$$= \frac{sL_f + R_f}{s^2L_fR_fC_f + sL_f + R_f}$$

The transfer function ($G_{LC}(s)$) of the filter without damping resistor R_f can be obtained from (5-1) by substituting $R_f \rightarrow \infty$, and;

$$G_{LC}(s) = \frac{1}{s^2L_fC_f + 1}. \quad (5-2)$$

Assuming that the input power factor is to be greater than 0.9 at 10% rated load or at higher power levels then the maximum value for C_f is given by ^[51];

$$\text{Maximum value of } C_f = \frac{P_{out} \tan(\varphi_i)}{3V_i^2 w_i}. \quad (5-3)$$

Considering the design specifications for the system in this thesis as P_{out} 100 W, V_i 26 V, and the input angular frequency, w_i 100π rad/sec, the maximum value of C_f results as, 76 μ F. C_f is chosen therefore as 10 μ F.

Then the inductor size L_f is chosen as 1.5 mH to give a resonance frequency much less than the switching frequency but sufficiently higher than the supply frequency.

Finally, the resistor, R_f should be suitable selected such that the power losses will be minimized while the damping set to a critical level. An optimal value for damping resistor is obtained as a suitable selection based on different transfer functions plotted against R_f . Here it came out to be 94 Ohm. The bode plots of the LC filter configurations are presented in the Fig.5. 3 and Fig.5. 4.

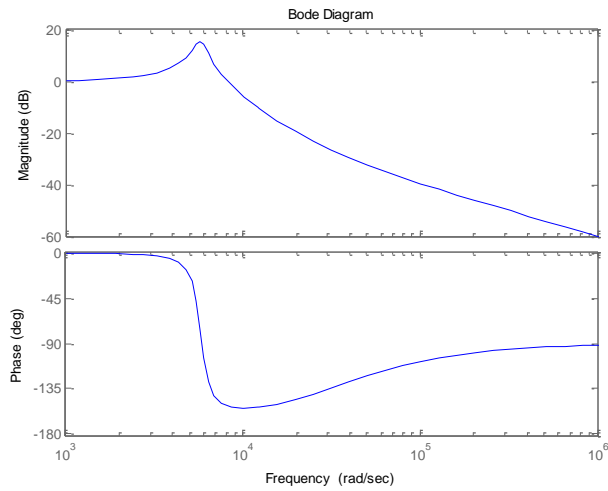


Fig.5. 3 Magnitude and phase plot of the LC filter with $R_f = 94$ Ohm

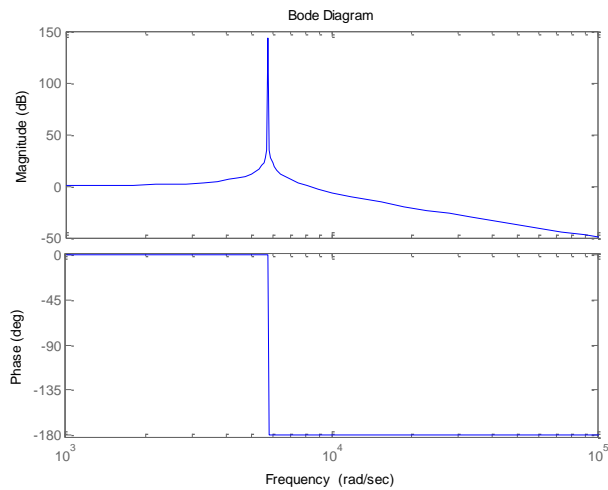


Fig.5. 4 Magnitude and phase plot of the LC filter without damping resistor

Plots in Fig.5. 3 and Fig.5. 4 show that both filter configurations seem as a good solution to reduce the harmonics at the AC input terminals with nearly zero dB gains and zero phase delays around the input frequency 50 Hz (314 rad/sec). However, the second order LC filter has great amplification at its resonance frequency without damping resistor R_f . If the input current has harmonics at the same or near frequency to the resonance frequency (5800 rad/sec), the system will be unstable. Hence in implementing the direct matrix converter use of a LC filter with parallel damping resistor configuration becomes much feasible to ensure the stability of the system.

The structure of the model of the direct matrix converter being simulated model is shown in Fig.5. 5.

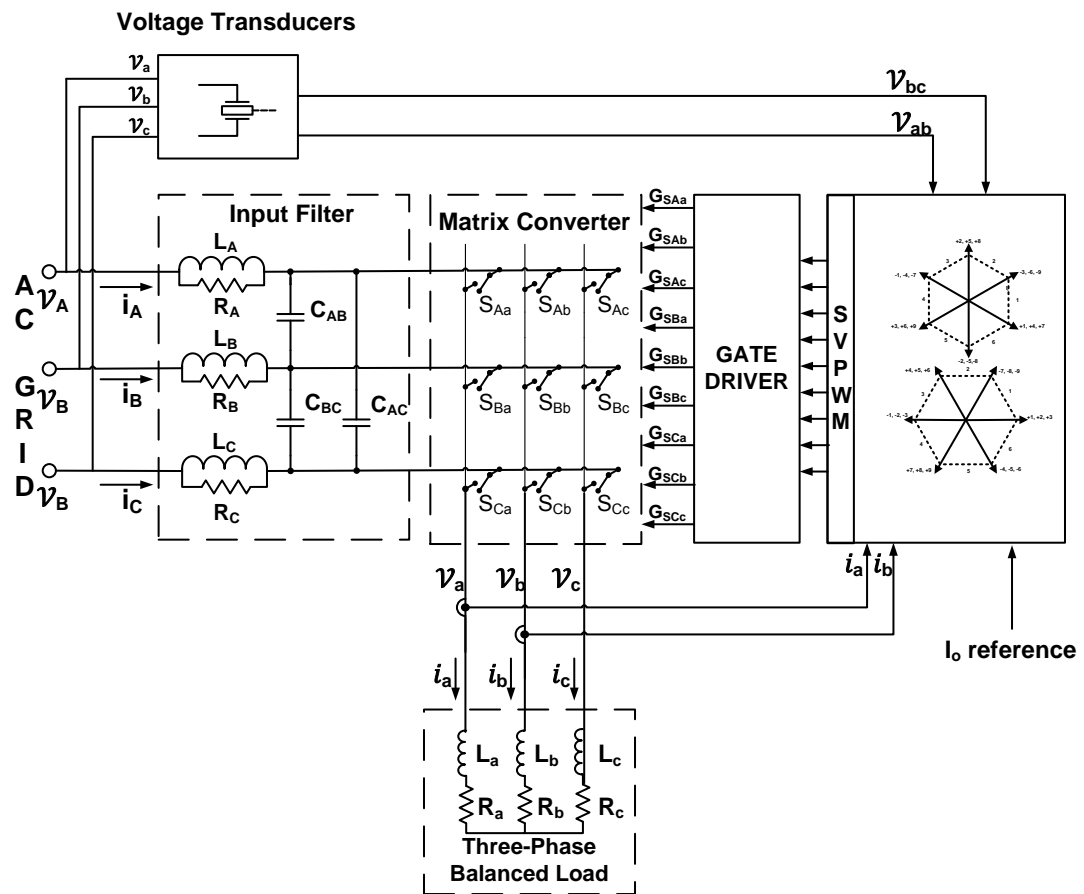


Fig.5. 5 The block diagram of the direct matrix converter model for simulation

5.1.2 Construction of Bi-directional Power Switch Structures

The main objects in the matrix converter power stage are the bi-directional (AC) switches. The switches have to block voltage in either polarity and allow current flow in both directions. Since, bi-directional switches are not commercially available, this switch structure here has to be built up with commercially available devices. In this study, N-channel power MOSFETs are used to build up the common source bi-directional switch structure and model.

5.1.3 Steps for the Simulation of Indirect Space Vector PWM for the Direct Matrix Converter

In Chapter 4, the modulation techniques of matrix converters were discussed and the derivation of indirect space vector modulation technique for direct matrix converters was presented. In this study, the indirect space vector PWM was simulated with direct matrix converter.

As an overview, the modulation procedure is described as follows:

- Calculate the angles of the input current reference vector and the output voltage reference vector in order to determine the sectors respectively,
- Select the suitable four active vectors and the zero vector. The two of the four active vectors are used to synthesize the input current reference vector and the remaining two active vectors are used for construction of output voltage reference vector,
- Calculate the duty-ratios required in constructing both the input current and the output voltage reference vectors,
- Finally, to synthesize the input current and output voltage vectors, necessary control signals of the bi-directional switches are created.

5.2 SIMULATIONS ON DIRECT MATRIX CONVERTER REGARDING TO OUTPUT CHARACTERISTICS

Simulink is a very effective tool for modeling of complex systems. These models can include both continuous and discrete-time components. Simpower System Tool Box of Simulink is used to construct the simulation model of the electrical power systems (e.g. consisting of continuous states). Besides, the standard block sets (e.g. including discrete components) of Simulink are used to construct the control structure of matrix converter. These two models can be easily incorporated. The separation between the control system and the converter power stage allows the user to simulate and analyze the complex systems easily.

During the implementation of matrix converter output current direction based four-step commutation was used. Both the switching frequency and the sampling frequency were set up to 10 kHz in Simulink model.

In this section, the overall simulation model of the direct matrix converter system is presented and the simulation results are investigated. The supply, input filter and the load parameters used in the simulations are as following;

Table 5. 1 Simulation parameters

Symbol	Name	Value	Unit
V_{AB}	Line-to-line supply peak voltage	26	V
L_f	Per-phase input filter inductor	1.54	mH
C_f	Per-phase input filter capacitor	10	μF
R_f	Per-phase input filter resistor	94	Ohm
R_{l-1}	Line-to-line load resistor	1.6	Ohm
L_{l-1}	Line-to-line load inductor	11.6	mH

This section starts with the investigation of open-loop controlled direct matrix converter system operating with a passive balanced load. The results obtained in the simulations verified the correct use of the implemented indirect space vector PWM algorithm. Results also show that the direct matrix converter operates correctly. Then, control performance of the direct matrix converter output line currents using PI controller is implemented. In fact the development of a closed-loop system is important for the control of the dynamic loads like electric motors. The purpose of the open-loop simulations is to verify the effectiveness

of matrix converter operation under passive load. In order to verify the operation of matrix converter integrated permanent magnet motor drive system, closed-loop control is preferred.

5.2.1 Simulations of Open-Loop System with Balanced R-L Load

At the beginning, a study has been carried out to investigate the effectiveness of the implemented SVPWM algorithm in generating the desired input current and output voltage waveforms. The analysis begins with the investigation of the output voltage and the output current in terms of the magnitudes and phases. The theoretical analysis is performed with using per-phase equivalent circuit model of three-phase balanced passive load shown in Fig.5. 6.

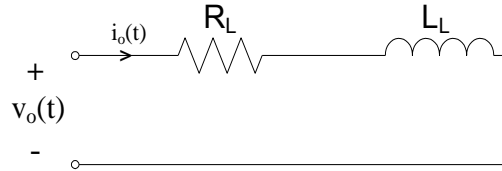


Fig.5. 6 Per-phase equivalent circuit model of three-phase balanced passive load

R_L and L_L are the per-phase equivalent resistor and inductor respectively.

The analytical model of the one-phase circuit is stated in (5-4).

$$v_o(t) = i_o(t)R_L + L_L \frac{di_o(t)}{dt} \quad (5-4)$$

After taking the Laplace transforms, the output voltage, $v_o(t)$ to output current, $i_o(t)$ transfer function, $G_{i_o v_o}(s)$ (i.e. the admittance at the input terminals of the circuit) can be obtained as follows:

$$V_o(s) = I_o(s)R_L + L_L s I_o(s) \quad (5-5)$$

$$I_o(s) = V_o(s) \frac{1}{(L_L s + R_L)} \quad (5-6)$$

Defining $\tau_e = \frac{L_L}{R_L}$ as the electrical time constant, the transfer function can be expressed as:

$$G_{I_o V_o}(s) \stackrel{\text{def}}{=} \frac{I_o(s)}{V_o(s)} = \frac{1}{R_L(\tau_e s + 1)} \quad (5-7)$$

Let the direct matrix converter considered as the SVPWM block shown in Fig.5. 7.

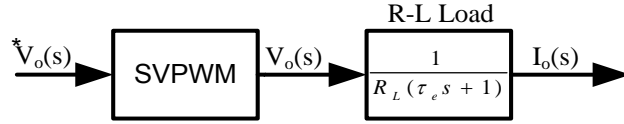


Fig.5. 7 Block diagram of direct matrix converter in open-loop and a R-L load

The SVPWM block denotes the PWM algorithm and converter circuit together. Ideally, the SVPWM block is expected to have unity gain and should not cause any phase lag/lead, and therefore, SVPWM block is assumed to have unity gain and no delay. Then, the model in Fig.5. 7 reduces to;

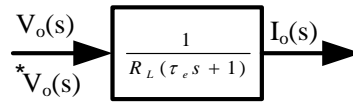


Fig.5. 8 Block diagram for the direct matrix converter with unity gain assumption and the R-L load

In order to verify this assumption, the space vector pulse width modulated direct matrix converter was simulated and simulation results were analyzed. The output voltage to output current transfer function gain and phase delay are observed using these simulation results. In order to show that SVPWM algorithm and the converter circuit model do not cause any effect on the transfer function, measured phase delay and transfer function ratio should be equal to the calculated phase delay and ratio for the inductive-resistive load. In other words, if SVPWM algorithm and converter circuit are ideal, direct matrix converter circuit can be thought as an ideal three-phase voltage source and the transfer function ratio and phase delay of the combined system (i.e. direct matrix converter and R-L load) must only depend on load characteristic. The theoretical (e.g. ideal) transfer function ratio and phase delay plots are shown in Fig.5. 9.

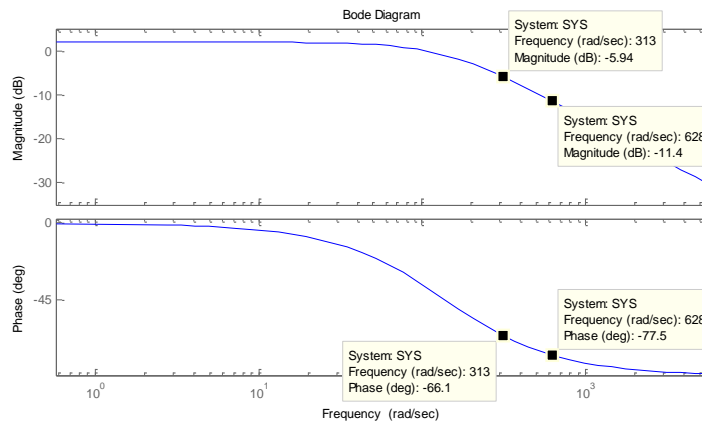


Fig.5. 9 Theoretical magnitude and phase plots of load transfer function

In Fig.5. 9, data cursors are placed at 50 Hz (314 rad/s) and 100 Hz (628 rad/s) frequencies. For the verification of SVPWM block that has unity gain and no phase delay, some simulation results are required. Hence, the simulation results are illustrated first. The verification of SVPWM block is postponed to the end of this section.

The open-loop steady-state simulation results for three-phase balanced passive load are obtained for the peak value of the load current at 5A (full load) and the output frequency is 50 Hz. The output voltage waveforms of the direct matrix converter are shown in Fig.5. 10 - Fig.5. 15. First three waveforms show the output phase voltages that are measured with respect to the neutral point and the remaining three waveforms show the output line-to-line voltages. These waveforms are obtained when the matrix converter is connected to a perfectly three-phase passive balanced load. Also, it should be noticed that no output filter is connected to the matrix converter.

In DC-link converters, the output voltage waveforms have flat shaped compared to the matrix converter output voltage waveforms because the AC voltages are first converted into DC voltage and then reconverted back to the AC voltage waveform. Hence, the output voltage peak values are always equal to the DC-link voltage. In the matrix converter topologies, the AC grid is directly connected to the output phases. Thus, there is not any energy storing elements and the input voltages are directly used for generating the output voltages. The following figures also verify this situation. The peak voltages have variable magnitudes because of the AC input voltage waveforms.

As shown in Fig.5. 10 - Fig.5. 15, the output phase and line-to-line voltage waveforms are symmetrical. Referring the Fig.5. 10, zero voltage line divides the waveform into two symmetrical halves. Generally for sinusoidal AC waveforms, the shape of the waveform above the zero voltage axis is same as the shape of the waveform below it. However, it is not possible to obtain symmetrical output phase and line-to-line voltage waveforms for all operating frequencies in this topology. The symmetrical output voltage waveforms are obtained at the output if the output operating frequencies are integer submultiples of input voltage frequency (e.g. f_i , $f_i/2$, $f_i/3$, ...). For the simulations in Fig.5. 10 - Fig.5. 15, input supply frequency and the output operating frequency are set to 50 Hz.

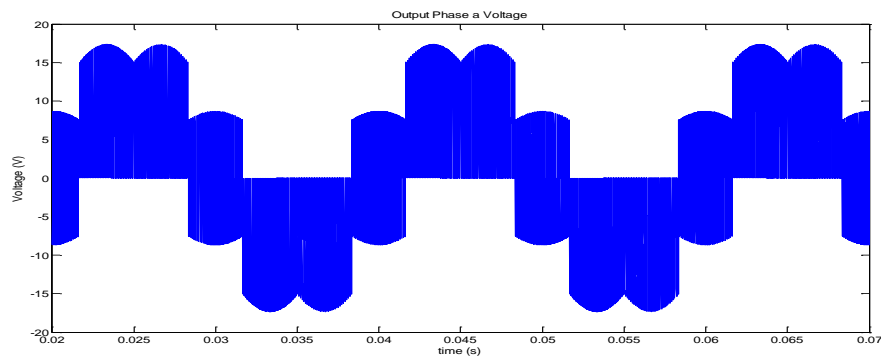


Fig.5. 10 Output phase “a” to neutral voltage, V_{an} ($f_o = 50$ Hz)

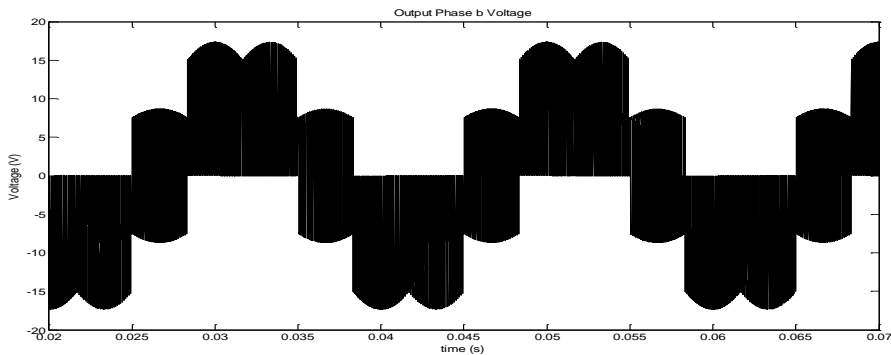


Fig.5. 11 Output phase “b” to neutral voltage, V_{bn} ($f_o = 50$ Hz)

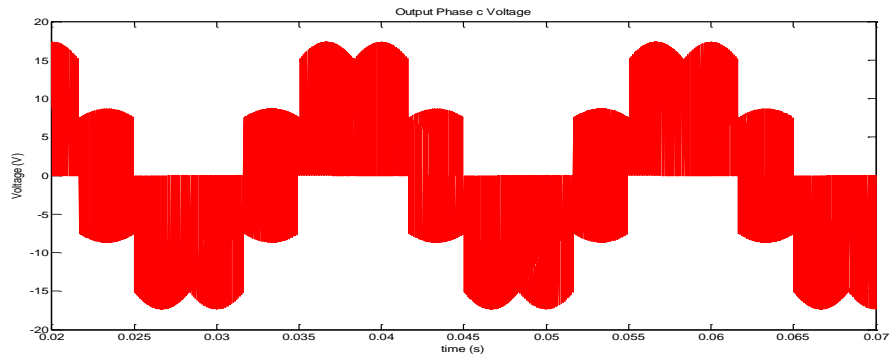


Fig.5. 12 Output phase “c” to neutral voltage, V_{cn} ($f_o = 50$ Hz)

The open-loop simulations were carried out to observe the effectiveness of the implemented algorithms for direct matrix converter. The following three waveforms show the output line-to-line voltages. It can be seen that the line-to-line output waveforms contain more than two voltage levels. However, the differences between the magnitudes of line-to-line output peak voltages are very close to each other. These output voltage waveforms mainly contains two absolute levels, 0 V and 26 V. Therefore, this converter structure is also a member of two-level converters.

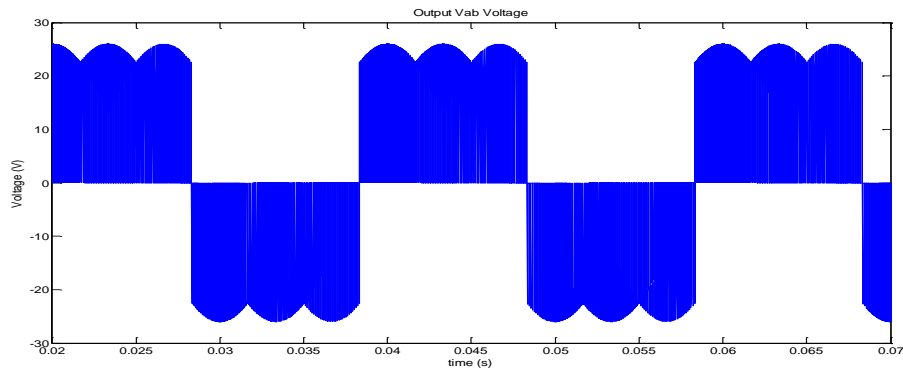


Fig.5. 13 Output line-to-line voltage V_{ab} ($f_o = 50$ Hz)

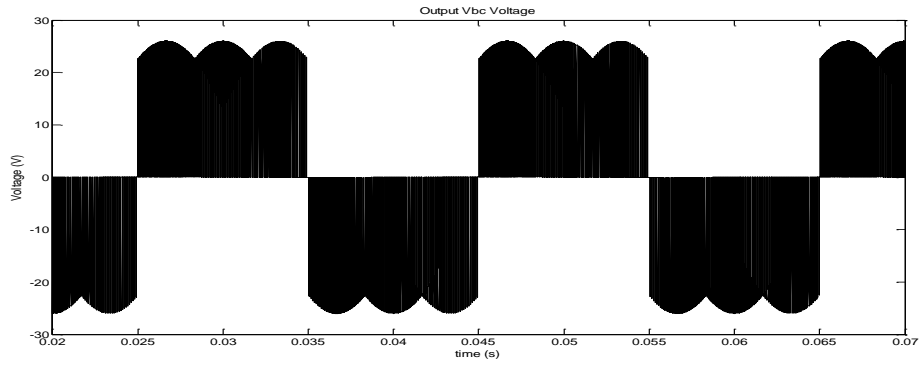


Fig.5. 14 Output line-to-line voltage V_{bc} ($f_o = 50$ Hz)

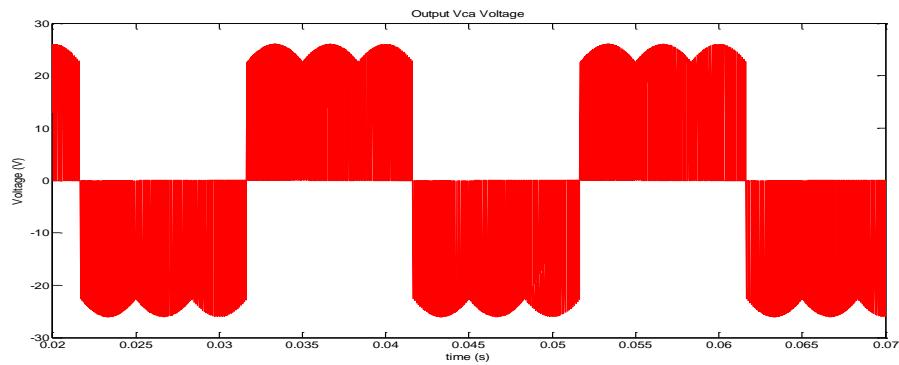


Fig.5. 15 Output line-to-line voltage V_{ca} ($f_o = 50$ Hz)

As we can see in Fig.5. 13 - Fig.5. 15, the output line-to-line voltages are not exactly sinusoidal waves. These waveforms also contain harmonic components. For the simulated line-to-line voltage waveform V_{ab} , the corresponding total harmonic distortion (THD) is given as 86.41%. The harmonic spectrum of the output line-to-line voltage V_{ab} is given in Fig.5. 16 with considerable high-frequency harmonics especially at integer multiples of switching frequency and at the side bands of these frequencies. The generation of harmonics is not exclusive to this topology. Almost all power converters have similar problem. For some applications, output filters will be needed to reduce high-frequency harmonic components. However, for the servo drive application this is not a mandatory situation.

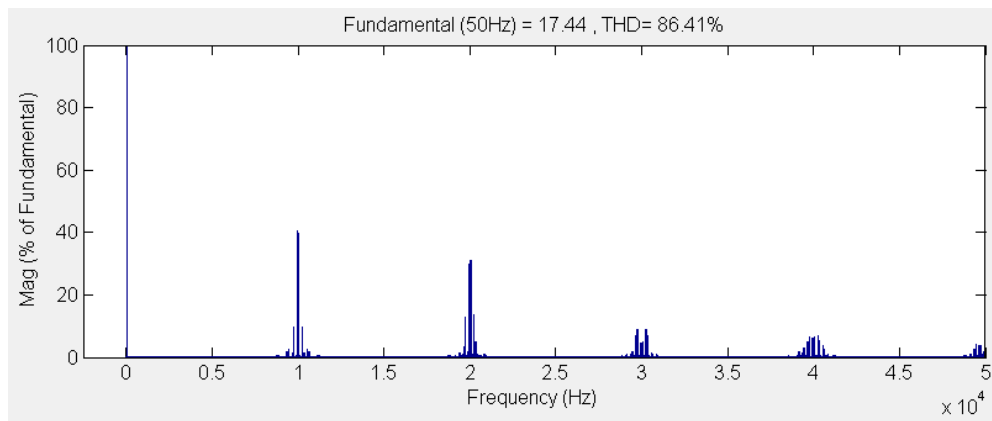


Fig.5. 16 Harmonic spectrum of output line-to-line voltage V_{ab} ($f_o = 50$ Hz)

Fig.5. 17 and Fig.5. 18 show the output load currents and the harmonic spectrum of phase “a” current. As we can see below, the total harmonic distortion on the load current is highly reduced as expected because the resistive-inductive load acts as a filter. This current waveform is quite adequate for smooth torque control operations. If this attenuation is needed for harmonic content of the output voltage waveforms, an output filter should be used before the load.

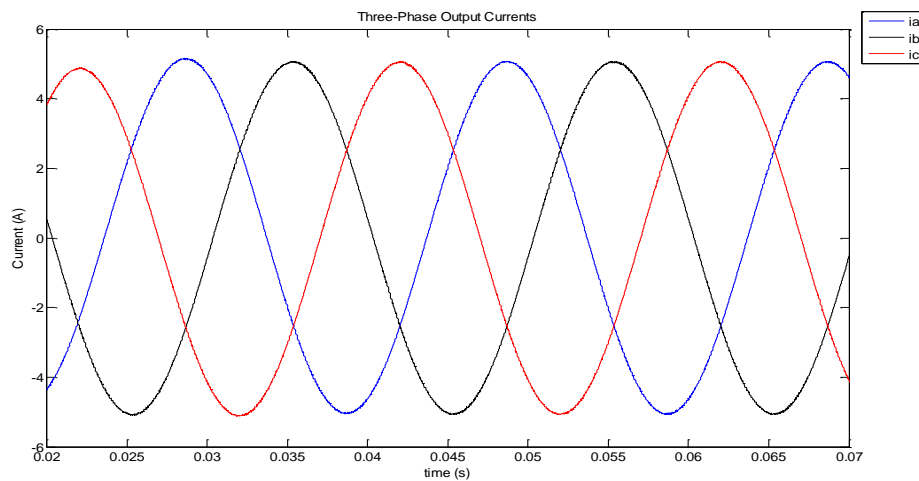


Fig.5. 17 Waveforms of the load currents ($f_o = 50$ Hz)

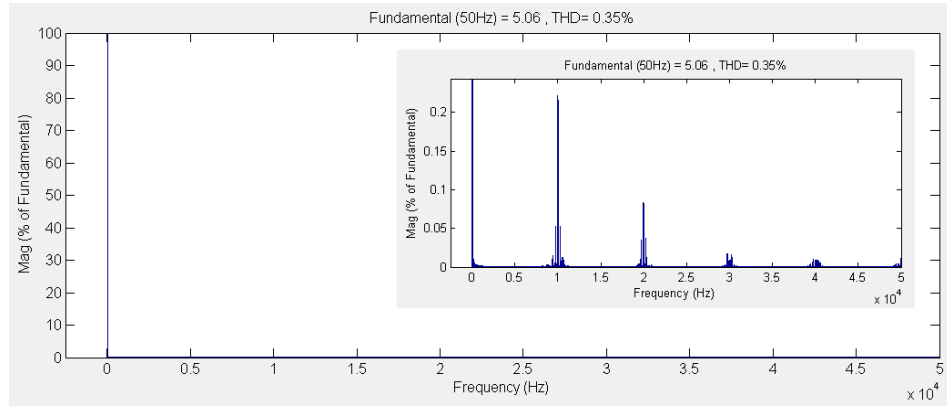


Fig.5. 18 Harmonic spectrum of the output phase “a” current ($f_o = 50$ Hz)

The three-phase voltages and currents are symmetric and have 120° phase shift from each other. For this reason, in the following illustrations only one line-to-line and one phase-to-neutral voltage waveform will be presented for ease tracking.

As mentioned in Section 1.1.2, cycloconverter is also a type of direct AC/AC converters. However, it has drawbacks like as the output frequency must have to be lower than the input frequency and cycloconverters have poor harmonic performance. To fill this gap, matrix converters have been developed. In order to show that matrix converter can operate at higher output frequencies than the input supply frequency, a simulation is performed for 50 Hz input and 100 Hz output frequency. The output phase “a” voltage, V_{an} with respect to the neutral point and the output line-to-line voltage, V_{ab} are shown in Fig.5. 19 and Fig.5. 20. These waveforms are obtained for a peak value of the load current is 3A and the output frequency is 100 Hz.

As shown in Fig.5. 19 - Fig.5. 20, the shapes of the output voltage waveforms above the zero voltage axes are not same as the shapes below the zero voltage axes (i.e. there is no half-cycle symmetry exactly). As mentioned above, it is not possible to obtain symmetrical output voltage waveforms if the output operating frequency is different from integer submultiples of input voltage frequency (e.g. f_i , $f_i/2$, $f_i/3$, ...).

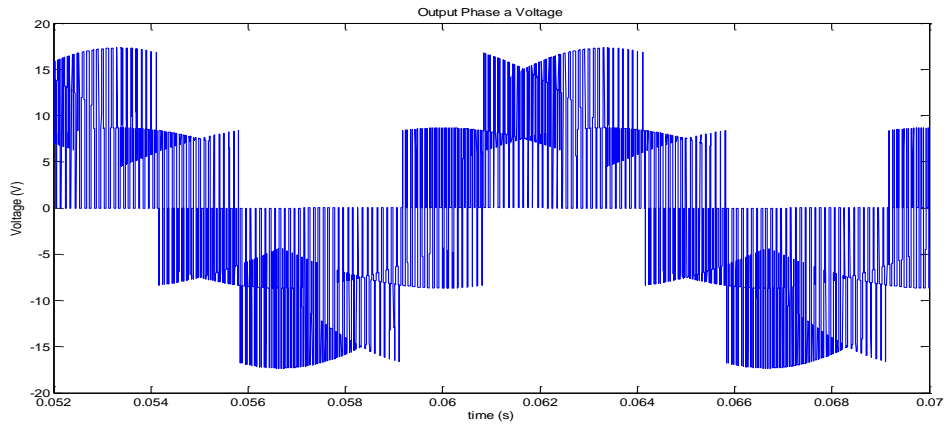


Fig.5. 19 Output phase “a” to neutral voltage, V_{an} ($f_o = 100$ Hz)

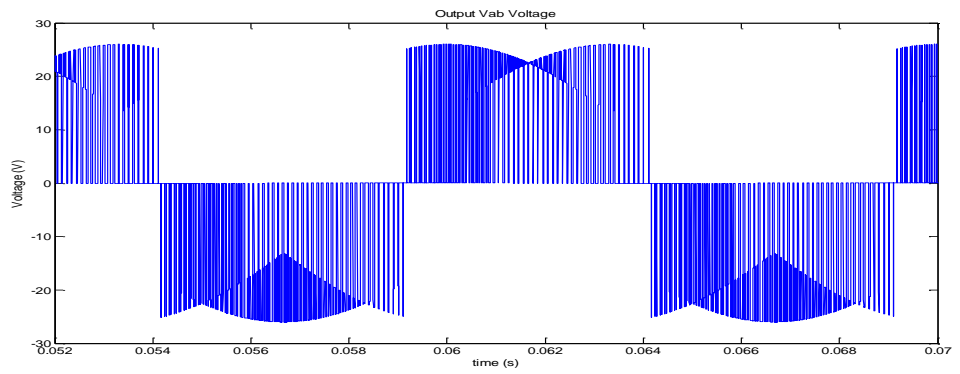


Fig.5. 20 Output line-to-line voltage V_{ab} ($f_o = 100$ Hz)

Fig.5. 21 shows the frequency spectrums of the output line-to-line voltage.

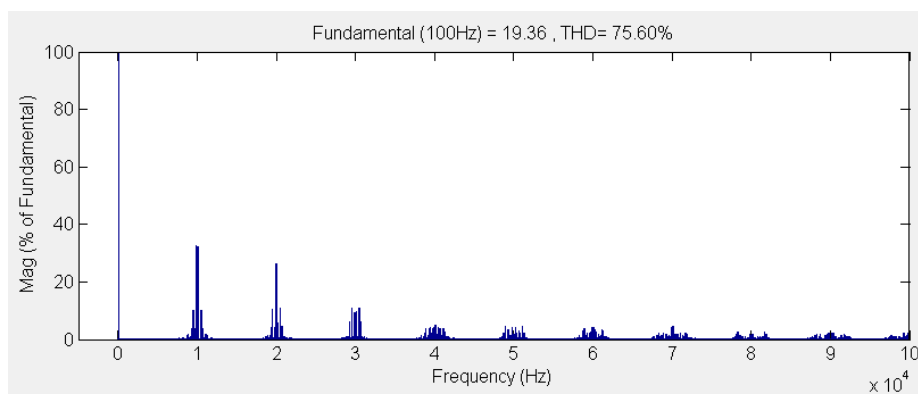


Fig.5. 21 Harmonic spectrum of output line-to-line voltage V_{ab} ($f_o = 100$ Hz)

As can be seen in Fig.5. 21, the harmonic distortion THD for $f_o = 100$ Hz is quite similar with the obtained waveforms for $f_o = 50$ Hz. These results also show that there are no significant low order harmonics in the output voltage waveforms. It should be noted that these higher frequency harmonics can easily be filtered out.

Fig.5. 22 and Fig.5. 23 show the output load currents and the harmonic spectrum of output phase “a” current.

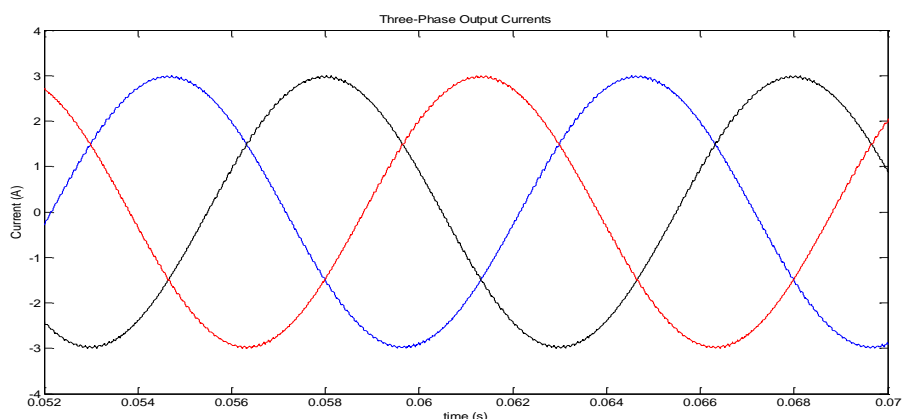


Fig.5. 22 Waveforms of the load currents ($f_o = 100$ Hz)

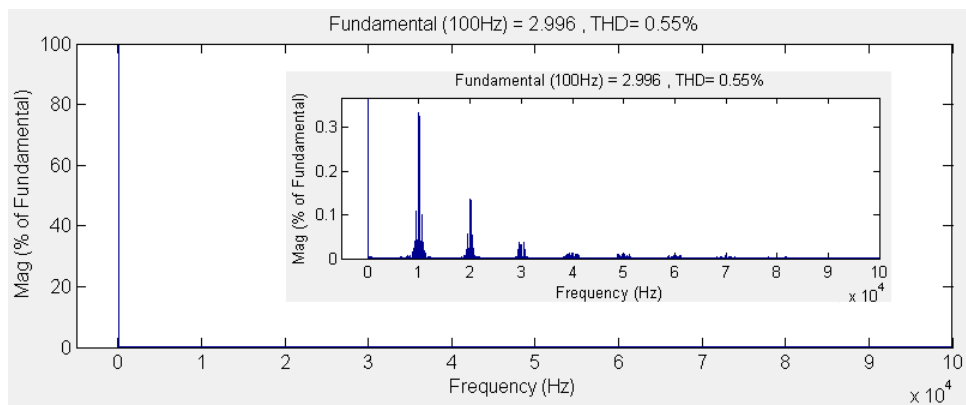


Fig.5. 23 Harmonic spectrum of the output phase “a” current ($f_o = 100$ Hz)

The current frequency spectrum includes familiar harmonic components which are switching frequency related and multiples of it. As expected, the harmonic component at switching frequency is dominant according to the other harmonic components.

At that point, we have all the required output voltage and current waveforms to verify that SVPWM block has unity gain and does not generate additional phase delay. Thus, we will continue with the verification of SVPWM block. The load impedance characteristics can be seen in Fig.5. 9. The ideal output voltage to output current ratio (gain) and phase delay can also be observed in Fig.5. 9. Those are theoretical values and stated in the Table 5. 2. These values will be compared with observed output voltage to output current ratio and phase magnitude values from simulation results to verify the assumption that the SVPWM block has unity gain and no additional phase delay.

Table 5. 2 Calculated theoretical gain and phase angles for R-L load

	50 Hz	100 Hz
Output Voltage to Current Gain	0.504 (-5.94 dB)	0.269 (-11.4 dB)
Phase Delay	-66.1°	-77.5°

Then considering Fig.5. 16 and Fig.5. 18, for the 50 Hz output frequency, peak value of the fundamental component of the output phase “a” current is observed as 5.06A and peak value of fundamental component of the line-to-line voltage is observed as 17.44V in the open-loop system involving the direct matrix converter and the passive R-L load. Then the output voltage to output current transfer gain for this open-loop system can be calculated from these results as $\left| \frac{I_{a_{peak}}}{V_{an_{peak}}} \right| = \frac{5.06}{(17.44/\sqrt{3})} = 0.503$. This result shows that the gain of the open-loop system is same with the calculated gain of the R-L load only indicating that the direct matrix converter itself has unity gain thus proving the assumption made of the beginning of the simulations. In similar way, same calculation can be done for 100 Hz output frequency.

Moreover, the additional phase delay generated from the SVPWM algorithm and converter circuit can be found easily by comparing the phase delay between the reference and observed line-to-line output voltage waveforms. The two waveforms should go through their zero voltage points at the same time and in the same direction. As seen is Fig.5. 24 the zero voltage crossing points are coincident. It shows that the waveforms are in phase. Therefore, SVPWM algorithm and matrix switches does not cause any phase delay in the simulation model. For the practical realization, this situation will be slightly different

because of the additional delays caused by data acquisitioning, processing systems, and the non-linear characteristics caused by the semiconductor switches like as turn-on/off times and the on state voltage drops.

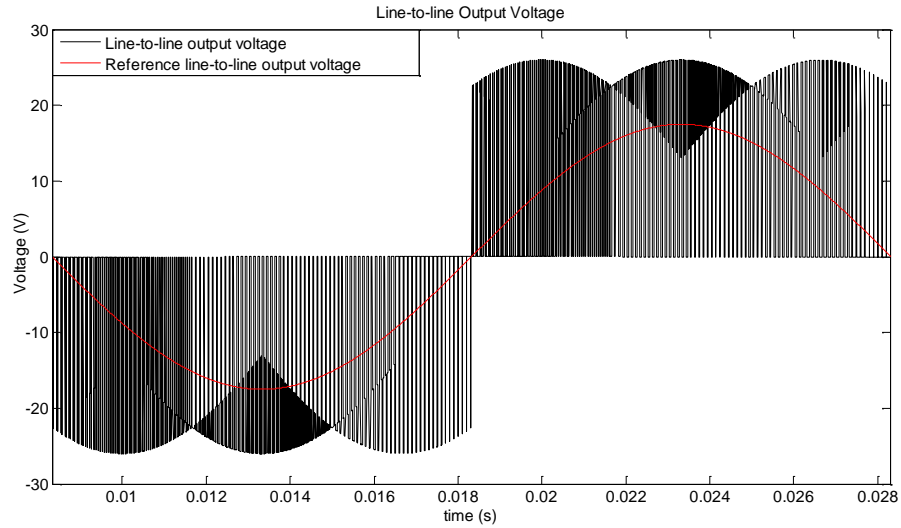


Fig.5. 24 Reference and observed output line-to-line voltage waveform, V_{ab}

Fig.5. 25 demonstrates the output current and voltage waveforms, and the control signals issued to the semiconductor switches at a commutation instant. Fig.5. 26 may be useful, in order to understand the explanations about the waveforms given in Fig.5. 25.

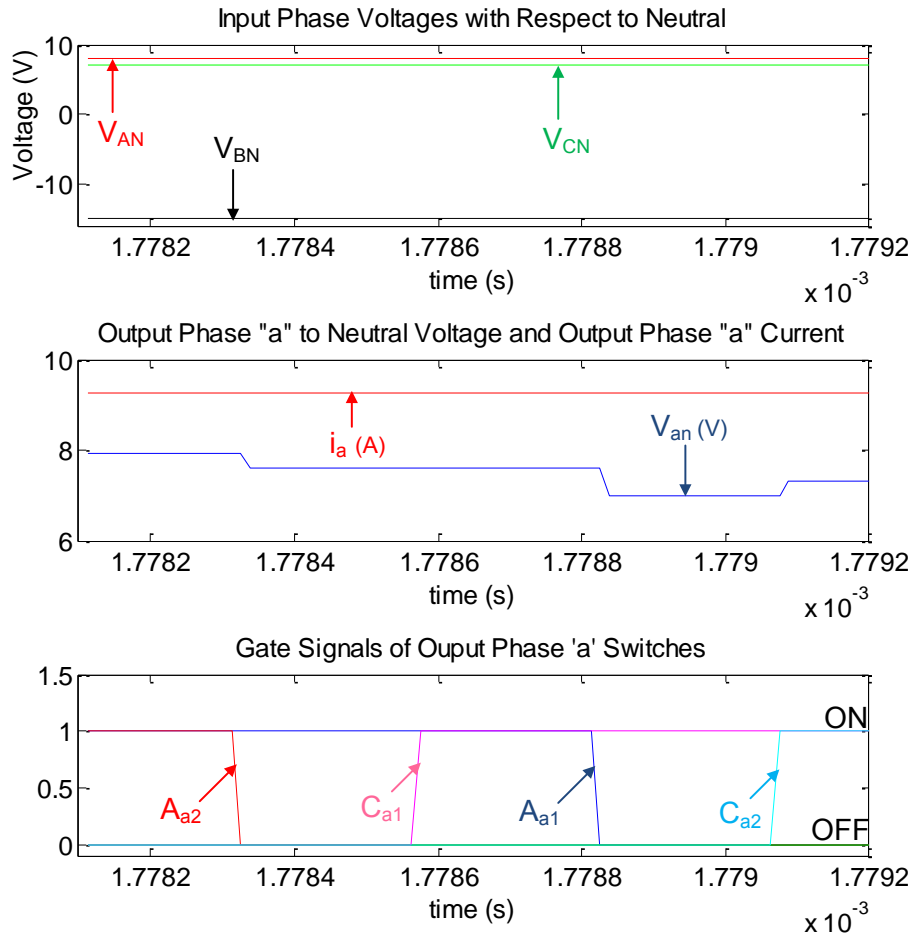


Fig.5. 25 Output current and voltage waveforms and the control signals of the semiconductor switches at a commutation instant

Considering Fig.5. 25, when the MOSFET A_{a2} is turned-off (at $t \cong 1.7783 \times 10^{-3}$ sec), the inductive load current flows through the free-wheeling diode, D_{Aa2} and the output phase "a" voltage, V_{an} is reduced by the amount of diode voltage drop.

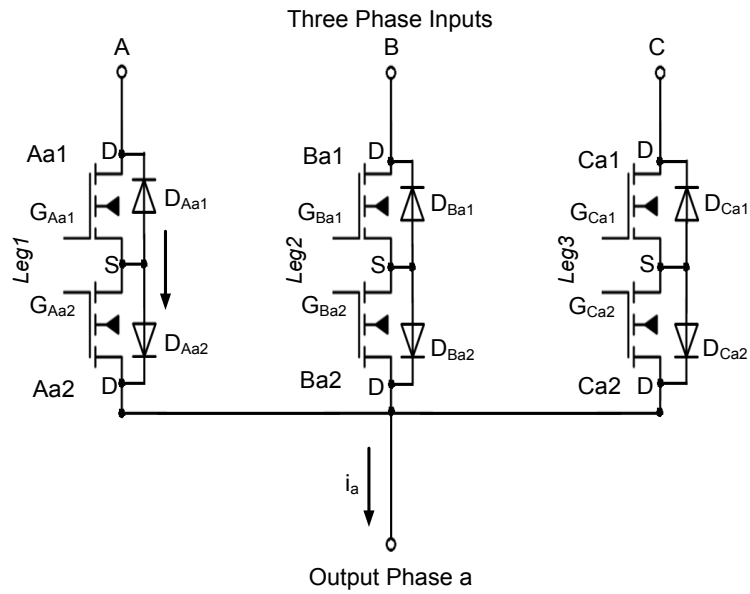


Fig.5. 26 Single phase output circuit structure

From the first plot in Fig.5. 25, we can see that V_{AN} is greater than V_{CN} . Therefore, we cannot expect any change at the output waveform when the MOSFET C_{a1} is turned-on at ($t \cong 1.7786 \times 10^{-3}$ sec) and is left turned-on. Because, the free-wheeling diode D_{Ca2} on the Leg3 is reversed biased and no electrical connection established. Later, the MOSFET A_{a1} is turned-off at ($t \cong 1.7788 \times 10^{-3}$ sec) and any current path does not remain on Leg1 anymore. The inductive current i_a flows through the diode D_{Ca2} . Now, the output phase “a” voltage is equal to difference of input phase “C” voltage and voltage drop of free-wheeling diode D_{Ca2} . Finally, MOSFET C_{a2} is turned-on at ($t \cong 1.7791 \times 10^{-3}$ sec) and the current flows through the MOSFETs on Leg3. In fact, the on state resistances of the MOSFETs are relatively low. Hence, for the low current levels the voltage drop on these MOSFETs can be negligible comparing with the diode forward voltages.

Ideally, the current flow has to be transferred immediately to the input phase “C” when the current commutation from input phase “A” to input phase “C” is required. However, it is not practical due to the finite turn-on and turn-off times of semiconductor devices. In addition to this, turn-on and turn-off times of semiconductor devices may show differences due to the manufacturing tolerances. Hence, in order to provide safe commutation between the semiconductor switches, when a switch is turned-off, turned-on of the other switch is delayed by a blanking time (dead-time). The effect of dead-time on the output voltage

magnitude is shown in Fig.5. 25. It can be easily seen that the voltage drops on semiconductor devices and the dead-time duration generate nonlinearity at the output voltage magnitude.

5.2.2 Closed-Loop Simulations with Balanced Three-Phase R-L Load

Closed-loop operation of direct matrix converter can be shown in block diagram form shown in Fig.5. 27. The output currents are measured separately and then used as feedbacks to the control system.

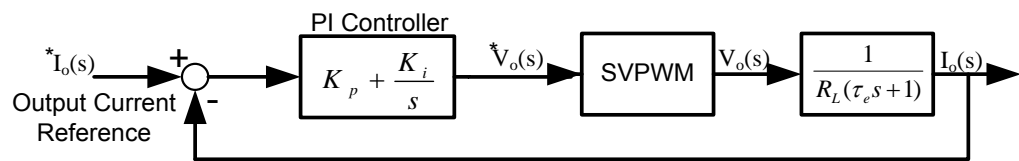


Fig.5. 27 Block diagram of the closed-loop system involving the direct matrix converter with RL load

Since the space vector pulse width modulated direct matrix converter (shown as SVPWM block in Fig.5. 27) is a unity gain with zero phase shift block as verified in the previous section, we can assume that the SVPWM direct matrix converter block has unity gain and does not cause any phase lag/lead. Then the model can be reduced to the one shown in Fig.5. 28.

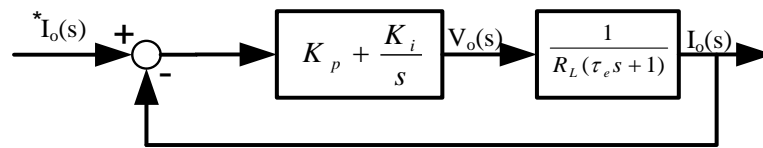


Fig.5. 28 Simple block diagram form of closed-loop direct matrix converter control system

Then, the closed-loop reference output current to output current transfer function $G_{I_o I_o^*}(s)$ can be written as:

$$G_{I_o I_o^*}(s) = \frac{I_o(s)}{I_o^*(s)} = \frac{sK_p + K_i}{sR_L(\tau_e s + 1) + sK_p + K_i} \quad (5-8)$$

The PI controller parameters are selected as $\frac{K_p}{K_i} = \tau_e$ to cancel the closed-loop pole due to the RL load. The bandwidth of the closed-loop transfer function linearly depends on the K_i . Hence, in order to obtain an approximately 300 Hz closed-loop bandwidth, K_i is selected as 1000. Then, the proportional gain, K_p is calculated as 14.5. For a perfectly accurate current sensor were perfectly accurate such a PI controller will function to give zero steady-state error. Note that these gains are calculated in s-domain. They will be transformed into z-domain using a bilinear transformation.

Applying the same conditions for the closed-loop steady-state simulations applied in the open-loop simulations such as the peak value of the load current of 5A and the output frequency of 50 Hz. Then, we obtain output voltages and currents shown in Fig.5. 29 - Fig.5. 31 for the closed-loop cases.

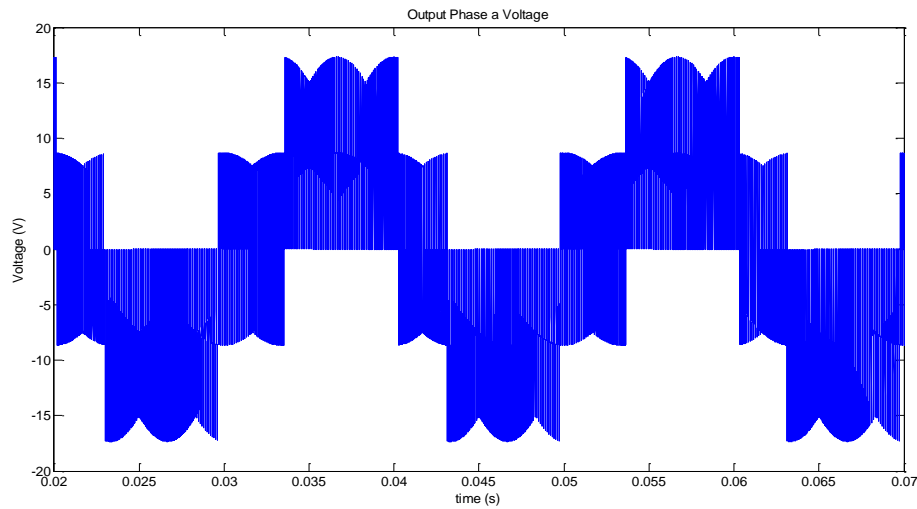


Fig.5. 29 Output phase “a” to neutral voltage, V_{an} ($f_o = 50$ Hz)

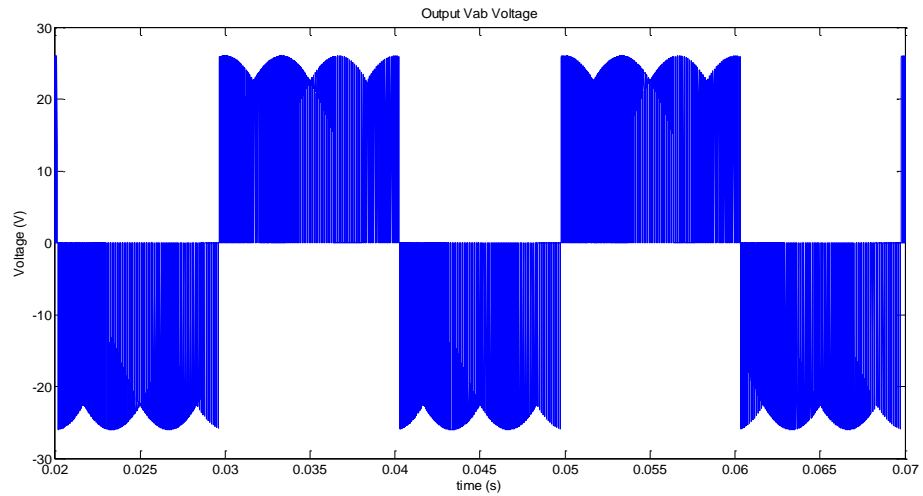


Fig.5. 30 Output line-to-line voltage V_{ab} ($f_o = 50$ Hz)

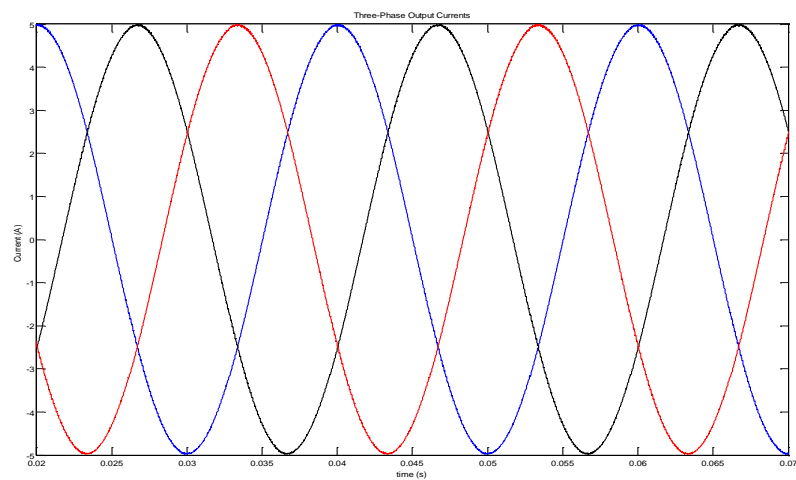


Fig.5. 31 Close-loop output currents ($f_o = 50$ Hz)

The designed PI controller works very well with d-q system model when the load is perfectly balanced. This kind of controller may cause some problems when the load is unbalanced. Because, the three-phase currents are transformed to two-phase equivalent currents with the assumption that the load is perfectly balanced. Otherwise, reference signals generated by the controller do not generate sinusoidal waveforms.

Fig.5. 32 and Fig.5. 33 show the frequency spectrums of the output line-to-line voltage, output phase current.

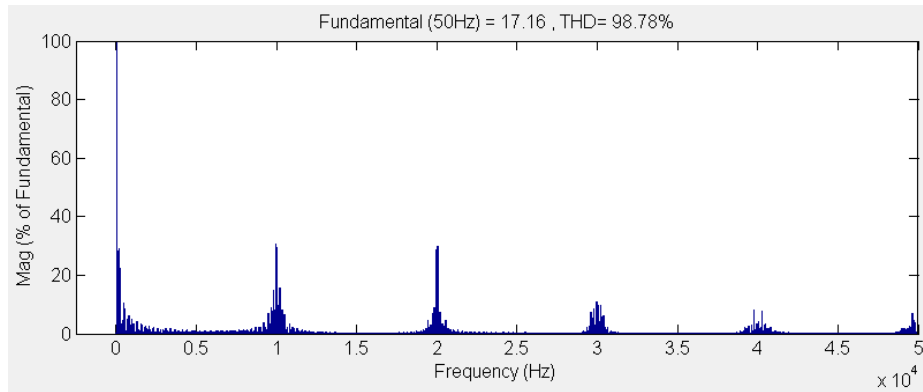


Fig.5. 32 Harmonic spectrum of output line-to-line voltage V_{ab} ($f_o = 50$ Hz)

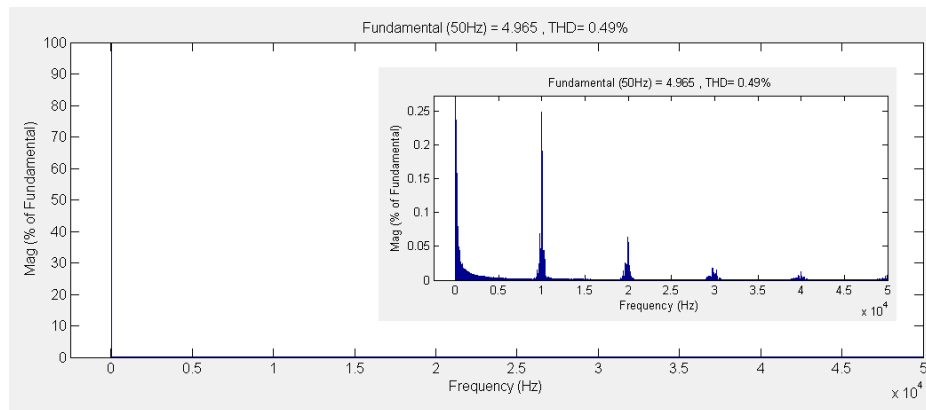


Fig.5. 33 Harmonic spectrum of output phase “a” current ($f_o = 50$ Hz)

At steady-state, the closed-loop current and voltage waveforms and their harmonic contents are expected to be similar with the open-loop current and voltage waveforms for passive load. However, the total harmonic distortion for the closed-loop simulation result at steady-state came out higher than that for the open-loop simulation. It is an unexpected condition for steady-state. This difference may be caused from the inaccurate tuned PI controller parameters. Actually, a big difference may exist only at the transient instant for a passive load due to the different dynamic responses. However, if the load is active, the distortion of waveforms and harmonic contents will be totally different.

For 100 Hz output frequency, the output phase “a” to neutral voltage, output line-to-line voltage V_{ab} , three-phase output currents and their harmonic contents are shown in the following figures. The demanded peak value of load current is 3A.

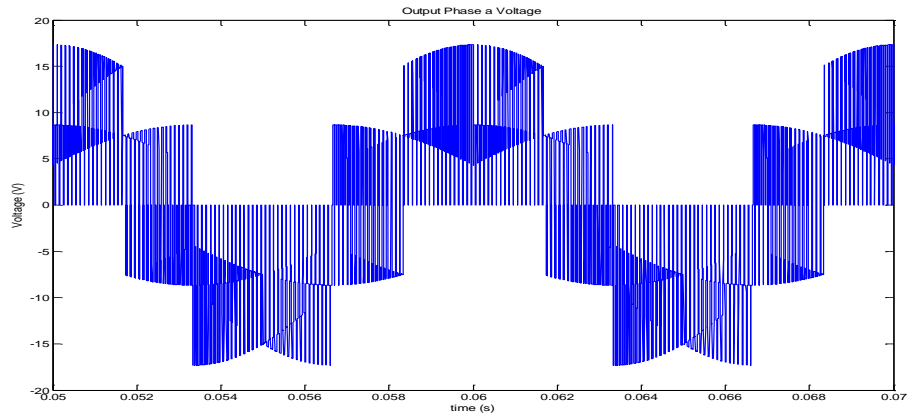


Fig.5. 34 Output phase “a” to neutral voltage, V_{an} ($f_o = 100$ Hz)

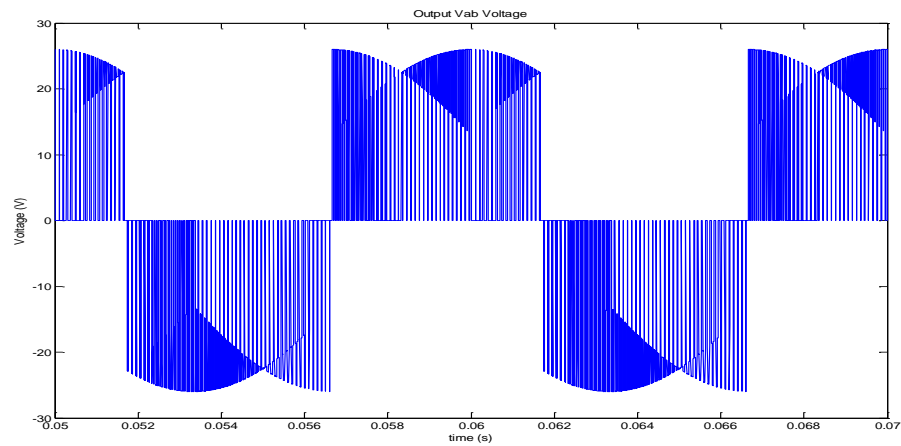


Fig.5. 35 Output line-to-line voltage V_{ab} ($f_o = 100$ Hz)

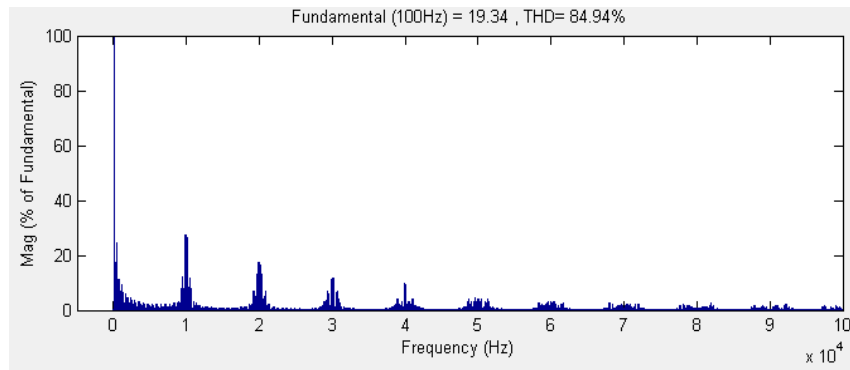


Fig.5. 36 Harmonic spectrum of output line-to-line voltage V_{ab} ($f_o = 100$ Hz)

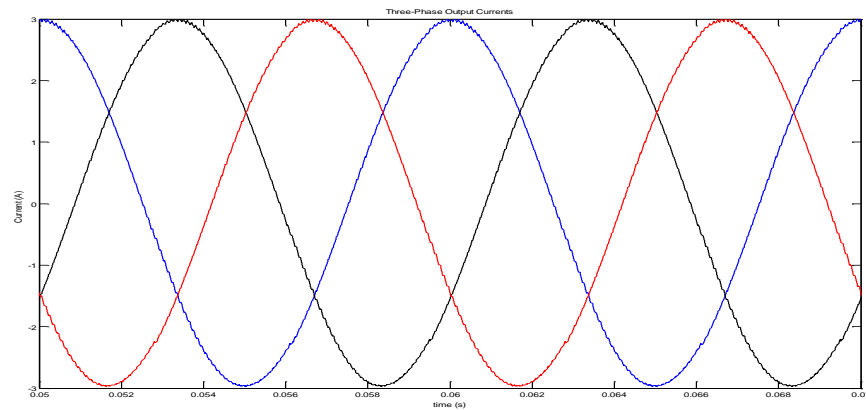


Fig.5. 37 Closed-loop output currents ($f_o = 100$ Hz)

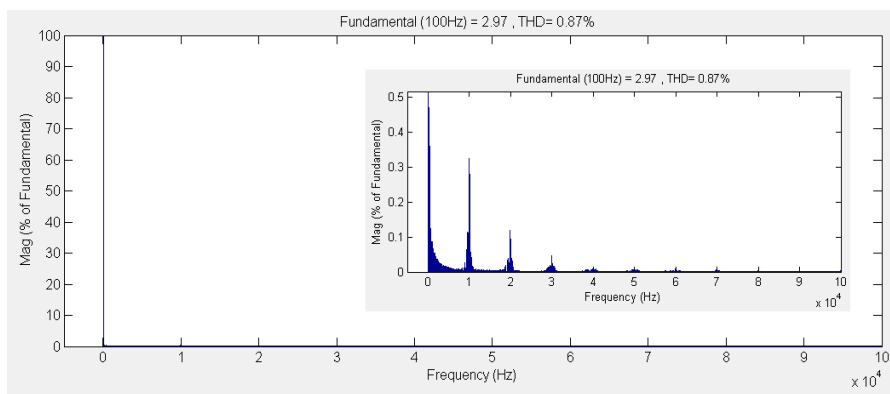


Fig.5. 38 Harmonic spectrum of output phase "a" current ($f_o = 100$ Hz)

The previous output waveforms still verify the validity of the assumption made for the direct matrix converter model. The output waveforms are sinusoidal as assumed at the beginning. Thus the, output voltage and current waveforms verify the prior assumptions made. To fully verify the validity of operational characteristics of direct matrix converter model assumed at the beginning, the input voltage and current waveforms should also be investigated.

5.3 SIMULATIONS ON DIRECT MATRIX CONVERTER REGARDING TO INPUT CHARACTERISTICS

The matrix converters also have sinusoidal input voltage and sinusoidal current waveforms according to the assumption made for the direct matrix converter model. Together with this, another feature of matrix converter has to be verified for the model is the input power factor control. Looking at Fig.5. 39, it can be verified that the control operates in order to keep the matrix converter input current in phase with the corresponding input phase voltage. The plots in Fig.5. 39 demonstrate the validity of the matrix converter input characteristics.

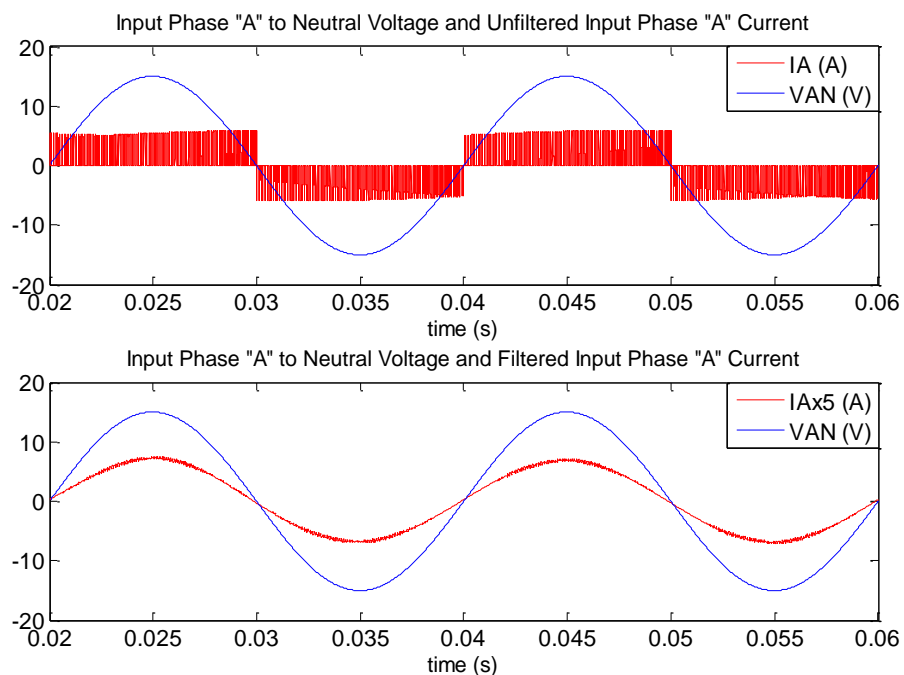


Fig.5. 39 Unfiltered and filtered input phase “A” current vs. input phase “A” voltage, V_{AN}

As far as the input power quality is concerned it has to be highlighted the significant reduction of the low order current harmonic components carried out by direct matrix converter compared to the diode-rectified voltage source inverters. Since the matrix converter is a switch-mode device, the harmonic components are at the switching frequency and multiples of it. Therefore, the reduction on the harmonic contents can be easily obtained by using an input filter. However, this is not possible for the diode-rectified structures due to the subharmonic contents. The harmonic spectrums of unfiltered and filtered input current waveforms are seen in Fig.5. 40 and Fig.5. 41.

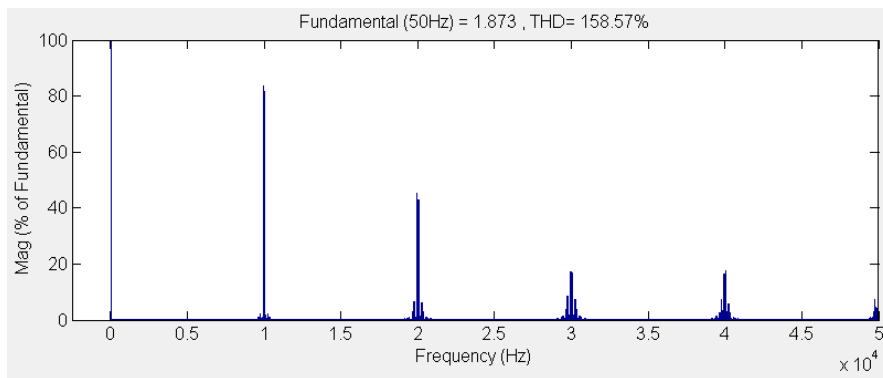


Fig.5. 40 Harmonic spectrum of unfiltered input phase current, I_A

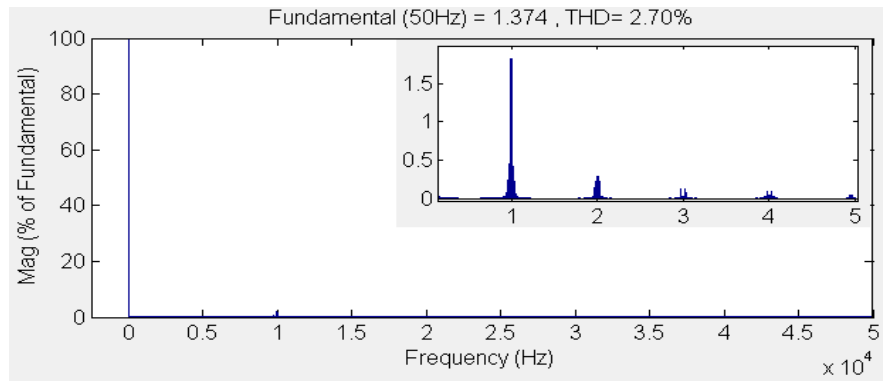


Fig.5. 41 Harmonic spectrum of filtered input phase current, I_A

The unfiltered input phase current has significant high frequency distortion. By using a low-pass LC filter (the filter cut-off frequency is at nearly 1.3 kHz), the switching frequency harmonics are filtered out so that a set of sinusoidal, balanced input currents are obtained at the supply side.

5.4 SIMULATIONS ON DIODE-RECTIFIED TWO-LEVEL VOLTAGE SOURCE INVERTER STRUCTURE

In order to compare the performance of the direct matrix converter with a diode-rectified voltage source inverter, the simulations were carried out for identical operational conditions and identical PWM techniques (e.g. space vector PWM) because, the voltage quality and the harmonic current content are highly dependent on the PWM method.

The operational conditions for the closed-loop steady-state simulations are same as those presented in closed-loop matrix converter simulations. The output waveforms are obtained for a peak the load current of 5A and the output frequency of 50 Hz. Fig.5. 42 - Fig.5. 46 show output phase “a” voltage, line-to-line voltage V_{ab} , three-phase output currents and the harmonic spectrums. The three-phase voltages and currents are symmetric and have 120° phase shift from each other. For this reason, in the following illustrations only one-phase output voltage and one line-to-line output voltage waveform are presented.

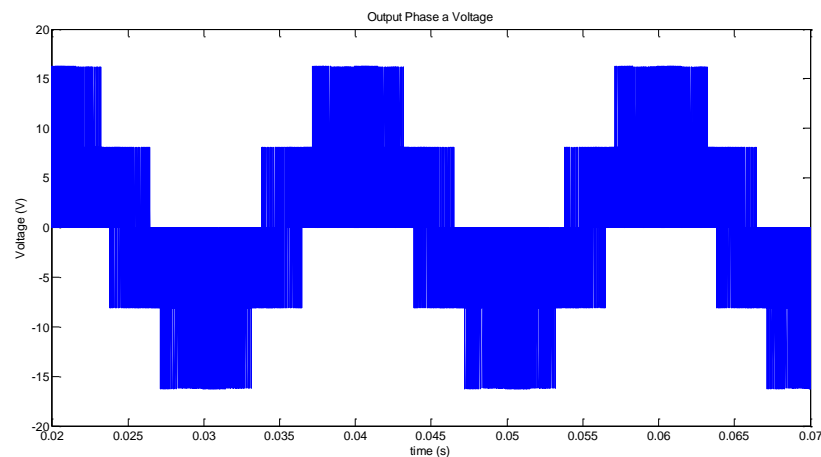


Fig.5. 42 Output phase “a” to neutral voltage, V_{an} ($f_o = 50$ Hz)

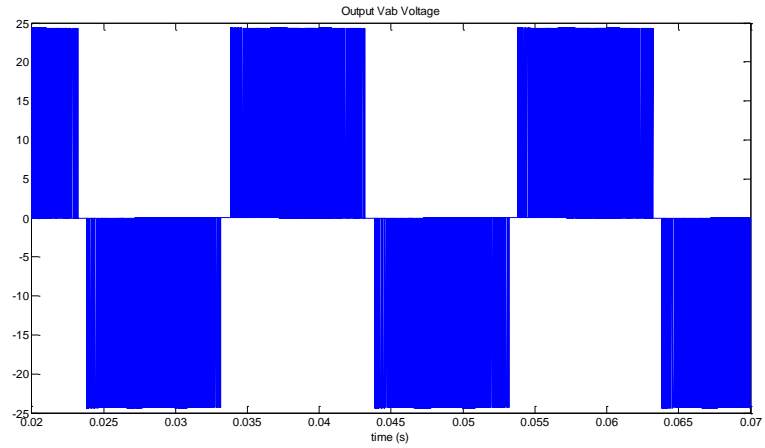


Fig.5. 43 Output line-to-line voltage V_{ab} ($f_o = 50$ Hz)

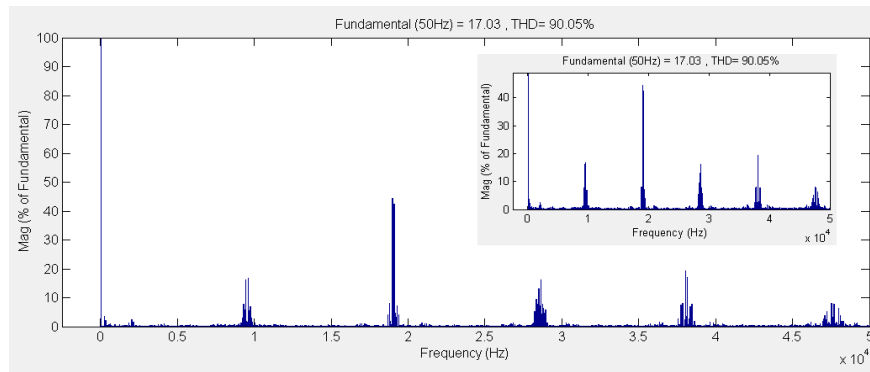


Fig.5. 44 Harmonic spectrum of output line-to-line voltage V_{ab} ($f_o = 50$ Hz)

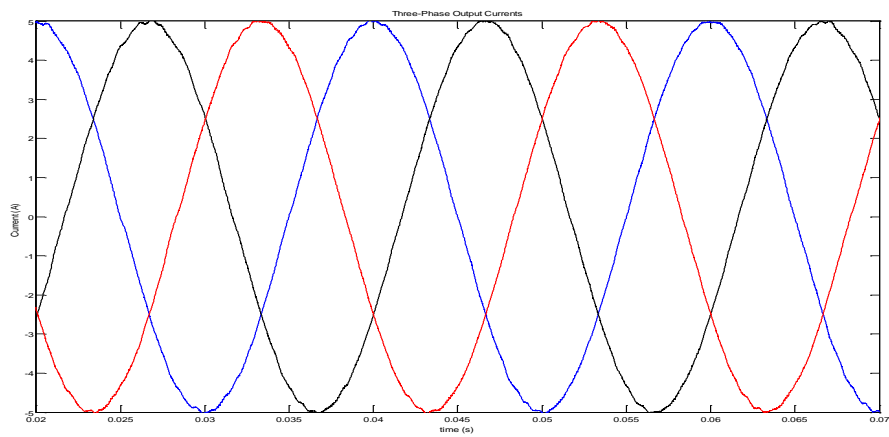


Fig.5. 45 Three-phase output currents ($f_o = 50$ Hz)

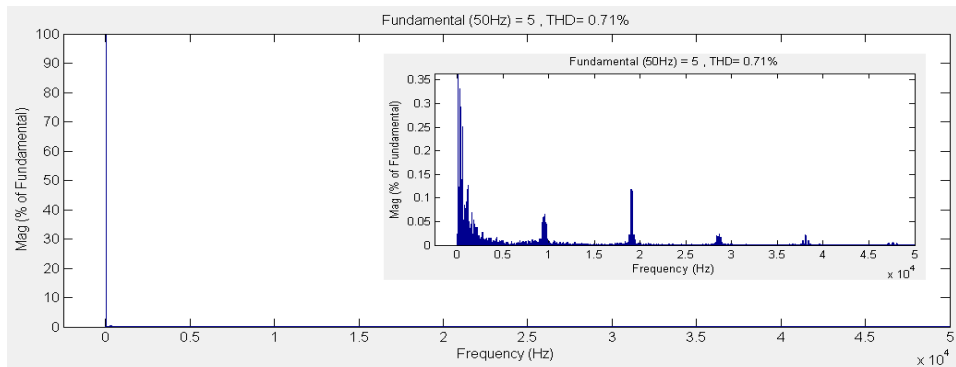


Fig.5. 46 Harmonic spectrum of output phase “a” current ($f_o = 50$ Hz)

The previous output waveforms show the diode-rectified two-level VSI operation at the load side. The output waveforms are sinusoidal as expected. The plots in Fig.5. 44 and Fig.5. 46 show that, diode-rectified two-level VSI possesses familiar harmonic content with the matrix converter output waveforms for the same switching frequency. However, from Fig.5. 44 and Fig.5. 46 we can see that the second order harmonic component (nearly at 20 kHz) is dominant for this case.

So far, the output voltage and current waveforms are demonstrated. In order to be able to fully compare the operational characteristics of diode-rectified two-level VSI, the input voltage and current waveforms should also be investigated. The input currents and the harmonic spectrum of input phase “A” current are presented in Fig.5. 47 and Fig.5. 48, respectively.

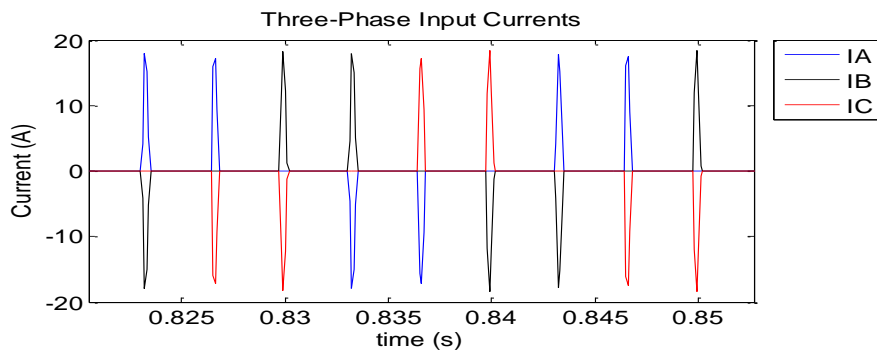


Fig.5. 47 Three-phase input currents ($f_i = 50$ Hz)

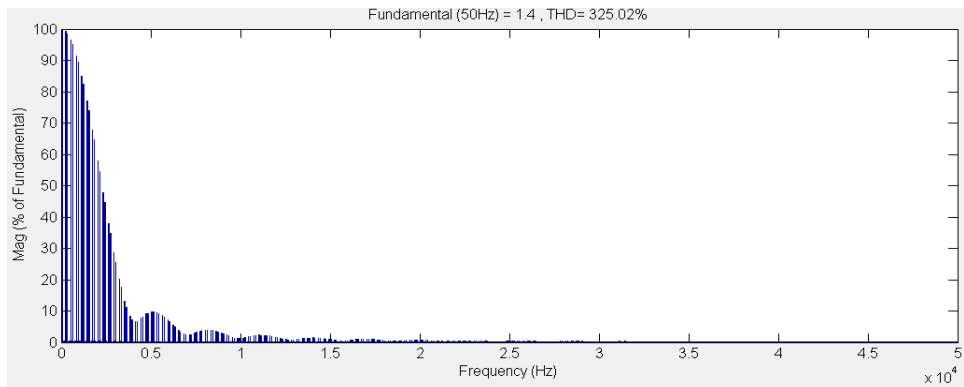


Fig.5. 48 Harmonic spectrum of input phase “A” current, I_A

As it is seen from the Fig.5. 48, the input current drawn by the three-phase diode rectifier is highly distorted especially at low frequencies. Also, it is not easily possible to attenuate these low frequency harmonics which are very close the mains operating frequency. Probably, these low frequency harmonics affect other systems connected to the same utility grid.

5.5 COMPARISON OF THE DIODE-RECTIFIED TWO-LEVEL VOLTAGE SOURCE INVERTER AND DIRECT MATRIX CONVERTER

In this section, two different converter systems are analyzed considering terminal variables only. They are the sinusoidal supply voltages, supply currents, output currents and voltages. In order to achieve a fair comparison, both systems were simulated to run on equal balanced, three-phase supply (line-to-line voltage $V_{L-L}=26V$ and frequency $f_i=50$ Hz) and equal balanced, three-phase load.

First, the previous simulation results are discussed to demonstrate the ability of the matrix converter. Simulation results show that the matrix converter can able to produce similar output current and voltage waveforms with diode-rectified two-level voltage source inverter. In order to investigate the output voltage linearity characteristics, the peak value of the fundamental output voltages vs. the voltage commands are plotted in Fig.5. 49.

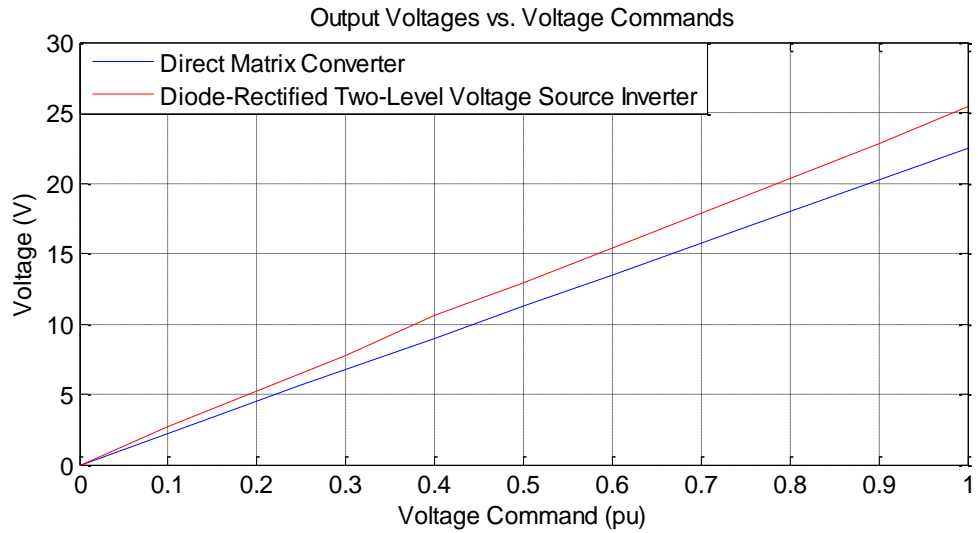


Fig.5. 49 Voltage linearity characteristics

As it can be seen, the maximum input/output transfer ratio of matrix converter is lower than the diode-rectified two-level VSI and is limited to a value of 0.866. For this reason, the industrial acceptance of the matrix converter is still in the early stage of development. The linearity characteristics of the both topologies seem similar up to their maximum input to output voltage transfer ratios.

Then, another comparison is done to show that the direct matrix converter is able to generate better quality input waveforms than the diode-rectified voltage source inverter. As it can be seen in previous simulation results, the diode-rectified two-level voltage source inverter produces highly distorted input current waveforms ($THD_i = 325.02\%$) with uncontrollable power factor due to its uncontrolled operational characteristics. Also, the diode-rectifier two-level voltage source inverter produces subharmonic contents and it is not possible to highly reduce the harmonic contents. Because the subharmonics are so close to the input supply main frequency. On the other hand, the direct matrix converter produces harmonic content at the switching frequency and its multiples. No subharmonic content is produced in this topology. Therefore, reduction in the harmonic content can be easily achievable by using input filters for these topologies. For example, unfiltered input current THD_i is equal to 158.57% and it was reduced to a value 2.70% by using an input filter which has the cut-off frequency nearly at 1.3 kHz. Therefore, irreducible harmonic contents of the input currents drawn by the diode-rectified two-level voltage source inverter may

cause the overheating of the equipment, malfunction of the solid-state equipment and the power quality degradation in distribution system ^[50, 51].

Finally, the regeneration capabilities are compared. For the diode-rectified VSI, the current direction in a diode rectifier cannot be reversed, some auxiliary circuits should be implemented to handle an eventual current flow reversal, as during a regenerating operation of the motor, in order to avoid that the DC-bus voltage can reach destructive levels. Hence, the regenerative energy cannot be given back to the utility grid without using auxiliary circuits. On the other hand, the matrix converter topology can provide a continuous operation for the regenerative loads due to the bi-directional power flow capability without need of auxiliary circuits.

Consequently, the outstanding advantages of matrix converters emerge as unity power factor control capability, sinusoidal input current waveforms with minimized harmonics, bi-directional power flow capability, and more integrating silicon structure with reduced passive components.

5.6 MODELING OF THE DIRECT MATRIX CONVERTER INTEGRATED DRIVE SYSTEM AND SIMULATIONS

The drive system model consists of a three-phase supply, a three-phase input filter, the direct matrix converter switches, a controller and a surface mounted permanent magnet synchronous machine model. The mathematical model of the surface mounted permanent magnet synchronous machines was investigated in Chapter 3. In this section, the matrix converter integrated drive system with field oriented control is presented first. Then, the model of a surface mounted permanent magnet synchronous motor is described. In this thesis, a surface mounted permanent magnet synchronous motor is the only type of permanent magnet motors.

5.6.1 Field Oriented Control of a Permanent Magnet Synchronous Motor

Early AC machine drives employed the constant volts-per-hertz (constant V/f) operation principle. The performance of the constant volts-per-hertz method was sufficient for fan and pump applications. However, it was not suitable for the applications requiring high motion quality such as high sensitive speed and position controls. The new generation AC

machine drives use modern control techniques which provide high motion quality and high bandwidth in torque, speed, and position control. The field oriented control method is used in most of the AC motor drives to obtain high torque bandwidth and control performance [53].

The principle of field oriented control of electrical drives is based on the control of both the magnitude and the phase of each phase current and voltage waveforms. In the field oriented control (FOC), phase currents and voltages are represented by vectors. In this control technique, some projections which transform a three-phase speed dependent system into a two co-ordinate (d and q co-ordinates) time invariant system are used to provide great simplification in expression of control equations. These transformations lead to a structure similar to that of a DC machine control [54]. There is a basic set of three requirements for vector control of the AC machines which are originating from the DC machine [55];

- An independently controlled armature (stator) current to overcome the effects of stator winding resistance, leakage inductance and induced voltage;
- An independently control of field flux;
- An independent control of spatial angle between the field (rotor) flux axis and the magneto motive force (MMF) axis to avoid the interaction of the MMF and the flux.

If all of these three requirements are met at every instant of time, the torque follows the current that allows an immediate torque control by controlling stator currents and also allows decoupled flux and torque regulation.

The basic concept of field orientation is based on knowing the position of rotor flux and positioning the stator current vector at orthogonal angle to the rotor flux for optimal torque output. Therefore, the information of the instantaneous rotor flux or rotor position is needed. This can be provided by position sensors such as resolver, encoder etc. or advanced estimation techniques [55]. In generally, the use of advanced estimation techniques is ideal for cost sensitive applications. In these techniques, rotor flux position information can be estimated from three-phase current and voltage measurements.

Field oriented controlled machines need two input references. These are the torque component (aligned with the q-axis) and the flux component (aligned with d-axis). The aim

of FOC is to perform real time control of torque and the flux components separately. As stated above, to perform field oriented control, the control equations are projected from a three-phase non-rotating frame into a two co-ordinate rotating frame by using mathematical transformations. The mathematical transformations have been named as Clarke and Park transformations (introduced in Appendix A) which simplify the expression of control equations and removes time dependencies. The good torque response, accurate speed control and full torque capability at zero speed are the advantages. The block diagram in Fig.5. 50 illustrates a permanent magnet synchronous motor control scheme based on field orientation principle.

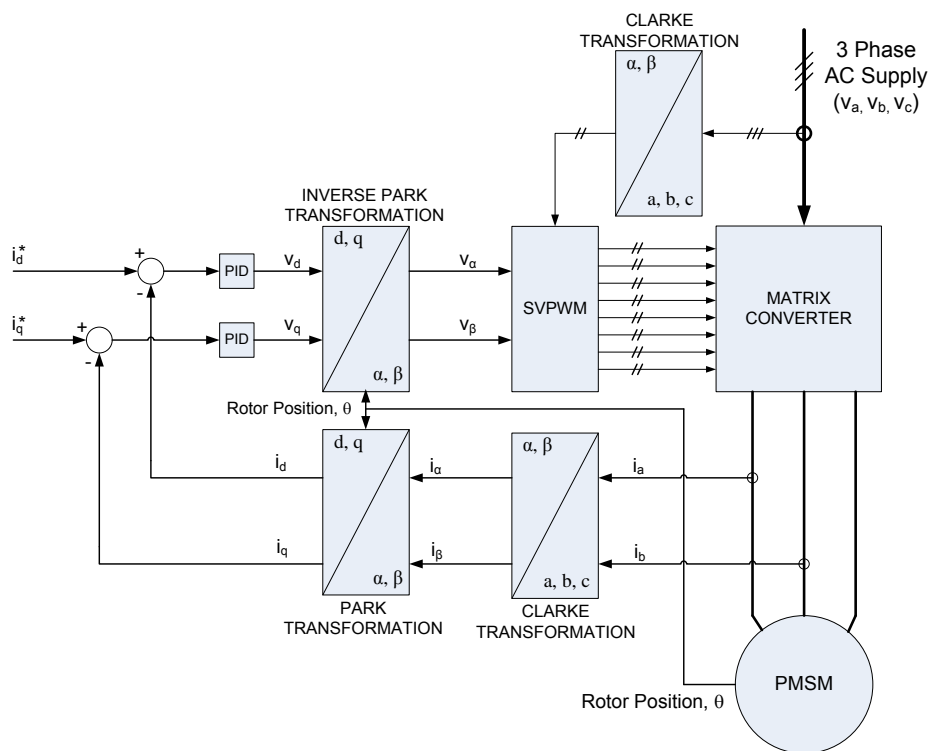


Fig.5. 50 Basic scheme of FOC for permanent magnet synchronous motor

i_d^* (flux reference) and i_q^* (torque reference) are the inputs of the system. The two of the three-phase stator currents are measured to provide the required feedbacks for the close loop control of the system. The unmeasured current can also be calculated from the measured two stator currents since $i_a + i_b + i_c = 0$.

Clarke and Park transformations should be applied to the measured currents to get rid of the time dependencies. Hence, the measured currents feed the Clarke transformation block.

This transformation provides the variables i_α and i_β from the measured stator currents i_a and i_b . i_α and i_β are time-varying quadrature current values as viewed from the perspective of the stator. Then, by using the Park transformation, the two axis coordinate system is rotated to align with the rotor flux using a transformation angle observed from a resolver. This transformation provides i_d and i_q variables from i_α and i_β . i_d and i_q are the quadrature currents transformed to the rotating coordinate system. For steady-state conditions, i_d and i_q are constant (e.g. no time dependency).

Then i_d and i_q feedback components are compared to the inputs (references or commands) of the control system which are i_d^* and i_q^* . Then the error signals are generated to feed the PI controllers. The i_d^* controls rotor magnetizing flux and i_q^* controls the torque output of the motor.

This control structure shows an interesting advantage. In permanent magnet synchronous motor, the rotor flux is fixed (determined by the magnets) there is no need to create the rotor flux. Hence, when controlling a PMSM, i_d^* should be set to zero. On the other hand, induction motors need a rotor flux creation in order to operate. Therefore, the flux reference must not be zero in this case. The i_q^* is used to provide the demanded torque value. It can also be the output of the speed and position regulator which depends on application areas. The outputs of the PI controllers are V_d and V_q which form the voltage vectors that will be sent to the motor. The V_d and V_q output values are rotated back to the stationary reference frame using inverse Park transformation. This transformation provides the quadrature voltage values V_α and V_β . The V_α and V_β are transformed back to the three-phase V_a, V_b and V_c in SVPWM block. These voltages are used to calculate PWM duty ratios and to select the voltage vectors which will be sent to the motor. The outputs of SVPWM block are the control signals which are used to drive the switches of matrix converter. Note that both Park and inverse Park transformations need the rotor flux position information.

As a consequence, FOC provides direct and separate control of the torque and flux of AC machines. Also, field oriented controlled AC machines obtain every DC machine advantage such as; instantaneous control of the separate quantities allowing accurate transient and steady-state operation.

5.6.2 Model of the PMSM and Simulation Results

The d-q axes circuit models and the electromechanical torque equation of surface mounted permanent synchronous motor (SMPMSM) in terms of d-q variables are given in Chapter 3. The SMPMSM simulation model includes both the Simpower System Tool Box components (to form the stator windings) and standard blocks of Simulink. The test motor has the parameters in Table 5. 3.

Table 5. 3 Parameters of the test motor

Symbol	Name	Value	Unit
P_{Rated}	Rated power	3.5	kW
P	Number of poles	8	
V_{Rated}	Rated voltage	322	V_{rms}
R_s	Stator phase resistance	0.8	Ohm
L_s	Stator phase inductance	5.8	mH
k_e	Motor back-emf constant	0.73	$V_p/\text{rad/s}$
k_t	Motor torque constant	0.69	Nm/A_p

In fact, the permanent magnet motor drive model is built in two main steps. Those are modeling of the stator windings and implementation of the motor equations. First, stator winding is modeled as R – L with a back-emf in series. The simulation model of stator windings is shown in Fig.5. 51.

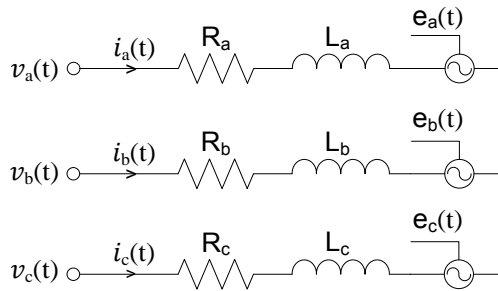


Fig.5. 51 Simulation model of the stator windings

In the second step, electromagnetic torque equation (3-23) is implemented. Motor three-phase currents are measured and transformed to d-q axes currents (i_d , i_q) by using Park and

Clarke transformation presented in Appendix A. Then, the output torque of the motor is calculated using the d-q axes currents and the output torque equation of the permanent magnet motor. From the output torque and the motor inertia, the instantaneous angular acceleration and the angular speed of the motor shaft are calculated. Then, the motor position is calculated from motor speed. For stabilizing the motor speed at a desired value, the measured back-emf voltage is compared with the motor back-emf voltage calculated using desired speed value. If the measured peak back-emf voltage reaches the calculated peak value, the motor speed is saturated at that speed. After that point, the motor speed does not increase any more.

For the PI controller design, following analysis is performed by using one-phase equivalent circuit model of SMPMSM as shown in Fig.5. 52.

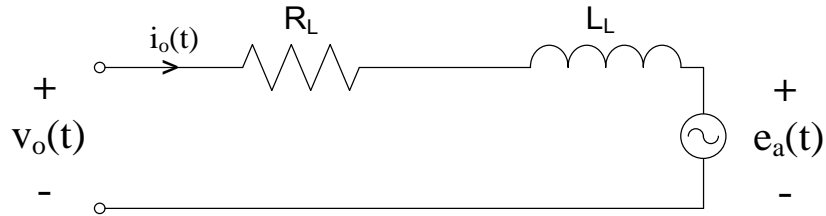


Fig.5. 52 One-phase equivalent circuit model of SMPMSM

R_L and L_L are the phase equivalent resistor and inductor, respectively. $e_a(t)$ is the motor back-emf voltage.

The mesh equation for the equivalent circuit yields;

$$v_o(t) = i_o(t)R_L + L_L \frac{di_o(t)}{dt} + e_a(t). \quad (5-9)$$

After taking the Laplace transforms, the transfer function can be obtained as follows:

$$V_o(s) = I_o(s)R_L + L_L s I_o(s) + E_a(s) \quad (5-10)$$

$$I_o(s) = (V_o(s) - E_a(s)) \frac{1}{L_L s + R_L} \quad (5-11)$$

After defining $\tau_e = \frac{L_L}{R_L}$ as the electrical time constant, the transfer function can be expressed as:

$$\frac{I_o(s)}{V_o(s) - E_a(s)} = \frac{1}{R_L(\tau_e s + 1)} \quad (5-12)$$

The closed-loop direct matrix converter operation can be expressed as block diagram form shown in Fig.5. 53.

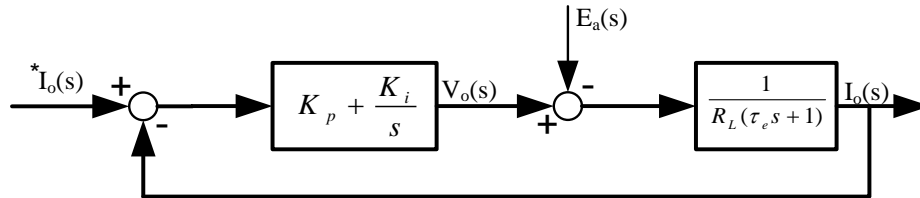


Fig.5. 53 Block diagram of closed-loop drive control system

Then,

$$I_o(s) = \frac{sK_p + K_i}{sR_L(\tau_e s + 1) + sK_p + K_i} I_o^*(s) - \frac{s}{sR_L(\tau_e s + 1) + sK_p + K_i} E_a(s)$$

At the beginning, controller parameters are selected same as the calculated for close-loop control of passive load. However, these parameters were not sufficient to control the permanent magnet motor model and the PI controller parameters were again tuned manually as to have a satisfactory torque response. The dynamic responses of the i_d and i_q currents with respect to the i_d^* and i_q^* references are given in Fig.5. 54.

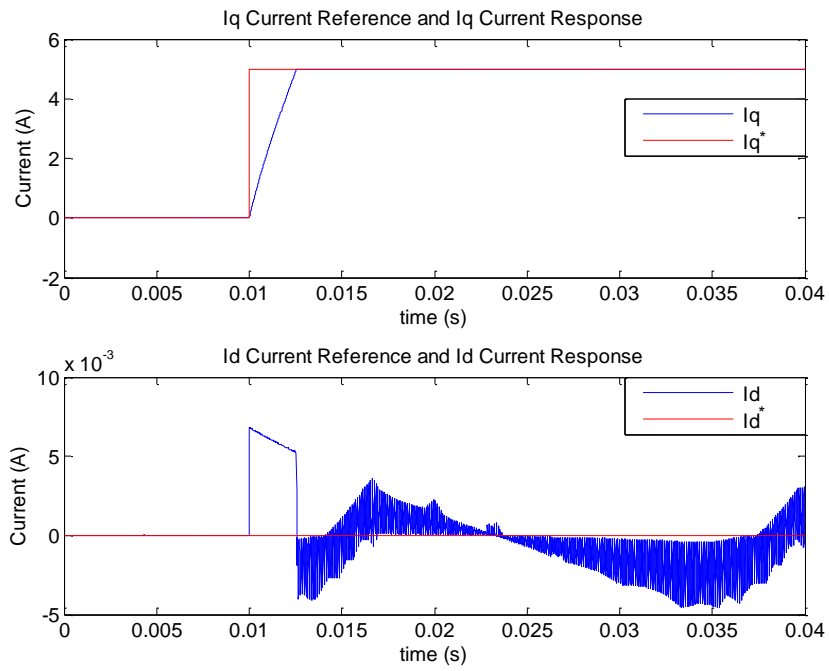


Fig.5. 54 Dynamic responses of d-axis (i_d) and q-axis (i_q) currents

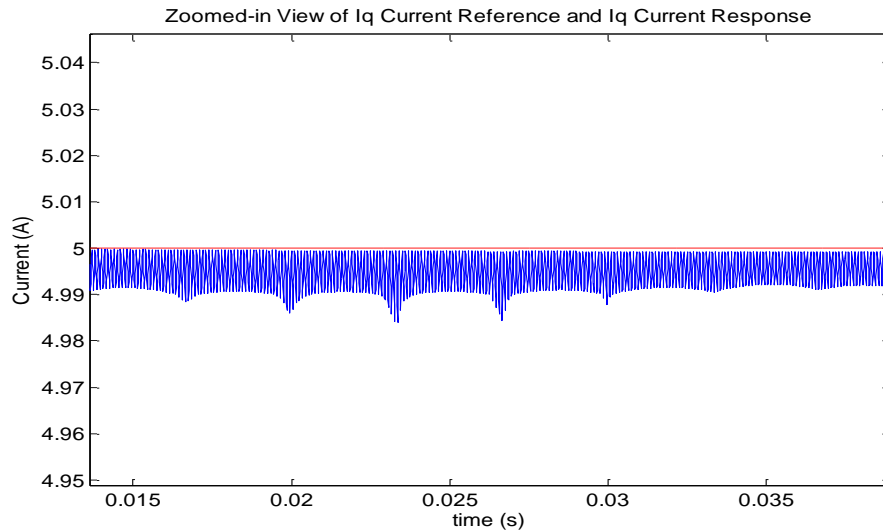


Fig.5. 55 Zoomed-in view of i_q reference and i_q

The simulations were carried out using PI controller and the motor operates at constant speed. During the simulations, field oriented control technique is used and the d-axis

current (i_d) is set to zero. Because, the output torque of the surface mounted permanent magnet synchronous motor is only linearly proportional to q-axis current (i_q). Fig.5. 56 - Fig.5. 58 show the output phase “a” voltage with respect to the neutral point, output line-to-line voltage, V_{ab} and three-phase output currents.

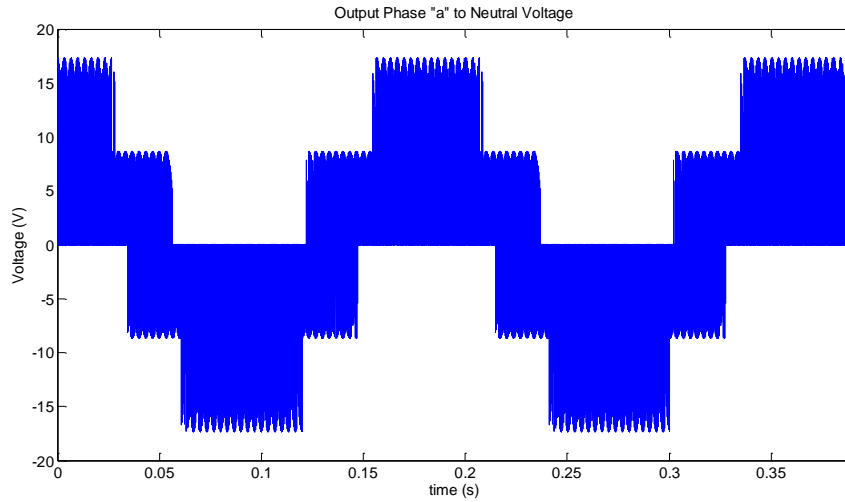


Fig.5. 56 Output phase “a” to neutral voltage, V_{an} ($f_o = 5.5$ Hz)

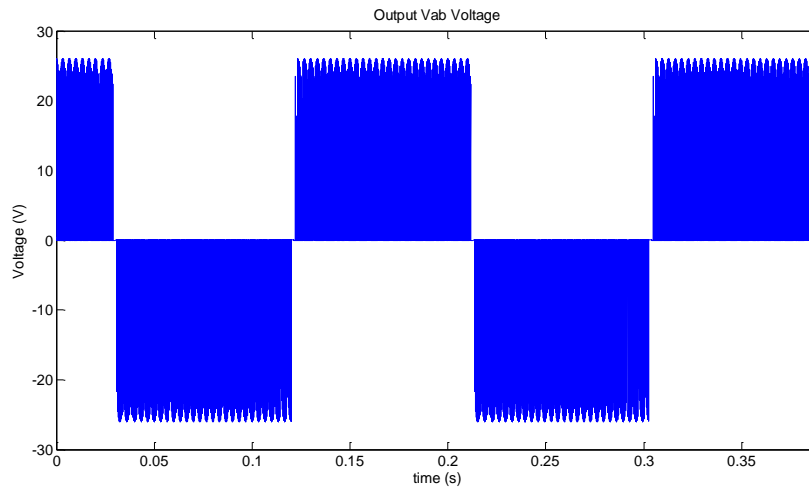


Fig.5. 57 Output line-to-line voltage, V_{ab} ($f_o = 5.5$ Hz)

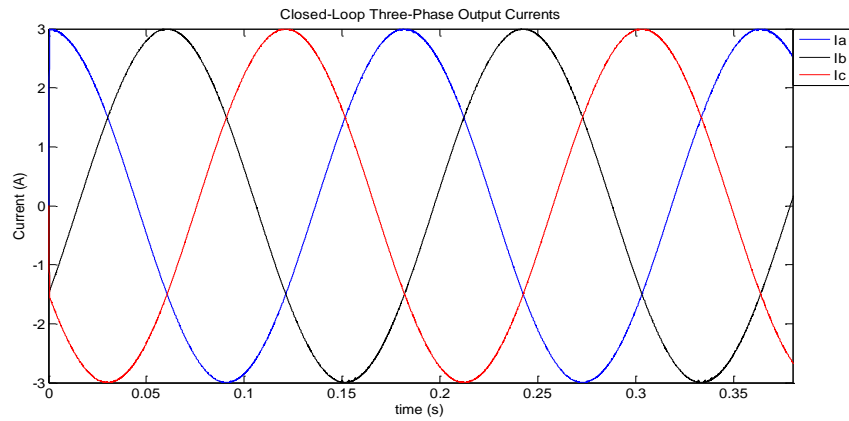


Fig.5. 58 Closed-loop three-phase output currents ($f_o = 5.5$ Hz)

Fig.5. 59 shows the developed electromechanical motor torque and the stator currents when the motor torque command was changed from a steady-state value of 0.63 Nm (e.g. 0.3pu motor torque) to 2.1 Nm (e.g. 1pu motor torque). In fact, the peak torque can be set higher than the 2.1Nm. However, due to the some unexpected restrictions caused by the matrix converter hardware, the line-to-line input supply voltage could not be increased higher than 26 V. For that reason, the stator current has to be limited at 3 A maximum value. Therefore, in order to obtain comparable figures with the experimental results, simulations were performed with same ratings.

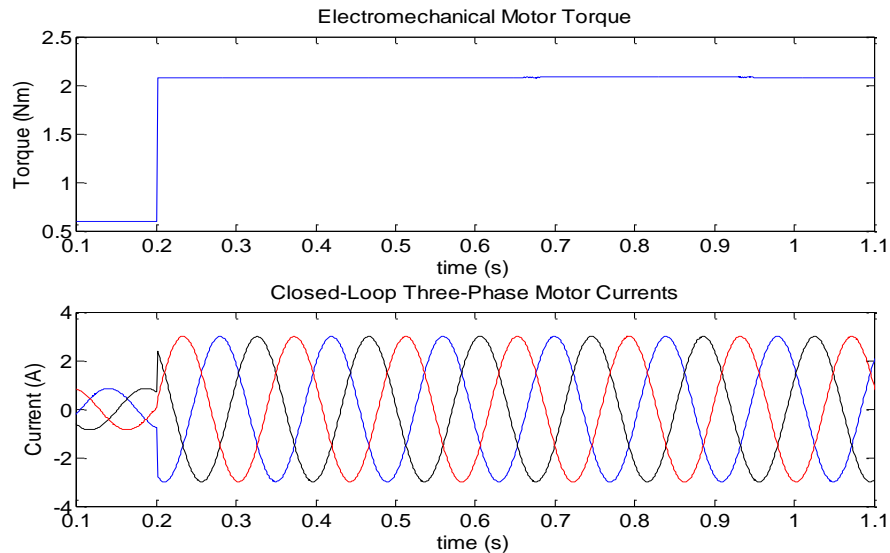


Fig.5. 59 Developed electromechanical motor torque and three-phase motor currents

The plots in Fig.5. 59, we can see that the motor phase currents are sinusoidal and quite adequate for torque control operations. So far, direct matrix converter operation is verified by simulation results. Hereafter, the direct matrix converter operation will be verified with the experimental results.

CHAPTER 6

EXPERIMENTAL WORK

After evaluating the performance of the direct matrix converter topology using Simulink, it is essential to experimentally validate the simulation results using a realistic power converter circuit. This chapter presents the hardware design, software implementations and the experimental results. First, the overall structure of the matrix converter circuit is described and the design of each part is explained in detail. Then, the experimental results are analyzed.

6.1 HARDWARE IMPLEMENTATION

In this study, a three-phase input filter, a direct matrix converter power circuit, an over voltage protection circuit and gate-driver circuit have been built to verify the simulation results. Fig.6. 1 shows the structure of the matrix converter circuit. Referring the Fig.6. 1, real time input voltage and output phase current data are gathering to implement the reliable commutation of bi-directional switches and to perform closed-loop control of matrix converter. The input filter should be used to reduce the harmonic pollution at the utility grid. The overvoltage clamp circuit is also used to prevent the matrix converter switches from any inevitable failure condition.

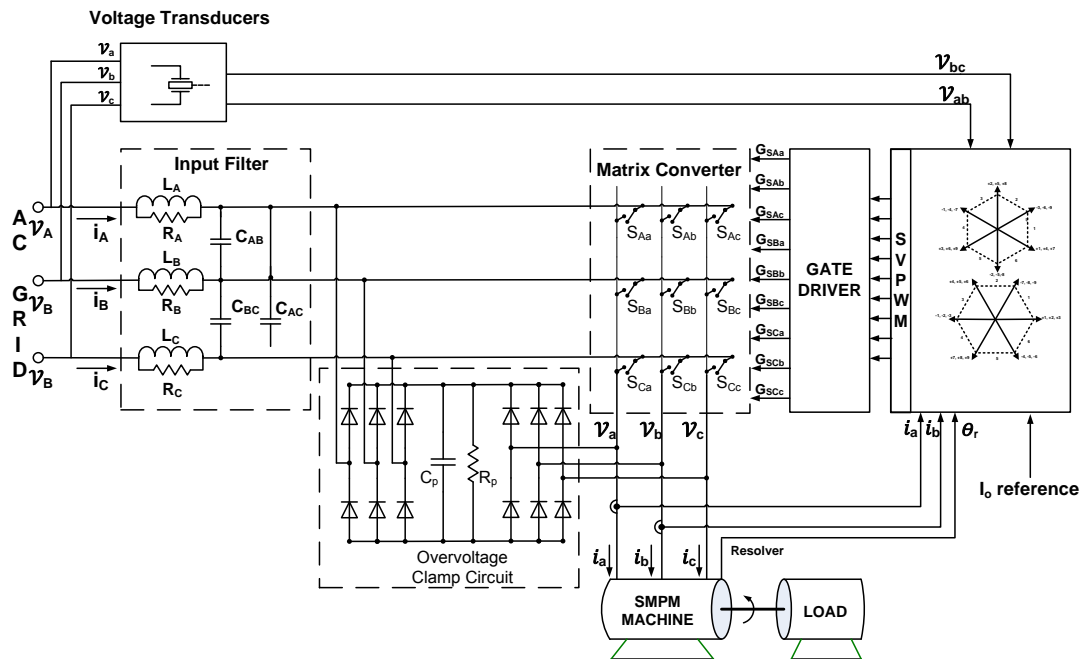


Fig.6. 1 Overall structure of the matrix converter circuit

The parameters of the input filter are same as those presented in Section 5.1.1. The filter inductance is 1.54 mH (rated current 5 Arms, designed by using Epcos ETD 54-28-19 cores), the supply filter capacitance is 10 μ F (A74S4, max. 100V_{ac}, manufactured by EUROFARAD) and the supply filter resistance is 94 Ω . For illustration purposes, one phase filter elements are presented in Fig.6. 2.

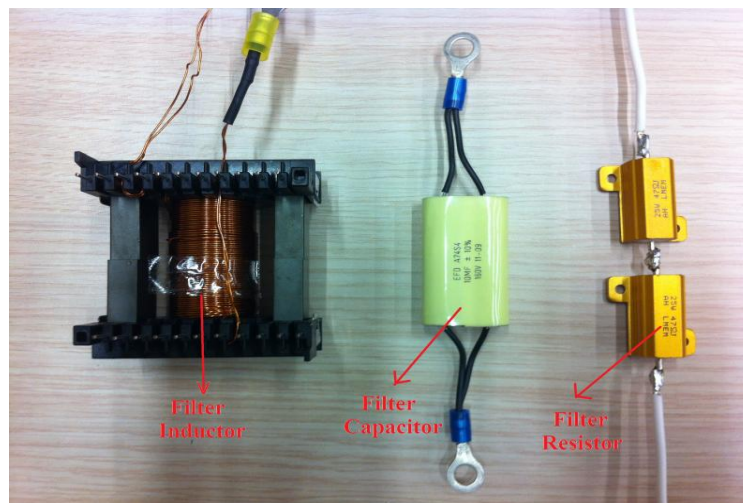


Fig.6. 2 One phase filter elements

In order to construct the power stage of three-phase to three-phase direct matrix converter, common-source connected MOSFETs (FAIRCHILD, FCB20N60F) are preferred because of their low losses. One MOSFET pairs forms the bi-directional switch structure as presented in Section 2.4.3. The voltage and the current ratings of the MOSFETs are 600 V and 20 A respectively. The current and voltage ratings are selected higher than the rated current and voltage of the system. The MOSFETs were soldered on a custom-designed twelve-layer printed circuit board (PCB) called as power circuit board and a photograph is shown in Fig.6. 3. Also, the current-voltage sensors and gate-source protection components (e.g. zener diodes) were placed on this PCB. The top and bottom layers of this PCB are the signal planes that consist of the sensors and gate-driver signals.

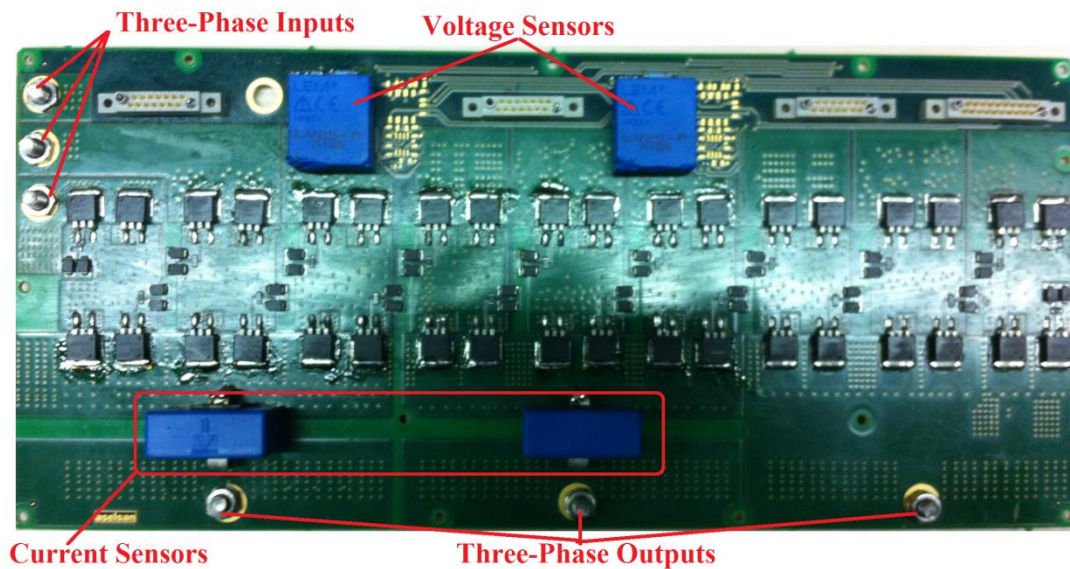


Fig.6. 3 Photograph of power circuit board

The values of output currents (two of three phase currents are enough) are required for open-loop and closed-loop control of the drive system and implementing the output current direction based four-step commutation technique. The current measurements are performed with LA 55-TP/SP1 closed-loop current sensors manufactured by LEM.

Also, measurements of the supply voltages are required to calculate the input current vector reference angle. The voltage measurements are performed with LV 25-P closed-loop voltage sensors manufactured by LEM.

To connect the MOSFETs to the input and output terminals, nine inner layers are used for power planes. The MOSFETs have no heat-sink connection. So, the cooling of the MOSFETs is considered during the layout process of this PCB. The power planes were taken as wide as possible to provide the cooling of MOSFETs. Also, the three-phase power planes are retired by overlapping to minimize the radiated noises.

The control algorithm is implemented on TMS28346 DSP board which had been provided from my workplace. This board also contains a FPGA (Xilinx XCS3S2000) and analog-to-digital (A/D) converters to perform the signal processing process. The FPGA is used to implement four-step commutation technique, read the A/D converter data, synchronize with the input voltages (e.g. phase angles) and generate the individual MOSFET gate control signals. The mathematical calculations are performed on DSP. The steps of the implemented algorithm are presented at below:

- Synchronize with the three-phase input supply,
- Update the registers,
- Calculate the angles of input current and output voltage reference vectors,
- Determine the sectors of input and output reference vectors,
- Calculate the magnitudes of the reference vectors,
- Define the usable active vectors and duty ratios,
- Construct the switching patterns to synthesize the output voltage and input current waveforms.

In order to generate the control signals of bi-directional switches and provide the isolated interface between the DSP board and the power circuit board, another custom-designed ten-layer printed circuit board was built and called as gate-driver board. Gate-driver board also consists of the all isolated power supplies to generate the required powers for card electronics and gate-drivers. The photographs of the gate-driver board are presented in Fig.6. 4 and Fig.6. 5.

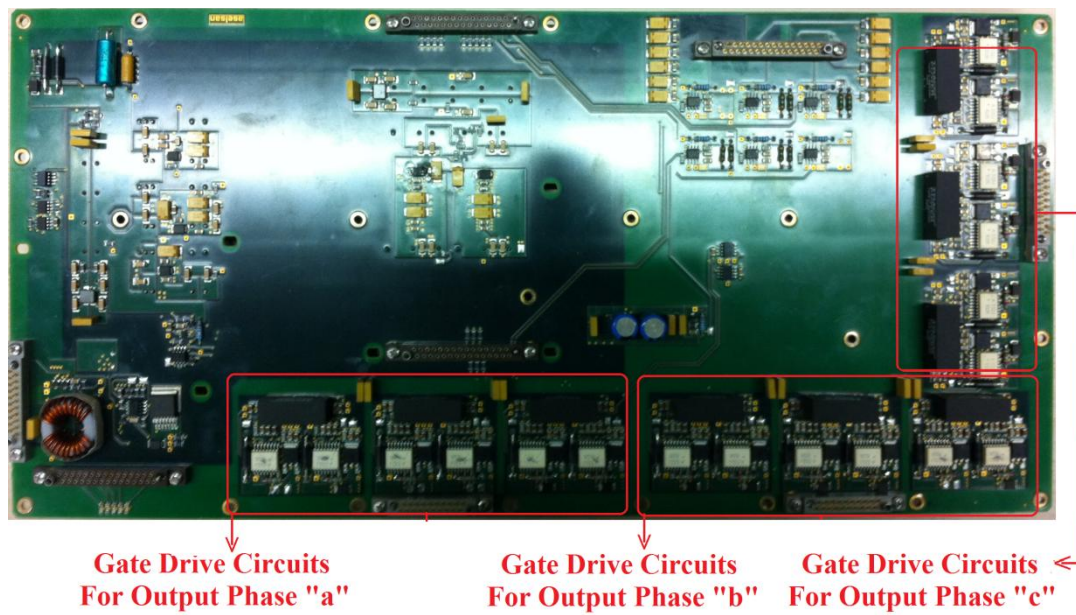


Fig.6. 4 Top view of gate-driver board

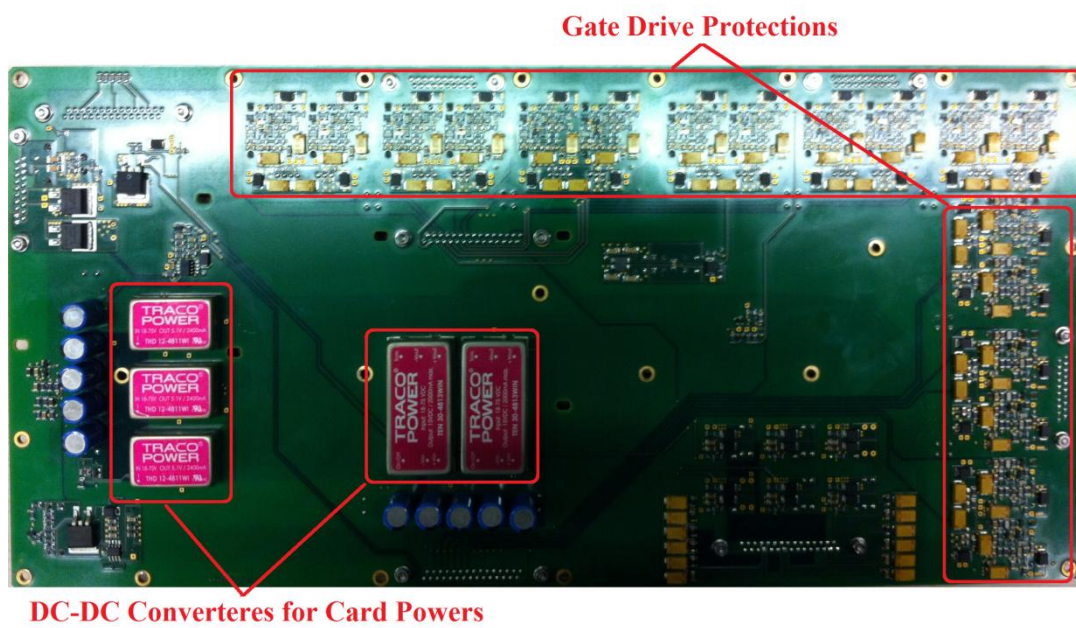


Fig.6. 5 Bottom view of gate-driver board

The gate-driver board consists of nine isolated power supplies required for all gate drivers in the case of common-source configuration, five isolated power supplies to generate the required powers for DSP board and the electronic components placed on gate-driver board.

The gate-driver board also contains the gate-driver optocouplers (AVAGO, ACPL 332J), voltage and current buffer circuits for measurements. To control each bi-directional switch two MOSFET gate-drive signals are needed. Hence, eighteen gate-driver optocouplers are used to control the nine bi-directional switches placed in the matrix converter power circuit. The gate-driver optocouplers must be mounted as close as possible to the gate of the semiconductor switches to avoid unwanted coupling of the transient signals which may result the failures of the semiconductor switches. The gate-driver board also provides the required isolation between the DSP board and the power circuit board of the direct matrix converter.

A photograph of the overall direct matrix converter circuit is given in Fig.6. 6.

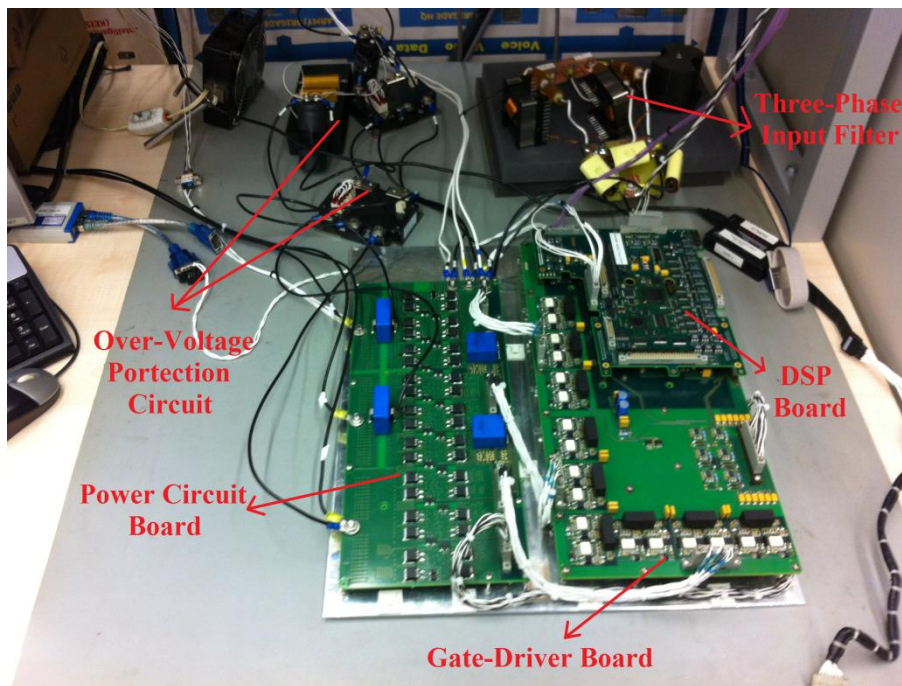


Fig.6. 6 The photograph of direct matrix converter circuit

6.2 MEASUREMENT EQUIPMENTS

During the measurements, a four-channel digital oscilloscope TDS3034B has been used. The currents have been measured with Tektronix TCP202 current probes. The voltage measurements were performed with Tektronix P5205 differential voltage probes.

6.3 EXPERIMENTAL RESULTS

This section presents the open-loop and closed-loop experimental results obtained from the designed and constructed direct matrix converter. These experimental results validate the simulation results and the implemented control structure. This section starts with the open-loop experimental results which verified the operation of space vector modulated direct matrix converter. Then the closed-loop operation of the direct matrix converter is presented. The capability of the direct matrix converter is tested for low ($f_o = 50$ Hz) and high ($f_o = 100$ Hz) output frequencies. Also, the peak current demands are 5A and 3 A, respectively.

The experimental studies were conducted with a balanced three-phase supply (line-to-line supply voltage $V_{L-L} = 26$ V and frequency $f_i = 50$ Hz), the three-phase input filter, the direct matrix converter, a three-phase R-L load and a three-phase star-connected 400 V / 3.5 kW surface mounted permanent magnet synchronous machine. The per-phase inductance and resistance of permanent magnet machine are 5.8 mH and 0.8 Ω , respectively. The passive three-phase R-L load was also obtained by locking the permanent magnet motor shaft. The three-phase balanced supply is fed to the direct matrix converter through a three-phase input filter. During the experiments, input-output current and voltage waveforms of direct matrix converter were measured and recorded with an oscilloscope. The recorded data in ISF files can be easily imported into Matlab and plotted again in a compact form. The experimental results follow the same sequence with the simulation results to have ease in testing of the produced matrix converter circuit.

6.3.1 Open-Loop Output Characteristics with Balanced R-L Load

In this section, the verification of the implemented algorithms and the output performances of the direct matrix converter circuit are evaluated. In the experiments, first direct matrix converter is operated at 50 Hz output frequency. The three-phase voltages are symmetric and have 120° phase shift from each other. Therefore, only one output phase voltage and line-to-line voltage are illustrated. The experimental waveforms shown in Fig.6. 7, Fig.6. 8 and Fig.6. 10 present output phase “a” to neutral voltage , line-to-line output voltage and three-phase output currents. Also, it should be noticed that no output filter is connected to the direct matrix converter output.

Waveforms displayed in Fig.6. 7, Fig.6. 8 and Fig.6. 10 comply with the simulation results shown in Fig.5. 10, Fig.5. 13 and Fig.5. 17. Thus, we may conclude that similar results are obtained with the simulation results. However, the experimental output phase voltage waveform is not clear as the simulation results. From the simulation results, the direct link between the sinusoidal input supply and the output are easily understood. However, the same situation cannot be said for the experimental results, especially low output operating frequencies ($f_o < 50$ Hz). The voltage waveforms are not seen clearly because of the voltage spikes due to the inevitable timing inaccuracies, dead-time durations used at bi-directional switch commutation instants and the parasitic inductances of the commutation paths carrying discontinuous currents ($L \frac{di}{dt}$) at the switching instants.

For each gate driver, the dead-time duration is adjusted by FPGA (Field Programmable Gate Array). Same dead-time durations are used for all the semiconductor switches. However, each gate-driver and also the semiconductor switches have different manufacturing tolerances. In other words, the delays for turn-on and turn-off durations may be different. For this reason, the dead-time durations are set with margin of safety. Hence, the use of single dead-time duration for all semiconductor switches may also cause additional distortions.

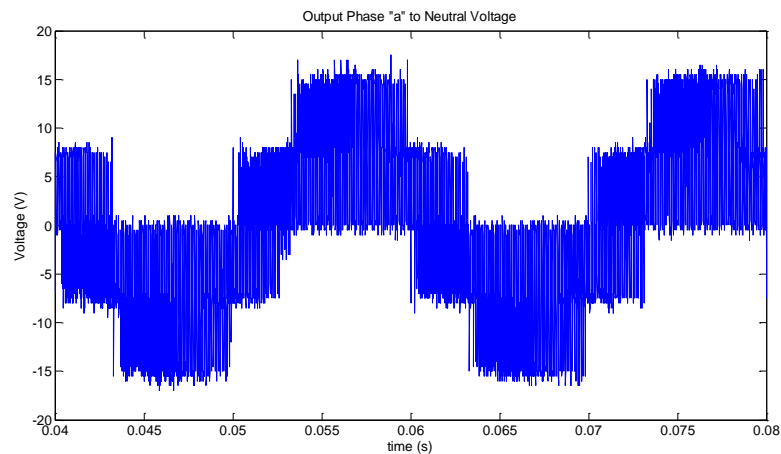


Fig.6. 7 Output phase “a” to neutral voltage, V_{an} ($f_o = 50$ Hz)

In Fig.6. 8, the direct link between the sinusoidal input supply and the load side is seen from the peak values of the line-to-line output voltage waveform. As mentioned above,

small distortion also appears as narrow spikes on this waveform. Except for these, the line-to-line output voltage waveforms have no important noticeable distortion. The output voltage waveform mainly contains two absolute levels, 0 V and 26 V. Hence, this converter structure is a member of two-level direct converters.

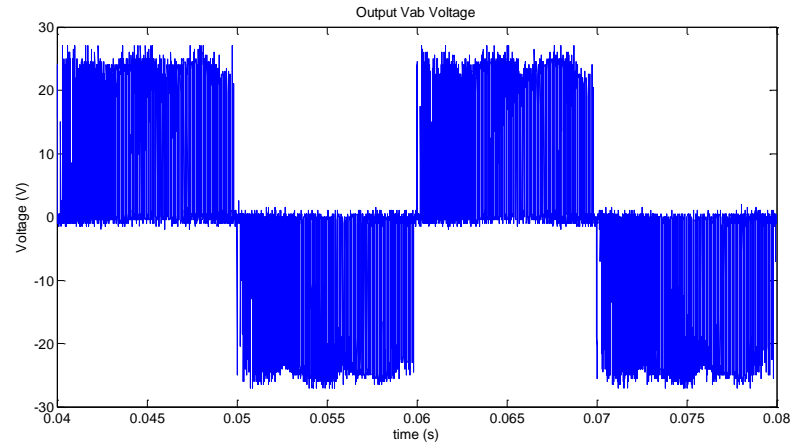


Fig.6. 8 Output line-to-line voltage V_{ab} ($f_o = 50$ Hz)

The corresponding total harmonic distortion (THD) of line-to-line voltage V_{ab} is shown in Fig.6. 9. There are considerable high-frequency harmonics especially at integer multiples of switching frequency and at the side bands of these frequencies. The results of experimental tests show very similar characteristics with the simulation results. However, although the magnitudes of low order frequency harmonics are still very small, the magnitudes are very slightly greater than the simulation result in Fig.5. 16.

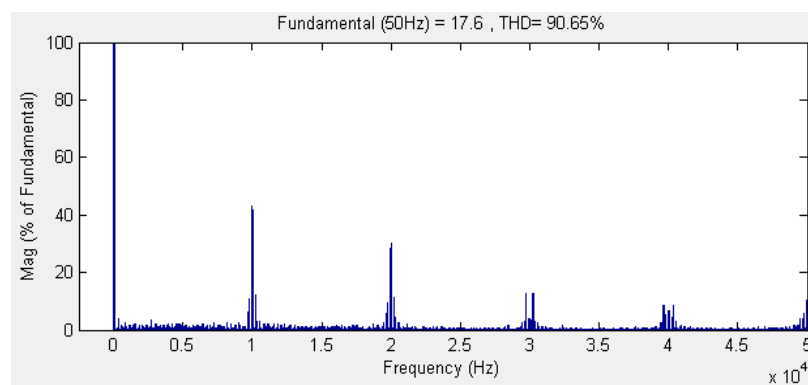


Fig.6. 9 Harmonic spectrum of output line-to-line voltage V_{ab} ($f_o = 50$ Hz)

Next, the three-phase output current waveforms are seen in Fig.6. 10. The load currents are nearly sinusoidal, balanced and the peak values of the currents are equal to demanded current reference. These current waveforms are quite adequate for smooth torque control operation.

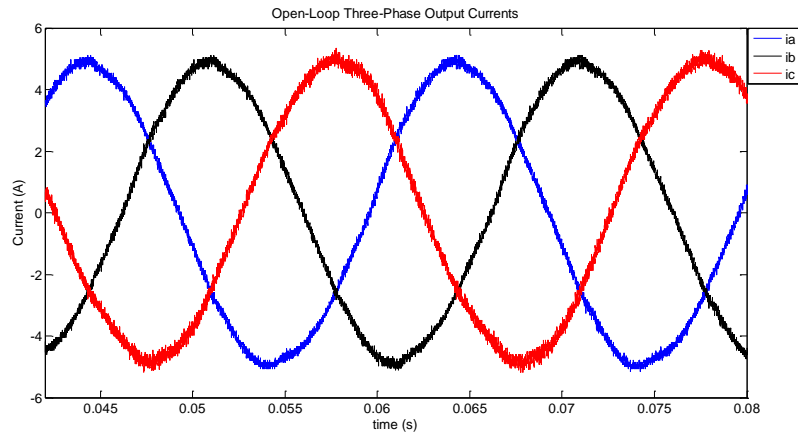


Fig.6. 10 Three-phase output currents ($f_o = 50$ Hz)

Fig.6. 11 shows the harmonic spectrum of output phase “a” current. As we can see below, the total harmonic distortion on load current is highly reduced comparing with the harmonic distortion of line-to-line output voltage V_{ab} . Since the harmonic components have high frequencies (e.g. switching frequency and its multiples), these components are naturally damped by the R-L load because the resistive-inductive load acts as a filter.

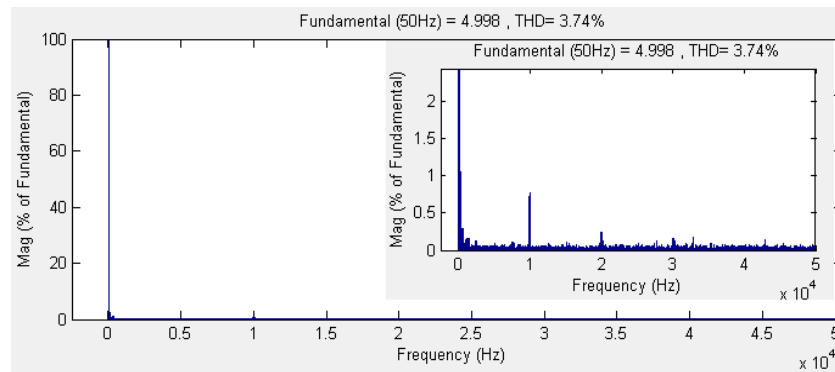


Fig.6. 11 Harmonic spectrum of the output phase “a” current ($f_o = 50$ Hz)

Finally, the voltage and current waveforms are taken at 100 Hz output frequency are illustrated. In Fig.6. 12 and Fig.6. 13 output phase “a” voltage and the output line-to-line

voltage are presented, respectively. As can be seen, the matrix converter does not restrict the output frequencies like as the cycloconverters. As mentioned in Chapter 1, cycloconverters have limited output frequencies and this limit is lower than the input supply frequency. To examine whether the direct matrix converter is properly operating higher frequencies than the input supply frequency to generate the desired output waveforms with low frequency harmonic distortions, the spectrum analysis was also performed on the 100 Hz output line-to-line voltage.

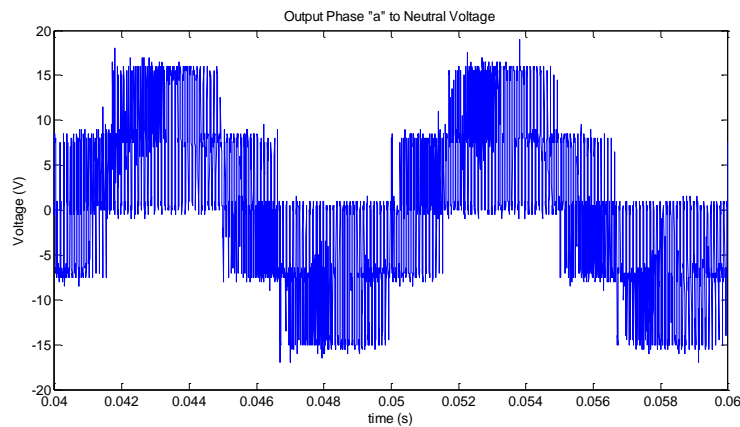


Fig.6. 12 Output phase “a” to neutral voltage, V_{an} ($f_o = 100$ Hz)

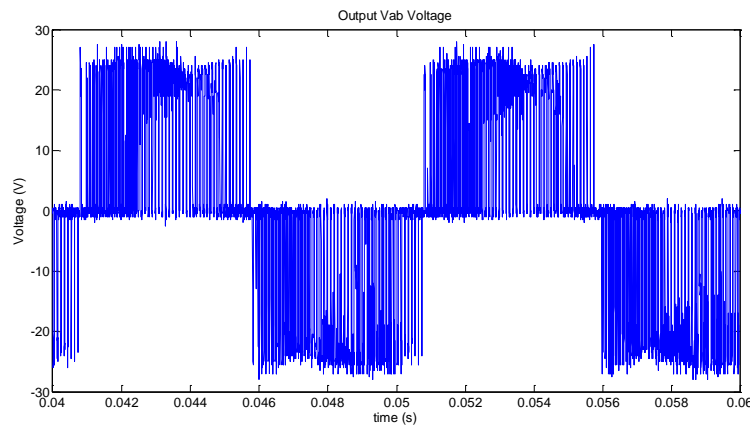


Fig.6. 13 Output line-to-line voltage V_{ab} ($f_o = 100$ Hz)

The harmonic spectrum of the line-to-line voltage is shown in Fig.6. 14. The spectrum clearly shows that there is no significant harmonics around the input and output fundamental frequencies. The significant harmonics appear around the integer multiples of

switching frequency and the side bands of these frequencies. This result also shows that the space vector modulated direct matrix converter does not produce considerable low order harmonics.

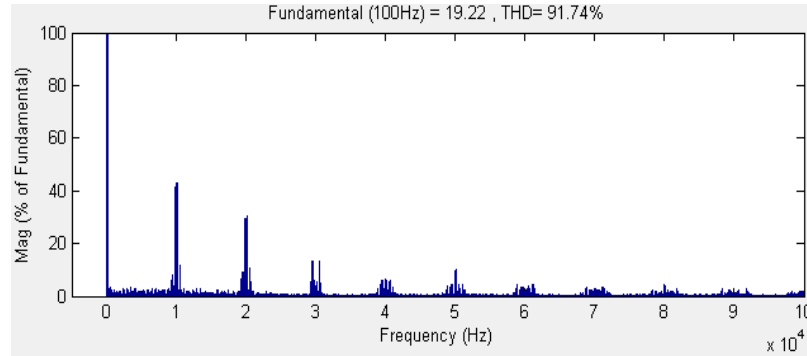


Fig.6. 14 Harmonic spectrum of output line-to-line voltage V_{ab} ($f_o = 100$ Hz)

The three-phase output current waveforms and the harmonic spectrum of the output phase “a” current are shown in Fig.6. 15 and Fig.6. 16, respectively. As seen in Fig.6. 15 the output currents are sinusoidal and balanced. Then, referring to the harmonic spectrum of output phase “a” current presented in Fig.6. 16, there are clearly some harmonics around the switching frequency and its multiples. However, the harmonics are not so significant which prove that the SVPWM strategy is able to modulate direct matrix converter to generate a set of balanced sinusoidal output currents with low harmonic contents. It should be also noticed that no extraordinary situation is obtained.

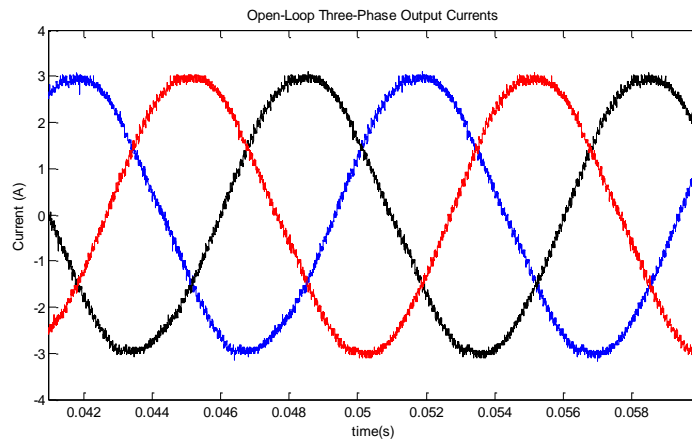


Fig.6. 15 Three-phase output currents ($f_o = 100$ Hz)

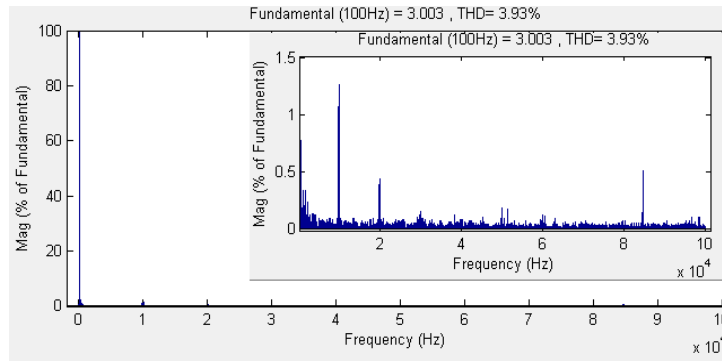


Fig.6. 16 Harmonic spectrum of the output phase “a” current ($f_o = 100$ Hz)

As it can be seen in Fig.6. 10 and Fig.6. 15 , the stator currents seems quite close to a pure sinusoidal waveform which is enough for smooth torque control operations. The open-loop experimental results also show that the matrix converter hardware implementation and control including communication and transfer of information between the power circuit board, the gate driver board and the DSP board were working perfectly. However, the open-loop implementation of the control results in high sensitivity to both inevitable timing inaccuracies in the control circuit as well as to distortions in the input/output waveforms. Therefore, the open-loop control is not recommended for the control of dynamic loads like as electric motors.

6.3.2 Closed-Loop Output Characteristics with Balanced R-L Load

This section presents the experimental R-L load results with closed-loop control. First, the PI controller parameters were tuned to give a satisfactory output response. In order to provide fast transient response by the control system, for example a response to a step change in the output reference, the bandwidth of the closed-loop should be high. The parameters tuning of the PI controller were examined in detailed in Section 5.2.2. Fig.6. 17 shows the response of the matrix converter circuit to a step command change for the output current. As seen in Fig.6. 17, the settling time of the i_q current is sufficiently fast. However, although the command value of the i_q current is only changed, i_d current is also effected from this situation. This situation is called as cross-coupling effect and it is caused from the synchronous frame transformations (Clarke and Park) expressed in Appendix A. These coupling effects can be removed by adding feed-forward compensation terms for them.

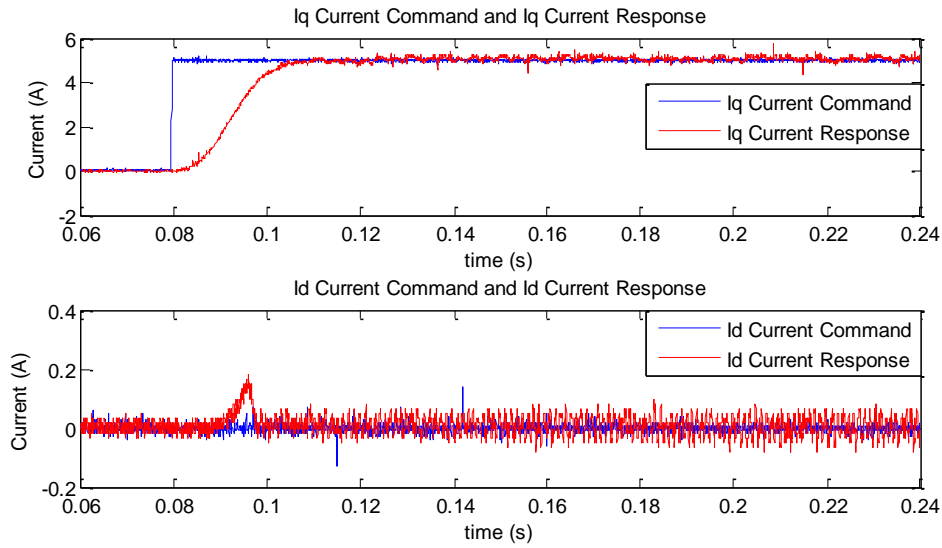


Fig.6. 17 Dynamic responses of the matrix converter circuit

In the past, the converters had to be operated in the square wave operation mode because of the long turn-on and off times of semiconductor switches. The line-to-line and phase output voltages of those converters have square shaped waveforms. That operation mode has a major drawback such that the output voltage has low order harmonics. Therefore, the filtering of these components is not practically possible and these components directly act the output currents. Today, the semiconductor switches have low turn-on and off times and this makes possible to utilize the pulse width modulation methods. In pulse width modulated converter outputs voltages results in pulsating voltage waveforms between some voltage levels. For example, in diode-rectified two-level VSI, these levels are absolutely equal to the DC-link voltage and the zero voltage. Also, the PWM converter output voltages can be decomposed into the fundamental frequency and the ripple voltages. The ripple voltages consist of the components at switching frequency and its multiples. In fact, these ripple voltages are also known as harmonic voltages and cause additional losses. In this case, since the switching frequencies are practically high (around a few kHz); it is possible to filter these harmonic components. In the light of mentioned above, the harmonic components of the output voltage and current waveforms depend on the modulation strategy. In this study, SVPWM technique is considered. To show the output characteristics of space vector pulse width modulated direct matrix converter, some experimental

waveforms are recorded. Also, it should be noticed that no output filter is connected to the matrix converter.

First, the output waveform results which are taken at $f_o = 50$ Hz, are illustrated. The three-phase voltages are symmetric and have 120° phase shift from each other. Therefore, only one output phase voltage and line-to-line voltage are illustrated. The output phase voltage shown in Fig.6. 18 is measured with respect to the neutral point. While the converter is operating at 50 Hz output frequency, very small gaps are generated in the output phase voltage waveform. At these points, the controller generated the duty ratios of switches very small. In other words, the generated time durations for turn-on signals of the switches is so small and the switch cannot be fully opened in these time intervals.

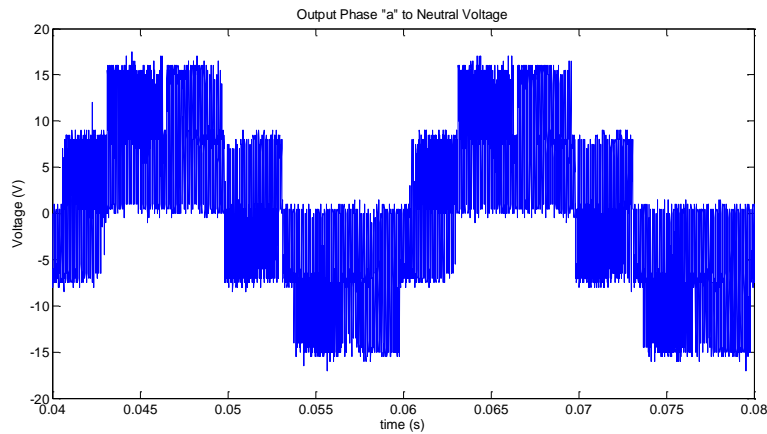


Fig.6. 18 Output phase “a” to neutral voltage, V_{an} ($f_o = 50$ Hz)

In Fig.6. 19, line-to-line output voltages V_{ab} , is presented. Also, it is easily seen that the trace of the sinusoidal input voltages appear at the output line-to-line voltage. To examine whether the voltage levels are properly applied to generate the desired outputs, the harmonic spectrum of the line-to-line voltage and the three-phase currents of the direct matrix converter are shown in Fig.6. 20 and Fig.6. 21, respectively. The three-phase currents are obviously balanced and sinusoidal. These results also clearly show that the direct matrix converter properly produces the desired output waveforms.

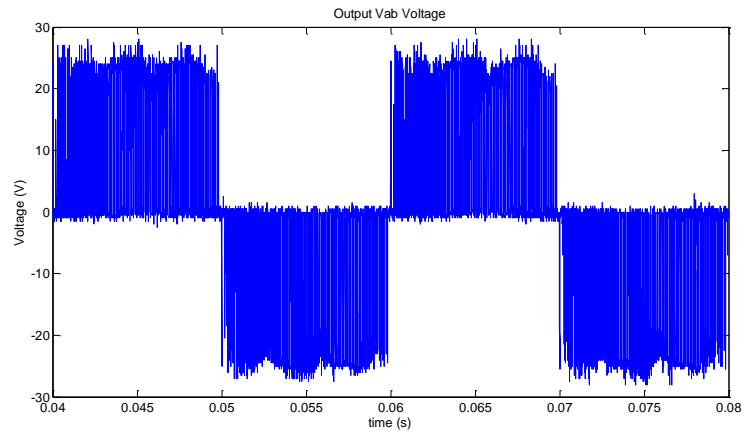


Fig.6. 19 Output line-to-line voltage V_{ab} ($f_o = 50$ Hz)

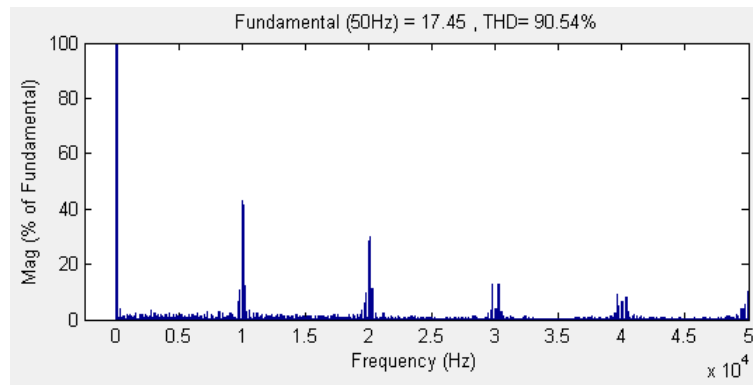


Fig.6. 20 Harmonic spectrum of output line-to-line voltage V_{ab} ($f_o = 50$ Hz)

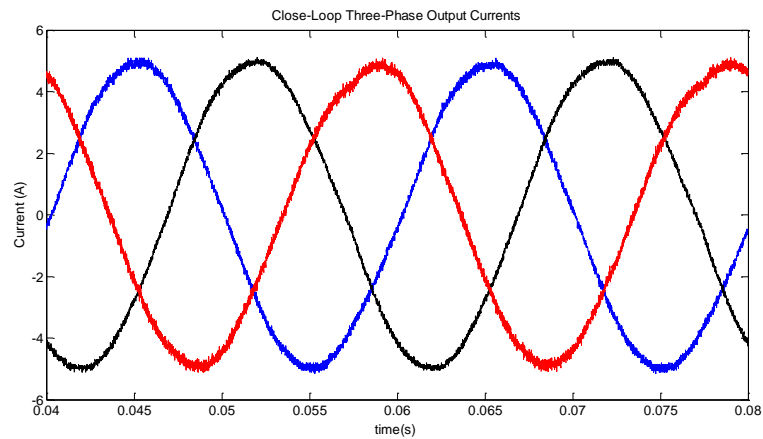


Fig.6. 21 Three-phase output currents at 50 Hz

After proving the direct matrix converter that generates the desired output voltages and the three-phase sinusoidal output currents, the harmonic analysis of the output phase current is also performed. The harmonic spectrum of the output phase “a” current is illustrated in Fig.6. 22. There is no considerable low order and high order frequency components.

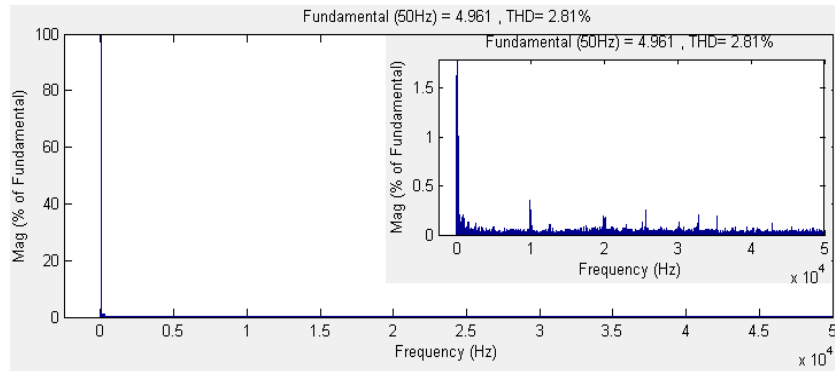


Fig.6. 22 Harmonic spectrum of the output phase “a” current ($f_o = 50$ Hz)

Second, to show the ability of direct matrix converter topologies to generate higher frequency output voltages than the input frequency, the closed-loop experimental results of the direct matrix converter at 100 Hz output frequency are presented in Fig.6. 23, Fig.6. 24 and Fig.6. 26. The three-phase voltages and currents are symmetric and have 120° phase shift from each other. Therefore, only one output phase voltage and line-to-line voltage are illustrated in Fig.6. 23 and Fig.6. 24. The output phase voltage is measured with the reference to the neutral point. As shown in Fig.6. 23 and Fig.6. 24, there are more voltage spikes (distortions) in the output voltage waveforms when compared with the simulation results due to the non-ideal switching characteristics (turn-on and turn-off times) of the switching devices.

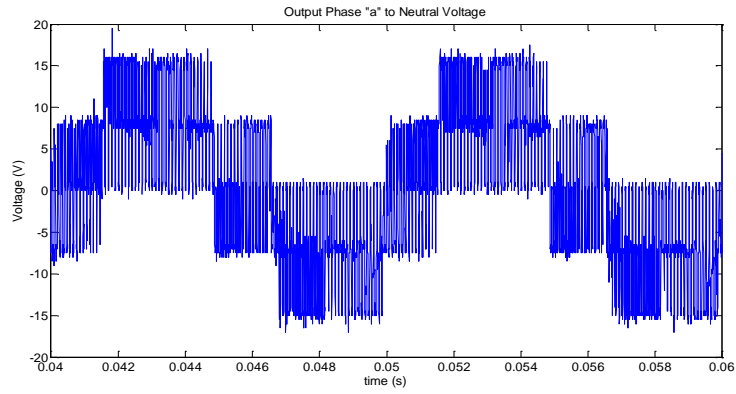


Fig.6. 23 Output phase “a” to neutral voltage, V_{an} ($f_o = 100$ Hz)

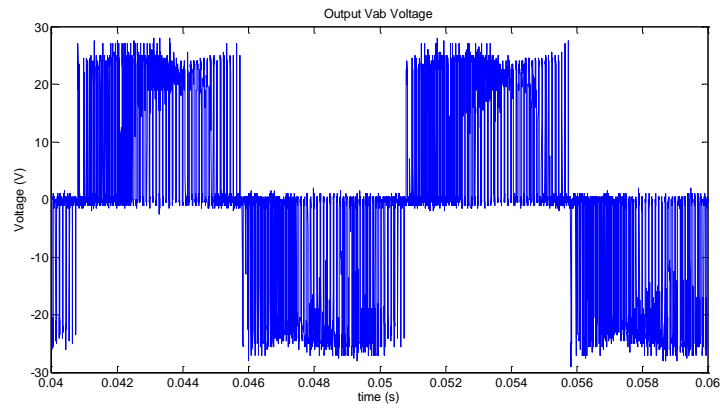


Fig.6. 24 Output line-to-line voltage V_{ab} ($f_o = 100$ Hz)

Besides plotting the output voltage waveform, the harmonic spectrums of the output line-to-line voltage is also presents in Fig.6. 25.

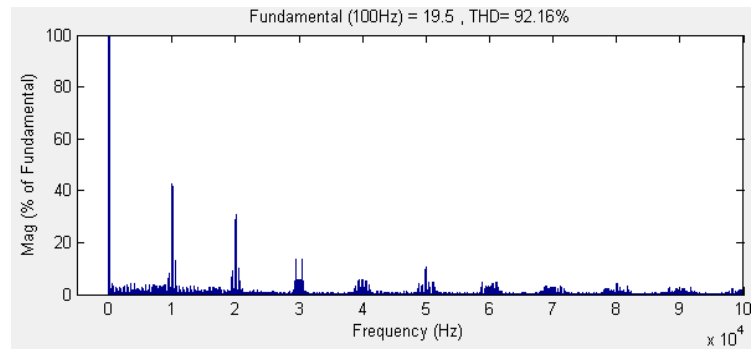


Fig.6. 25 Harmonic spectrum of output line-to-line voltage V_{ab} ($f_o = 100$ Hz)

Referring the Fig.6. 26, the output current waveforms of the direct matrix converter are balanced and sinusoidal. The harmonic spectrum of the output phase “a” current is illustrated in Fig.6. 27. These results evidently show that the modulation strategy is able to modulate the direct matrix converter to generate a set of sinusoidal and balanced output currents.

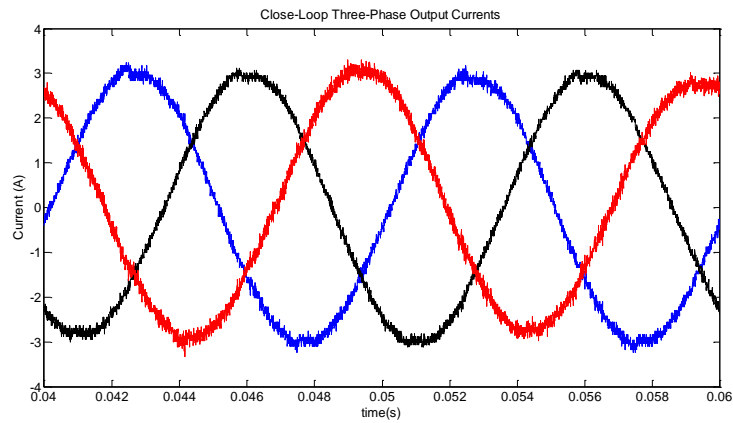


Fig.6. 26 Three-phase output currents ($f_o = 100$ Hz)

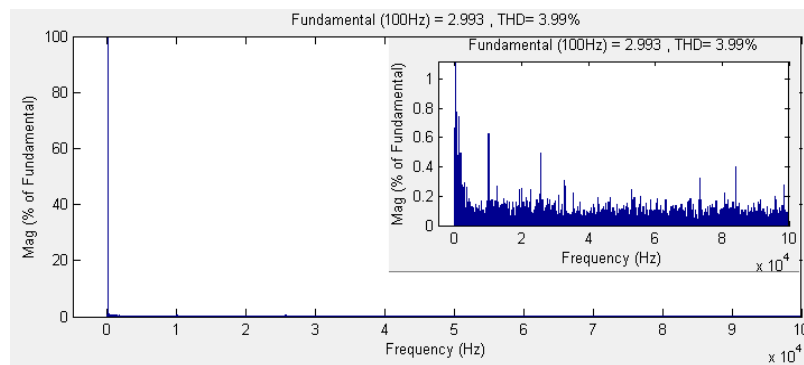


Fig.6. 27 Harmonic spectrum of the output phase “a” current ($f_o = 100$ Hz)

The previous closed-loop output waveforms verify the matrix converter operation at the load side and also show that the feedbacks (output currents and input voltages) are perfectly evaluated in the control loop. The output waveforms are sinusoidal as claimed. To fully verify the operational characteristics of matrix converter, the input voltage and current waveforms should also be investigated experimentally. Since no energy storage components are presented between the input and output sides of the matrix converter, the output voltage waveforms are generated directly from the input voltages. In other words,

each output voltage waveform is directly synthesized from AC input voltage waveforms. Therefore, the sampling rate had to be set much higher than frequencies of input and output waveforms. In fact, the input supply and load side waveform qualities are affected from the discontinuous conduction of the semiconductor switches. As mentioned before, inevitable timing inaccuracies and dead-time used at bi-directional switch commutation instants and the parasitic inductances of the commutation paths carrying discontinuous currents ($L \frac{di}{dt}$) at the switching instants results the distortion at the output waveforms. However, these are not the only reason of the distortions seen at output waveforms. Also, the output regulation of the input supply is effected from the discontinuous switching and it is directly linked to the output voltage waveforms since no energy storage components are used. The visual examples are illustrated in the next section.

6.3.3 Unity Power Factor Control

The controllable input power factor is the another feature of the matrix converter. The control algorithm only needs phase information of the input voltages for unity power factor control. It does not require the knowledge of the output phase angles. Fig.6. 28 and Fig.6. 30 show the input current and voltage waveforms in both filtered and unfiltered forms. As shown in Fig.6. 28, the unfiltered input current is discontinuous and has also nearly unity power factor distribution.

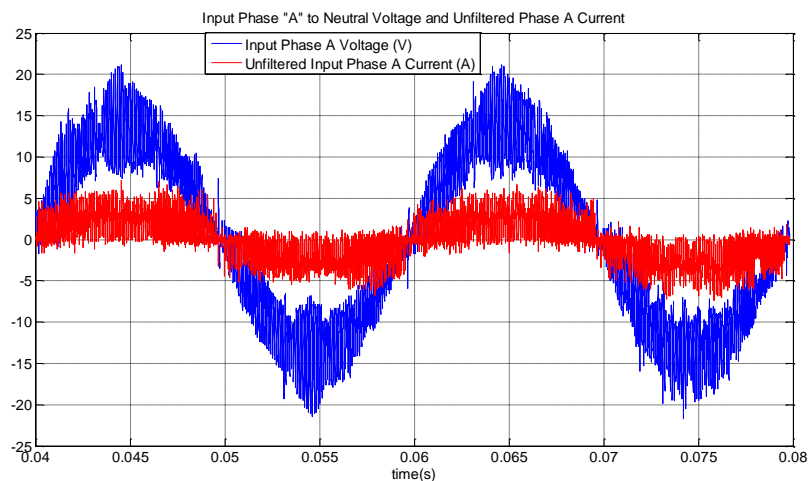


Fig.6. 28 Input phase “A” to neutral voltage, V_{AN} and unfiltered input current, I_A

As seen in Fig.6. 28, the input supply is highly affected from the discontinuous current drawn by matrix converter. Also, these disruptive effects are directly link to the output due to the nature of the matrix converter circuit because; there is not any energy storage element. As mentioned in Section 2.3.2, an input filter is required to reduce the harmonic pollution generated from matrix converter circuit. The input filter acts as an interface between the matrix converter and the input supply. Also, the input filter protects the matrix converter against to the unwanted changes like as voltage spikes arising from the input supply.

In Fig.6. 29, the harmonic spectrum of the unfiltered (discontinuous) input current is shown. As seen in figure, the total harmonic distortion of the discontinuous input current is high. Unless remedial actions are taken, the power system disturbances caused from these high harmonics can disrupt the other electrical operations performed on the line.

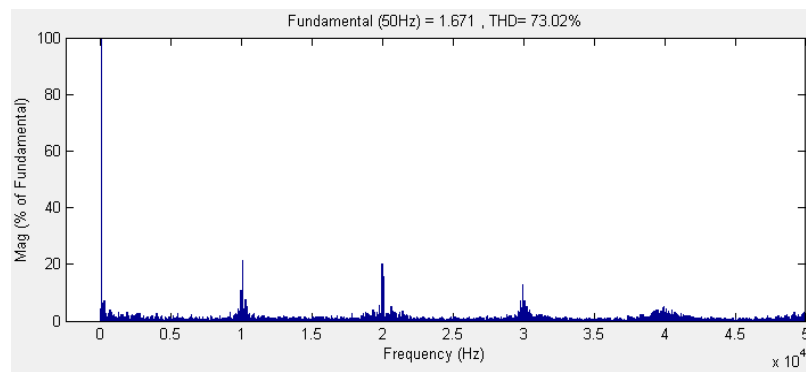


Fig.6. 29 Harmonic spectrum of the unfiltered input phase “A” current ($f_i = 50$ Hz)

In fact these harmonic components have practically high frequencies (around 10 kHz and above). Thus, the attenuation of these harmonics is not problematic. These components can be practically filtered using input filters. Fig.6. 30 shows the filtered input phase “A” current waveform and the input phase “A” voltage waveform with respect to neutral point while the matrix converter is operating at 5 A/ 50 Hz output current reference. It can be easily seen that input phase “A” to neutral voltage and filtered input phase “A” current are in phase. Thus, it proves the unity power factor control performance of direct matrix converter. Also, the use of input filter reduces the harmonic distortion in the input current waveform. As seen in Fig.6. 31, the high frequency range harmonics (e.g. switching frequency and its multiples) appeared in unfiltered input current is attenuated with the input filter designed with a cut-off frequency of nearly 1.3 kHz.

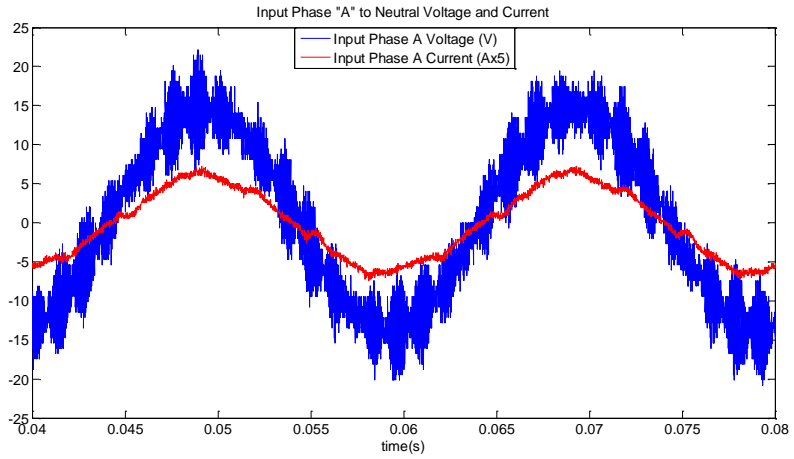


Fig.6. 30 Input phase “A” to neutral voltage, V_{AN} and filtered input current, I_A ($f_i = 50$ Hz)

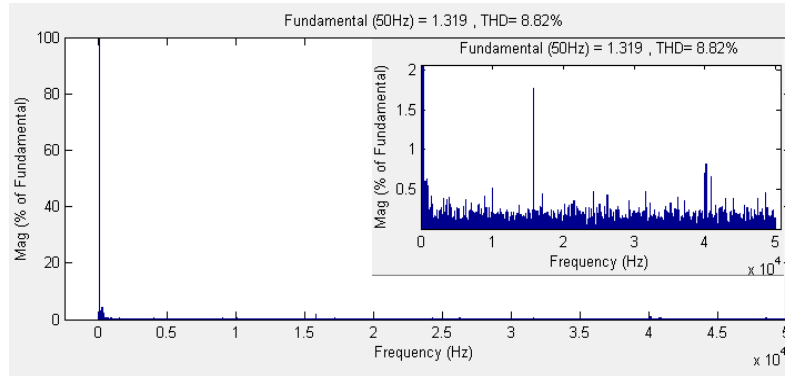


Fig.6. 31 Harmonic spectrum of the filtered input phase “A” current ($f_i = 50$ Hz)

The three-phase input currents are presented in Fig.6. 32.

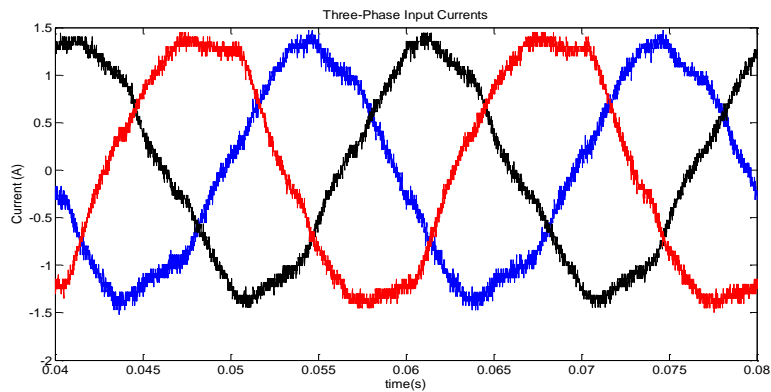


Fig.6. 32 Three-phase input currents

As it is seen, the three-phase input currents are nearly balanced and sinusoidal. This result also confirms that the matrix converter input currents are sinusoidal. However, some disturbances still exist in current waveforms. The disturbances in current waveforms may be caused from the overvoltage protection circuit. Fig.6. 30 shows that the input voltages are highly distorted despite the use of input filter. In fact, the input filter is a low pass filter (cut-off frequency is nearly 1.3 kHz) and matrix converter is operated at 10 kHz switching frequency. Therefore, the distortions which will be caused from the higher frequencies are filtered. However, the direct matrix converter structure also consists of a clamp circuit to protect the semiconductor switches for any high voltage spike caused from any inevitable timing inaccuracies at the switching instant or any reasons that require emergency stop. The clamp circuitry, presented in Section 2.4.5, is a basic three-phase diode rectifier. As presented in Section 5.4, the diode rectifier produces highly distorted input currents waveform especially in low frequency range. Therefore, the disturbances in input voltages are mostly caused from this problem and this problem may also affect the three-phase input currents.

6.3.4 Experiments with Surface Mounted Permanent Magnet Machine Load

In this section, the tests were performed with a surface mounted permanent magnet machine load described in Table 5. 3. Following figures show the closed-loop output phase voltage, line-to-line voltage and current waveforms of the matrix converter when the demanded peak current value is 3A. Fig.6. 33 and Fig.6. 34 corroborate the output voltage waveforms. The absolute peak value of the pulses in the output phase voltage is nearly 15V. Note that the voltage levels have some higher values than 15 V due to the inevitable timing inaccuracies at the bi-directional switch commutation instants and the parasitic inductances of the commutation paths carrying discontinuous currents ($L \frac{di}{dt}$) at the switching instants.

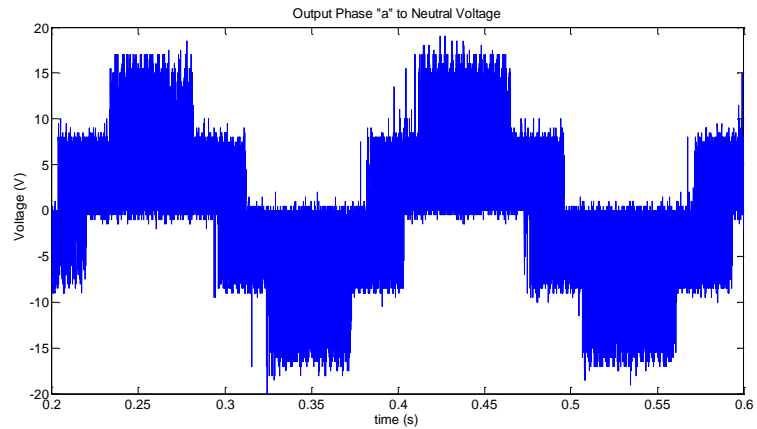


Fig.6. 33 Output phase “a” to neutral voltage, V_{an} ($f_o = 5.5$ Hz)

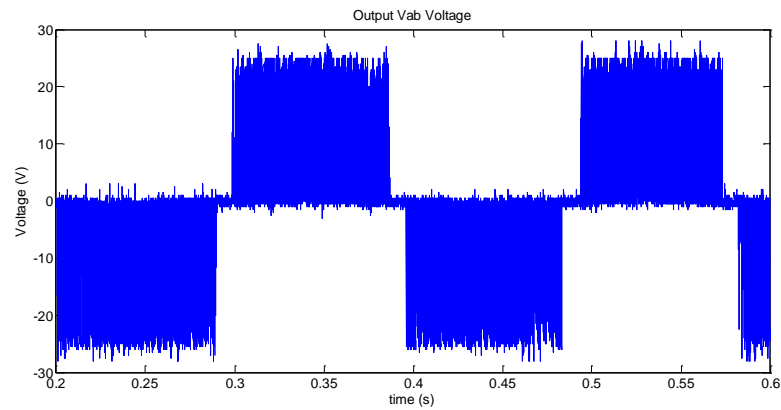


Fig.6. 34 Output line-to-line voltage V_{ab} ($f_o = 5.5$ Hz)

Fig.6. 35 shows the three-phase stator currents. The current waveforms are sinusoidal with a switching ripple at 10 kHz. The peak-to-peak ripples in three-phase motor currents were higher than the peak-to-peak ripples measured on passive load currents because while the motor is running it generates back-emf voltage and the generated back-emf also resists the supply voltage. Thus, the usable voltage capacity to regulate the output currents gets smaller.

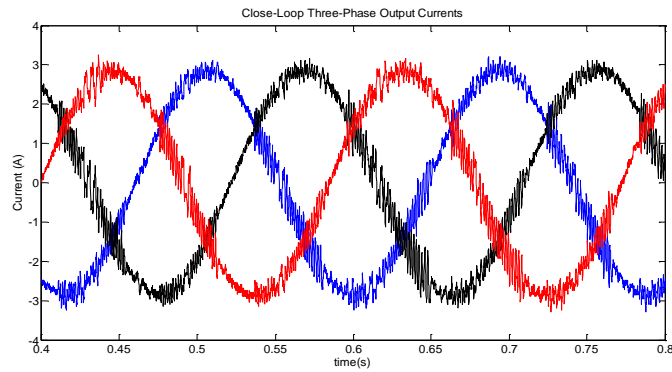


Fig.6. 35 Three-phase output currents ($f_o = 5.5$ Hz)

Fig.6. 36 shows the developed motor torque and the stator currents when the motor torque command was changed from a steady-state value of 0.63 Nm (e.g. 0.3pu motor torque) to 2.1 Nm (e.g. 1pu motor torque). Also, it should be noticed that the motor speed is kept constant using another dynamic load. In fact, the peak torques of the test motor and the dynamic load are higher than the 2.1Nm. However, due to the some unexpected restrictions caused from the matrix converter circuit, the input supply voltage is not increased higher than $26 V_{L-L}$. For that reason, the stator current has to be limited to a maximum value of 3 A. The maximum current value is set to 5 A for passive R-L load due to the lack of back-emf effect. As mentioned in Chapter 3, for surface mounted permanent magnet synchronous machines, the output torque is linearly controlled with the q-axis current demand. D-axis current does not directly affect the output torque. Hence, the only q-axis current demand (torque demand) is adjusted.

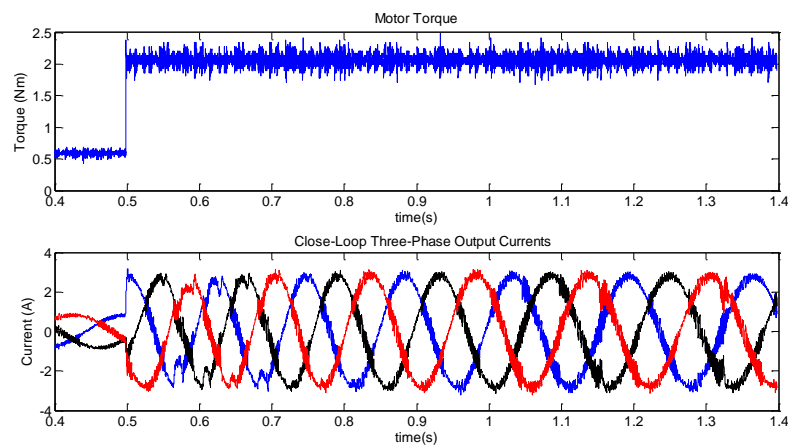


Fig.6. 36 Developed motor torque and converter output currents

Comparing the experimental results with the simulation results it can be stated that there is a good accordance. This proves the validity of the produced circuits and implemented models. And also, the input and output current waveforms of the direct matrix converter prove the ability of SWM to perform sine-wave-in/sine-wave-out operation.

As discussed in many times, the matrix converter circuit consists of an array of bi-directional semiconductor switches and the input voltage source is directly connected to the output load without any intermediate energy storage elements. It means that the matrix converters are more sensitive to input power disturbances than conventional diode-rectified voltage source inverters due to the absence of dc-link. Therefore, under power disturbances such as transients and short term power interruption has become more important issue for matrix converters.

CHAPTER 7

CONCLUSIONS AND FUTURE WORKS

This study has comprehensively addressed the direct matrix converter control for a three-phase balanced load and a surface mounted permanent magnet synchronous machine. Actually, matrix converter is a switch-mode device and generates harmonic components especially at switching frequencies. Thus, we need to understand the spectrum of the input and output waveforms. In this thesis, the harmonic spectrums of the currents and voltages are analyzed. It is seen that an unfiltered matrix converter highly pollutes the utility grid. As a result, a practical filter was designed and simulated with the integrated matrix converter model. The total harmonic distortions (THDs) for the unfiltered and filtered input phase current are obtained as 158.57 % and 2.70 %, respectively. It observed that the dominant frequency harmonics especially at switching frequency and its multiples were suppressed. Moreover, THD values for the output voltage and current are obtained less than 100 % and 1 %, respectively. The observed THD of voltage waveforms are quite high and the considerable harmonic components are at integer multiples of switching frequency and side bands of these frequencies. Also, the high harmonic contents are not seen in the output currents waveforms because the R-L load attenuates these high frequency harmonics. Thus, the effect of these harmonics on the electromagnetic torque is negligible. However, these high harmonic components on the output voltage waveforms cause additional power losses.

In light of simulation results presented in Chapter 5, the developed and implemented algorithms for controlling the direct matrix converter in order to generate three-phase output voltages/currents as well as maintain a set of balanced, sinusoidal input currents with unity power factor are quite satisfactory. Moreover, the current control loop is also verified under step and constant loading cases. For the high current control bandwidths, the settling time should be small. In fact, the settling time depends on the electrical time constant of the

load. For a typical permanent magnet synchronous machine, the electrical time constant is less than 10 ms. The closed-loop simulation results show that the settling time bringing the output peak currents to 5 A (1pu) is 2.5 ms which is quite enough for the motor control applications.

During the simulations, any unexpected situation, related with the operational characteristics of direct matrix converter, was not encountered except the theoretical difficulties because the matrix converter topologies have unfamiliar power conversion stage and power switch structures than customary (DC-link) converters. In direct matrix converter topology, the AC input power phase lines are directly connected to the converter outputs. Moreover, bi-directional switch structures are used to block voltages in either polarities and allow current flow in either direction. Actually, these switches have important role in the realization of the direct matrix converter. Besides, these positive characteristics, the bi-directional switches also bring some challenges such as the lacking of the free-wheeling paths for inductive load currents. Therefore, the output current direction based four-step commutation technique has also been utilized to resolve this difficulty during the commutation instants.

In addition, in order to assess the performance of the direct matrix converter, the converter was compared with the diode-rectified two-level voltage source inverter. Compared to the diode-rectified two-level VSIs, the direct matrix converter topologies obviously generate similar output voltage and current waveforms and better quality input waveforms in terms of the harmonic contents and power factor. Also, considering the power flow direction, we can say that the direct matrix converter can work inherently in four quadrant operation regions as well. However, by referring Fig.5. 49, we can say that the diode-rectifier two-level voltage source inverter has superior input voltage to output voltage transfer ratio than the direct matrix converter in the linear operating regions of both converters.

After the validation of direct matrix converter operation by simulation results, the designed matrix converter is verified by experimentally. The experimental results clearly correspond well to the simulation results, proving the abilities of the direct matrix converter to generate three-phase output voltages/currents and a set of balanced, sinusoidal input currents with unity power factor. The harmonic spectrums of the input current, output voltage and output current obtained experimentally comply with the simulation results. The output voltage and

current THDs are less than 93 % and 4 %, respectively. Moreover, the total harmonic distortions (THDs) for the unfiltered and filtered input phase current are obtained as 73.02 % and 8.82 %, respectively. The dominant frequency harmonics in the input current waveform especially at switching frequency and its multiples are suppressed. Although a second order LC filter (cut-off frequency is nearly 1.3 kHz) was also used for experimental studies to reduce the impact of the harmonic currents on power supply, the harmonic contents of the input current waveforms could not be reduced as in the simulation results. Because, the simulation results of the direct matrix converter topology discussed in this study based on the assumption that the AC mains feeding the direct matrix converter is distortion-free. In practice, this may be true for the large power utility grids. However, in this thesis another switch mode AC power supply is used during the experimental works and this assumption is not true for this case. In fact, there are two critical factors which can heavily distort the quality of the input current. Those are the effect of the overvoltage protection circuit and the regulation capability of the AC source.

Moreover, the current control loop is also verified experimentally under step loading case. The closed-loop experimental results show that the settling time to bring the output peak currents to 5 A (1pu) is 20 ms. Although this time duration was enough during the experimental studies, the settling time reached by simulations could not be obtained by experimentally. This difference may be caused from the delays occurred during the data acquisition, processing and PWM generation. Moreover, three-phase motor current ripples obtained experimentally are much higher than the obtained results by simulations. I think that this difference is also related to the low settling time and the harmonics on the input voltage.

Consequently, the following advantages can be stated for a direct matrix converter system:

- It has been shown that the size of the reactive components can be reduced significantly,
- It has been demonstrated that the unity power factor control at the input side can be obtained although the load is inductive,
- It is shown that the better quality input waveforms can be obtained in terms of the harmonic contents,

- Finally, the direct matrix converter system can inherently provide bi-directional power flow for the adjustable speed drive applications.

This work has practically investigated the operational principles of the direct matrix converter under balanced input voltage and output load conditions. However, further studies are absolutely necessary and some of the possible studies are identified below;

- The further investigation of the semiconductor devices to construct the optimum bi-directional switches for matrix converter,
- The investigation of multilevel matrix converter topologies in order to decrease the harmonic components in the output waveforms,
- The derivation of alternative modulation strategies that can increase the input voltage to output voltage transfer ratio,
- Implementation of the direct matrix converter with unbalanced voltage supply and load to check on the performance and reliability.

REFERENCES

- [1] L. Gyugyi, "Generalized theory of static power frequency changers", UK, Salford University Press, 1970.
- [2] P. D. Ziogas, S. I. Khan, and M. H. Rashid, "Some improved forced commutated cycloconverter structures", IEEE Trans. On Industry Applications, vol. 21, no:5, pp. 1242–1253, 1985.
- [3] L. Helle, K. B. Larsen, A. H. Jorgensen, and S. M. Nielsen, "Evaluation of Modulation Schemes for Three-Phase to Three-Phase Matrix Converter", IEEE Trans. On Industrial Electronics, vol. 51, no:1, Feb. 2004.
- [4] A. Alesina and M. G. B. Venturini, "Solid-state conversion: A fourier analysis approach to generalized transformer synthesis", IEEE Trans. On Circuits and Systems, vol. CAS-28, no:4, pp. 319-330 , April 1981.
- [5] L. Huber and D. Borojevic, "Space vector modulation with unity input power factor for forced commutated cycloconverters", in Conference Record of the 1991, IEEE Industry Applications Society Annual Meeting, vol. 1, pp. 1032–41, 1991.
- [6] A. Alesina, M. Venturini, "Analysis and Design of Optimum-Amplitude Nine-Switch Direct AC-AC Converters", IEEE Trans. on Power Electronics, vol. 4, no:1, pp. 101-112, Jan. 1989.
- [7] P.W. Wheeler and D.A. Grant, "Optimised Input Filter Design and Low-loss Switching Techniques for A Practical Matrix Converter" ,IEE Proc. of Electric Power Applications, vol. 144, no:1, pp. 53-60, Jan. 1997.
- [8] N. Mohan, T. M. Undeland, W. P. Robbins, "Power Electronics", 3rd Edition, John Wiley & Sons, 2003.
- [9] N. Burany, "Safe Control of Four-Quadrant Switches", Conference Records of IEEE- IAS Annual Meeting, vol:1, pp. 1190-1194, 1-5 Oct. 1989.

- [10] P. Tenti, L. Malesani and L. Rossetto, "Optimum Control of N-Input K-Output Matrix Converters", IEEE Trans. On Power Electronics, vol. 7, no:4, pp. 707-713, Oct. 1992.
- [11] A. Zuckerberger, D. Weinstck and A. Alexandrovitz, "Single-Phase Matrix Converter", IEE Proc. of Electric Power Applications, vol 144, no:4, pp. 235-240, July 1997.
- [12] A. Khoei and S. Yuvarajan, "Single-Phase AC-AC Converters Using Power MOSFETs", IEEE Trans. On Industrial Electronics, vol. 35, no:3, pp. 442-443, Aug. 1988.
- [13] Z. Idris, M.K. Hamzah and M. F. Saidon, "Implementation of Single-Phase Matrix Converter as a Direct AC-AC Converter with Commutation Strategies", Proc. of IEEE Power Electronics Specialists Conference, PESC'06, pp. 1-7, Jeju, Korea, June 18-22 2006.
- [14] P. W. Wheeler, J. C. Clare and N. Mason, "Space Vector Modulation for a 4-Leg Matrix Converter", Proc. of IEEE Power Electronics Specialists Conference, PESC'05, pp. 31-38, Recife, Brazil, June 12-16 2005.
- [15] D. Katsis, P. W. Wheeler, J. C. Clare and L. Empringham, "A Utility Power Supply Based on a Four-Output Leg Matrix Converter", Proc. of IEEE Industry Applications Society Annual Meeting, IAS 2005, vol. 4, pp. 2355-2359, Hong Kong, China, October 2-6, 2005.
- [16] C. Klumpner and F. Blaabjerg, "Modulation method for multiple drive system based on a two-stage direct power conversion topology with reduced input current ripple", IEEE Trans. On Power Electronics, vol. 20, no:4, pp. 922-929, July 2005.
- [17] S. L. Arevalo, "Matrix Converter for Frequency Changing Power Supply Applications", Ph.D. Thesis, University of Nottingham, Jan. 2008.
- [18] M. Jussila, H. Tuusa, "Comparison of Direct and Indirect Matrix Converters in Induction Motor Drive", Proc. of IEEE-IECON'06, pp.1621-1626, 2006.
- [19] R.R. Beasant, W.C. Beattie, A. Refsum, "An Approach to the Realisation of a High Power Venturini Converter", Proc. of IEEE/PESC'90, pp. 291-297, 1990.
- [20] J. Mahlein, M. Braun, "A Matrix Converter without Diode clamped Over-Voltage Protection", Proc. of IEEE-IPEMC 2000, vol. 2, pp. 817-822, 2000.
- [21] P. Nielsen, F. Blaabjerg, J.K. Pedersen, "New Protection Issues of a Matrix Converter: Design Considerations for Adjustable-Speed Drives", IEEE Trans. on Industry Applications, vol. 35, no:5, pp. 1150-1161, Sept./Oct. 1999.

- [22] J. Mahlein, M. Bruckmann and M. Braun, "Passive Protection Strategy for a Drive System With a Matrix Converter and an Induction Machine", IEEE Trans. On Industrial Electronics, vol. 49, no:2, April 2002.
- [23] T. Svensson, M. Alaküla, "The Modulation and Control of a Matrix Converter Synchronous Machine Drive", Proc.of EPE'91, vol. 4, pp. 469-476, 1991.
- [24] L. Empringham, P.W. Wheeler, J.C. Clare, "A Matrix Converter Induction Motor Drive Using Intelligent Gate Drive Level Current Commutation Techniques", Proc of IEEE/IAS Conference 2000, vol. 3, pp. 1936-1941, 2000.
- [25] M. Ziegler, and W. Hofmann, "Implementation of a Two Steps Commutated Matrix Converter", in Proc. IEEE PESC'99, vol. 1, pp. 175 – 180. 1999.
- [26] Hongwu She, Student Member, IEEE, Hua Lin, Member, IEEE, Bi He, Xingwei Wang, Limin Yue, and Xing An, "Implementation of Voltage-Based Commutation in Space-Vector-Modulated Matrix Converter", IEEE Trans. on Industrial Electronics, vol. 59, no:1, Jan. 2012.
- [27] K. Kato, J. Itoh, "Improvement of Input Current Waveforms for a Matrix Converter Using a Novel Hybrid Commutation Method", Proc. of IEEE-PCCON'07 , Nagoya , 2-5 Apr. 2007.
- [28] L.C. Herrero, S. de Pablo, F. Martin, J.M. Ruiz, J.M. Gonzalez and B. Rey Alexis "Comparative Analysis of the Techniques of Current Commutation in Matrix Converters" , IEEE International Symposium on Industrial Electronics, pp. 521-526, 4-7 June 2007.
- [29] M. Ziegler, W. Hoffman, "Semi Natural Two Steps Commutation Strategy for Matrix Converters" , Proceedings of IEEE/PESC'98, vol. 1, pp. 727-731, 22 May 1998.
- [30] J. Mahlein, J. Igney, M. Braun, O. Simon, "Robust Matrix Converter Commutation without explicit Sign Measurement", IEEE Trans. On Industrial Electronics, vol. 49, no:2, pp. 407-414, 2002.
- [31] R. Krishnan, "Permanent Magnet Synchronous and Brushless DC Motor Drives", London New York, CRC Press, 2010.
- [32] B. S. Guru and H. R. Hızıroğlu, "Electric Machinery and Transformers", 3rd Edition, New York, Oxford University Press, 2001.
- [33] R. Krishnan, "Electric Motor Drives (Modeling, Analysis, and Control)", Prentice-Hall, 2003.

- [34] M. Matteini, "Control Techniques For Matrix Converter Adjustable Speed Drives", Ph.D. Thesis, University of Bologna, 2001.
- [35] M. Venturini, "A new sine wave in, sine wave out conversion technique which eliminates reactive elements", Proc. of Powercon'07, pp. 310-315, 1980.
- [36] P.D. Ziogas, S.I. Khan, and M.H. Rashid, "Analysis and Design of Forced Commutated Cycloconverter Structures with Improved Transfer Characteristics," IEEE Trans. on Industry Applications, vol. IE-33, no:3, pp. 271-280, Aug. 1986.
- [37] A. Alesina and M. Venturini, "Intrinsic Amplitude Limits and Optimum Design of 9-Switches Direct PWM AC-AC Converters," Proceedings of IEEE/PESC'88, vol. 2, pp. 1284-1291, 1988.
- [38] G. Roy, and G-E. April, "Cycloconverter Operation Under a New Scalar Control Algorithm", Conference Records of IEEE PESC 1989, Milwaukee, WI, pp. 368-375, June 26-29, 1989.
- [39] L. Huber, D. Borojevic, "Space Vector Modulator for Forced Commutated Cycloconverters" Proceedings of IEEE/PESC'89, pp. 871-876, 1989.
- [40] D. Casadei, G. Grandi, G. Serra, A. Tani, "Space Vector Control of Matrix Converters with Unity Input Power Factor and Sinusoidal Input/Output Waveforms," Proceedings of IEEE PE'93, Vol. 7, pp. 170-175, 1993.
- [41] J.W. Kolar, M. Baumann, F. Schafmeister and H. Ertl, "Novel Three-Phase AC-DC-AC Sparse Matrix Converter", Proceedings of Applied Power Electronics Conference and Exposition, vol. 2, pp. 777 – 791, March 2002
- [42] L. Huber, D. Borojevic, "Space Vector Modulated Three-Phase to Three-Phase Matrix Converter with Input Power Factor Correction", IEEE Trans. on Industry Applications, vol. 31, no:6, pp. 1234-1246, 1995.
- [43] D. O. Neacsu, "Space Vector Modulation", The 27th Annual Conference of the IEEE Industrial Electronics Society, 2001
- [44] Y. Tadano, S. Urushibata, M. Nomura, Y. Sato, and M. Ishida, "Direct Space Vector PWM Strategies for Three-Phase to Three-Phase Matrix Converter", Power Conversion Conference- Nagoya, 2007. PCC'07, pp. 1064-1071, 2-5 April 2007.
- [45] Y. Lu, "An Optimization-Based Space Vector Modulation Method for the Three-Phase to Three-Phase Matrix Converter", Ph.D. Thesis, University of Idaho, 2007.

- [46] D. Casadei, G. Serra, A. Tani, and L. Zarri, "Matrix Converter Modulation Strategies: A New General Approach Based on Space-Vector Representation of the Switch State", *IEEE Trans. on Industrial Electronics*, vol. 49, no:2, pp. 370-381, 2002.
- [47] C. Klumpner and F. Blaabjerg, "Two Stage direct Power converter: An alternative to Matrix converter", *IEE seminar on matrix converters*, pp. 7/1 – 7/9, Aalborg University, Denmark, April 2003.
- [48] K. You and M. F. Rahman, "Modulations for Voltage Source Rectification and Voltage Source Inversion Based on General Direct Space Vector Modulation Approach of AC-AC Matrix Converter Theory", *Industrial Electronics, IEEE International Symposium*, vol. 2, pp. 943-948, July 2006.
- [49] P.W. Wheeler, H. Zhang and D.A. Grant, "A Theoretical and Practical Investigation of Switching Frequency Harmonics in a Matrix Converter". *Proceedings of UPEC'93*, pp. 502–505, 1993.
- [50] R.D. Middlebrook, "Input Filter Considerations in Design and Application of Switching Regulators", *Conference Records of IEEE/IAS Society Annual Meeting*, pp. 91-107, Chicago, 1976.
- [51] M. Y. Lee, "Tree-level Neutral-point-clamped Matrix Converter Topology", Ph.D.. Thesis, University of Nottingham, March 2009
- [52] R. A. Petrocelli, "New Modulation Method for Matrix Converters", Ph.D. Thesis, University of Manchester, May 2002.
- [53] Bimal K. Bose, "Modern Power Electronics and AC Drivers". Penitence Hall PTR, October 2001.
- [54] R. D. Doncker, D. W.J. Pulle and A. Veltman, "Advanced Electrical Drives", London New York, Springer, 2011.
- [55] D. W. Novotny and T. A. Lipo. "Vector Control And Dynamics Of AC Drives," Oxford University Press, 1996.

APPENDIX A

PARK AND CLARKE TRANSFORMATIONS

A.1. CLARKE TRANSFORMATION

The purpose of this transformation is that the stator current space vector is expressed in another reference frame with two orthogonal axes. Assuming that the axis “a” and the axis “ α ” are in the same direction then we have the following vector diagram.

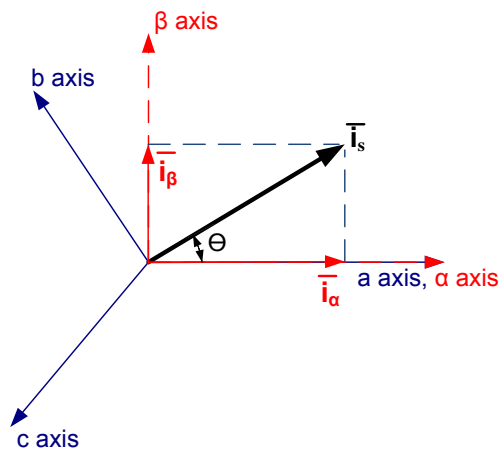


Fig. A. 1 Stator current representation in two co-ordinate stationary frame

The stator current space vector can be projected into two orthogonal axes. The real part of the stator current space vector is equal to the value of the direct-axis stator current component (i_α) and the imaginary part is equal to the quadrature-axis stator current component represented as (i_β) which are shown in Fig. A. 1. Then, the stator current space vector can be expressed in the reference frame as:

$$\bar{i}_s = i_\alpha + j i_\beta \quad (\text{A-1})$$

The projection of the stator current space vector on the orthogonal α , β axes can be derived as the following:

$$i_\alpha = |\bar{i}_s| \cos(\Theta) \quad (\text{A-2})$$

$$= |k(i_a + a i_b + a^2 i_c)| \cos(\Theta) \quad (\text{A-3})$$

$$= k(i_a - i_b \cos\left(\frac{\pi}{3}\right) - i_c \cos\left(\frac{\pi}{3}\right)) \quad (\text{A-4})$$

where $i_c = -i_a - i_b$

$$i_\alpha = k\left(\frac{3}{2}\right) i_a \quad (\text{A-5})$$

k is the transformation constant, chosen as $k = 2/3$ to select $i_\alpha = i_a$

Similarly, i_β can be derived and found as the following:

$$i_\beta = |\bar{i}_s| \sin(\Theta) \quad (\text{A-6})$$

$$i_\beta = \frac{1}{\sqrt{3}} i_b - \frac{1}{\sqrt{3}} i_c \quad (\text{A-7})$$

Then the matrix form of the stator current transformation can be written as:

$$[f_{\alpha\beta 0}] = [T_{\alpha\beta 0}][f_{abc}]$$

$$\begin{bmatrix} i_\alpha \\ i_\beta \\ i_0 \end{bmatrix} = \frac{2}{3} \begin{bmatrix} 1 & -\frac{1}{2} & -\frac{1}{2} \\ 0 & \frac{\sqrt{3}}{2} & -\frac{\sqrt{3}}{2} \\ \frac{1}{2} & \frac{1}{2} & \frac{1}{2} \end{bmatrix} \begin{bmatrix} i_a \\ i_b \\ i_c \end{bmatrix} \quad (\text{A-8})$$

$$[T_{\alpha\beta 0}] = \begin{bmatrix} 1 & -\frac{1}{2} & -\frac{1}{2} \\ 0 & \frac{\sqrt{3}}{2} & -\frac{\sqrt{3}}{2} \\ \frac{1}{2} & \frac{1}{2} & \frac{1}{2} \end{bmatrix} \quad (\text{A-9})$$

$[T_{\alpha\beta 0}]$ is the transformation matrix.

Zero sequence component i_0 stated in the equation (A-8) is equal to zero for balanced three phase loads. The each phase of three phase balanced stator windings is displaced with $\frac{2\pi}{3}$ radians phase shifts in space shown in Fig. A. 2(a). And its two axes equivalent has two orthogonal windings as shown in Fig. A. 2(b). Orthogonal windings guarantee that there is no interaction between perpendicular windings.

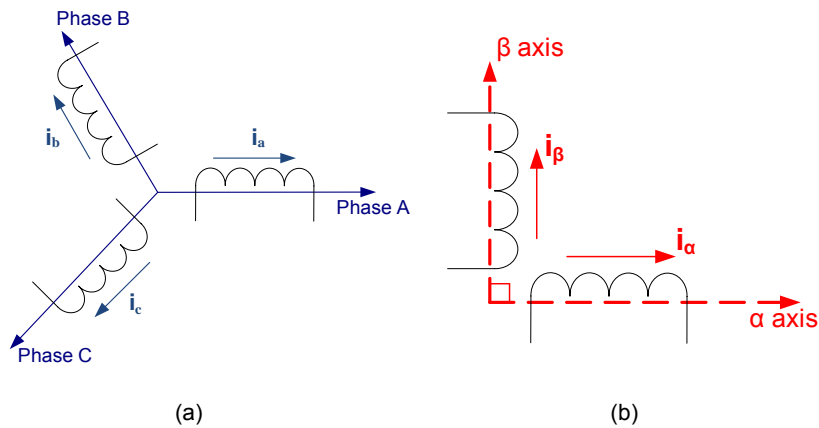


Fig. A. 2 (a) Three-phase balanced windings and (b) its two axes equivalent

After this transformation the torque equation is still dependent on the position of the rotor flux. In order to remove the dependency, second transformation called as Park Transformation must be applied.

A.2. PARK TRANSFORMATION

This transformation modifies the stationary two-phase orthogonal system α, β in the d, q rotating reference frame where d -axis is aligned with the rotor flux. In this frame, the torque expression is independent from the position of the rotor flux. Hence, working on this rotating reference frame makes the control easy. The next figure shows the relationship between the two reference frames.

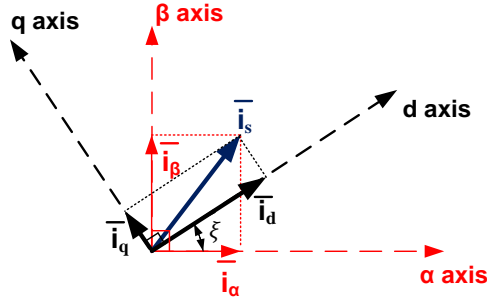


Fig. A. 3 D, q rotating reference frame

ξ is the instantaneous angle between the d axis and α axis.

The projection of the direct-axis stator current component (i_α) and the quadrature-axis stator current component (i_β) on the rotating d, q axes can be derived as the following:

$$i_d = i_\alpha \cos(\xi) + i_\beta \sin(\xi) \quad (\text{A-10})$$

$$i_q = -i_\alpha \sin(\xi) + i_\beta \cos(\xi) \quad (\text{A-11})$$

The matrix form of the Park Transformation can be written as:

$$\begin{bmatrix} i_d \\ i_q \end{bmatrix} = \begin{bmatrix} \cos(\xi) & \sin(\xi) \\ -\sin(\xi) & \cos(\xi) \end{bmatrix} \begin{bmatrix} i_\alpha \\ i_\beta \end{bmatrix} \quad (\text{A-12})$$

Also i_d and i_q are obtained directly from i_a , i_b and i_c .

$$\begin{bmatrix} i_d \\ i_q \end{bmatrix} = \begin{bmatrix} \cos(\xi) & \sin(\xi) \\ -\sin(\xi) & \cos(\xi) \end{bmatrix} \frac{2}{3} \begin{bmatrix} 1 & -\frac{1}{2} & -\frac{1}{2} \\ 0 & \sqrt{\frac{3}{2}} & -\sqrt{\frac{3}{2}} \end{bmatrix} \begin{bmatrix} i_a \\ i_b \\ i_c \end{bmatrix} \quad (\text{A-13})$$

$$\begin{bmatrix} i_d \\ i_q \end{bmatrix} = \frac{2}{3} \begin{bmatrix} \cos(\xi) & \cos(\xi - \frac{2\pi}{3}) & \cos(\xi + \frac{2\pi}{3}) \\ -\sin(\xi) & -\sin(\xi - \frac{2\pi}{3}) & -\sin(\xi + \frac{2\pi}{3}) \end{bmatrix} \begin{bmatrix} i_a \\ i_b \\ i_c \end{bmatrix} \quad (\text{A-14})$$

And inverse park transformation has the following equations:

$$\begin{bmatrix} i_\alpha \\ i_\beta \end{bmatrix} = \begin{bmatrix} \cos(\xi) & -\sin(\xi) \\ \sin(\xi) & \cos(\xi) \end{bmatrix} \begin{bmatrix} i_d \\ i_q \end{bmatrix}$$